THE CONTACT ANGLE, INTERFACIAL TENSION AND VISCOSITY OF RESERVOIR FLUIDS: EXPERIMENTAL DATA AND MODELLING

by

ZAID KHAMIS SARBOOKH AL-SIYABI

BSc. PE & AMath, MEng PE

Submitted for the Degree of Doctor of Philosophy in

PETROLEUM ENGINEERING

Department of Petroleum Engineering

Heriot-Watt University

Edinburgh, UK

February 2000

DEDICATION

This work is dedicated to my late brother (*May Allah rest his soul in peace and grant him paradise*), parents, wife and son, brothers and sisters, relatives and friends.

TABLE OF CONTENTS

LIST OF SYMBOLS

ABBREVIATION

AAD	:Absolute Average Deviation.
AD	:Average Deviation.
CCE	:Constant Composition Expansion.
cP	:centipoise.
CS1	:One-reference Fluid Corresponding State.
CS2	:two-reference Fluids Corresponding State.
DMF-1	:Drilling Mud Filtrate Number One.
DMF-3	:drilling mud filtrate Number Three.
DSS	:Direct Sampling System.
EOS	:Equation of State.
GOR	:Gas-Oil Ratio.
HPHT	:High Pressure-High Temperature.
HW1	:Heriot-Watt Correlation 1.
HW2	:Heriot-Watt Correlation 2.
IFT	:Interfacial Tension.
IOR	:Improved Oil Recovery.
JST	:Jossie-Stiel-Thodos.
LBC	:Lohrenz-Bray-Clark.
PRT	:Platimnum Resistance Thermometers.
PVT	:Pressure, Volume, Temperature.
SD	:Standard Deviation.
STLV	:Stock Tank Liquid Volume.
TRAPP	:TRAnsport Properties Prediction.
VLE	:Vapour-Liquid Equilibrium.
WK	:Weinaug-Katz.

NOMENCLATURES

a, b, c :Viscosity-EOS parameters.

A_c :Parameter used by the Scaling Law, Equation (4.5), which depends on the critical properties and boiling temperature of component.

A, B :Coefficients in Equation (6.6).

B :Parameter in Equation (4.5), which is estimated from component's IFT.

C :Conversion Constant in Equation (2.1).

d :Molecular Diameter.

D :Internal Diameter of the Capillary Tube Viscometer.

d_e :Equatorial Diameter of the suspended drop, Equation (2.2).

d_s :Diameter of the Drop Measured at the Height (d_e) above the Bottom of the Drop.

E_i :Standard Error Associated with a Measurable Quantity.

f_x, h_x :Corresponding State Reducing Ratios, used by Equation (5.5).

g : Gravitational Acceleration.

h :Vapour-Liquid Meniscus/interface Height..

H :Drop Shape factor, correlated as a function of the ratio d_s/d_e.

K :Vapour-Liquid Equilibrium Factor.

L :Length of the Capillary Tube Viscometer.

MW :Molecular Weight.

P :Pressure.

ΔP :Differential Pressure Across the Capillary Tube Viscometer.

P_c :Capillary Pressure across curved interface.

P_k :Convergence Pressure

$P_{\sigma i}$:Parachor Value of component i,

P_L :Parachor-equivalent Coefficients of Liquid Phase

P_V :Parachor-equivalent Coefficients of Vapour Phase

q :Cut-off Wave Number.

Q	:flow rate.
r	:Radius of Cylindrical Capillary Tube, Equation (3.1).
R	:Universal Gas Constant.
R_b	:Radius of Curvature of the Liquid Meniscus, Equation (2.4).
R_c	:Radius of Curvature of the Corner of Square Capillary, Equation (2.4).
R_t	:Radius of Curvature at the Top of Liquid Filament, Equation (2.4).
SG	:Specific Gravity.
T	:Temperature.
u	:Velocity.
υ_i	:Volume Fraction of Component i in the Mixture.
V	:Volume.
x_i	:Mole Fraction of Component i in the Liquid Phase.
y_i	:Mole Fraction of Component i in the Vapour Phase.
z	:Universal Critical Exponent, 0.054< z <0.065.
Z	:Compressibility Factor.
ΔZ	:Height of Liquid Filament.

GREEK LETTERS

α	:Rotational Coupling Factor.
α_c	:Riedel Parameter.
ϕ	:Half Corner Angle of a Wedge.
Φ	:Shape Factor, Equation (5.5).
η	:Viscosity.
$\Delta\eta$	:Residual or Excess Viscosity.
$\Delta\eta_c$	:Critical Viscosity Enhancement Component.
$\Delta\eta^1(\rho,T),\Delta\eta^2(\rho,T)$	:Viscosity terms in Equations (B.1) which govern the dense fluid region.
θ	: Contact Angle.

θ_b :Base-Value Contact angle.

Θ :Shape Factor, Equation (5.5).

ρ :Density.

$\Delta\rho$:Density Difference Between Two Immiscible Phases.

σ :Interfacial Tension.

ω :Acentric Factor.

Ω_{η}^{*} :Collisional Integral.

ξ :Correlation Length.

Ψ :Term in CS Models to Account for the High Density Behaviour.

ζ :Viscosity Reducing Parameter or the Inverse of the Critical Viscosity.

SUBSCRIPTS

b :Boiling State

c :Critical State

calc. :Calculated Value

eq. :Equivalent Value

exp. :Experimental Value

f :Freezing State

l :Liquid

v :Vapour

m :Molar Value

mix :Mixture

n :Normal State

o :Dilute State

pred. :Predicted Value

r :Reduced State

ref :Reference Component

LIST OF TABLES

LIST OF FIGURES

ACKNOWLEDGEMENTS

In The Name of Allah, The Most Gracious, The Most Merciful

I would like to take this opportunity to express my appreciation to all people who have helped me during my study. Special thanks to my parents, wife and son, brothers and sisters, nieces and nephews for their endless encouragement during my study. My sincere gratitude and thanks go to my supervisors, professor Ali Danesh and Dr. Bahman Tohidi for providing me this excellent opportunity to study under their guidance and their valuable advices throughout my study. I am also very grateful to professors Dabir Tehrani and Adrian Todd for their constructive comments and advices.

The financial support by the **Ministry of Oil and Gas** of Oman and **Petroleum Development Oman** (PDO) LLC is highly appreciated. I owe a great appreciation to Messrs. Keith Bell, Ken Malcolm, Alastiar Reid and Rod Burgass for their immense help with all experimental work, Dr. F. Gozalpour for his kind help with the Fluid Phase Equilibria (FPE) program, Messrs. Andrew Kidd, Ian Chislom, Robert Stables for their help with computer matters, and to all the colleagues in the department, especially Messrs. M. Jamiolahmady, M. Sohrabi, K. Østegaard and B. Al-Kharusi.

Finally, I would like to thank my friends (Dr. Said Al-Harthy, Isam Al-Zadjali, Suleiman Al-Siyabi, Suleiman Al-Zakwani, Mohammed Al-Salhi, Hamed Al-Hashmi, Abdullah Al-Mabsali) for their encouragement and motives.

ABSTRACT

Surface and viscous forces play a major role in the flow characteristics of fluids in petroleum reservoirs, hence, in the recovery of hydrocarbons. In reservoir engineering, surface forces are expressed by the interfacial tension (IFT) between different co-existing phases and the contact angle between the reservoir rock and in-situ fluids; whereas viscous forces are expressed by the viscosity of the flowing phases. The determination of these properties are essential in planning, management and operation of reservoirs for optimum recovery.

Novel techniques based on the characteristics of gas-liquid interface have been developed and employed for measuring the liquid-vapour-solid contact angle and IFT of various binary and real reservoir fluids. The results show that the contact angle remains fairly constant for a wide range of IFT values and then decreases as the fluid approaches its critical region. A generalised correlation between the contact angle and IFT was developed and evaluated using the generated data.

A systematic investigation of viscosity of pure compounds at various pressure and temperature levels indicated the need to include both structural and thermal effects for accurate viscosity prediction of dense fluids. A residual viscosity method has been modified to include the above effects and its reliability for calculating viscosity of mixtures has been demonstrated. Furthermore a model to predict the viscosity enhancement at near-critical conditions has been developed and tested against measured data at such conditions.

A methodology has been developed to determine the viscosity and IFT of the original reservoir fluid from samples contaminated by drilling fluids. The method, which relies on retrieving the original fluid composition and fluid property predictive models, has been tested for a large number of volatile oil and gas condensate samples contaminated at different levels with satisfactory results.

CHAPTER 1

INTRODUCTION

The characteristics of the flow of fluids in pipelines, wellbore and porous media are directly related to their viscosity and the capillary pressure. Viscosity is a configurational property which reflects the effect of inter-molecular motion and interaction which tends to oppose any dynamic change in fluid motion. Capillary pressure can be loosely defined as the pressure difference existing across an interface between immiscible fluids in equilibrium. Capillary pressure is a complex property which is a function of surface forces between the flowing phases expressed by the interfacial tension (IFT) and the wetting characteristics as expressed by the contact angle between the equilibrium fluids and the solid surface in contact with.

Reservoir fluids are known to compose of many hydrocarbon components. The distribution of these compounds has a very important effect in the flow characteristics of the in-situ fluids within reservoir rocks. Compositional effects that result through the depletion process and/or during improved oil recovery (IOR) processes materially affects the behaviour of viscosity, IFT and contact angle. For black oil simulation, sets of tables of these properties, for both liquid and vapour, are provided as function of pressure which usually are sufficient for a simulator to carry out flow calculation. On the other hand, when dealing with processes such as miscible gas-injection, multi-contact miscibility, volatile oil and gas-condensate systems where vigorous inter-phase interactions occur, the necessity of acquiring means of capturing fluid property changes for each grid block

is given too much attention in the petroleum industry. The means of capturing these changes is either by conducting very laborious experiments or modelling these changes with an equation. The latter option is very attractive and more effective than the first option which is very difficult to achieve and involves too much time and cost.

In the advent of highly sophisticated technologies in hydrocarbon exploration, drilling and recovery schemes, HPHT reservoirs are now being discovered and exploited in various parts of the world. Reservoir fluids present in these adverse conditions can give rise to peculiar behaviour for volumetric and fluid properties. The development of these reservoirs depends on the profitability and productivity of hydrocarbon. The literature contains many methods for predicting the above properties, (especially for viscosity and interfacial tension), ranging from mathematically rigorous to totally empirical. However, the majority of these methods are inapplicable at these conditions. Therefore, it is preferred to have models which could be applied to a wider range of conditions with an acceptable accuracy.

Any fluid produced from a reservoir can provide valuable information on its phase behaviour and flow characteristics within its reservoir rock. Oil-based drilling muds are widely used drilling fluids which are known to minimise drilling-induced damage to hydrocarbon bearing formation. These drilling muds range from simple synthetic to multi-component natural fluids. Reservoir fluid samples obtained are often contaminated with mud filtrate, particularly if it is completely miscible with reservoir fluid, and can, therefore, affect its properties. Despite advances in downhole sampling technology, obtaining a mud-free reservoir fluid sample still remains a challenging and time consuming operation. Therefore, it is essential to be able to retrieve the properties of the original fluid from contaminated samples. To retrieve the properties of the original fluid, predictive tools are often used. To do so, fluid samples need to be fully characterised and extensively tested in laboratory.

The most extensively used instruments for the measurement of fluid viscosity are capillary tube viscometers. For these instruments, the viscosity of the fluid of interest is

determined from the nature of its flow through capillaries of relatively small diameters. The theory of capillary flow viscometry entails that the pressure drop between the inlet and the outlet ends, of the tube, is related to the viscosity of the flown fluid. Viscosity is then calculated from a well-known theoretically based formulation of Hagen-Poiseuille[1]. A coiled capillary tube viscometer has been shown to generate reliable viscosity data for a variety of fluids ranging from simple single component to complex multi-component fluids.

The petroleum industry uses several methods for viscosity prediction, ranging from mathematically rigorous to completely empirical. The residual viscosity method by Lohrenz-Bray-Clark (LBC)[2] is the most popular method of predicting the viscosity of hydrocarbon fluids. Other techniques which are based on the principle of corresponding state[3,4] have also been used. In general, the LBC method is found to be more reliable than others, however it is not adequate for the dense fluids. This in turn emphasises the need for an accurate model, which can predict the viscosity of dilute and dense fluid phases with reasonable accuracy. A liquid, with molecules much more closely spaced than a gas, has cohesion forces much larger than in a gas. Momentum transport in liquids may occur by the action of intermolecular forces of the neighbouring molecules; while in gases momentum is predominantly transferred by the free-motion of molecules. A systematic investigation of density and viscosity of pure compounds at various pressures and temperatures indicated the need to include both structural and thermal effects in addition to density, which were not accounted for in the Jossi *et al* (JST) correlation[5].

Fluid viscosity appears to diverge from the normal trend as the critical point is approached, for a variety of model and multi-component near-critical fluids. This critical divergence is attributed to compressibility enhancement resulting in non-linear coupling between the various hydrodynamic modes (mainly viscous and diffusive) of the system. Predictive models[2-4,6], described previously, were observed to behave unreliably in the vicinity of critical point. To ensure reliable viscosity prediction at such conditions, a simple two-parameter corresponding state viscosity model has been developed[7], using

critical enhancement data on pure fluids. The model has been tested against various binary and multi-component reservoir fluids near their critical points.

As mentioned previously, capillary pressure is a complex property which is a function of the interfacial tension (IFT) between different co-existing phases and the contact angle between reservoir rock and in-situ fluids. Interfacial tension is defined as the surface-free energy which is required to bring the molecules from their bulk phases to the boundary surface separating them. The formation of the boundary surface results from the imbalance between the molecular forces at the interface caused by the physical attraction between molecules. It has been established that relative permeability relationships, which determine the flow behaviour of reservoir fluids in porous media, strongly depend on the interfacial tension at high pressure conditions[8-10]. Therefore, accurate and reliable information on interfacial tension (IFT) is of major importance in the petroleum industry.

The most commonly used method for the experimental measurement of interfacial tension is the pendant drop technique[11]. The method involves suspending a droplet of liquid in its equilibrium vapour and measuring various droplet dimensions. However, the size of droplet that can be generated is limited by the diameter of the tube from which it is suspended. So fluids with low interfacial tensions cannot be measured unless the tube is replaced by one with a smaller diameter. This would involve a great deal of effort to change the pendant dropper for fluids with differing interfacial tensions. For gas-condensate and near-critical fluid systems, where the interfacial tension is typically very low, a novel technique (using the height of the interface) has been developed, for the measurement of interfacial tension[12]. The technique utilises the meniscus height that forms between any equilibrated hydrocarbon liquid and vapour phases against the solid glass window inside a PVT cell. Previously, the technique was limited to measure the IFT of low tension fluids. However, a systematic comparison of the measured data by this technique and the pendant drop method demonstrated its reliability for high IFT measurements. Since then, this technique along with the conventional pendant drop method are routinely employed on all test fluids. As is usually the case with many fluid properties, the time and cost involved in obtaining sufficient experimental data for wide

ranges of conditions are prohibitive. Hence, predictive, often empirical, techniques are usually employed to estimate such properties. The two most commonly used methods of predicting the interfacial tension are the parachor method[13] and the scaling law[14]. Both techniques have previously been evaluated and modified by this Department[15].

Generally, the measured capillary pressure data on a core at laboratory conditions are transposed to reservoir conditions employing crude assumptions, such as zero or constant contact angle at all conditions. Recent reports on capillary pressure data measured at reservoir conditions[16,17], have indicated the unreliability of the current practice, particularly at low IFT conditions. Christoffersen *et al*[16] concluded that linear up-scaling of laboratory capillary pressure data to reservoir condition is not valid at IFT conditions lower than a threshold value of about 5 $mN.m^{-1}$. Longeron *et al*[17] conducted series of gas-oil capillary pressure measurements on sandstone cores over a range of IFT values and concluded that the standard transposition of laboratory capillary pressure data to reservoir conditions is only valid for IFT values higher than 3.7 $mN.m^{-1}$. The authors suggested changing the contact angle for lower IFT values, which is in agreement to those conclusions reported by Christoffersen *et al*[17]. However, there exists little information, in the literature, in the variation of contact angle with pertinent parameter.

The contact angle is a measure of the relative strength of adhesion of the fluid to the solid surface and to itself. Contact angle has a major influence on the hydrocarbon distribution as well as any water present within reservoir rocks. The main interest in the contact angle in petroleum engineering is its contribution to the capillary pressure as expressed by the Laplace-Young equation. A literature search was conducted to establish the techniques available for the measurement of contact angle at elevated conditions of pressure and temperature similar to those encountered in hydrocarbon reservoirs. The most widely used techniques for the measurement of contact angle are the sessile drop and the Wilhelmy plate methods[18]. A method based on filament rise in square capillary tubes has recently been shown to provide accurate contact angle data[19].

In the sessile drop method, the contact angle between liquid droplet and a solid surface is measured visually through a comparator microscope fitted with goniometric scale, thereby measuring the contact angle directly. The Wilhelmy plate method relies on the liquid rise on a vertical flat plate partially immersed in a pool of liquid for which the contact angle is to be determined. The contact angle can then be measured directly using similar viewing devices or indirectly using an equation. However, the contact angle would be impossible to measure in real porous media with heterogeneous rock properties and rough surfaces.

The method which is based on the characteristics of filament rise in square capillary tube has been used for contact angle measurements[20]. The tube is held rigidly inside one of the equilibrium cells (in the VLE facility). Contact angle data were measured for various binary and real reservoir fluids in the near critical region. The results showed that the contact angle remains relatively constant for a wide range of IFT values and then decreases as the fluid approaches its critical region (i.e., IFT approaches zero). This behaviour has not been reported before and could have significant implications in the management of hydrocarbon reservoirs when fluid composition is continuously changing. Based on the observed behaviour, a generalised correlation between contact angle and IFT was developed and evaluated against independent data of real reservoir fluids[21].

The objectives of work presented in this thesis were to understand the changes that viscosity, interfacial tension and contact angle undergo and to evaluate/improve industrial practice by generating reliable experimental data and improving predictive methods to be used for simulating flow of multi-phase processes. The thesis comprises of eight chapters. After the above brief review of the essence of work presented in this thesis, a description of the content of each subsequent chapters is presented as follow:

Chapter 2 gives a description of the experimental facilities used in generating the required contact angle, viscosity and IFT data. The procedures for carrying out a specific property measurement were also presented in this chapter.

In **Chapter 3**, the variation of interfacial tension (IFT) and contact angle were studied for four binary mixtures of C_1/n-$_{C4}$, C_1/n-$_{C8}$, C_1/n-$_{C10}$ and C_1/n-$_{C14}$ and two real reservoir fluids, namely; a near critical fluid referred to as NCF and a rich gas-condensate referred to as GCA. The IFT data were measured by both the pendant drop and meniscus height techniques, while the contact angle data were measured using a square capillary technique. Error analysis on the measured data was carried out and smoothed contact angle data for all tested fluids were derived and discussed. The measured contact angle data were, then, used to develop a generalised correlation between the contact angle and IFT. The developed correlation was then tested against contact angle data of two multi-component reservoir fluids.

Chapter 4 discusses the most commonly used methods for predicting the interfacial tension in the petroleum industry. The possibility of calculating the IFT of mixture of fluids using various averaging methods was investigated. The volumetric averaging method was found to be the best, with uncertainty comparable to that of experimental accuracy. Measured interfacial tension data of ternary mixtures of Methane/n-Octane/n-Decane and mixtures of real reservoir fluids were used to test this approach. A comparison between the calculated IFT by the volumetric average and the original Weinaug-Katz was made and discussed in this chapter.

In **Chapter 5**, an introduction on the mechanisms of fluid viscosity and the effect of composition, pressure and temperature on the behaviour of fluid viscosity for different fluid states is given. Various viscosity predictive models, used by the petroleum industry, were also discussed in this chapter. A systematic evaluation of density and viscosity of pure compounds at various pressures and temperatures indicated the need to include both structural and thermal effects, in additional to density, for improved viscosity predictions. Based on the above evaluation, the JST correlation was modified and discussed in this chapter. The modified correlation was extended for calculating the viscosity of real reservoir fluids, whereby a correlation for the critical volume of the plus-fraction was developed and discussed. A comprehensive evaluation of the modified correlation for

variety of binary and multi-component real reservoir fluids has been conducted and discussed in this chapter too.

Chapter 6 discusses the divergence of fluid viscosity in the vicinity of critical point. The two most commonly approaches for predicting viscosity enhancement were briefly discussed in this chapter. Viscosity data on near-critical binary and multi-component real reservoir fluids were measured inside and outside their critical regions. An evaluation of the residual viscosity models and those based on the principle of corresponding states to predict the observed viscosity enhancement of the above tested fluids was carried out. Discussion on the developed two-parameter corresponding state viscosity model, for viscosity enhancement, and the methodology employed for developing the model is discussed. Comparison between model predictions and the observed (measured) viscosity enhancement of the tested fluids has been made.

Chapter 7 presents experimental viscosity and interfacial tension data on a number of volatile oil and gas condensate samples in their original states and with various contamination levels. The aim of this chapter is to investigate whether the viscosity and IFT of the un-contaminated reservoir fluids can be retrieved from samples contaminated by drilling mud, especially those of oil-based which are completely miscible with reservoir fluid and effect its properties. The effect of mud filtrate contamination on the viscosity and interfacial tension of the original (un-contaminated) fluid and methodology employed in retrieving the properties of the un-contaminated fluids is also discussed.

Chapter 8 presents the conclusions drawn from the above studies along with recommendations for future work.

REFERENCES

[1] Bird, R. B., Stewart, W. E. and Lightfoot, E. N. : Transport Phenomena, Wiley & Sons Inc., New York (1960).

[2] Lohrenz, J., Bray, B. G. and Clark, C. R. : "Calculating Viscosities of Reservoir Fluids from Their Compositions", J. Pet. Tech. (JPT), 1171-1176, (Oct., 1964).

[3] Pedersen, K. S. and Fredenslund, Aa. : "An Improved Corresponding States Model for the Prediction of Oil and Gas Viscosities and Thermal Conductivities", Chem. Eng. Sci., **42**, 182-186, (1987).

[4] Petersen, Aa., K., Knudsen, K. and Fredenslund, Aa. : "Prediction of Viscosities of Hydrocarbon Mixtures", Fluid Phase Equilib., **70**, 293-308, (1991).

[5] Jossi, J. A., Stiel, L. I. and Thodos, G. : "The Viscosity of Pure Substances in the Dense Gaseous and Liquid Phases". AICHEJ, **8**(1), 59-63, (1962).

[6] Dandekar, A., Danesh, A., Tehrani, D. H. and Todd, A. C. : "A Modified Residual Viscosity Method for Improved Prediction of Dense Phase Viscosities", Paper presented at the 7th European Improved Oil Recovery (IOR) Symposium in Moscow, Russia, Oct. 27-29, (1992).

[7] Al-Siyabi, Z. K., Danesh, A., Tohidi, B. and Todd, A. C. : "Abnormal Viscosity Behaviour of Near Critical Fluids, Experimental Data and Modelling", paper No. 57 presented at the 10th Improved Oil Recovery Symposium held in Brighton, UK, Aug. 18-21, (1999).

[8] Bardon, C. and Longeron, D. G. : "Influence of Very Low Interfacial Tension on Relative Permeability", Soc. Pet. Eng. (SPEJ), 391-401 (Oct., 1980).

[9] Henderson, G. D., Danesh, A., Tehrani, D. H. and Peden, J. M. : "The Effect of Velocity and Interfacial Tension on the Relative Permeability of Gas Condensate Fluids in the Wellbore Region,", 8th IOR Symposium, Vienna, (May 1995).

[10] Al-Siyabi, Z. K. : Modelling The Effect of Interfacial Tension on Gas and Oil Relative Permeability, MEng Thesis, Heriot-Watt University, Edinburgh, UK (1996).

[11] Andreas, J. M., Hauser, E. A. and Tucker, W. B. : "Boundary Tension by Pendant Drops", Presented at the 50th Colloid Symposium, held at Cambridge, Massachusetts (1938).

[12] Danesh, A., Todd, A. C., Somerville, J. and Dandekar, A. : "Direct Measurement of Interfacial Tension, Density, Volume and Compositions of Gas Condensate Systems", Trans. I Chem. E, **68**A, 325-330, (1990).

[13] Weinaug, C. F. and Katz, D. L. : "Surface Tension of Methane-Propane Mixtures", Ind. Eng. Chem. (I & EC), **35**(2), 239-246, (1943).

[14] Lee, S. T. and Chien, M. C. H. : "A New Multicomponent Surface Tension Correlation Based on Scaling Theory", paper SPE 12643 presented at the SPE/DOE Enhanced Oil Recovery Symposium, Tulsa, Oklahoma, (1984).

[15] Danesh, A., Dandekar, A., Todd, A. C. and Sarkar, R. : "A Modified Scaling Law and Parachor Method for Improved Prediction of Interfacial Tension of Gas Condensate Systems", SPE 22710, Proceeding of the 66th Annual Conference, (Oct., 1991).

[16] Christoffersen, K. R., Whitson, C. H., de Silva, F. V. and Haldoupis, A. J. : "Measuring Capillary Pressure of Chalk Samples at Elevated Pressures and Varying Interfacial Tension", paper presented at the 4th North Sea Chalk Symposium, Deauville, France, Sep. 21-23. (1992).

[17] Longeron, D. G., Kalaydjian, F., Bardon, C. and Desremaux, L. M. : "Gas/Oil Capillary Pressure: Measurements at Reservoir Conditions and Effect on Gas-Gravity Drainage", paper SPE 28612 presented at the SPE 69th Annual Technical Conference and Exhibition held in New Orleans, LA, USA, Sep. 25-28 (1994).

[18] Neumann, A. W. and Good, R. J. : "Techniques of Measuring Contact Angles". Surf. & Colloid Sci., Vol. II, Experimental Methods, R. J. Good and R. R. Stromberg, Eds., Plenum Press, New York, (1979).

[19] De Ramos, A. L. and Cerro, R. L. : "Liquid Filament Rise in Corners of Square Capillaries: A Novel Method for the Measurement of Small Contact Angles". Chemical Engineering Science, **49**(14), 2395-2398, (1994).

[20] Al-Siyabi, Z., Danesh, A., Tohidi, B. and Todd, A. C. : "Measurement of Gas-Oil Contact Angle at Reservoir Conditions", Paper No. 57 presented at 9th Symposium on Improved Oil Recovery, 20-22 October, The Hague, The Netherlands, (1997).

[21] Al-Siyabi, Z. K, Danesh, A., Tohidi, B. and Todd, A. C. : "Variation of Gas-Oil Contact Angle with Interfacial Tension", Petroleum Geoscience, **5**, 37-40, (1999).

CHAPTER 2

EXPERIMENTAL EQUIPMENTS AND PROCEDURES

2.1 OBJECTIVE

The objective of this chapter is to give a description of the experimental facilities and procedures employed for measuring the required contact angle, viscosity and interfacial tension data that were used in the subsequent chapters of this thesis.

2.2 INTRODUCTION

The PVT and Phase Behaviour Laboratory in the Department of Petroleum Engineering at Heriot-Watt University has targeted its effort over two decades towards the measurement and modelling of properties and behaviour of reservoir fluids. Novel experimental techniques have been developed to generate reliable compositional[1], volumetric and density data on all fluid phases at reservoir and surface conditions for improving phase behaviour modelling. The measurement of interfacial tension (IFT) has been pursued by developing a novel method of using the gas-liquid meniscus curvature[2] to accurately determine low to relatively high IFT. This technique along with the conventional pendant drop method[3] are routinely employed on all test fluids. Capillary tube viscometers are used to provide reliable viscosity data on gas and liquid phases formed by different reservoir processes, hence allowing investigation of viscosity variations due to compositional, temperature and pressure changes. A novel technique

based on the characteristics of gas-liquid interface has been developed and employed for measuring the gas-liquid-solid contact angle[4].

The above capabilities have been employed in generating the experimental data that are presented in the subsequent chapters. The experimental facilities and procedures employed in carrying out a specific property measurement are described throughout the subsequent sections of this chapter.

2.3 EXPERIMENTAL FACILITIES

2.3.1 Vapour-Liquid-Equilibrium Facility

The schematic representation of Figure 2.1 gives the general layout of the main compartments constituting the Vapour-Liquid-Equilibrium (VLE) facility. The VLE facility consists of two 200 cm^3 high pressure (5,700 psia) equilibrium windowed cells, mounted side by side inside a constant temperature air bath controlled to within $\pm$ 0.1 °C. The pressure inside the system is maintained with two 250 cm^3 proportional mercury pumps. The equilibrium pressure is monitored in the cells by two Quartzdyne pressure transducers to within 0.001 psi. The equilibrium cells are connected with pipework incorporating a direct sampling system (DSS) and a high pressure (10,000 psia) Anton Paar densitometer, allowing in-situ density measurement with an accuracy of better than $\pm$ 0.0003 $gr.cm^{-3}$. A side tapping on each of the cells is also utilised to mount a stainless steel tube, which is used for measuring interfacial tension (IFT) by the conventional pendant drop technique. A square capillary glass tube is held rigidly inside one of the equilibrium cells and is used for contact angle measurements. A stainless steel capillary tube viscometer has been coiled and mounted above the PVT cells, within the temperature controlled bath, and connected to each of the Rheodyne valves with high pressure fittings.

Furthermore, the VLE facility is equipped with a video camera mounted on a microscope enabling image magnifications to 50 and 125 times. The resulting images in each test could be viewed on the monitor and stored on the video recorder. An image quantifier is

used to dimension live images from the camera and/or those stored on the video recorder, for interfacial tension calculation.

2.3.2 Gas Condensate Facility

The gas condensate (GC) experimental facility, schematically shown in Figure 2.2, consists of an equilibrium cell divided into two chambers connected by a narrow neck. The larger, upper chamber has a volume of 4000 cm^3 and contains a floating piston with the smaller, lower chamber having a volume of 500 cm^3. The connecting neck, has a diameter of one centimetre, is used to allow visual inspection of the fluid being studied, by means of two opposing sapphire windows. The cell, which has a test pressure of 26,000 psia and a maximum working pressure of 17,600 psia, has been modified by the Department to facilitate the development of a Direct Sampling System (DSS)[1] and a high pressure densitometer, similar to that in the VLE facility· The entire cell is enclosed in a thermostatically controlled enclosure which has an operating limit of -20 °C to +200 °C. The temperature is controlled by a Eurotherm 905S high precision temperature controller which can maintain the cell temperature to ±0.05 °C. Pressure is measured by a Quartztronics C20K high pressure (20,000 psia) resonating quartz crystal transducer with a resolution equal to those for the VLE facility. The position of the piston and the pressure within the cell are controlled by pumping mercury into or out of the top of the cell while at the same time pumping mercury in the opposite direction out of or into the lower chamber.

The viewing system incorporated for the GC facility is very much similar to that used for the VLE facility.

2.3.3 High Pressure-High Temperature Facility

The existing High Pressure-High Temperature (HPHT) facility, schematically shown in Figure 2.3, is capable of making highly accurate saturation pressure, volumetric and viscosity measurements on multi-component hydrocarbon fluids, with or without the presence of water, to pressures up to 20,000 psia and temperature up to 200 °C. The

facility consists of two small volume (15 cm^3) high pressure cells linked at the top. Located at the top of one of the cells is a sight cell which can be viewed via a camera and monitored from outside the oven. Pipework from the base of each cell is connected to opposite ends of a push-pull pump. Mercury is used to confine the sample within the high pressure cells, to adjust the sample volume and to manoeuvre the sample from one cell to the other. The push-pull pump is comprised of a solid rod each end of which protrudes into a cylinder filled with mercury. The movement of the push-pull pump is measured using a linear transducer and the movement in terms of volume can be read to within 0.000755 cm^3. The push-pull pump is motorised and has an accurate variable speed controller (maximum flow rate 180 $cm^3.hr^{-1}$). There are two platinum resistance thermometers (PRT) mounted on the pipework in the oven in order to monitor the temperature. The pressure is monitored using two high pressure (30000 psia) Quartzdyne pressure transducers with a quoted accuracy of better than 3 psi. The pressure transducers are arranged so that they are connected to opposite sides of the push-pull pump. The sight cell, pumps and pipework are all rated to at least 29,000 psia and can withstand temperatures to at least 200 °C.

A capillary tube viscometer, similar to that in the VLE facility, has been installed to enhance the rig capabilities to viscosity measurements at high pressure and high temperature conditions.

2.4 EXPERIMENTAL PROCEDURES

The following section provides detailed description of the procedures and methods employed in generating the experimental contact angle, IFT and viscosity data.

2.4.1 Viscosity Measurement Procedure

The VLE and HPHT facilities were equipped with stainless steel capillary tube viscometers. Viscometer arrangement and procedures for measuring fluid viscosity are very much the same, which is outlined below.

Figure 2.4 gives a more detailed picture of the individual component parts connected with the capillary tube viscometer housed in the VLE facility. The direction of flow is always from the delivery cell (1) as the fluid for test must then flow through the filter (3), which has been specially modified to remove as much dead volume as possible. So all particulate matter and any mercury droplets are removed before the fluid can reach the Rheodyne stream selection valves (4). Here, the flow can be directed either through the capillary tube viscometer (5) or through a short length of by-pass tube (6) which helps to measure the entire system resistance to flow. The emergent stream of fluid then appears in the receiving cell (7).

The physical measurement of viscosity is made by first closing the top valves of each of the PVT cells, recording the resting pressures, then simultaneously starting data collection from each of the two Quartzdyne transducers, which are coupled to the mercury pumps and starting to pump the fluid from the delivery cell to the receiving cell, through the capillary tube. The pumps are then stopped and the top valves are opened again-allowing the pressure to stabilised and a resting pressure is recorded. This then results in two readings for each side of the capillary (i.e., dynamic and static). The differential pressure for that run can then be calculated by summing the results obtained from subtracting the resting from dynamic values. This process is repeated through the short tube-bypassing the viscometer- and the differential pressure again is calculated as above. This value is then subtracted from the capillary differential to give the pressure drop across the capillary tube due to flow of fluid.

For the HP-HT facility, the procedure above for measuring fluid viscosity is very much the same, but without a blank tube. The pressure drop due to system resistance was evaluated which turned out to be very small compared to that due to fluids at higher pressure conditions.

The pressure drop across the capillary tube for laminar flow is related to viscosity, tube characteristics and flow rate according to the theoretically-based formulation of Hagen-Poiseuille[5];

$$\frac{\Delta P}{Q} = C\left(\frac{L}{\pi D^4}\right)\eta \qquad (2.1)$$

where;

ΔP: differential pressure across the capillary tube viscometer, psi.

Q: flow rate, $cm^3.sec^{-1}$.

L: Length of the capillary tube, cm.

D: internal diameter of the capillary tube, cm.

η: viscosity of the flown fluid, cP.

C: unit conversion factor, equal to $1.450377439x10^{-7}$ if the above units are used.

For the VLE viscometer tube, the calculated diameter of the tube, which has a nominal value of 0.254 mm was calculated by matching the measured and literature viscosities for pure components[6]. Whereas, the average diameter of the HP-HT viscometer tube was established by measuring the volume of the tube and its length. The effect of pressure and temperature on the length and diameter of the tube were calculated and found to have no significant effects on the calculated viscosity. Thereafter, tube internal diameters established above were used for viscosity measurements of all other fluids. Table 2.1 lists the characteristics of both viscometers, hosted within the VLE and HP-HT facilities. Figures 2.5 through 2.7 show comparisons between the calculated and literature viscosities for both tubes. Very good agreements between the calculated and literature viscosities can be seen, demonstrating the reliability of both viscometers which then can be used with confidence for measuring the viscosity of mixtures.

2.4.2 Interfacial Tension Measurement Procedure

As mentioned above, two techniques have been routinely used, by the Department, for the measurement of interfacial tension. The pendant drop technique[3] involves suspending a droplet of liquid in its equilibrium vapour, as schematically shown in Figure 2.8, and measuring the droplet dimensions (d_e and d_s). The dimensions of the droplet

together with the vapour-liquid density difference is used for IFT measurement using the formulation below[7]:

$$\sigma = \frac{\Delta\rho g d_e^2}{H} \qquad (2.2)$$

where;

σ: interfacial tension, $mN.m^{-1}$.

$\Delta\rho$: density difference between vapour and liquid phases, $gr.cm^{-3}$.

g: acceleration due to gravity, 9.81 $m.sec^{-2}$.

d_e: equatorial diameter of liquid droplet, cm.

H: liquid droplet shape factor, tabulated as a function of the ratio d_e/d_s, and

d_s: diameter of the liquid droplet measured at a distance d_e from the bottom of the droplet.

The pendant drop technique is utilised principally for black and volatile oils which have a relatively high interfacial tension. For low tension fluids (e.g., gas-condensates, near-critical fluids), their interfacial tensions cannot be measured unless the tube is replaced by one with a smaller diameter or a wire. This would involve a great deal of effort to change the pendant dropper for fluids with differing interfacial tensions.

Therefore, low interfacial tensions are now measured during laboratory testing of a fluid by the meniscus height technique[2]. The technique utilises the meniscus height that forms between any equilibrated hydrocarbon liquid and vapour phases, as shown in Figure 2.9. A rigorous relationship between the height of liquid-vapour interface and the IFT was derived which has the following form[2]:

$$\sigma = \frac{\Delta\rho\, g\, h^2}{2(1 - \sin\theta)} \qquad (2.3)$$

where; σ, $\Delta\rho$ and g as defined for Equation (2.2).

d_e: equatorial diameter of liquid droplet, cm.

h: height of the vapour-liquid interface, cm.

θ: three-phase (vapour-liquid-solid) contact angle, deg.

Previously, the technique was limited to measure the IFT between low tension fluids. However, a systematic comparison of the measured data by this technique and the pendant drop method demonstrated its reliability for high IFT measurements. Since then, this technique along with the conventional pendant drop method are routinely employed on all test fluids.

Furthermore, it has been found that the meniscus height technique could also be used for acquiring highly accurate volumetric data for low shrinkage oils, where the liquid phase is generally dark. This in turn result in the liquid phase volume being over-estimated. Therefore, volumetric data for such fluids are subject to some errors. In these cases, if the IFT is known, it is then possible to back calculate the meniscus height using Equation (2.3), thereby enabling more accurate liquid and vapour volumes to be derived.

2.4.3 Contact Angle Measurement Procedure

There exist various methods for measuring the liquid-solid contact angle in the literature[8]. However; the most widely used techniques are the sessile drop and the Wilhelmy plate methods. A method based on filament rise in square capillary tubes has recently been shown to provide accurate contact angle data[9].

In the sessile drop method, the contact angle between liquid droplet and a solid surface is measured visually through a comparator microscope fitted with goniometric scale, thereby measuring the contact angle directly. The Wilhelmy plate method relies on the liquid rise on a vertical flat plate partially immersed in a pool of liquid for which the contact angle is to be determined. The contact angle can then be measured directly using

similar viewing devices or indirectly using an equation similar to Equation (2.3). provided the IFT and meniscus height are known.

The method which is based on the characteristics of filament rise in a square capillary tube, schematically shown in Figure 2.10, has been used for contact angle measurements. The tube is held rigidly inside one of the equilibrium cells (in the VLE facility). The characteristics of the glass tube are listed in Table 2.2. It has been established[10,11] that if the sum of the contact angle of the fluid and the half angle of a wedge is smaller than 90°, the liquid filament should rise unbounded (i.e., there is no equilibrium position for the surface). However there exist no perfect corners in nature, and that square capillaries have corners with very small non-zero radius of curvature. For this imperfection, De Ramos and Cerro[9] concluded that the liquid filament rises to a level where the radius of curvature of the filament (R_t) intersects with the radius of corner (R_c) at an angle so-called equilibrium contact angle (θ). At this point, system equilibrium is established with the boundary conditions being the contact angle and surface and gravity force balance.

The physical measurement of the three-phase contact angle begins by making a stable image of the square capillary glass tube with the test fluids inside, both on the monitor and for video recording, utilising the highly complex array of video and electronic equipment so that the height of the filament rise (ΔZ), the radius of curvature of the liquid meniscus in the capillary tube (R_b) are dimensioned, Figure 2.10. Those measured quantities together with the radius of curvature of the corner of the capillary tube (R_c), the vapour-liquid density difference and the measured IFT are used to calculate the vapour-liquid-solid contact angle (θ), from the following formulations[9]:

$$\tan\theta = -\frac{R_c - \sqrt{2R_t^2 - R_c^2}}{\sqrt{2\sqrt{R_t^2 + R_c\sqrt{2R_t^2 - R_c^2}}}} \tag{2.4}$$

and

$$\Delta Z = \frac{\sigma}{\Delta\rho g}\left(\frac{1}{R_t} - \frac{2}{R_b}\right) \tag{2.5}$$

where; σ, $\Delta\rho$, g and θ are as defined previously.

ΔZ: height of the filament rise, cm.

R_c: radius of curvature of the corner of the capillary tube, cm.

R_b: radius of curvature of the liquid meniscus in the capillary tube, cm.

R_t: radius of curvature of the liquid filament, cm.

The above set-up provided novel ability of measuring vapour-liquid-solid contact angle at reservoir conditions with real reservoir fluids.

2.5 DESIGN AND PREPARATION OF FLUID SYSTEMS

The fluid systems investigated for the viscosity, IFT and contact angle studies were those with phase behaviour similar to naturally occurring hydrocarbons. The investigated fluid systems ranges from single component to multi-component fluids and their mixtures. The preparation and transfer of these mixtures together with the time taken to reach equilibrium plus the various viscosity, IFT and contact angle measurements represent a considerable effort in time.

2.5.1 Binary Fluids

Binary mixtures of both gas condensates and oil systems can be prepared by the simple addition of one component into the other, at the temperature of interest. In this way the dew point or bubble point of the binary mixture can be accurately controlled.

If for example an oil system was required, a PVT cell would be loaded with a quantity of the heavier component to which the lighter component would be added. The addition of the lighter component would be carried out at, or slightly above, the bubble point pressure. After the addition of some of the lighter component, the PVT cell would be shaken and the system pressure is measured. More additive steps would then be made, if required, until the required saturation pressure was reached. Likewise, a gas condensate

system can be generated in a similar manner so the generated binary mixture will have a dew point pressure.

Although, in practice, most fluids could be prepared in a manner described above, near-critical fluids posed their own problems. The addition of the pure light component on its own was found to lead to prolonged process. It was found that a much simpler and relatively quicker process is to inject the light component once it had been saturated with the heavier component. The ever-present danger when preparing a near critical fluid is the likelihood of driving the system past the critical point (i.e., from liquid to gas condensate system or vice versa). To minimise the chance of this happening, as the saturation pressure approaches the target pressure the volume of addition is reduced to give better control until the required saturation pressure is attained.

2.5.2 Reservoir Fluids

In this laboratory fluids are prepared to meet the requirements of computer modelling. Fluids would therefore be designed by computer models to produce the required phase behaviour (i.e., saturation pressure, maximum liquid fraction...etc.) The prepared reservoir fluid would be based around a dead hydrocarbon fluid of known density and composition to which light components (C_1 to C_5) would be added to produce the active reservoir fluid. Intermediate components (C_5 to C_8) are then added (possibly with additional C_1, if needed) until the fluid exhibits the required phase behaviour. The order in which intermediate and light components are added to the dead hydrocarbon fluid is not important.

Once the fluid has been modelled, the mass of each component required to produce, say 100 cm^3, is calculated. This *recipe* is then used in the laboratory to make the actual reservoir fluid. This will be performed firstly by combining the required mass of the light components, one at a time, in an appropriate high pressure vessel. Next, the intermediate components are gravimetrically added to the vessel, finally, the dead hydrocarbon fluid is added to complete the fluid. The prepared fluid is then compressed to a pressure well in

excess of the predicted saturation pressure and thoroughly mixed to ensure homogeneity amongst the components-the fluid would then be ready for use.

A common method for preparing reservoir fluids would be the simple recombination of separator gas and liquid samples, provided the samples are representative. This basically involves adding the required volume of separator liquid into a known volume of separator gas to reproduce the field Gas Oil Ratio (GOR).

2.6 CONCLUSIONS

The existing experimental facilities within the PVT and Phase Behaviour Laboratory in the Department of Petroleum Engineering at Heriot-Watt University provide novel capabilities to generate reliable compositional, volumetric, density, viscosity, interfacial tension and contact angle data while conducting routine PVT testing, required by different reservoir processes. Hence allowing investigating the variation of the above properties with temperature, pressure and compositional changes.

REFERENCES

[1] Danesh, A. and Todd, A. C. : "A Novel Sampling Method for Compositional Analysis of High Pressure Fluids", Fluid Phase Equilib., **57**, 161-171, (1990).

[2] Danesh, A., Todd, A. C., Somerville, J. and Dandekar, A. : "Direct Measurement of Interfacial Tension, Density, Volume and Compositions of Gas Condensate Systems", Trans I Chem E, **68**A, 325-330, (1990).

[3] Andreas, J. M., Hauser, E. A. and Tucker, W. B. : "Boundary Tension by Pendant Drops", presented at the 50th Colloid Symposium, held at Cambridge. Massachusetts (1938).

[4] Al-Siyabi, Z., Danesh, A., Tohidi, B. and Todd, A. C. : "Measurement of Gas-Oil Contact Angle at Reservoir Conditions", Paper No. 57 presented at 9th Symposium on Improved Oil Recovery, 20-22 October, The Hague, The Netherlands, (1997).

[5] Bird, R. B., Stewart, W. E. and Lightfoot, E. N. : Transport Phenomena, Wiley & Sons Inc., New York (1960).

[6] Lee, A. L. : "Viscosity of Light Hydrocarbons", Monograph on API Research Project 65, American Petroleum Institute, New York, (1965).

[7] Niedrehauser, D. O. and Bartell, F. E.: "A Corrected Table for Calculation of Boundary Tensions by Pendant Drop Method", Research on Occurrence and Recovery of Petroleum, A Contribution from API Research Project 27, 114-146, (1947).

[8] Neumann, A. W. and Good, R. J. : "Techniques of Measuring Contact Angles", Surf. & Colloid Sci., Vol. II, Experimental Methods, R. J. Good and R. R. Stromberg, Eds., Plenum Press, New York, (1979).

[9] De Ramos, A. L. and Cerro, R. L. : "Liquid Filament Rise in Corners of Square Capillaries: A Novel Method for the Measurement of Small Contact Angles", Chemical Engineering Science, **49**(14), 2395-2398, (1994).

[10] Concus, P. and Finn, R. : "On the Behaviour of Capillary Surface in Wedge", Proc. Nat. Acad. Sci. USA, **63**, 292-299, (1969).

[11] Pomeau, Y. : "Wetting in a Corner and Related Questions", J. of Colloid Interf. Sci., **113**, 5-11, (1986).

Table 2.1 - The Characteristics of the Capillary Tube Viscometers.

	VLE Facility	HP-HT Facility
Material	Stainless Steel	Stainless Steel
Length, cm	1543	1484.5
Calculated ID, cm	0.027778	0.029935

Table 2.2 - The Characteristics of the Square Capillary Tube Inside The VLE Facility.

	Characteristics
Material	Borosilicate Glass
Length, cm	12
Dimension, mm	2 x 2
Corner Diameter, mm	0.103

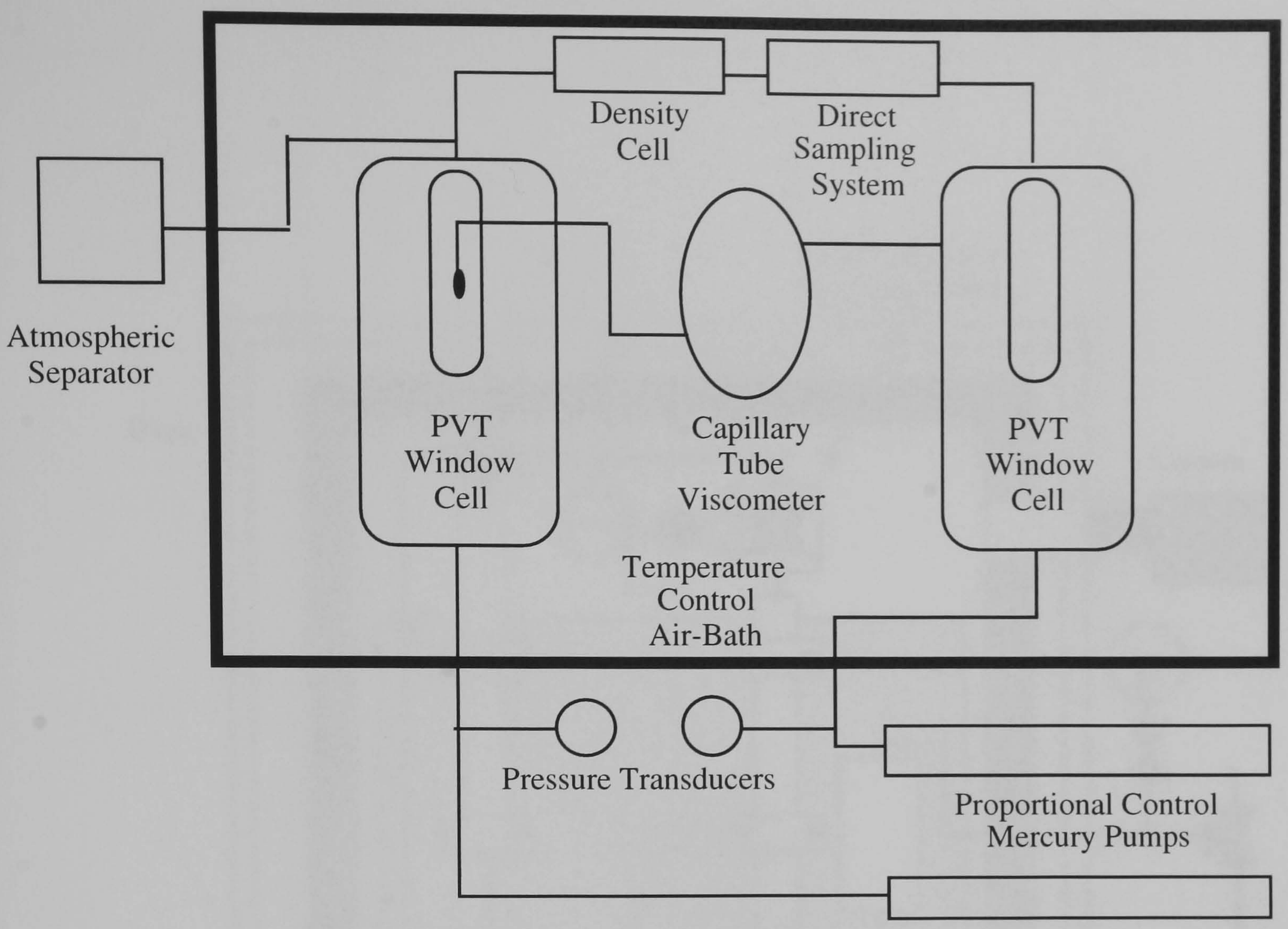

Figure 2.1 - Schematic Representation of the Vapour-Liquid Equilibrium (VLE) Experimental Facility.

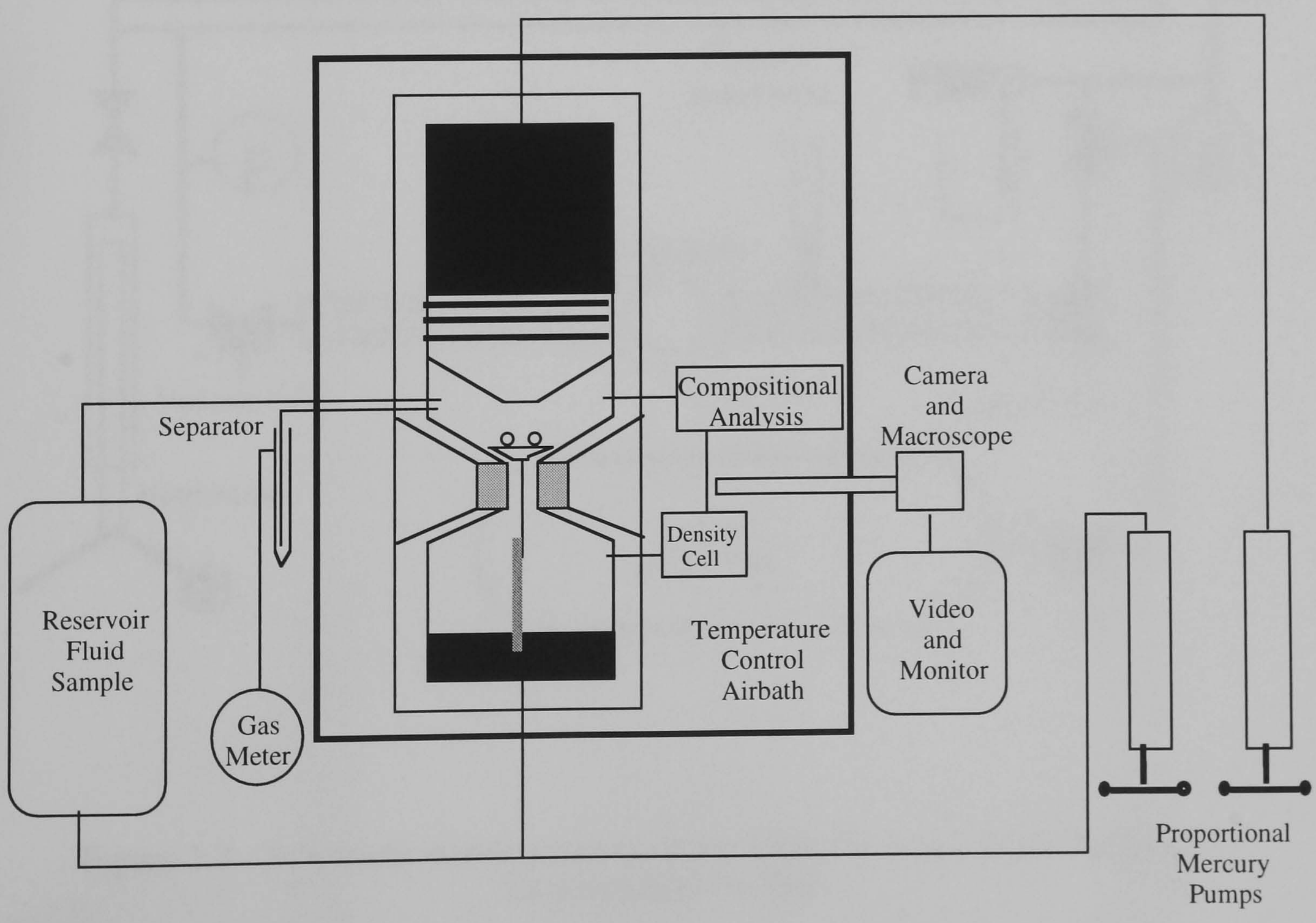

Figure 2.2 - Schematic Representation of the Gas Condensate Experimental Facility.

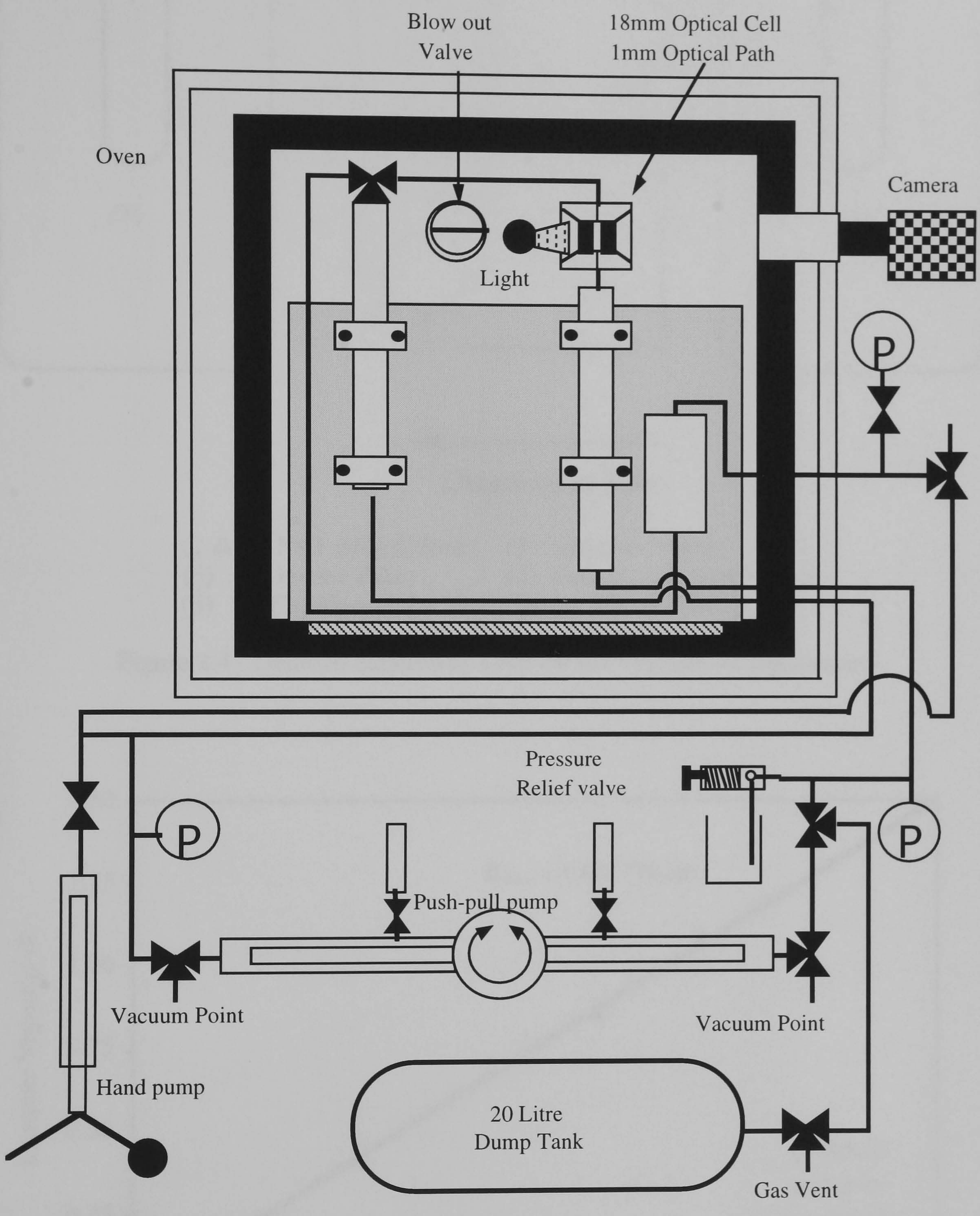

Figure 2.3 - Schematic Representation of the High Pressure - High Temperature Experimental Facility.

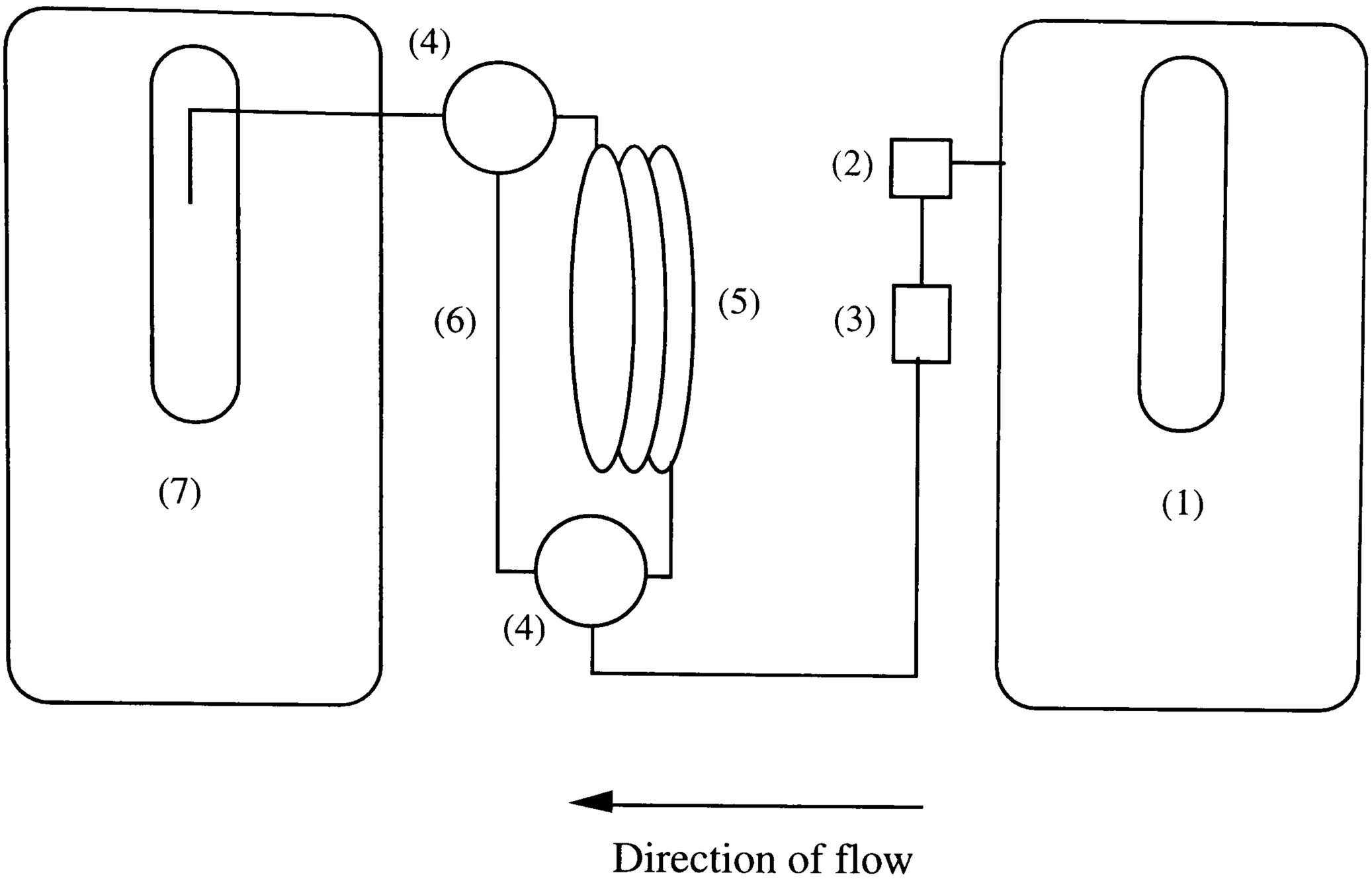

(1 & 7) PVT cells (200cc) (2) Isolation Valve
(3) In-line Filter (4) Stream Selection Valves
(5) Capillary Tube Viscometer (6) By-pass Line

Figure 2.4 - Detailed Schematic View Of the Viscometer Equipment.

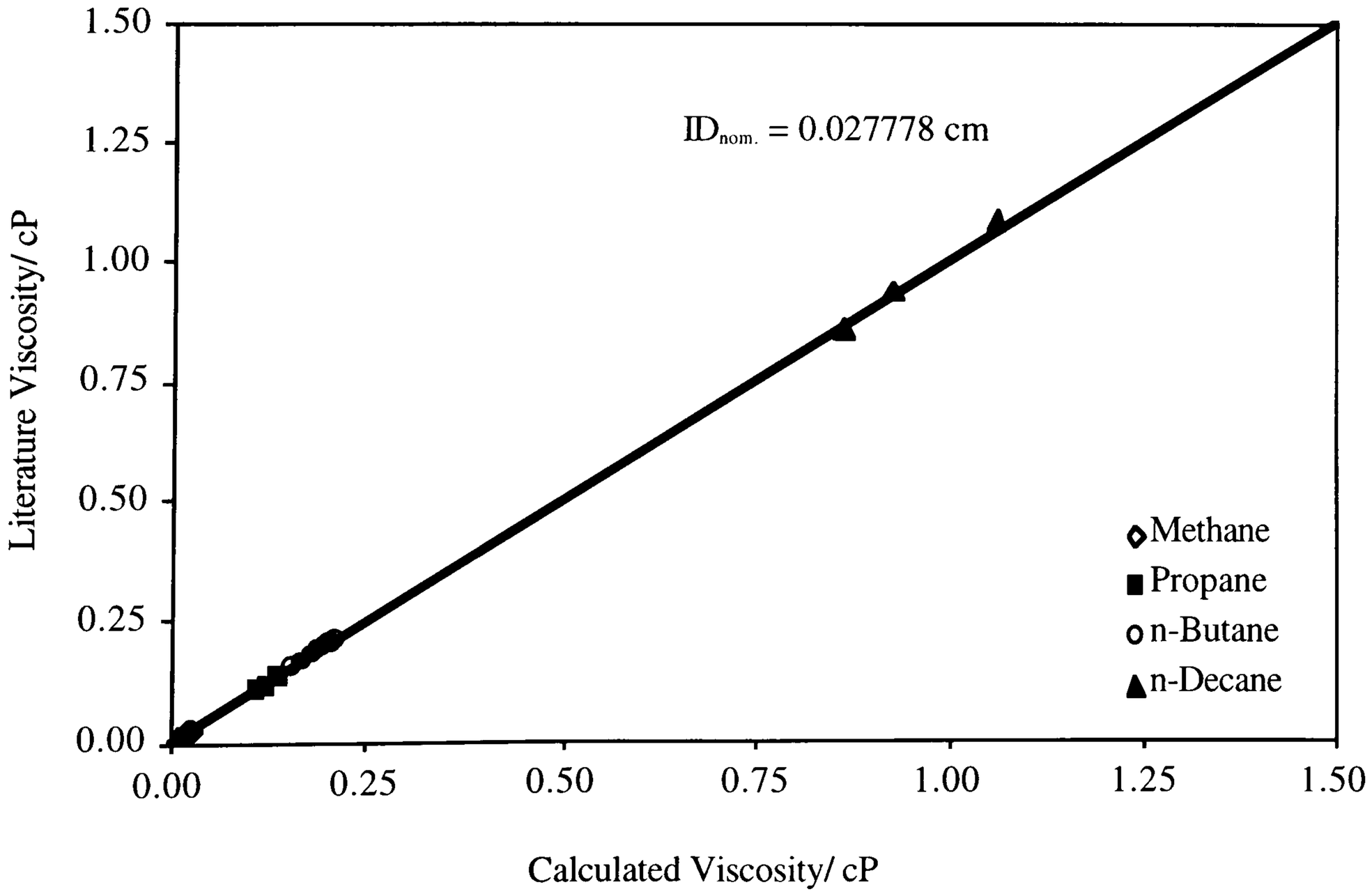

Figure 2.5 - The VLE Capillary Tube Viscometer Calibration at 37.8 °C.

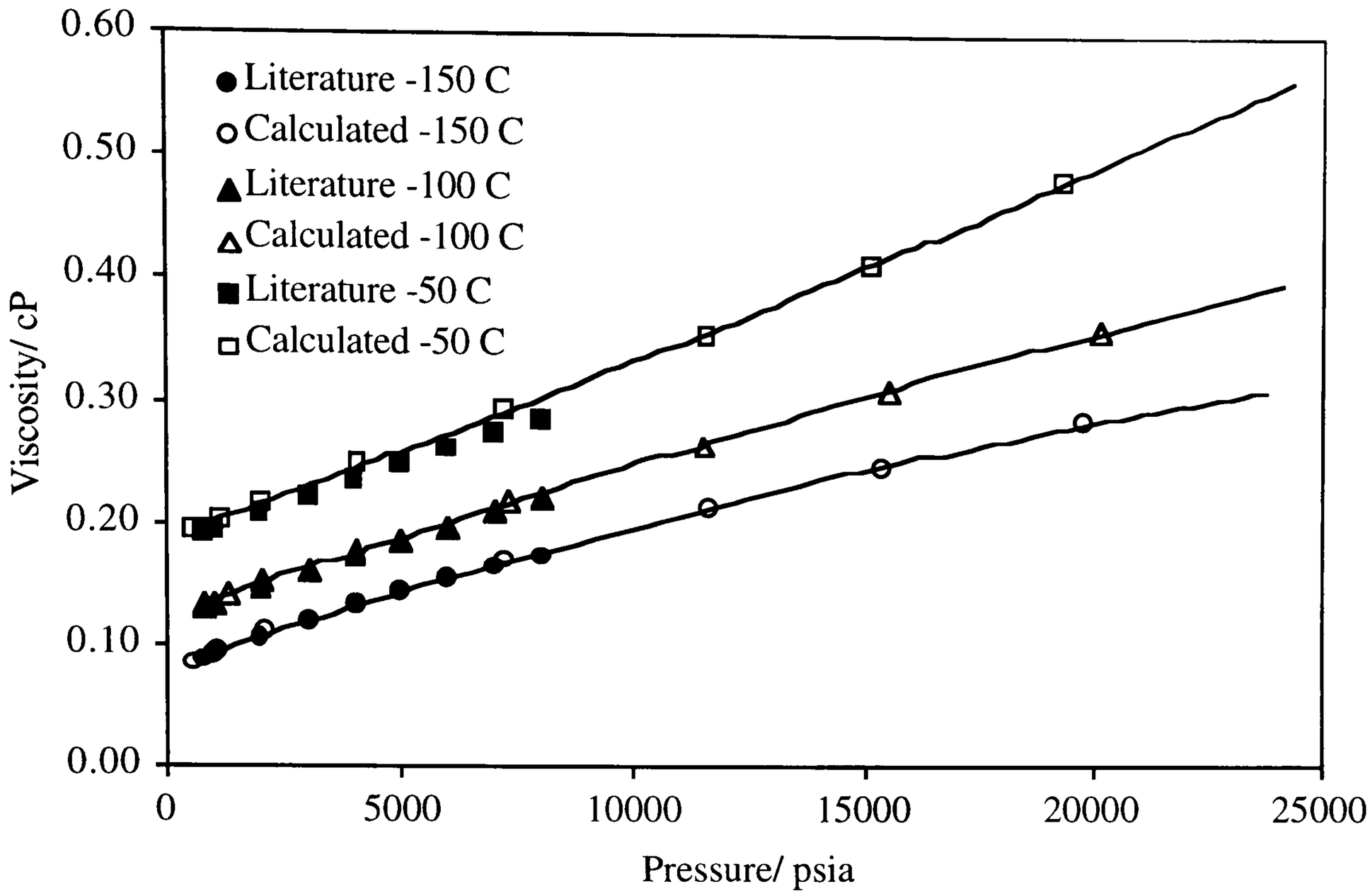

Figure 2.6 - Comparison Between the n-Pentane Literature and Calculated Viscosity from the HP-HT Capillary Tube Viscometer at Various Temperatures.

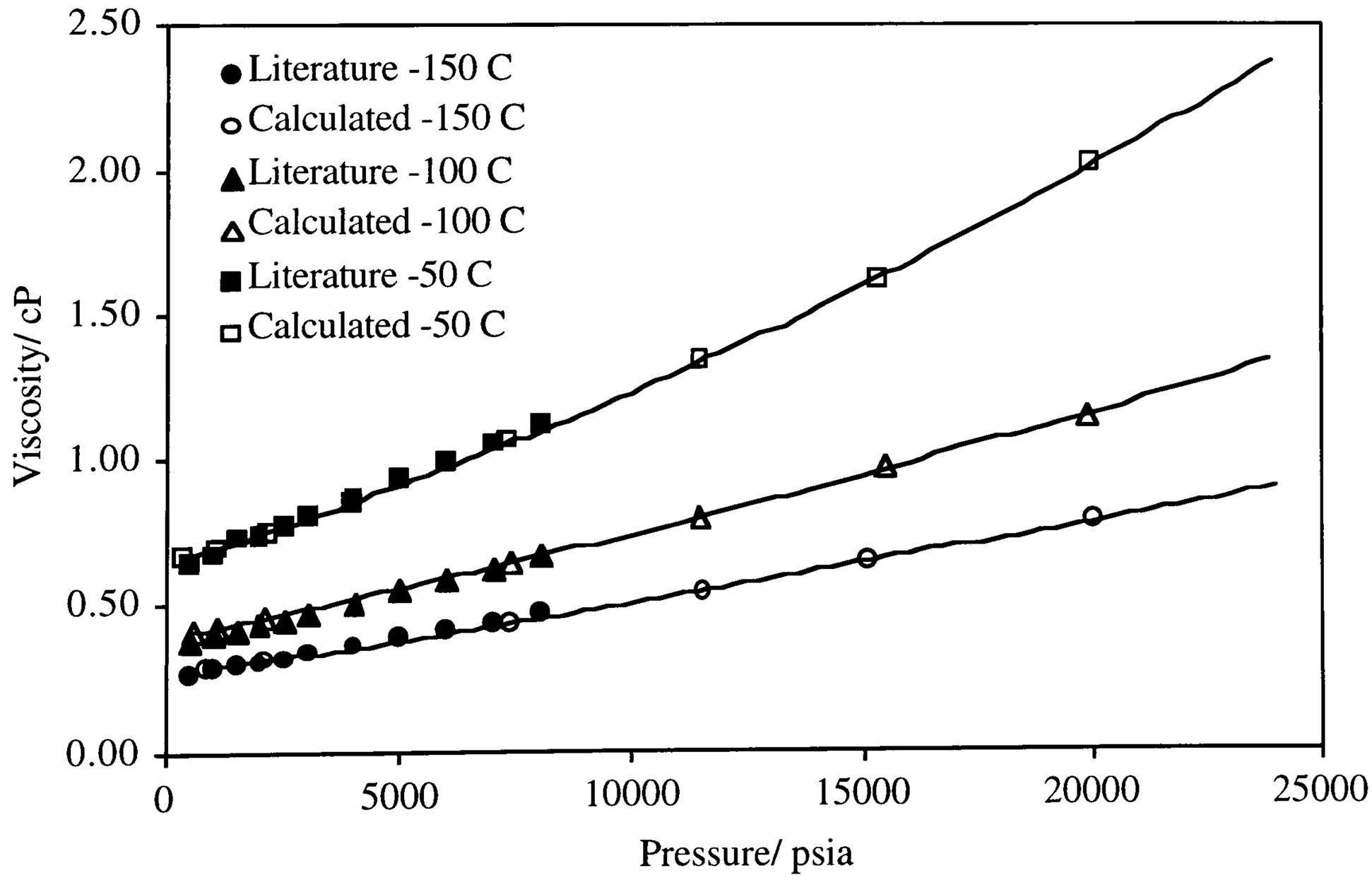

Figure 2.7 - Comparison Between the n-Decane Literature and Calculated Viscosity from the HP-HT Capillary Tube Viscometer at Various Temperatures.

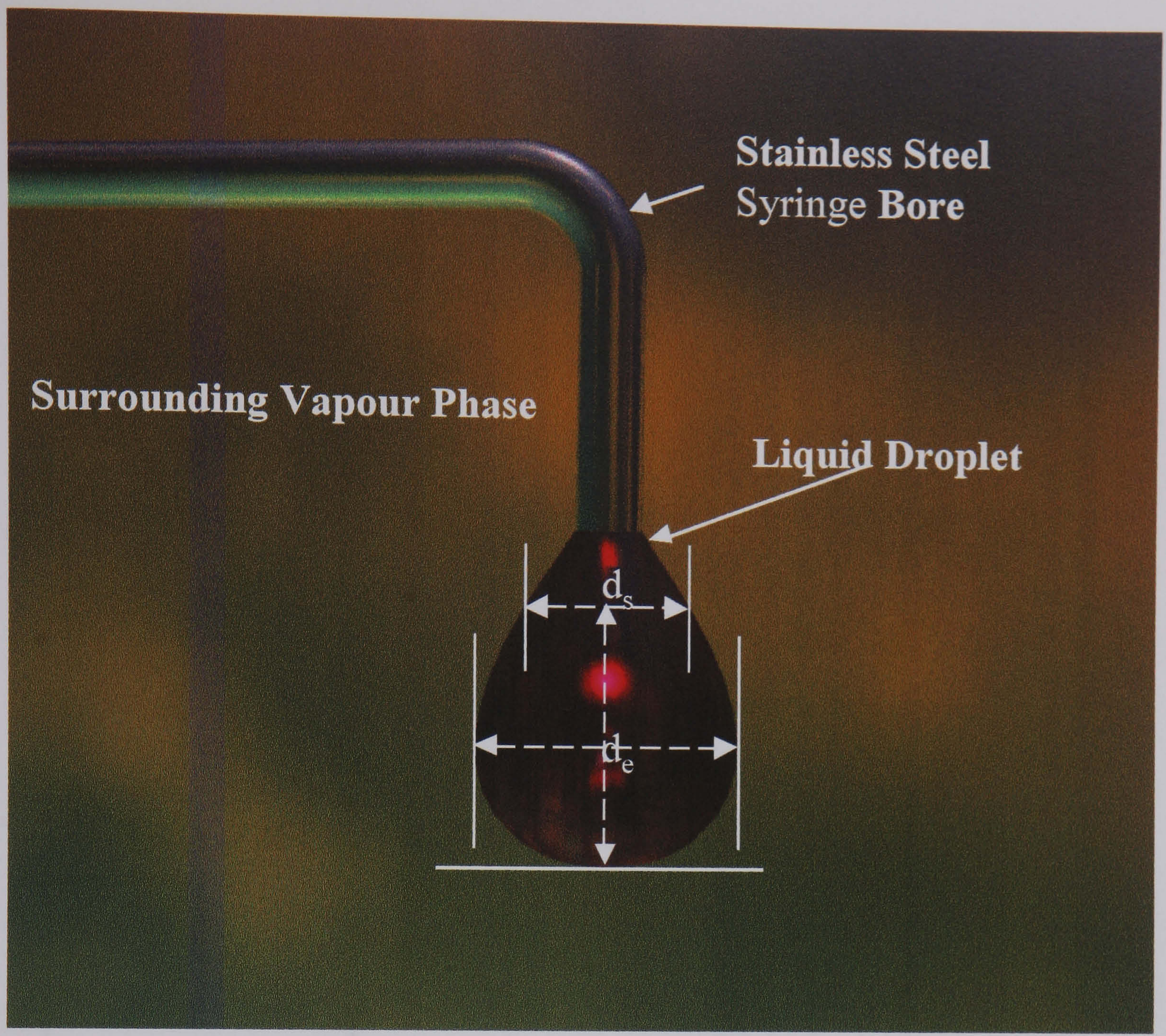

Figure 2.8 - Pendant Dropper (Hosted inside the VLE Facility) for Interfacial Tension Measurements.

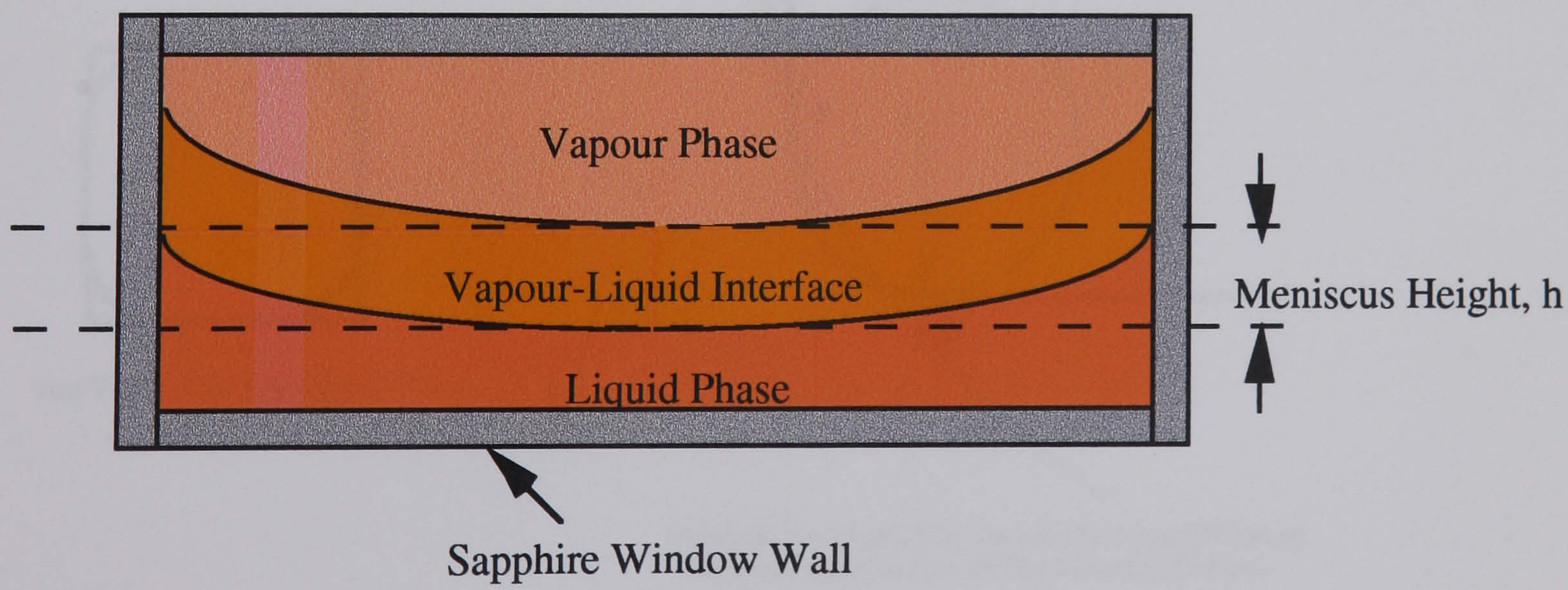

Figure 2.9 - Front View of the Vapour-Liquid Interface as seen on the TV Monitor.

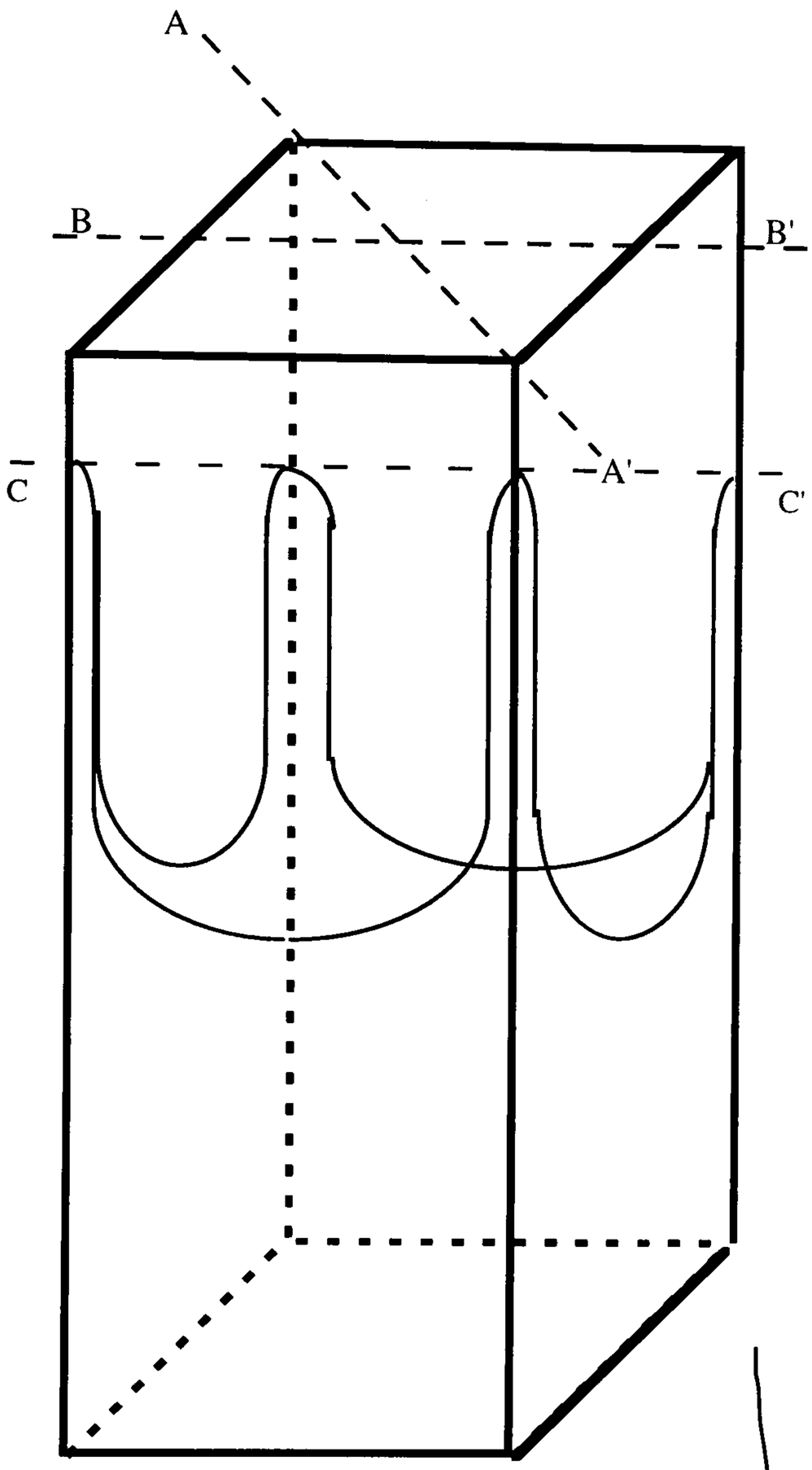

Square Capillary Tube

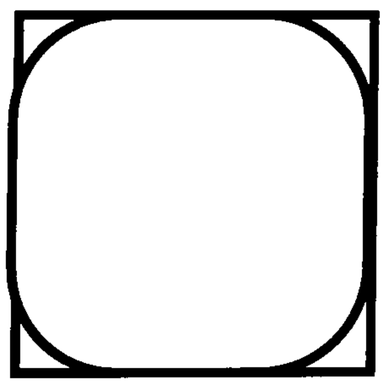

Top View , Cut T hrough C - C'

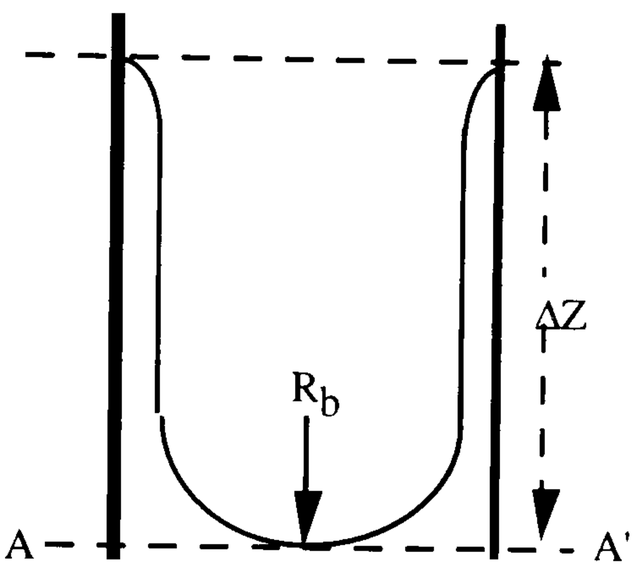

Diagonal View, Cut Through A - A'

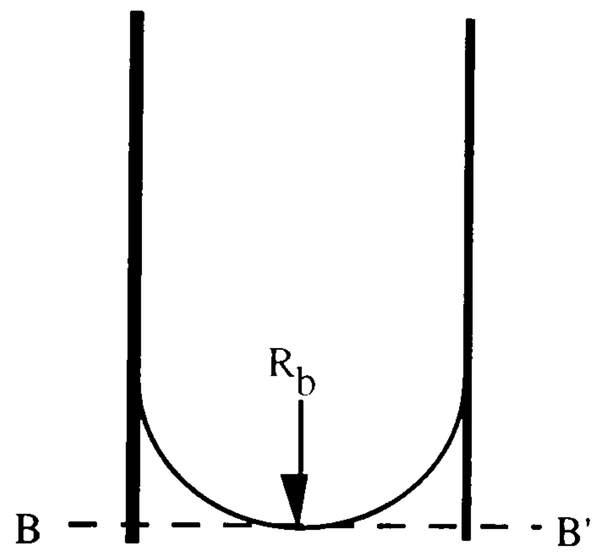

Side View, Cut Through B - B'

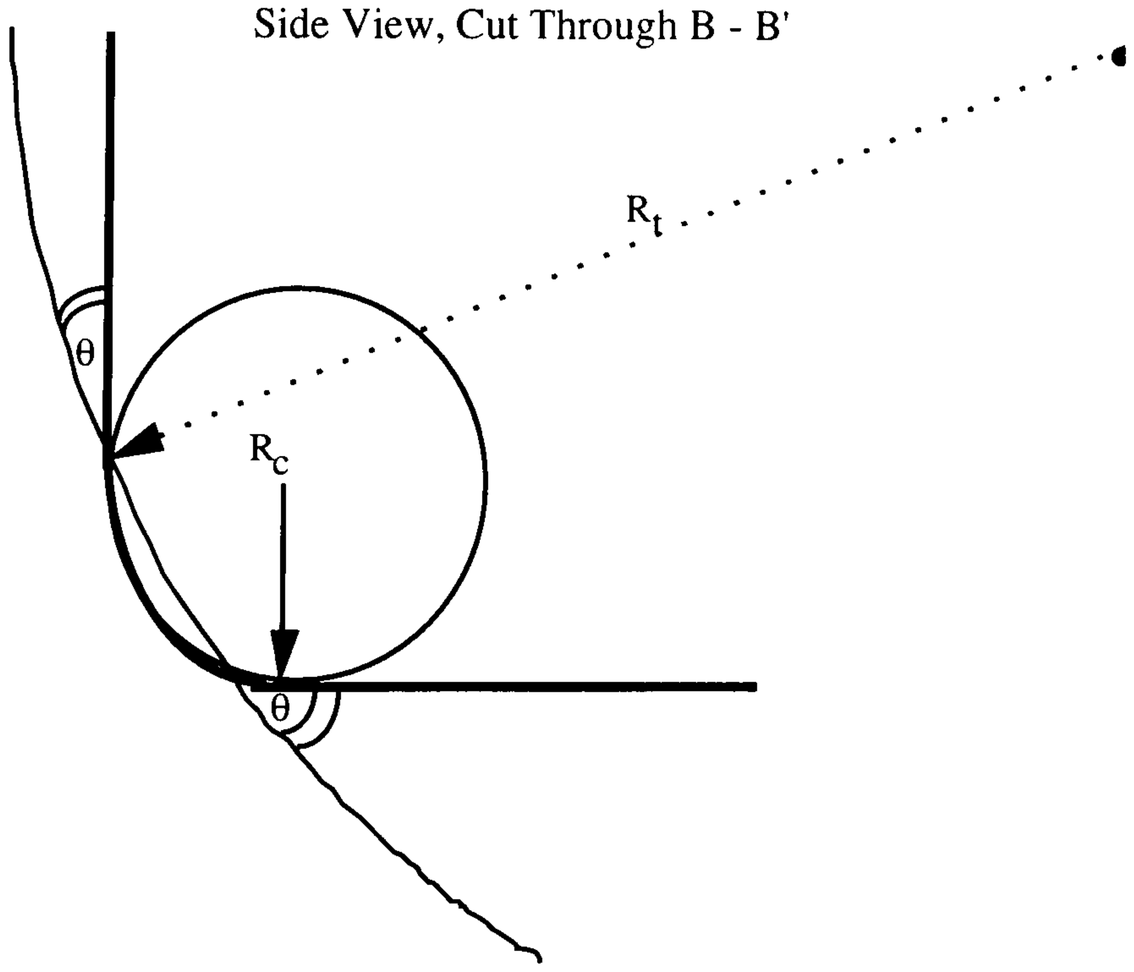

Detailed View into The Top of The Liquid Filamant
Intersecting With One of The Rounded Corners.

Figure 2.10 - Schematic Representation of the Square Capillary and Liquid Filament Diagonal, Side and Top Views.

CHAPTER 3

GAS-OIL-SOLID CONTACT ANGLE AT RESERVOIR CONDITIONS AND ITS VARIATION WITH INTERFACIAL TENSION

3.1 OBJECTIVES

The contact angle is a measure of the relative strength of adhesion of the fluid to the solid surface and to itself. It has a major influence on the distribution of hydrocarbons as well as any water present within reservoir rocks. The main interest in the contact angle in petroleum engineering is its contribution to the capillary pressure as expressed by the Laplace-Young equation. The objectives of this preliminary research has been twofold:

- To find a practical method that could be easily incorporated into the existing vapour-liquid equilibrium (VLE) experimental facility for measuring gas-oil-solid contact angle at conditions similar to those found for oil and gas condensate reservoirs.
- To investigate the variations of contact angle at reservoir conditions with measured fluid properties, towards the development of a generalised correlation to predict the pattern of contact angle variation for use in reservoir simulation.

3.2 INTRODUCTION

Surface forces between fluids and rocks play a major role in the flow characteristics of fluids in petroleum reservoirs, hence, in the recovery of hydrocarbons. In reservoir

engineering, surface forces are expressed by the interfacial tension (IFT) between different co-existing phases, and the contact angle between the reservoir rock and in-situ fluids. The determination of these properties are essential in planning, management and operation of reservoirs for optimum recovery.

The interfacial tension between vapour and liquid is traditionally measured by the pendant drop method[1]. An alternative method which is based on the measurement of the height of vapour -liquid interface curvature on a glass surface[2] is being routinely used in conjunction with the pendant drop method. Both of these methods have been described in details in Chapter 2.

The contact angle is a measure of the relative strength of adhesion of the fluid to the solid surface and to itself. It has a major influence on the distribution of hydrocarbons as well as any water present within reservoir rocks. The main interest in the contact angle in petroleum engineering is its contribution to the capillary pressure as expressed by the Laplace-Young equation[3]. In the case of a small cylindrical capillary tube the interface surface can be approximated as hemispherical in shape and hence the two radii are identical and equal to the radius of sphere, r. The capillary pressure across the curved interface can then be calculated by the Laplace-Young equation of the following form:

$$P_c = \frac{2\sigma\cos\theta}{r} \tag{3.1}$$

where;

P_c: capillary pressure, mPa.

σ: interfacial tension, $mN.m^{-1}$.

θ: three-phase (vapour-liquid-solid) contact angle, deg.

r: radius of the capillary tube, m.

The contact angle would be impossible to measure in real porous media with heterogeneous rock properties and rough surfaces. Generally, the measured capillary

pressure data on a core at laboratory conditions are transposed to reservoir conditions employing crude assumptions, such as zero or constant contact angle at all conditions. Recent reports on capillary pressure data measured at reservoir conditions[4,5], have indicated the unreliability of the current practice, particularly at low IFT conditions. Christoffersen *et al*[4] measured capillary pressure (at different IFT values) on a chalk cores and concluded that linear up-scaling of laboratory capillary pressure data to reservoir condition is not valid at IFT conditions lower than a threshold value of about 5 $mN.m^{-1}$. Longeron *et al*[6] conducted a series of gas-oil capillary pressure measurements on sandstone cores over a range of IFT values and concluded that the standard transposition of laboratory capillary pressure data to reservoir conditions is only valid for IFT values higher than 3.7 $mN.m^{-1}$. The authors suggested changing the contact angle for lower IFT values, which is in agreement with those conclusions reported by Christoffersen *et al*[4]. McCaffery[6] performed interfacial tension and contact angle experiments, on three liquid hydrocarbon-brine systems, as a function of temperature. His study revealed that the contact angle remained almost constant at low temperature, hence high IFT values, and started to decline thereafter. He suggested that the decrease in IFT may alone be responsible for the decrease in contact angle with temperature.

There is little information on the variation of gas-oil-rock contact angle with pertinent parameters in the literature. Fowkes[7] correlated the cosine of the contact angle, $\cos(\theta)$, of hydrocarbons on various solids as a function of the ratio between the square root of the liquid dispersion component (σ_l) of the IFT and the total IFT (σ). However, his correlation breaks down when IFT approaches zero.

In this chapter, the variation of interfacial tension and contact angle were studied for four binary mixtures of C_1/n-C_4, C_1/n-C_8, C_1/n-C_{10} and C_1/n-C_{14} and two real reservoir fluids, namely; a near critical fluid referred to as NCF and a rich gas-condensate referred to as GCA. The IFT data were measured by both the pendant drop and meniscus height techniques[1,2]. The contact angle data were measured using a square capillary technique. The detailed procedures for measuring both properties were described in Chapter 2.

Error analysis on the measured data was carried out and smoothed contact angle data for all tested fluids were derived as described in Section 3.3. The measured contact angle data were, then, used to develop a generalised correlation between the contact angle and IFT. The developed correlation was then tested against contact angle data of two multi-component reservoir fluids which will be demonstrated in Section 3.4. The conclusions drawn from this study are stated in Section 3.5.

3.3 EXPERIMENTAL DATA

As previously mentioned, the variations of contact angle and IFT were investigated for fluid systems with phase behaviour similar to naturally occurring hydrocarbons. Four near-critical binary fluid mixtures of methane/n-Butane, methane/n-Octane, methane/n-Decane and methane/n-Tetradecane and two multi-component mixtures, obtained from samples supplied by oil companies, namely; a near critical fluid NCF, and a rich gas-condensate GCA, were tested. The preparation and transfer of these mixtures together with the time taken to reach equilibrium plus the various IFT measurements represent a considerable effort in time. Some basic properties of the investigated fluids are listed in Table 3.1. The procedures for preparing these fluids has been outlined in Chapter 2. Compositional data were available for some of the fluids and listed in Tables 3.2 and 3.3.

Contact angle and gas-liquid interfacial tension measurements were conducted at a temperature of 37.8 °C (100 °F) and various pressures for the above mentioned fluid systems. An example of un-smoothed data indicating the reliability of measurements by the two methods are shown in Figure 3.1. The error band (Table 3.4) in the measured contact angle data was estimated by calculating the propagated errors as described in Appendix A.

Taking into account the derived error bands in the calculated contact angle data, smoothed values for all tested fluid systems were obtained and listed in Tables 3.5 through 3.10. Figure 3.2 shows the variation of IFT with pressure for all fluid systems investigated in this study. The results show that IFT decreases with increasing pressure

and decreases toward zero at the critical point. These results have important applications in reservoir management, in particular hydrocarbon recovery by depressurisation. In the depressurisation study conducted by Mackay *et al*[8], it has been observed that the capillary forces (indexed by gas-water and gas-oil interfacial tensions) play an important role in bubble nucleation which in turn restrict upon expansion and coalescence of gas bubbles in maximising hydrocarbon recovery.

The variation of vapour-liquid-solid contact angle for the systems investigated as a function of IFT is plotted in Figure 3.3. It can be seen that the contact angle remains relatively constant over a wide range at high IFT values and monotonically decreases at low IFT values, approaching zero at the critical point. The commencement of this contact angle decline in the IFT range between 2 to 5 $mN.m^{-1}$ for the fluids tested, which is in agreement with the studies conducted by Christoffersen *et al*[4] and Longeron *et al*[5] where authors suggested to change the contact angle to match measured capillary pressure data at reservoir conditions.

The behaviour observed above has not been reported before and could have significant implications in the management of hydrocarbon reservoirs when fluid composition is continuously changing either due to production or deliberate changes when improved oil recovery (IOR) and depressurisation schemes are implemented. A more precise quantification and understanding of the physics of bubble growth during depressurisation process and other IOR processes, where capillary pressure forces dominate, can be gained by incorporating contact angle variations, which are apparent from this study, into the calculation of capillary pressure.

The commencement of contact angle decline could also be tied-in to the relationship between density difference of liquid and vapour phases and IFT, which is used in interfacial tension prediction, as described in Chapter 4. Investigators[9,10] observed that the universal critical exponent relating IFT to density difference was not constant and different exponents were needed to match their experimental data for low and high IFT

values. The confirmation of these observations could become clearer when more IFT and contact angle data become available.

3.4 DEVELOPMENT OF A GENERALISED CORRELATION

The generated data were used to develop a generalised correlation between the contact angle, interfacial tension and other measurable parameters of the system. Several models were tested on the generated results. The following correlation was developed to relate contact angle to interfacial tension:

$$\theta = \theta_b(1 - e^{-C\sigma}) \tag{3.2}$$

where,

θ: three-phase (vapour-liquid-solid) contact angle, deg.

θ_b: base (constant) contact angle at high IFT values which depends on the characteristics of the solid-fluid system, deg.

σ: interfacial tension, $mN.m^{-1}$.

C: correlation constant.

The established values for the constant C, for all mixtures studied, are listed in Table 3.11. All the binary data tested in this laboratory approached the critical pressure at 37.8 °C. It was noticed that the constant C could be correlated linearly with the critical (saturation) pressure. The correlation was then generalised to multi-component systems by using the convergence pressure, which is equivalent to the critical pressure for the binary mixtures.

Based on the limited data generated on binary mixtures, the following correlation was developed:

$$C = -0.0009 \times P_k + 6.5228 \tag{3.3}$$

where P_k is the convergence pressure of the system, defined as the pressure where vapour-liquid equilibrium factor (K) has a value of unity (i.e., the compositions of both liquid and vapour phases become identical).

Equation (3.2) was used to predict the measured contact angle data for the multi-component NCF and GCA fluids, listed in Tables 3.9 and 3.10, respectively. It should be noted that those experimental data are independent and have not been used in the optimisation of Equation (3.3). The convergence pressure was calculated for each mixture by converting the fluid into a pseudo-binary composed of methane and the rest of the components lumped together as the pseudo heavy component. The critical properties of the pseudo-component were calculated by weight averaging of its constituents. Table 3.11 contains the critical and convergence pressures of tested fluid systems.

Figures 3.4 and 3.5 present the experimental and predicted contact angle for the NCF and GCA fluids at 37.8 °C, using Equations (3.2) and (3.3). The predicted contact angles are in good agreement with the experimental data demonstrating the reliability of the developed correlation.

3.5 CONCLUSIONS

This exploratory study into contact angle and IFT for hydrocarbon mixtures has provided some stimulating results both from a theoretical as well as a practical perspectives. The employed square capillary tube technique provided a novel ability of measuring vapour-liquid-solid contact angle at condition relevant to reservoir operations, thus allowing investigation of contact angle variation (with pertinent parameter) due to compositional changes. The variation of the three-phase contact angle with interfacial tension has concluded the following:

- The contact angle has been shown (in Figure 3.3) to remain relatively constant over a wide range of interfacial tension values (above a threshold value between 2 to 5 $mN.m^{-1}$) and declines at a variable rate, depending on the volatility of the mixture, approaching zero at the critical point.
- The current practice of assuming zero or constant contact angle, when transposing laboratory capillary pressure data to reservoir conditions, has been demonstrated to be invalid at low IFT values. Capillary pressure curve which takes into account the contact angle variation must be incorporated for fluid flow simulation purposes.
- A predictive correlation between the vapour-liquid-solid contact angle, interfacial tension and convergence pressure has been developed (Equation (3.2)) which can be easily incorporated in numerical reservoir flow simulators.
- The predicted contact angle data for two multi-component real reservoir fluids, using the developed correlation, were in good agreement with their experimental data (Figures 3.4 and 3.5) , demonstrating the reliability of the developed correlation.

REFERENCES

[1] Andreas, J. M., Hauser, E. A., and Tucker, W. B. : "Boundary Tension by Pendant Drops," Presented at the 50th Colloid Symposium, held at Cambridge. Massachusetts (1938).

[2] Danesh, A., Todd, A. C., Somerville, J. and Dandekar, A. : "Direct Measurement of Interfacial Tension, Density, Volume and Compositions of Gas Condensate Systems", Trans I Chem E, **68A**, 325-330, (1990).

[3] Adamson, A. W. :Physical Chemistry of Surfaces, 4th Edition, John Wiley and Sons, New York City (1982).

[4] Christoffersen, K. R., Whitson, C. H., de Silva, F. V. and Haldoupis. A. J. : "Measuring Capillary Pressure of Chalk Samples at Elevated Pressures and Varying Interfacial Tension", paper presented at the 4th North Sea Chalk Symposium, Deauville, France, Sep. 21-23. (1992).

[5] Longeron, D. G., Kalaydjian, F., Bardon, C. and Desremaux, L. M. : "Gas/Oil Capillary Pressure: Measurements at Reservoir Conditions and Effect on Gas-Gravity Drainage", paper SPE 28612 presented at the SPE 69th Annual Technical Conference and Exhibition held in New Orleans, LA, USA, Sep. 25-28 (1994).

[6] McCaffery, F. G. : "Measurement of Interfacial Tension and Contact Angles at High Temperature and Pressure", J. Cand. Pet. Tech. (JCPT), **11**(3), 26-31 (1972).

[7] Fowkes, F. M. : "Dispersion Force Contributions to Surface and Interfacial Tensions, Contact Angle, and Heat Immersion", Adv. Chem. Series, **11**, 99-111, (1964).

[8] Mackay, E. J., Henderson, G .D., Tehrani, D. H. and Danesh, A. : "The Importance of Interfacial Tension on Fluid Distribution During Depressurisation", SPE 38919, paper presented at the 1997 SPE Annual Technical Conference held in San Antonio, Texas, Oct. 5-8, (1997).

[9] Danesh, A. S., Dandekar, A. Y., Todd, A. C. and Sarkar, R. : "Modified Scaling Law and Parachor Method Approach for Improved prediction of Interfacial Tension of Gas-Condensate Systems", SPE22710, presented at the 66th SPE Annual Technical Conference held in Dallas, Texas, Oct. 6-9, (1991).

[10] Huygens, R. J. M., Ronde, H. and Hagoort, J. : "Interfacial Tension of Nitrogen and Volatile Oil Systems", SPE 26643, presented at the 68th SPE Annual Technical Conference and Exhibition held in Houston, Texas, Oct. 3-6 (1993).

Table 3.1 - Properties of the Investigated Fluids at Temperature of 37.8 °C.

Fluid Mixture	Saturation Pressure (psia)	Fluid Type
C_1 / n-C4	1870	Near Critical Oil
C_1 / n-C8	4018	Near Critical Oil
C_1 / n-C10	5250	Near Critical Oil
C_1 / n-C14	-	Volatile Oil
NCF	4427	Multi-components Near Critical Oil
GCA	4184	Multi-components Rich Gas Condensate

Table 3.2 - Measured Molar Compositions of Methane/n-Octane and Methane/n-Decane Binary Mixtures.

Component	Methane/n-Octane	Methane/n-Decane
C1/ %	85.11	89.39
n-C8/ %	14.89	-
n-C10/ %	-	10.61

Table 3.3 - Measured Molar Compositions of the Multi-component NCF and GCA Fluids.

Comp.	NCF		GCA	
	Mole %	MW.	Mole %	MW.
N2	0.36	28.01	0.69	28.01
C1	68.74	16.04	72.12	16.04
CO2	0.27	44.01	1.17	44.01
C2	9.88	30.07	8.64	30.07
C3	4.22	44.10	3.99	44.10
i-C4	0.48	58.12	0.50	58.12
n-C4	1.49	58.12	1.43	58.12
i-C5	0.32	72.15	0.38	72.15
n-C5	0.86	72.15	0.74	72.15
C6	1.00	84	0.92	84.5
C7	2.02	89	1.71	90.0
C8	2.33	103	1.87	102
C9	1.78	114	1.32	114
C10	1.25	132	0.90	131
C11	0.89	148	0.64	148
C12	0.64	165	0.47	162
C13	0.52	177	0.39	175
C14	0.65	187	0.48	186
C15	0.48	204	0.35	202
C16	0.36	218	0.26	217
C17	0.24	234	0.17	232
C18	0.25	250	0.17	249
C19	0.20	262	0.14	262
C20+	0.79	346	0.56	349

Table 3.4 - Calculated Overall Propagated Error in the Computed Contact Angle.

IFT ($mN.m^{-1}$)	Calculated Overall Error (± deg.)
$\sigma > 2$	2.0
$1 \leq \sigma \leq 2$	1.0
$0.1 < \sigma < 1$	0.5
$\sigma < 0.1$	0.2

Table 3.5 - Smoothed Contact Angle and IFT Values of C_1/n-C_4 Binary Fluid Mixture at 37.8 °C.

Pressure (psia)	IFT ($mN.m^{-1}$)	Contact Angle (deg.)
500	6.94	24.5
800	4.81	24.5
1000	3.57	24.5
1250	2.22	24.5
1500	1.09	24.4
1750	0.250	18.0
1800	0.110	10.9

Table 3.6 - Smoothed Contact Angle and IFT Values of C_1/n-C_8 Binary Fluid Mixture at 37.8 °C.

Pressure (psia)	IFT ($mN.m^{-1}$)	Contact Angle (deg.)
1500	7.79	22.8
2000	5.29	22.8
2500	3.24	22.8
3000	1.79	22.8
3250	1.25	22.2
3500	0.736	20.1
3750	0.370	15.0
3900	0.097	5.6
4000	0.010	0.6

Table 3.7 - Smoothed Contact Angle and IFT Values of C_1/n-C_{10} Binary Fluid Mixture at 37.8 °C.

Pressure (psia)	IFT ($mN.m^{-1}$)	Contact Angle (deg.)
100	20.3	22.3
250	19.0	22.3
500	16.9	22.3
800	14.6	22.3
1000	13.2	22.3
1250	11.5	22.3
1500	9.93	22.3
1750	8.47	22.3
2000	7.15	22.3
2500	5.04	22.3
3000	3.72	22.2
3500	2.40	21.8
4000	1.49	20.1
4250	1.10	18.3
4500	0.766	15.5
5000	0.167	5.1
5100	0.094	3.0
5150	0.058	1.9
5200	0.026	0.9

Table 3.8 - Smoothed Contact Angle and IFT Values of C_1/n-C_{14} Binary Fluid Mixture at 37.8 °C.

Pressure (psia)	IFT ($mN\ m^{-1}$)	Contact Angle (deg.)
100	19.6	20.5
250	18.5	20.5
500	17.0	20.5
800	15.3	20.5
1000	14.2	20.5
1250	12.8	20.5
1500	11.6	20.5
1750	10.4	20.5
2000	9.31	20.5
3000	5.73	20.4
4000	3.43	19.8
5000	2.17	18.1

Table 3.9 - Smoothed Contact Angle and IFT Values of the Multi-components NCF Fluid Mixture at 37.8 °C.

Pressure (psia)	IFT ($mN\ m^{-1}$)	Contact Angle (deg.)
1000	9.39	21.9
1500	6.50	21.9
2000	4.00	21.9
2500	2.27	21.9
3000	1.21	21.6
3500	0.508	18.5
4000	0.152	9.4
4250	0.052	3.8
4300	0.027	2.1

Table 3.10- Smoothed Contact Angle and IFT Values of the Multi-components GCA Fluid Mixture at 37.8 °C.

Pressure (psia)	IFT ($mN\ m^{-1}$)	Contact Angle (deg.)
1000	9.12	21.5
1250	7.59	21.5
1500	6.20	21.5
2000	4.00	21.5
3000	1.19	19.5
4000	0.255	8.5
4500	0.067	2.7

Table 3.11 - The Base Contact Angle, Constant C Values and Convergence Pressure for All Fluid Systems at 37.8 °C.

Fluid Mixture	Base Contact Angle (deg.)	Constant C	Convergence Pressure (psia)
C_1/n-C_4	24.5	4.80	1870
C_1/n-C_8	22.8	2.87	4018
C_1/n-C_{10}	22.3	1.58	5250
C_1/n-C_{14}	20.5	1.2	6150
NCF	21.9	2.57	4400
GCA	21.5	2.27	4800

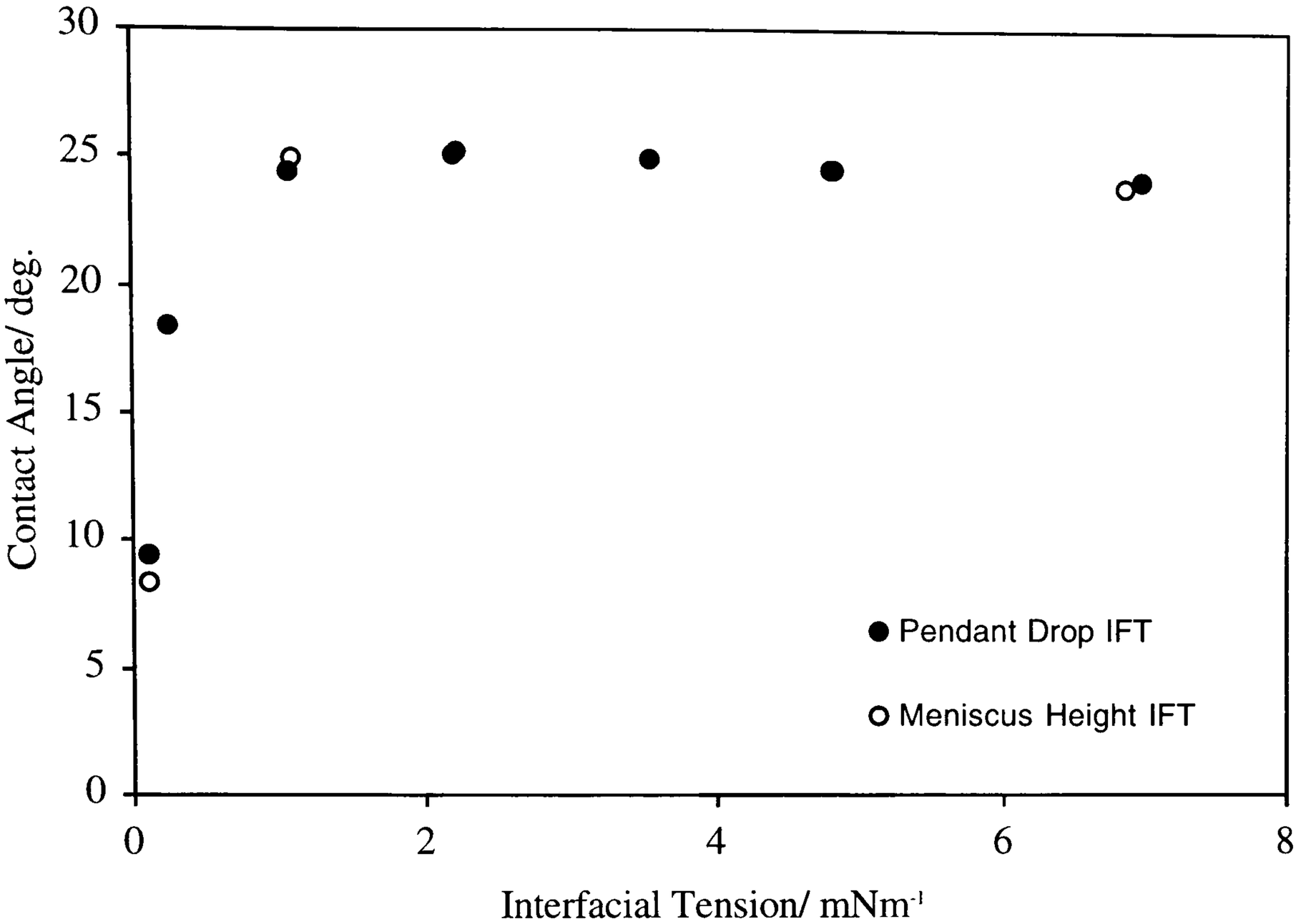

Figure 3.1 - The Variation of Measured Contact Angle With Interfacial Tension for the Binary Fluid Mixture of C_1/n-C_4 , Using IFT Data Measured by both The Pendant Drop and Meniscus Height Techniques.

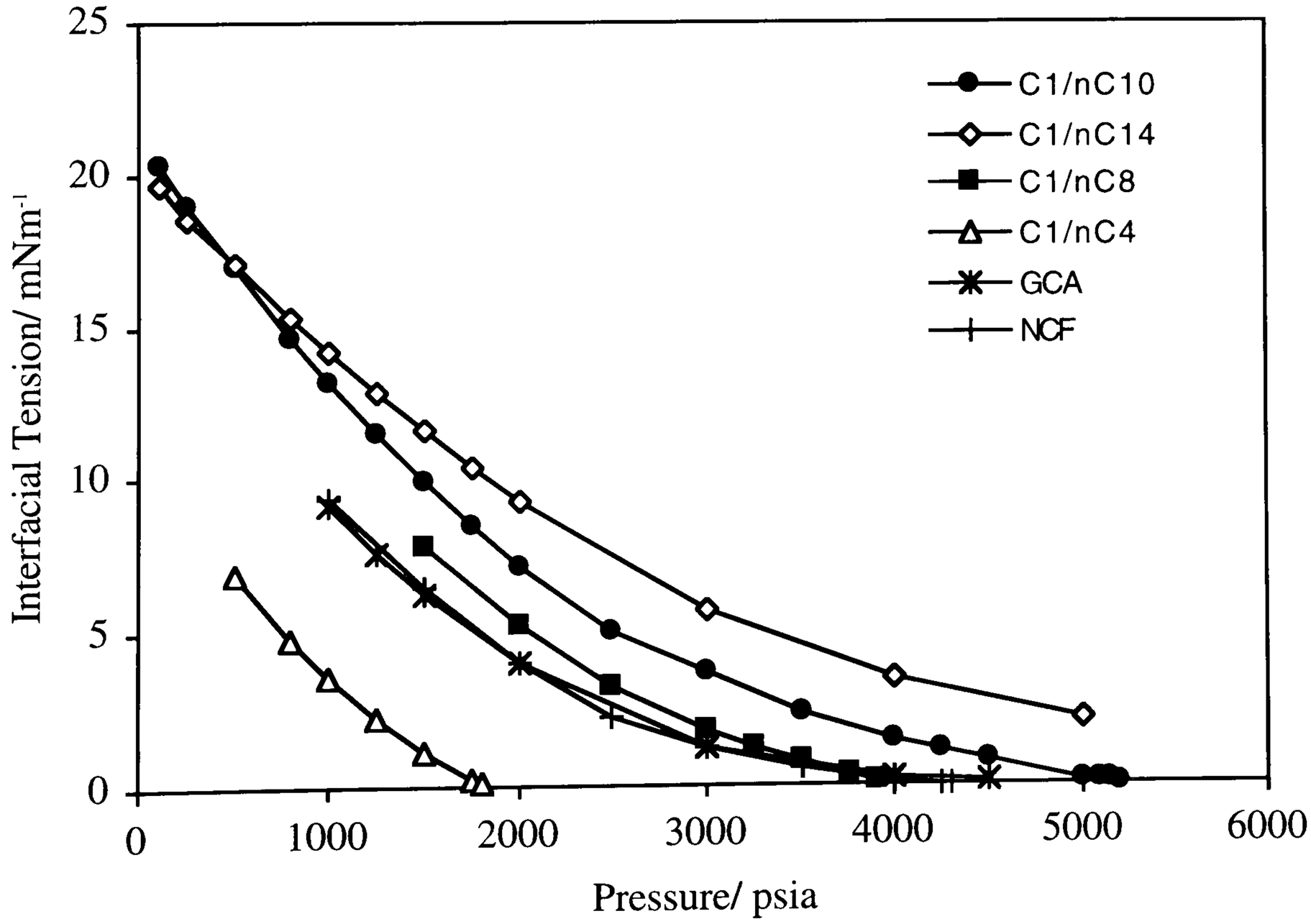

Figure 3.2 - Interfacial Tension vs. Pressure for All Tested Fluids.

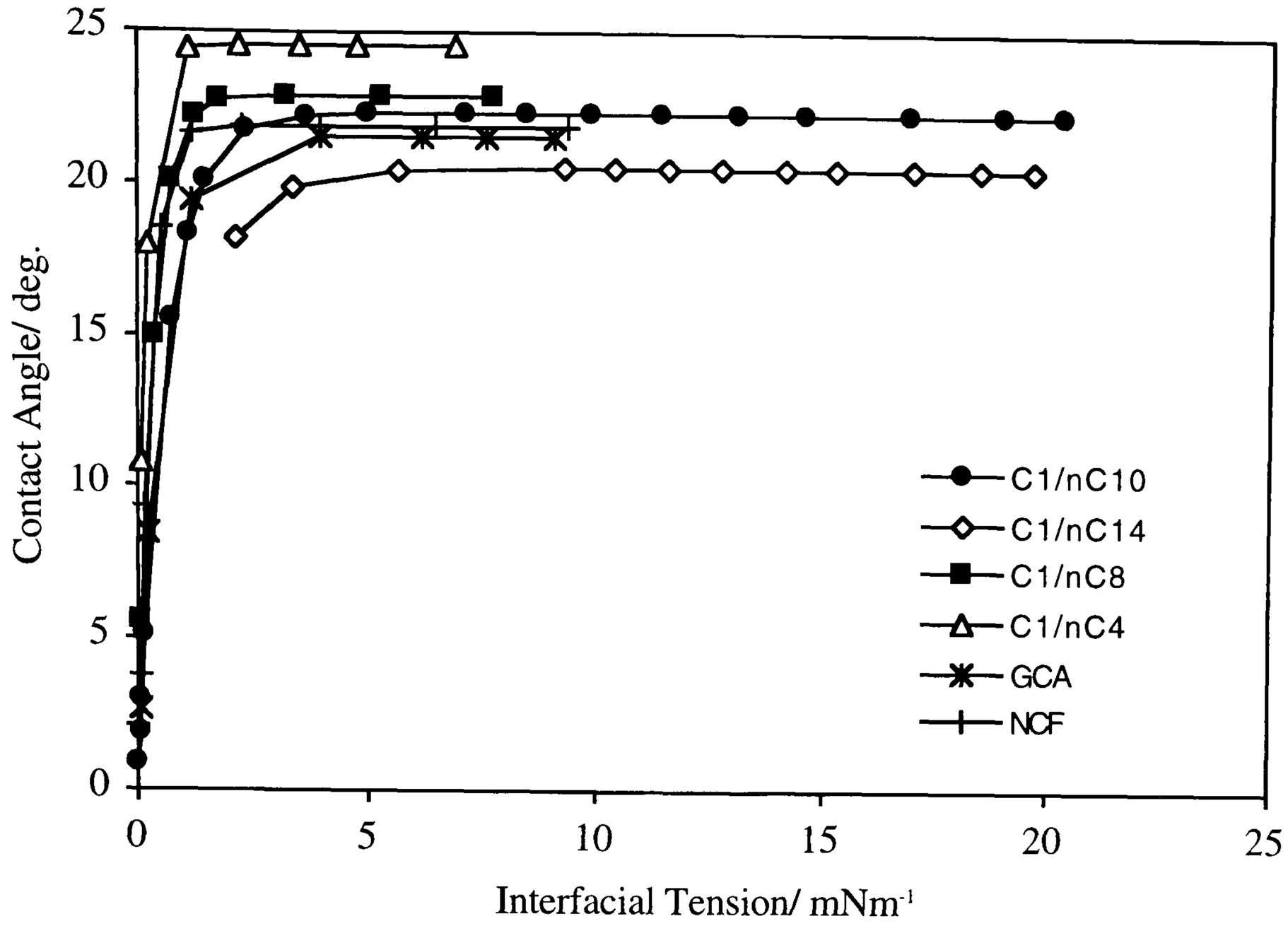

Figure 3.3 - Smoothed Contact Angle vs. IFT for all Tested Fluids.

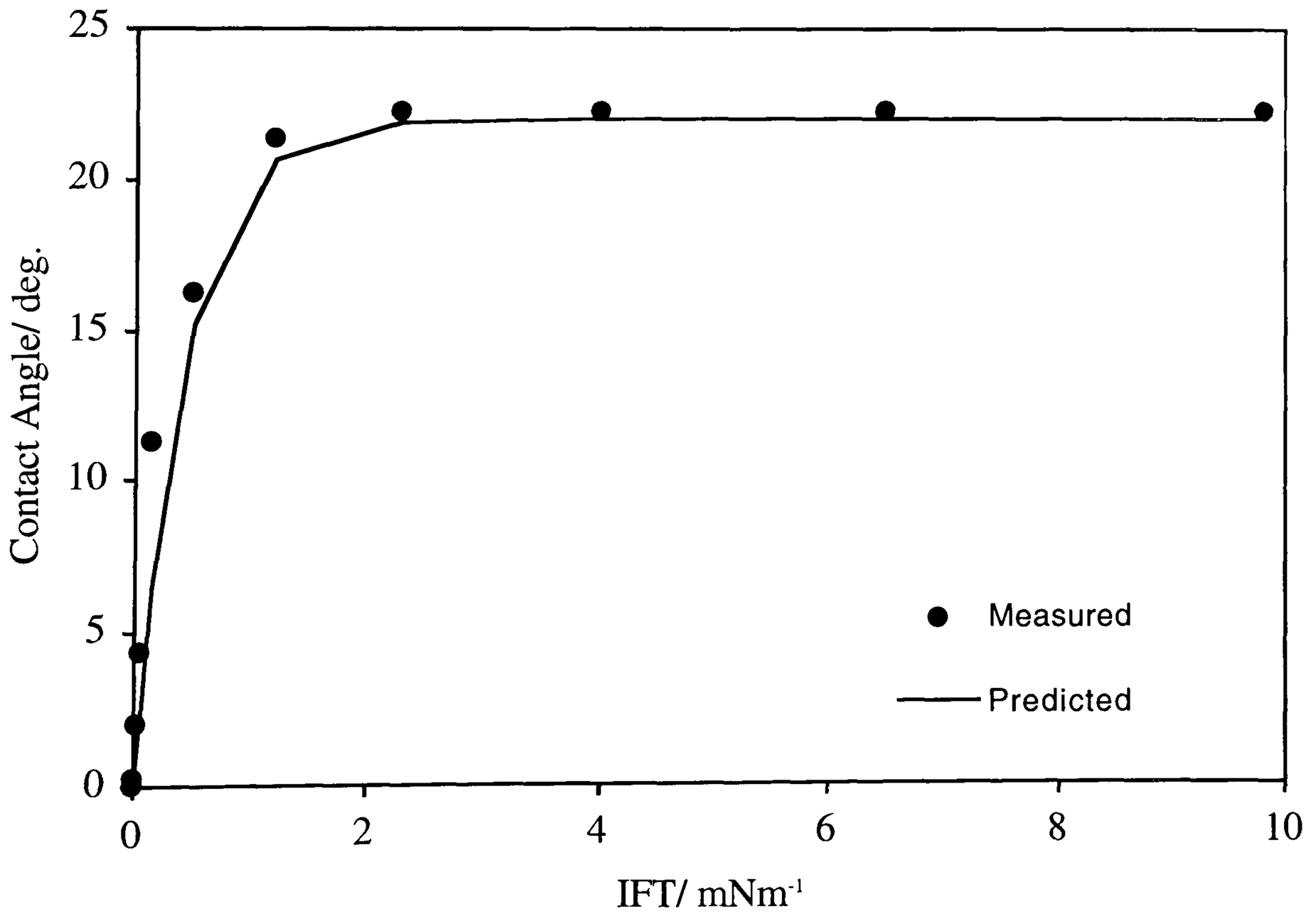

Figure 3.4 - Comparison of Measured and Predicted Contact Angle vs. IFT for the Multi-components Near-Critical NCF Mixture at 37.8 °C.

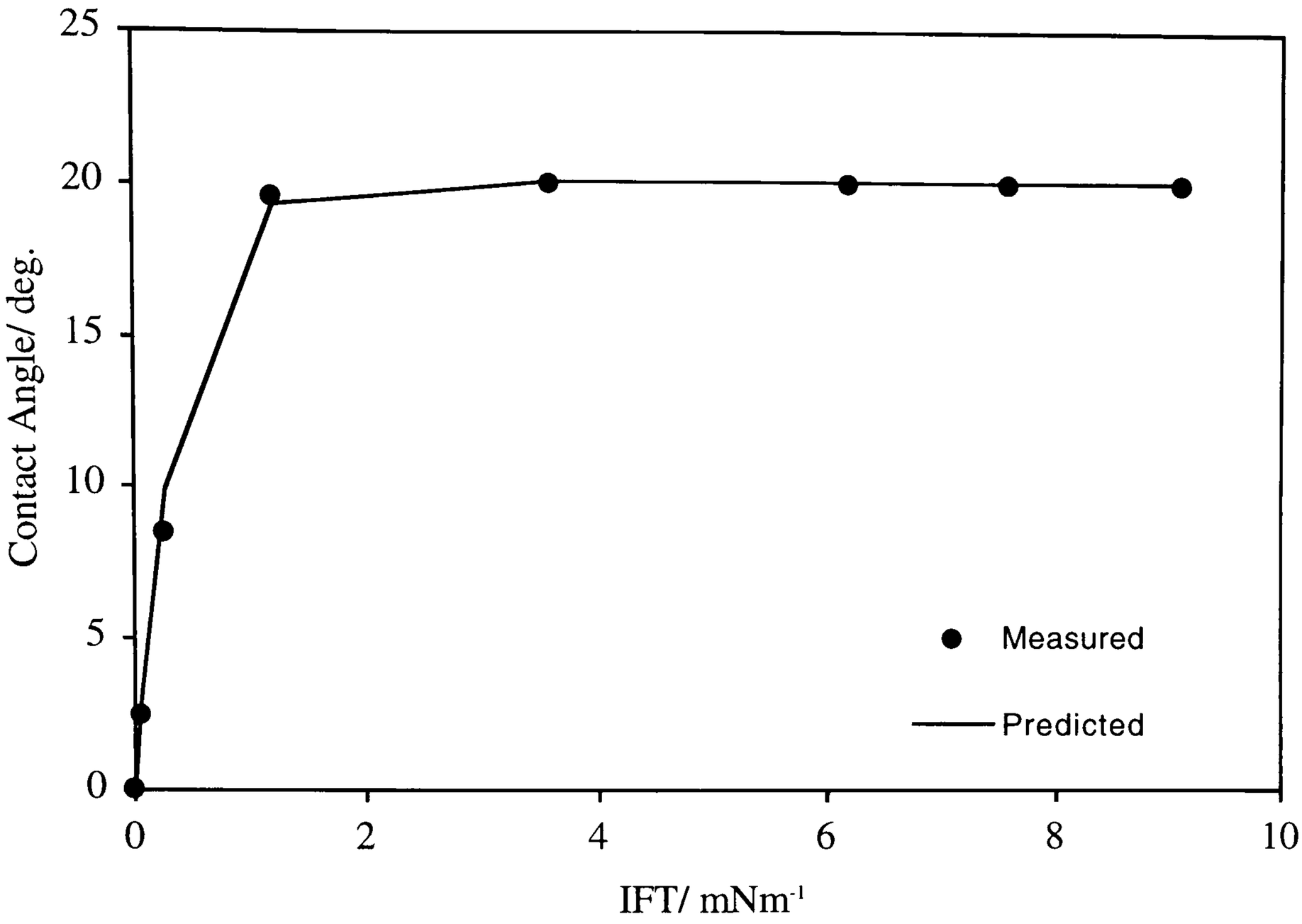

Figure 3.5 - Comparison of Measured and Predicted Contact Angle vs. IFT for the Multi-components Rich Condensate GCA Mixture at 37.8 °C.

CHAPTER 4

INTERFACIAL TENSION OF RESERVOIR FLUIDS

4.1 OBJECTIVES

Accurate and reliable information on interfacial tension (IFT) is of major importance in both petroleum and chemical engineering. The objectives of this chapter are:

- To give a description of the most commonly used methods for predicting the interfacial tension in the petroleum industry and the tuning procedure normally employed to ensure reliable interfacial tension prediction for real reservoir fluids for reservoir simulation purposes.
- To investigate the possibility of calculating the IFT of mixture of fluids using various averaging (e.g., volumetric, molar and weight) methods. A comparison between the calculated interfacial tensions, of two ternary mixtures of Methane/n-Octane/n-Decane and two mixtures of real reservoir fluids, by the volumetric average and the Weinaug-Katz model were made and discussed in this chapter.

4.2 INTRODUCTION

When two immiscible fluids are in contact with each other, they are separated by a thin layer of uniform thickness called the *interface*, which results from the imbalance of molecular forces (at the interface) caused by the physical attraction between molecules[1]. The formation of this interface can be visualised on the basis of surface energy or work per

unit area required to bring the molecules to the surface. The surface tension is then the stretching force required to form the film. From a mechanical point of view, the system behaves as if it consisted of two homogeneous fluids separated with a stretched membrane of infinitesimally uniform thickness. At the interface, there exist different force-fields than the bulk phases and consequently those atoms, at the interface, possess different internal pressure, intermolecular spacing and chemical potential.

Accurate and reliable information on interfacial tension (IFT) is of major importance in both petroleum and chemical engineering. The importance of IFT is magnified when dealing with IOR processes where the relative magnitude of interfacial (capillary), gravitational and viscous forces considerably affect the recovery of hydrocarbons. The relative permeability relationships which determine the flow behaviour of reservoir fluids in porous media strongly depend on the interfacial tension at high pressure conditions[2-4].

As is usually the case with many fluid properties, the time and cost involved in obtaining sufficient experimental data for wide ranges of conditions are prohibitive. Hence, predictive, often empirical, techniques are usually employed to estimate such properties. The two most commonly used methods of predicting the interfacial tension are the parachor method[5] and the scaling law[6]. Both these techniques have previously been evaluated and modified by this Department[7]. A brief discussion on IFT predictive models and the associated tuning approach for real reservoir fluids is given in Section 4.3.

Reservoir fluids with different phase behaviour are normally mixed together in a single pipeline as they transported to production or loading units where they are processed and/or exported. The properties of the mixed fluids are essential for the design of pipelines as well as surface facilities. It was found that if the interfacial tensions of the individual make-up fluids are known, the interfacial tension of the overall mixture can be reasonably calculated by volumetric averaging with uncertainty levels comparable to that of experimental accuracy. Measured interfacial tension data of two ternary mixtures of Methane/n-Octane/n-Decane and two mixtures of two real reservoir fluid were used to test

this approach. A comparison between the calculated interfacial tensions by this approach and by that of parachor method[5] with experimental data is discussed in Section 4.4.

4.3 PREDICTION OF INTERFACIAL TENSION IN MULTI-COMPONENT FLUIDS

A rapid, straight forward and low cost predictive technique with satisfactory accuracy is appreciated in reservoir simulation. However, there is no consistent standard by which this may be accomplished. Most of the techniques use the properties of the bulk phases to predict IFT, where it is known that there exist different force-fields between molecules at the surface of tension and those of bulk fluids. Hence, component composition in bulk phases is different from those at the surface. The disadvantage of these techniques is that they are largely empirical in nature and therefore cannot be developed in theoretical applications.

The two most commonly used methods of predicting the interfacial tension are the parachor[5] and the scaling law[6]. Based on experimental observations, MacLeod[8] recognised the following relation between surface tension and densities

$$\frac{\sigma}{(\rho_l - \rho_v)^4} = C \tag{4.1}$$

Sugden[9] related the constant C to chemical composition of the substance and called it Parachor, P_σ, which is believed to be a measure of the molecular volume and chemical composition:

$$P_\sigma = \frac{MW}{\rho_l - \rho_v}\sigma^{1/4} \tag{4.2}$$

where;

σ: interfacial tension.

ρ_l: density of liquid phase.

ρ_v: density of vapour phase.

MW: molecular weight.

P_σ: parachor.

Weinaug and Katz[5] extended the Macleod-Sugden equation (Equation 4.2) for multi-component systems, treating a mixture as a one-component fluid by using the molar average rule for calculating its parachor value. The extended formulation is described below:

$$\sigma^{1/4} = \left[\sum_{i=1}^{i=n} P_{\sigma i} x_i\right](\rho_l)_m - \left[\sum_{i=1}^{i=n} P_{\sigma i} y_i\right](\rho_v)_m \qquad (4.3)$$

where;

$(\rho_l)_m$: molar density of liquid phase.

$(\rho_v)_m$: molar density of vapour phase.

MW: component molecular weight.

$P_{\sigma i}$: parachor value of component *i* in the mixture.

x_i: molar composition of component *i* in the liquid phase.

y_i: molar composition of component *i* in the vapour phase.

Lee and Chien[6] developed a semi-empirical approach, based on the critical scaling theory[10], for calculating the interfacial tension between two equilibrium phases. Their formulation is described below:

$$\sigma^{1/3.911} = \left[P_{\sigma l}(\rho_l)_m\right] - \left[P_{\sigma v}(\rho_v)_m\right] \qquad (4.4)$$

For each component, the parachor is calculated from Equation (4.5):

$$P_\sigma = A_c^{45/176}\left(V_c\right)_m / B \tag{4.5}$$

where;

$(V_c)_m$: molar critical volume of component.

A_c: a constant, depends on critical properties and boiling temperature of component, calculated from the expression below:

$$A_c = P_c^{2/3} T_c^{1/3}\left(0.133\alpha_c - 0.281\right) \tag{4.6}$$

where;

P_c: critical pressure of component.

T_c: critical temperature of component.

α_c: Riedel parameter evaluated from the expression below:

$$\alpha_c = 0.9076\left[1.0 + \frac{\left(\ln\left(P_c/P_a\right)\left(T_b/T_c\right)\right)}{\left(1 - T_b/T_c\right)}\right] \tag{4.7}$$

where;

T_b: boiling temperature of component.

P_a: atmospheric pressure.

and

B: a constant which could be estimated from component's IFT. For some pure hydrocarbon compounds, B has been correlated to critical compressibility factor (Z_c) as in Equation (4.8):

$$B = 1.854426 Z_c^{-0.52402} \tag{4.8}$$

For multi-component fluids, the molar average mixing rule is used to calculate the values of the above parameters, both for the liquid and vapour phases.

The above techniques were modified by the Department[7], whereby the value of exponent of interfacial tension (1/E) was considered to be a function of the liquid-vapour molar density difference. Correlations were determined for both the parachor and the scaling methods by regressing E to minimise the deviations of the predicted results. The developed correlations for the Lee-Chein and Weinaug-Katz methods are stated below, respectively:

$$E = 3.535 + 17.76\left[(\rho_l)_m - (\rho_v)_m\right] \tag{4.9}$$

$$E = 3.583 + 0.16\left[(\rho_l)_m - (\rho_v)_m\right] \tag{4.10}$$

Other predictive models[11-13] have also been used in the literature for IFT prediction. These models have more or less the same functional form, except that they employ different values of critical exponent, E.

Another approach, known as the *gradient theory*, has also been used for IFT calculation[14]. In the gradient theory, the *interface* is assumed as a third phase with properties varying from those of the other two bulk fluids. However, the approach uses a cumbersome thermodynamic calculations, utilising an equation of state. The main drawback of the gradient theory, as with most of the theoretically-based models, is the mis-handling of the lumped-fraction which differs from a mixture to another, depending on the range of lumped single carbon number (SCN) groups and the distribution of paraffin, naphthene and aromatic (PNA) compounds. Hence, it has not being thoroughly tested for modelling the interfacial tension of real reservoir fluids.

The correlation of Firoozabadi *et al*[15] is normally used to calculate the parachor of petroleum fraction. The correlation uses the molecular weight of the fraction to calculate its parachor value as in the following relationship:

$$P_\sigma = -11.4 + 3.23MW - 0.0022MW^2 \qquad (4.11)$$

The above equation, Equation (4.11), has been used for estimating the parachor value of the single carbon number (SCN) groups and plus-fractions for IFT calculation of real reservoir fluids, described in Chapter 7.

4.4 MIXTURE OF SEVERAL RESERVOIR FLUIDS

As the properties of mixed fluids are essential for the design of pipelines and surface facilities, a simple, yet reliable, method for calculating the IFT of a mixture of fluids would be essential. Various averaging methods (volumetric, molar and weight) were evaluated for calculating the IFT of mixture of fluids. The volumetric averaging method, below;

$$\sigma = \sum_{i=1}^{N} \upsilon_i \, \sigma_i \qquad (4.12)$$

(where υ_i and σ_i are the volumetric ratio and the IFT of mixture i in the overall mixture of fluids, respectively) was proved to be quite reliable for mixtures of volatile oil and a near-critical fluid. The reliability of the volumetric averaging method was further investigated by conducting test on mixtures of binary fluids which confirmed the above finding. Section 4.4.1 presents the IFT measurement for the tested fluids. In Section 4.4.2, after a brief review of previous studies investigating the applicability of averaging method (Equation (4.12)) in IFT calculation, a comparison between the measured and predicted IFT by both the volumetric averaging method and the original Weinaug-Katz (WK) model is discussed.

4.4.1 Experimental Results

The interfacial tension measurements with the meniscus height technique[16] were compared with the literature data[17-19] and those measured (in-house) by the pendant drop method[20] for the binary Methane/n-Butane and Methane/n-Decane fluid systems. As shown in Figure 4.1, the IFT measurements with the meniscus height technique are in good agreement with those measured by the standard pendant drop technique and literature data, even at relatively high IFT values. As a result of this good agreement, the technique has been routinely used to measure interfacial tension in conjunction with the classical pendant drop method for all fluids during PVT testings.

Interfacial tension measurements between equilibrated vapour and liquid phases of mixtures of several reservoir and model fluids are presented in this section. The measurements were performed during CCE experiments at reservoir and surface temperatures and various equilibrium pressures using both pendant drop and meniscus height techniques.

Interfacial tension data for two mixtures of multi-component gas condensate GCA94-1 and a near-critical fluid, NCF, are listed in Tables 4.1 and 4.2. The compositional data of the NCF fluid can be found in Table 3.2 of Chapter 3, while Table 4.3 lists those data for the GCA94-1 fluid. Shown in Figures 4.2 and 4.3 is the variation of interfacial tension with pressure for the above fluids at 110 °C and 37.8 °C, respectively. The IFT of the GCA94-1/NCF mixtures, at both temperatures, is observed to decrease with the volumetric addition of NCF fluid. Moreover, the agreement in IFT measurement between the meniscus height and pendant drop techniques is very good, as shown in Figure 4.3, supporting the earlier statement endorsing the meniscus height technique as a robust method for measuring low and high IFT.

In Table 4.4, IFT data of two mixtures of the multi-component volatile oil, LRA97-1, and the near-critical fluid NCF are listed. Figure 4.4 shows the variation of IFT of the two LRA97-1/NCF mixtures as a function of pressure. As expected, the mixtures IFTs were seen to decrease with increasing amount of the lighter NCF mixture, approaching those of the latter at higher mixing proportions. In addition of the multi-component fluids.

interfacial tension data of two ternary mixtures of Methane/n-Octane/n-Decane are tabulated in Table 4.5 and graphically shown in Figure 4.5. The behaviour of mixture's IFT observed for these model fluids was the same as that seen for the multi-component mixtures (i.e., the IFT of the ternary mixture is seen to decrease with increasing the amount of Methane/n-Octane).

4.4.2 Additive Approach for Interfacial Tension Calculation

When two fluids of known properties are mixed together, the physical properties of their mixture could be calculated (with reasonable accuracy) by applying some forms of mixing rules. Attempts[21,22] have been made to investigate the applicability of the above approach for IFT calculation, using various averaging methods (e.g., volumetric , molar and weight), for mixtures of low pressure fluids. However, experiments have shown none of them is of universal application. Worely[21] compared measured IFTs of various liquid mixtures with those calculated from volumetric average. He deduced the following rules; **(i)** if at any given temperature the vapour pressures of two liquid mixtures agree with those calculated by the mixture rule in molecular proportions, then at that temperature the surface tensions of the mixtures agree with those calculated by volumetric average, **(ii)** if the vapour pressures are greater than those calculated, then the surface tensions are less than those calculated, **(iii)** if the vapour pressures are lower than those calculated, then the surface tensions are greater than those calculated. Morgan and Mary[22] employed the weight average to calculate the IFT of twenty-four liquid mixtures, ranging from binary to quinary. Their calculated IFTs were in good agreement with measured ones for only ten mixtures. It is worth noting, from their conclusions, that the deviation in the remaining mixtures was not due to chemical interaction between components but rather to the dominance of some components which might influence the property of the others (i.e., physical interaction between molecules which tend to change the overall force-fields of molecules).

4.4.3 Calculating the Interfacial Tension of Real Reservoir Fluid Mixtures by the Additive Approach

When multi-component fluids of different phase behaviour are mixed together, major changes in fluid composition may take place, especially those of vapour phase which can drastically effect the overall mixture's IFT. However, it was found that the mixture's IFT could be calculated by a simple volumetric averaging of the IFT of the make-up fluids.

The above ternary and the multi-component LRA/NCF mixtures were used to test the validity of the volumetric averaging approach. The molar compositions of these mixtures are listed in Tables 4.6 and 4.7. A comparison between the calculated IFTs using a volumetric average approach and the original WK model with experimental data are tabulated in Tables 4.8 and 4.9. As can be seen from these tables (Tables 4.8 and 4.9), the calculated IFTs using the simple volumetric averaging are in close agreement with the measured values. Whereas those calculated using WK model show large deviation from the measured values which in turn makes the volumetric averaging approach to be much more superior, at least for the fluid mixtures studied in this work.

4.5 CONCLUSIONS

- The measured interfacial tension data by the pendant drop and meniscus height techniques are in excellent agreement and is less than ±2% in most cases.
- As expected, the IFT of mixture of fluids is observed to decrease with the addition of more volatile fluid, approaching the values of the latter at higher proportion ratios.
- The volumetric average approach (Equation (4.12)) was successfully applied to calculate the IFT of mixed fluid streams using model and multi-component fluids. The calculated IFTs by the simple volumetric approach were in better agreement with the experimental data than those predicted by the Weinaug-Katz model.

REFERENCES

1] Danesh, A. : PVT and Phase Behaviour of Petroleum Reservoir Fluids, Elsevier Science B. V., The Netherlands (1998).

2] Bardon, C. and Longeron, D. G. : "Influence of Very Low Interfacial Tension on Relative Permeability", Soc. Pet. Eng. J. (SPEJ), 391-401 (Oct., 1980).

3] Henderson, G. D., Danesh, A., Tehrani, D. H. and Peden, J. M. : "The Effect of Velocity and Interfacial Tension on the Relative Permeability of Gas Condensate Fluids in the Wellbore Region", 8th IOR Symposium, Vienna, (May 1995).

4] Al-Siyabi, Z. K. : Modelling The Effect of Interfacial Tension on Gas and Oil Relative Permeability, MEng Thesis, Heriot-Watt University, Edinburgh, UK (1996).

5] Weinaug, C. F. and Katz, D. L. : "Surface Tension of Methane - Propane Mixtures", Ind. Eng. Chem. (I & EC), **35**(2), 239-246, (1943).

6] Lee, S. T. and Chien, M. C. H. : "A New Multicomponent Surface Tension Correlation Based on Scaling Theory", paper SPE 12643 presented at the SPE/DOE Enhanced Oil Recovery Symposium, Tulsa, Oklahoma, (1984).

[7] Danesh, A., Dandekar, A., Todd, A. C. and Sarkar, R. : "A Modified Scaling Law and Parachor Method for Improved Prediction of Interfacial Tension of Gas Condensate Systems", SPE 22710, Proceeding of the 66th Annual Conference, (Oct., 1991).

[8] MacLeod, D. B.: "On a Relation Between Surface Tension, Density", Trans. Faraday Soc., **19**, 38-43, (1923).

[9] Sugden, S. : "A Relation between Surface Tension, Density and Chemical Composition", J. Chem. Soc., **168**, 1177-1189, (1924).

[10] Stanley, H. E. : Introduction To Phase Transitions and Critical Phenomena, Oxford University Press, New York (1971).

[11] Brock, J. R. and Bird, R. B. : "Surface Tension and the Principle of Corresponding States", AICHEJ, **56**, 996-999, (1952).

[12] Hough, E. W. and Stegemeier, G. L. : "Correlation of Surface and Interfacial Tension of Light Hydrocarbons in The Critical Region", Soc. Pet. Eng. J. (SPEJ), 259-263, (Dec., 1961).

[13] Hugill, J. A. and van Welsenes, A. J. : "Surface Tension: A Simple Correlation for Natural Gas + Condensate Systems", Fluid Phase Equilib., **29**, 383-390, (1986).

[14] Bongiorno, V., Scriven, L. E. and Davis, H. T. : "Molecular Theory of Fluid Interfaces", J. Colloid Interf. Sci., **57**(3), 462-475, (1976).

[15] Firoozabadi, A., Katz, D. L., Soroosh, H. and Sajjadian, V. A. : "Surface Tension of Reservoir Crude-Oil/Gas Systems Recognising the Asphalt in the Heavy Fraction", SPE Res Eng, 265 - 272, (Feb., 1988).

[16] Danesh, A., Todd, A. C., Somerville, J. and Dandekar, A. : "Direct Measurement of Interfacial Tension, Density, Volume and Compositions of Gas Condensate Systems", Trans. I Chem E, **68A**, 325 - 330, (July, 1990).

[17] Stegemeier, G. L., Pennington, B. F., Brauer, E. B. and Hough, E. W. : "Interfacial Tension of Methane-Normal Decane System", Soc. Pet. Eng. J. (SPEJ), 257-260, (Sep., 1962).

[18] Pennington, B. F. and Hough, E. W. : "Interfacial Tension of Methane-Normal Butane System,", Prod. Month., 4, (Jul., 1965).

[19] Amin, R. and Smith, T. N. : "Interfacial Tension and Spreading Coefficient under Reservoir Conditions", Fluid Phase Equilib., **142**, 231 - 241, (1998).

[20] Andreas, J. M., Hauser, E. A., and Tucker, W. B. : "Boundary Tension by Pendant Drops", presented at the 50th Colloid Symposium, held at Cambridge, Massachusetts (1938).

1] Worley, R. P. : "The Surface Tension of Mixtures. Part II. Mixtures of Perfectly Miscible Liquids and the Relation between Their Surface Tension and Vapour Pressures", J. Chem. Soc., **105**, 273-282, (1914).

2] Morgan, J. L. R. and Mary, A. G. : "The Properties of Mixed Liquids. III. The Law of Mixtures", J. Chem. Soc., **108**, 2261-2275, (1917).

Table 4.1 - Interfacial Tension Data of the Mixed GCA94-1 and NCF Fluids at Reservoir Temperature of 110 °C.

Pressure/ psia	IFT (GCA94-1)/ $mN.m^{-1}$	IFT(Mix 1*)/ $mN.m^{-1}$	IFT(Mix 2**)/ $mN.m^{-1}$
3000	1.31	0.990	0.715
3500	0.784	0.530	0.296
3800	0.559	-	-
4000	-	0.241	0.099
4100	0.410	-	-
4400	0.293	-	-
4500	-	0.086	0.024
4600	0.235	-	-
4700		-	0.013
4800	0.181	-	-
4900		-	0.007
5000	-	0.034	-

* - Mix 1 (70.7% GCA94-1 / 29.3% NCF, by volume).
** - Mix 2 (48.5% GCA94-1 / 51.5% NCF, by volume).

Table 4.2 - Interfacial Tension Data of the GCA94-1/NCF Mixture (48.5% GCA94-1 / 51.5% NCF, by volume) at 37.8 °C.

Pressure/ psia	IFT (NCF, MH)/ $mN.m^{-1}$	IFT (Mix 2, MH)/ $mN.m^{-1}$	IFT (Mix 2, PD)/ $mN.m^{-1}$
1000	9.39	9.12	9.12
1500	6.50	6.00	6.20
1750	-	4.44	4.50
2000	4.00	3.47	3.31
2500	2.27	-	-
3000	1.21	1.10	1.12
3500	0.508	-	-
4000	0.152	0.232	0.222
4250	0.052	-	-
4300	0.027	-	-
4400	0.003	-	-
4600	-	0.067	-

Mix 2 - (48.5% GCA94-1 / 51.5% NCF, by volume).
MH - Meniscus Height Technique.
PD - Pendant Drop Technique.

Table 4.3 - Measured Molar Compositions of the Multi-component GCA94-1 Fluid.

Comp.	GCA94-1	
	Mole %	MW
N2	1.02	28.01
C1	75.54	16.04
CO2	2.09	44.01
C2	7.38	30.07
C3	3.76	44.10
i-C4	0.53	58.12
n-C4	1.37	58.12
i-C5	0.44	72.15
n-C5	0.61	72.15
C6	0.83	85
C7	1.41	91.0
C8	1.40	101
C9	0.85	114
C10	0.54	130
C11	0.38	147
C12	0.30	158
C13	0.25	173
C14	0.31	185
C15	0.22	200
C16	0.16	215
C17	0.11	230
C18	0.09	247
C19	0.08	261
C20+	0.33	352

Table 4.4 - Interfacial Tension Data of the Mixed LRA97-1 and NCF Fluids at 37.8 °C.

Pressure/ psia	IFT(LRA97-1)/ $mN.m^{-1}$	IFT (Mix 1)/ $mN.m^{-1}$	IFT (Mix 2)/ $mN.m^{-1}$
2000	4.71	4.60	4.05
2500	2.89	2.80	2.32
3000	1.80	1.69	1.32
3500	1.21	-	0.652

Mix 1 - (85.2% LRA97-1 / 14.8% NCF, by volume).
Mix 2 - (18.5% LRA97-1 / 81.5% NCF, by volume).

Table 4.5 - Interfacial Tension Data of Methane/n-Octane, Methane/n-Decane Binaries and Their Ternary Mixtures at 37.8 °C.

Pressure/ psia	IFT/ $mN.m^{-1}$		IFT / $mN.m^{-1}$	IFT / $mN.m^{-1}$
	C1/n-C8	C1/n-C10	(A)	(B)
2500	3.35	5.04	4.39	4.76
3000	1.84	3.74	2.84	3.38
3500	0.686	2.58	1.63	2.09
3750	0.295	2.07	1.16	1.48
4000	0.013	1.49	0.696	0.997

(A) - Mixture of C1/n-C8 (51%) and C1/n-C10 (49%) by volume.
(B) - Mixture of C1/n-C8 (70%) and C1/n-C10 (30%) by volume.

Table 4.6 - Calculated Molar Compositions of Methane/n-Octane/n-Decane Ternary Mixtures.

Comp.	Methane/n-Octane/n-Decane	
	(A)	(B)
C1/ %	87.29	88.14
n-C8/ %	7.30	4.35
n-C10/ %	5.41	7.51

Table 4.7 - Calculated Molar Compositions of LRA97-1 / NCF Mixtures.

Comp.	NCF / LRA97-1 Mixes (Mix 1) | (Mix 2)			
	Mole %	MW	Mole %	MW
N2	0.06	28.01	0.30	28.01
C1	58.10	16.04	66.68	16.04
CO2	0.05	44.01	0.23	44.01
C2	9.88	30.07	9.88	30.07
C3	5.42	44.10	4.45	44.10
i-C4	1.06	58.12	0.59	58.12
n-C4	1.93	58.12	1.57	58.12
i-C5	0.97	72.15	0.44	72.15
n-C5	1.74	72.15	1.03	72.15
C6	1.45	87.2	1.09	84.6
C7	2.13	91.5	2.04	89.5
C8	2.63	103	2.38	103
C9	1.95	116	1.81	114
C10	1.62	132	1.33	132
C11	1.23	147	0.95	148
C12	0.90	162	0.69	164
C13	1.10	175	0.64	177
C14	0.82	189	0.69	187
C15	0.80	200	0.54	203
C16	0.62	218	0.41	218
C17	0.46	232	0.28	234
C18	0.51	249	0.3	250
C19	0.53	258	0.27	261
C20+	4.02	441	1.42	364

Table 4.8 - Comparison between Measured and Calculated IFT of the Methane/n-Octane/n-Decane Mixtures at 37.8 °C Using the Weinaug-Katz Model and Volumetric Averaging Approach.

Pressure/ psia	IFT(A)/ $mN.m^{-1}$			IFT(B)/ $mN.m^{-1}$			% Deviation (A)		(B)	
	Exp.	VA	WK	Exp.	VA	WK	VA	WK	VA	WK
2500	4.39	4.18	3.47	4.76	4.53	3.80	-5	-62	-5	-52
3000	2.84	2.77	1.93	3.38	3.16	2.34	-2	-56	-7	-46
3500	1.63	1.61	0.857	2.09	2.01	1.21	0	-47	-4	-42
3750	1.16	1.16	0.508	1.48	1.53	0.796	0	-32	3	-31
4000	0.696	0.738	0.268	0.997	1.05	0.484	6	-21	5	-20
					AAD / %		**3**	**44**	**5**	**38**

(A) - Mixture of C1/n-C8 (51%) and C1/n-C10 (49%) by volume.
(B) - Mixture of C1/n-C8 (70%) and C1/n-C10 (30%) by volume.
(VA) - Denotes for Volumetric Average.
(WK) - Denotes for Weinaug-Katz Model

Table 4.9 - Comparison between Measured and Calculated IFT of the LRA97-1/NCF Mixtures at 37.8 °C Using the Weinaug-Katz Model and Volumetric Averaging Approach.

Pressure/ psia	IFT(A)/ $mN.m^{-1}$			IFT(B)/ $mN.m^{-1}$			% Deviation (Mix 1)		(Mix 2)	
	Exp.	VA	WK	Exp.	VA	WK	VA	WK	VA	WK
2000	4.05	4.13	3.13	4.60	4.61	2.98	2	-23	0	-35
2500	2.32	2.38	1.48	2.80	2.79	1.71	3	-36	0	-39
3000	1.32	1.32	0.603	1.69	1.71	0.794	0	-54	1	-56
3500*	0.652	0.637	0.186	-	-	-	-2	-71	-	-
				-	**AAD / %**		**1**	**46**	**0**	**43**

Mix 1 - Mixture of NCF (81.5%) and LRA97-1 (18.5%) by volume.
Mix 2 - Mixture of NCF (14.8%) and LRA97-1 (85.2%) by volume.
(VA) - Denotes for Volumetric Average.
(WK) - Denotes for Weinaug-Katz Model.
* - Using Extrapolated IFT Value for LRA97-1.

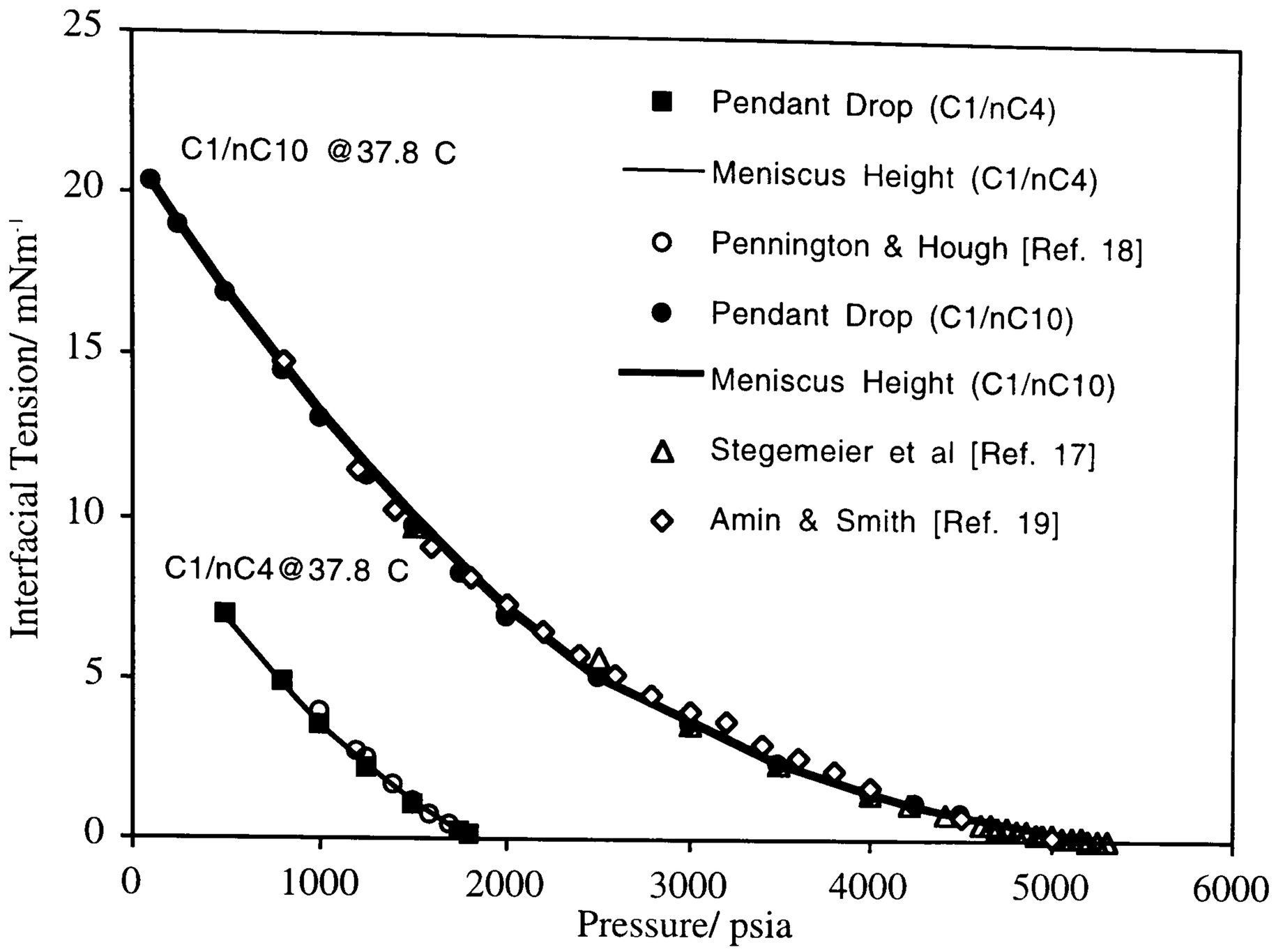

Figure 4.1 - Comparison Between Measured and Literature Interfacial Tension (IFT) vs. Pressure for C_1/n-C_4 and C_1/n-C_{10} Mixtures at 37.8 °C.

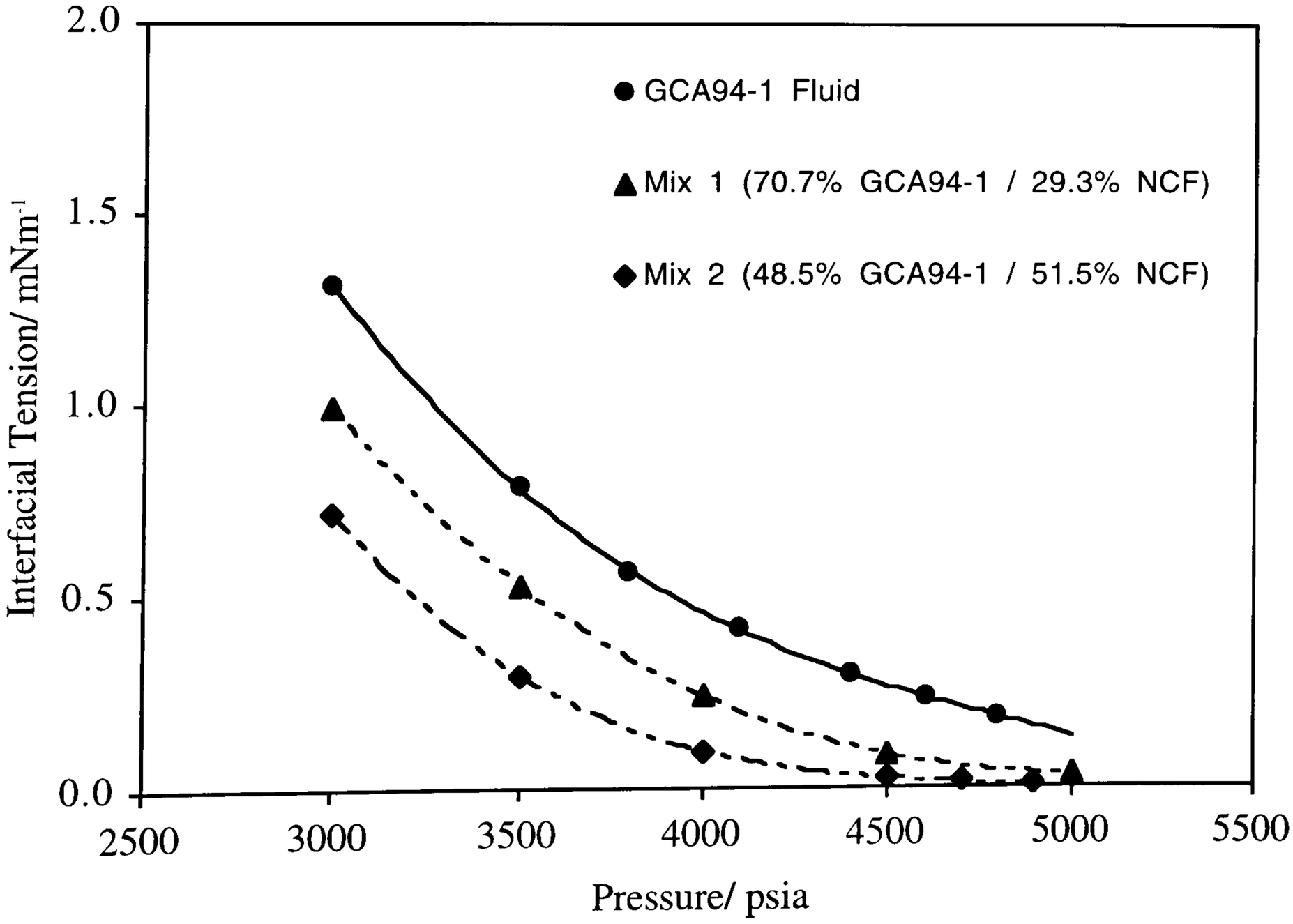

Figure 4.2 - Variation of Interfacial Tension With Pressure of GCA94-1 / NCF Mixtures at Reservoir Temperature of 110 °C.

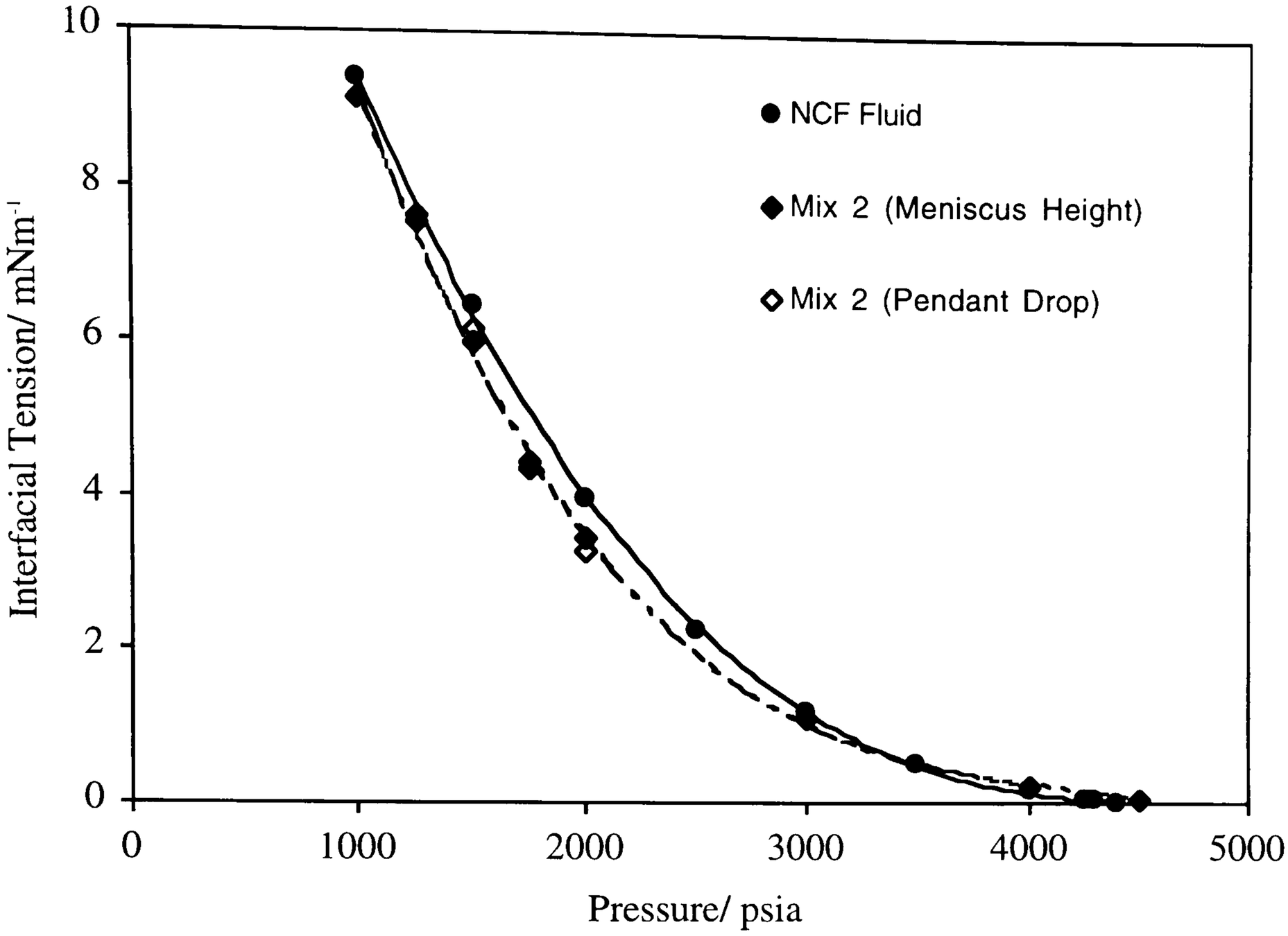

Figure 4.3 - Variation of Interfacial Tension With Pressure of GCA94-1 / NCF Mixtures at Surface Temperature of 37.8 °C.

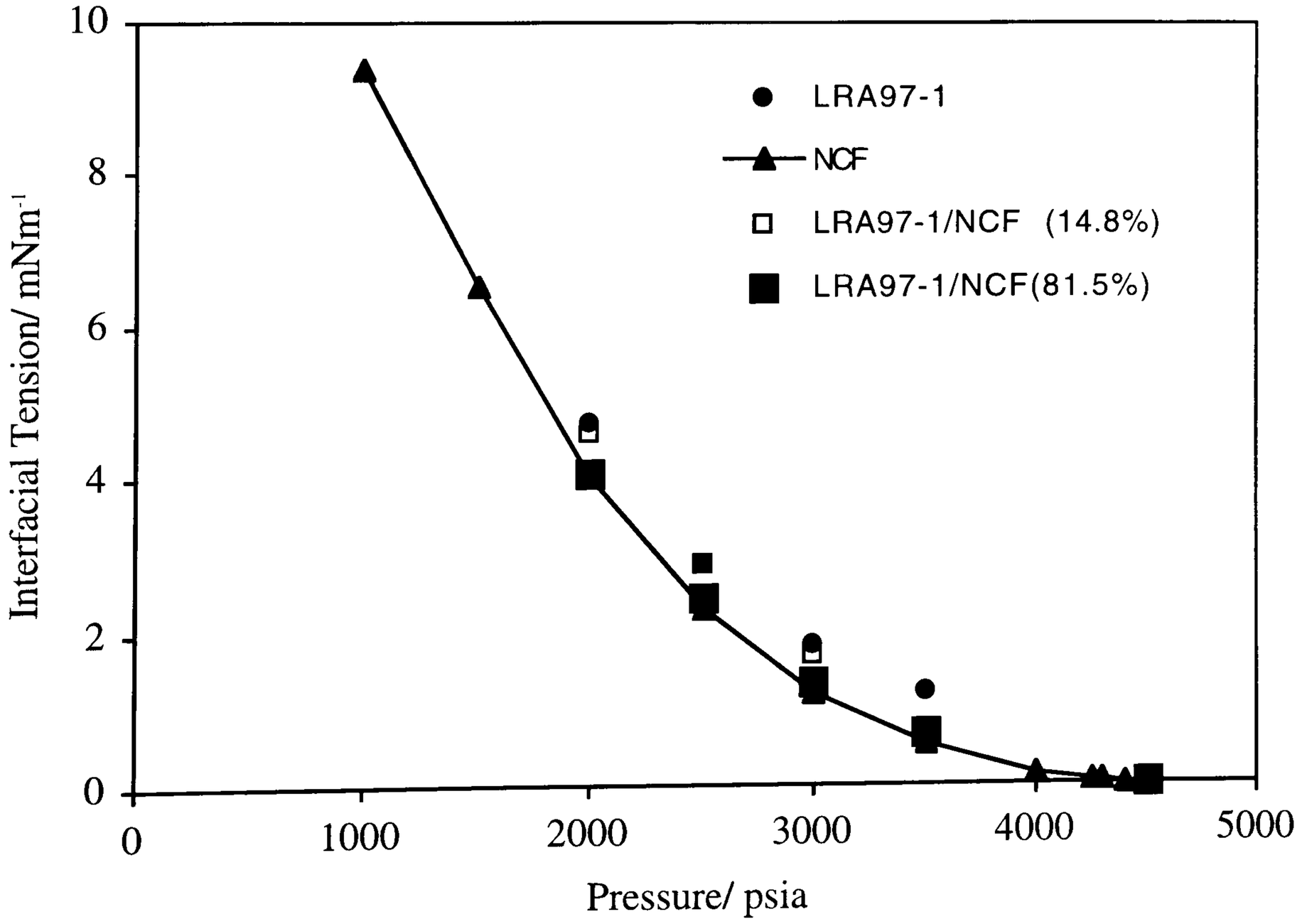

Figure 4.4 - Variation of Interfacial Tension With Pressure of LRA97-1 / NCF Mixtures at Surface Temperature of 37.8 °C.

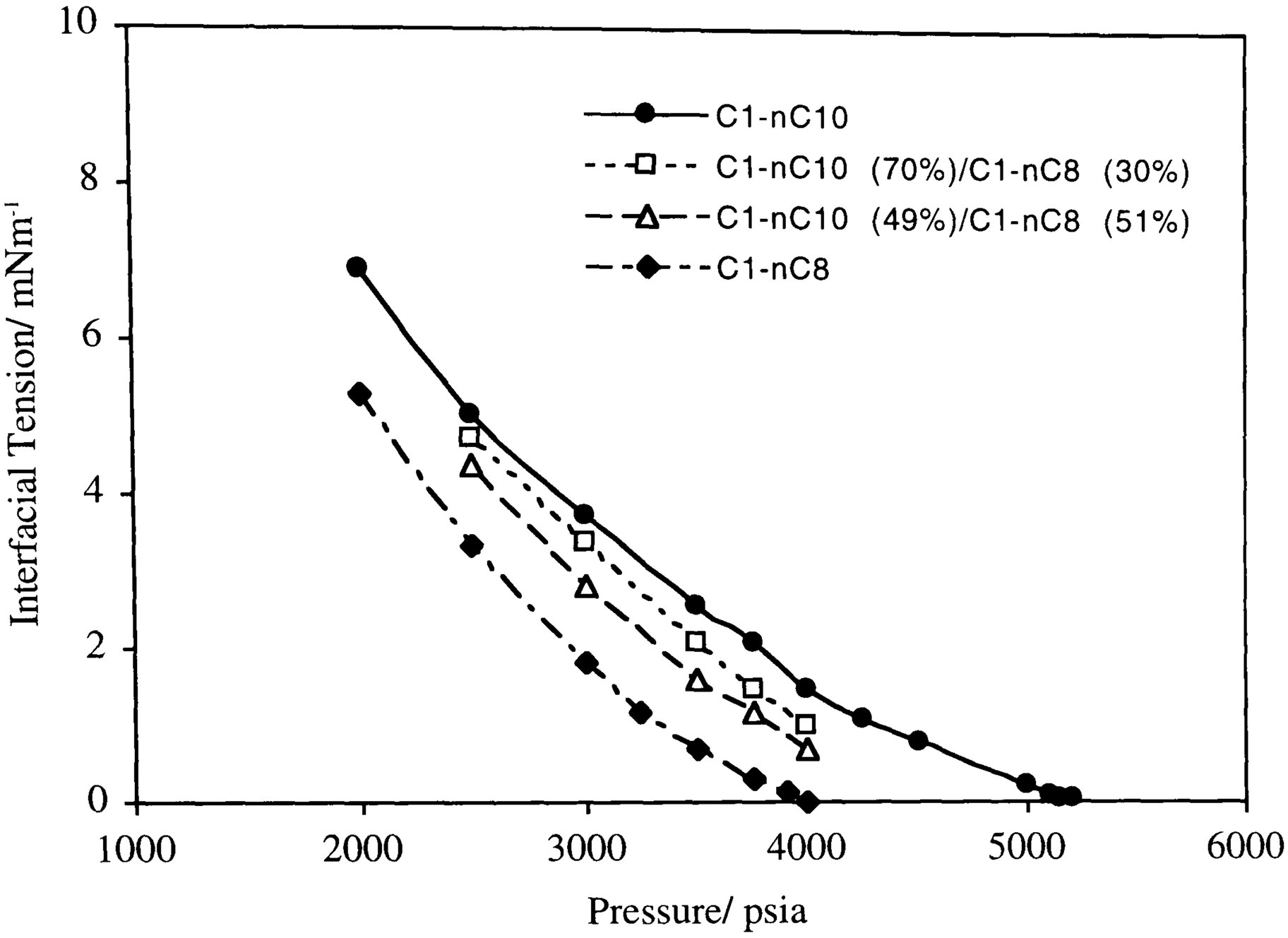

Figure 4.5 - Variation of Interfacial Tension With Pressure of methane/n-Octane, Methane/n-Decane and Their Ternary Mixtures at 37.8 °C.

CHAPTER 5

METHODS OF PREDICTING VISCOSITY

5.1 OBJECTIVES

In multi-phase flow calculations, reliable information on the viscosity of all flowing phases over a wide range of equilibrium conditions is essential for optimum process design and operational management. Viscosity predictive techniques used by the petroleum industry have been reviewed in this chapter. The residual viscosity method by Lohrenz-Bray-Clark (LBC) is the most popular method for predicting the viscosity of reservoir fluids and it is widely used in majorities of reservoir flow simulators. However, viscosity predictions, by the LBC method, for dense fluids was found to inadequate. Hence, the main objective of this chapter is:

- To modify the residual viscosity method by Lohrenz-Bray-Clark (LBC) to improve prediction of viscosity in dense fluid states.

5.2 INTRODUCTION

Viscosity is a configurational, non-equilibrium, property which reflects the effect of inter-molecular motion and interaction which tends to oppose any dynamic change in fluid motion. From a phenomenological point of view, fluid viscosity characterises the non-equilibrium process of momentum when the fluid is perturbed from equilibrium state by the application of a velocity gradient. A well known example to illustrate this transport property is to consider a fluid (e.g., gas or liquid) contained between two large

parallel plates of an area A as shown in Figure 5.1, uniformly separated by a distance y. Imagining the fluid system is initially at rest. If one further assumes that at any time, say t=0, the lower plate was set in motion and moves with a constant velocity denoted by u. As time proceeds, depending on the fluid under consideration, the fluid gains momentum and steady-state velocity profile is attained. To maintain this steady-state motion of the lower plate, a constant force, F, is required. For laminar flow behaviour, this force can be expressed as ;

$$\frac{F}{A} = \eta \frac{u}{Y} \tag{5.1}$$

or in a more general and explicit form as;

$$\tau_{xy} = -\eta \frac{du_x}{dy} \tag{5.2}$$

where,

η: viscosity.

τ_{xy}: shear stress applied on a fluid expressed as force, F, per unit area, A.

$\frac{du_x}{dy}$ the velocity gradient in the direction perpendicular to applied stress.

Equations (5.1) and (5.2) state that the shear force per unit area is proportional to the local velocity gradient, a relationship known as the *Newton's law of viscosity*[1]. Equation (5.2) also demostrates that in order for an ideal viscous fluid to start flowing it must suffers a higher strain, hence higher stress, to overcome the internal friction between molecules. The class of fluids which conform to the above relationship are termed *Newtonian* fluids, for which all gases and most simple liquids belong to. For those *Newtonian* fluids, viscosity is independent of the magnitude of the applied rate of shear or the shearing stress. Fluid systems for which the above linear relationship (Equation 5.2) is not applicable, are termed *non-Newtonian* fluids (e.g., polymers, liquid metals, slurries, colloids...etc). Unlike the *Newtonian* fluids, the viscosity of the *non-Newtonian* fluids **does** depend on the magnitude of the applied shear velocity. Different viscosity

formulations[1] have been employed to deal with the *non-Newtonian* fluids, depending on the observed fluid behaviours as shown in Figure 5.2.

Since viscosity is defined as a shear stress divided by shear velocity or rate, it should have the dimensions of $[F].[L^{-2}].[L][t^{-1}].[L]$. If one uses cgs units system where force, [F], has the units of $gr.cm.sec^{-2}$ or dyne, the length, [L], has the unit of cm and the time, [t], has the unit of sec., one may solve for the units of viscosity, η, as follows:

$$\frac{F/A}{du/dy} = -\eta = \frac{gr.cm.\sec^{-2}/cm^2}{cm.\sec^{-1}/cm} = g.cm^{-1}\sec^{-1} \qquad (5.3)$$

The resulting combined units for the viscosity, $gr.cm^{-1}.s^{-1}$, is called the *Poise*; however, most viscosity data are usually reported in *centipoises*, cP (1 cP = 0.01 Poise).

5.3 EFFECT OF TEMPERATURE AND PRESSURE ON FLUID VISCOSITY

Viscosity can be used to define the state of fluid, hence it is affected by the pressure and temperature under which the fluid is subjected under. However, the effects of those two parameters on gases are different from those on liquids. At low pressure and higher temperature conditions, gas viscosity is strongly dependent on temperature. Under these conditions, the viscosity of gases increases with increasing temperature; due to the view that increasing temperature increases the rate of momentum transfer (i.e., increasing collision frequency) between molecules, hence viscosity increases. On the other hand, gas viscosity is strongly dependent on pressure at the saturation or vapour pressure line. Generally, increasing the pressure, molecules are brought closer to each other and their mutual attraction is strengthened, hence viscosity increases. At high pressure conditions, gases behave like liquids where the increase in temperature helps the kinetic energy of molecules in overcoming the inter-molecular forces, hence viscosity decreases. Figure 5.3 illustrates the above-mentioned behaviour for gases.

The viscosity of liquids is different from that of gases both in magnitude and action. The magnitude of liquid viscosity is much higher than that of gas. Due to various inter-molecular forces that exist between liquid molecules, the effect of pressure and temperature on liquid viscosity makes it different from their effect on gas viscosity. Increasing temperature decreases liquid viscosity quite drastically. Also, at high pressure conditions, liquid viscosity was observed to increase quite sharply[2]. Figure 5.4 illustrates the above-mentioned behaviour for liquids.

The literature contains many methods for viscosity prediction, ranging from mathematically rigorous to completely empirical. Some of the techniques used for calculating fluid viscosity, in the petroleum industry, are reviewed below. More detailed descriptions about these techniques can be found in Appendix B.

5.4 KINETIC THEORY

The kinetic theory is one of the oldest theoretical description, in the literature, which describes the process of relaxation to equilibrium of transport properties from a perturbed state caused by a gradient in velocity, temperature and composition. The theory seeks to explain and relates the observable macroscopic properties of the bulk fluid to the microscopic properties in term of molecular encounters and the forces between molecules[3].

The kinetic theory treats dilute gases as ensemble of molecules each moving on its own independent path. The interaction between molecules is assumed to be through binary encounters only and the time between collisions is so large that the velocities of the two molecules which are about to collide are un-correlated. For dilute monatomic species, the viscosity at any temperature can be calculated from the following rigorous expression;

$$\eta = 0.002669 \frac{\sqrt{MW\,T}}{d^2} \tag{5.4}$$

where,

η: viscosity, cP.

MW: molecular weight, gr.mol^{-1}.

T: temperature, K.

d: molecule diameter, angstrom (°A).

However, for polyatomic gases two additional features needed to be included into the description of Equation (5.4). These features are; **(1)** molecules may possess internal energy in rotational and vibrational mode, and **(2)** the intermolecular pair potential are dependent on the orientation of the molecules[4]. Taking these features into account, the viscosity of all gasses in the dilute state can be calculated from the expression:

$$\eta = 0.002669 \frac{\sqrt{MW\,T}}{d^2 \Omega_\eta^*} \tag{5.5}$$

where, η, MW, T and d are as defined for Equation (5.4) and Ω_η^* is the viscosity collisional integral in units of square angstrom, which is related to inter-molecular pair potential functions[5]. Thus provided that the inter-molecular pair potential for the interaction is known, it is possible to calculate the viscosity of the gaseous system at any temperature to the desired degree of accuracy.

5.5 HARD-SPHERE THEORY

The most successful theoretically-based predictive techniques for predicting the transport properties of the dense fluid states are those based upon the van der Waals model[6]. The van der Waals model considers the molecules to interact through a weak long range attractive energy, as shown in Figure 5.5 (a). For real systems, the dependence of the pair

inter-molecular potential energy is much more complicated as shown in Figure 5.5 (b). The model is expected to be most applicable at high temperature where the repulsive forces dominate and at high densities where the attractive potential is more realistic.

Based on the above model, the van der Waals model has been considered for calculating the transport properties of fluids. Dymond[7] applied the Enskog[8] and modified it for the evaluation of transport properties of dense fluids, mainly liquids. For viscosity, the modified expression has the following form:

$$\eta^* = \frac{\eta}{\eta_0}\left(\frac{V}{V_0}\right)^{2/3} = 9.118x10^7 \eta V^* \Big/ \sqrt{MW\,TR} \qquad (5.6)$$

where, η, MW and T are as defined for Equation (5.4)

η^*: dimensionless viscosity function, $\eta/\eta_0(V^*)$.

η_0: viscosity of the dilute gas phase, calculated from Equation (5.4).

V: molar volume, $cm^3.mol^{-1}$.

V_0: core volume of molecule, $cm^3.mol^{-1}$.

V^*: dimensionless volume, (V/V_0).

R: universal gas constant, $gr.cm^2sec^{-2}.mol^{-1}.K^{-1}$.

The above expression (5.6) has been evaluated and found to represent the viscosity of hydrocarbon very well[7].

5.6 PRINCIPLE OF CORRESPONDING STATE METHODS

The concept of corresponding states for viscosity asserts that the reduced viscosity of fluids can be expressed as a function of reduced properties such as reduced temperature, reduced pressure or density. Hence, a reduced property of one substance is equal to that of another (reference) substance if both are evaluated at the same reduced conditions. Methods based on the above concept require methodologies to choose the optimum

reference fluid and to calculate the critical properties for plus-fraction cuts. In these methods, mixture is represented by a hypothetical pure component fluid with critical properties and molecular weight calculated using some mixing rules[9.10].

5.6.1 The Extended Corresponding State Method (TRAPP and SUPERTRAPP)

Ely and Hanley[11] have presented a corresponding state model for the prediction of fluid viscosity. The viscosity of a fluid at a given density and temperature is calculated using the functional form below;

$$\eta(\rho,T) = \eta_{ref}\left(\rho_{ref}, T_{ref}\right) F_{\eta} \tag{5.7}$$

where;

$\eta(\rho,T)$: viscosity of fluid of interest.

$\eta_{ref}(\rho_{ref},T_{ref})$: viscosity of reference fluid.

ρ_{ref} , T_{ref}: equivalent density and temperature, evaluated from expressions in Appendix B.

F_{η}: corresponding state reducing factor, evaluated from expressions in Section B.1.1 of Appendix B.

The original version of the above corresponding state method (TRAPP) uses methane as a reference fluid for viscosity calculation. However, since methane freezes at low reduced temperatures (T_r<0.4), the reference fluid has been changed to propane in its newer version.. The method uses two shape factors, $\Theta(T_r, V_r, \omega)$ and $\Phi(T_r, V_r, \omega)$, to account for deviations from the corresponding state principle. The method has been tested for variety of fluids and their mixtures and found to predict the viscosity to within an absolute deviation of 8%.

The TRAPP method was further modified to improve viscosity prediction for cyclic compound and highly branched alkanes[12]. The modified version is called

SUPERTRAPP which was found, generally, to improve viscosity prediction, especially those for cyclic compounds and branched alkanes[6,12].

5.6.2 The One-reference Fluid (CS1) Method

The origin of the above method is the method of Tham and Gubbin[13] which was developed for predicting the viscosity of pure liquid hydrocarbons. As in the extended corresponding state method, the one-reference fluid method, above, uses methane as the reference fluid. Due to molecular size and density effects, a rotational coupling factor, α_{TG}, was introduced to account for the non-conformance of some substances from the above corresponding states principle. Pedersen *et al* [14,15] generalise the above method for gas and liquid mixtures by employing Mo and Gubbin mixing rules[10] for calculating mixture critical properties. Based on the above method, the viscosity of any substance can be determined from the following expression;

$$\eta(P,T) = \left(\frac{\eta_c}{\eta_{c,ref}}\right)\eta_{ref}\left(P_{ref}, T_{ref}\right)F_\eta \qquad (5.8)$$

where,

$\eta(P,T)$: viscosity of fluid of interest.

$\eta_{ref}(P_{ref},T_{ref})$: viscosity of reference fluid.

P_{ref} , T_{ref}: equivalent pressure and temperature, respectively, evaluated from expressions in Section B.1.2 of Appendix B.

η_c: critical viscosity, $\eta_c = C\dfrac{MW^{1/2}\,P_c^{2/3}}{T^{1/6}}$ (5.9)

P_c , T_c: critical pressure (atm) and temperature (K), respectively.

C: constant.

F_η: corresponding state reducing factor, taken as the ratio of the rotational coupling factor of fluid of interest and the reference fluid. The rotational coupling factors for the reference fluid and the fluid of interest are evaluated from expressions in Appendix B.

The viscosity of the reference fluid and other fluid properties are evaluated as described in Section B.1.2 of Appendix B. The model give reasonable results for simple fluids, however, it poorly predicts the viscosity of hydrocarbon mixtures whose size and shape are considerably different from that of the reference component. However, if proper characterisation of the plus-fraction is performed, the method found to give good prediction for predicting the viscosity of real fluids[16].

5.6.3 The Two-reference Fluids (CS2) Method

Due to the deficiency of the above one-reference method for systems which are considerably different from methane, Petersen *et al* [17] developed an improved method which uses two reference fluids. The chosen reference fluids are methane and n-Decane. The model predicts the viscosity of any fluid from the reduced viscosity of the reference components using the molecular weight as an interpolating parameter using the expression below;

$$\eta(P,T) = \frac{\eta_c \eta_1(T_1,P_1)}{\eta_{c1}} \left(\frac{\eta_2(T_2,P_2)\eta_{c1}}{\eta_1(T_1,P_1)\eta_{c2}} \right)^K \tag{5.10}$$

where;

K: an interpolating factor, $K = \dfrac{MW - MW_1}{MW_2 - MW_1}$ (5.11)

1, 2: 1 refers to methane and 2 refers to n-Decane.

The viscosity of the reference fluids and fluid molecular weights are evaluated as described in Section B.1.3 of Appendix B. The model has been tested, by the authors, against pure component and mixture viscosities. Good agreement with experimental data were obtained, however, authors do not recommend to use the model for mixtures containing large amount of naphthenic components and for reduce temperature less than 0.47.

5.7 RESIDUAL VISCOSITY CORRELATIONS

The concept of residual viscosity was based on the empirical observation that the difference between the viscosity of dense phase and that of the dilute gas is approximately independent of temperature and primarily a function of density. For viscosity calculation, the normal viscosity of fluid is expressed as the sum of two viscosity terms both evaluated at the same temperature;

$$\eta(\rho,T) = \Delta\eta(\rho) + \eta_0(T) \qquad (5.12)$$

where;

$\Delta\eta$: residual viscosity term.

η_0: viscosity of dilute gas phase.

5.7.1 The Jossi-Stiel-Thodos (JST) Method

Jossi *et al* [18] utilised Abas-zade relationship[19] for thermal conductivity, to correlate the viscosity data of substances in gaseous and liquid states. A generalised relationship between viscosity and fourth degree polynomial of the reduced density (ρ_r), of the form below, for non-polar gaseous and liquid substances, was formulated;

$$\left[(\eta-\eta_o)\zeta+10^{-4}\right]^{1/4} = a_0 + a_1\rho_r + a_2{\rho_r}^2 + a_3{\rho_r}^3 + a_4{\rho_r}^4 \qquad (5.13)$$

where;

ζ: viscosity reducing parameter which is the inverse of critical viscosity, Equation (5.9).

ρ_r: reduced density.

$a_{0\text{-}4}$: correlation coefficient having the values; 0.10230, 0.023364, 0.058533, -0.040758 and 0.0093324, respectively.

For monatomic compounds, the dilute gas viscosity, η_o, can either be evaluated from kinetic theory (Equation (5.4)) or obtained from the following empirical expression as a function of reduced temperature, T_r;

$$\eta_o \zeta_i = 0.00034 T_r^{0.94} \qquad \text{for } T_r \leq 1.5 \qquad (5.14)$$

$$\eta_o \zeta_i = 0.0001778 \left[4.58 T_r^{0.94} - 1.67 \right]^{5/8} \qquad \text{for } T_r > 1.5 \qquad (5.15)$$

The properties (T_r and ρ_r) are evaluated from the following equations;

$$\rho_r = \frac{\rho}{\rho_c} \qquad (5.16)$$

$$T_r = \frac{T}{T_c} \qquad (5.17)$$

The above correlation is valid in the range of $0.1 \leq \rho_r < 3$. For polar compounds, different correlations were developed. The major drawbacks from the above correlation is that it is very sensitive to changes in density which can lead to severe error in the calculated viscosity if miscalculated.

5.7.2 The Lohrenz-Bray-Clark (LBC) Method

Lohrenz *et al* [20] extended the above correlation for calculating the viscosity of mixtures of naturally occurring hydrocarbons. A procedure for calculating viscosities of hydrocarbon mixtures has been developed through the application of appropriate mixing rules[9,21]. The mixture reducing parameter, Equation (5.9), can be calculated by molar averaging mixture critical properties and molecular weight, as shown below:

$$\zeta = \frac{\sum_{i=1}^{n}\left(x_i\, T_{ci}\right)^{1/6}}{\sum_{i=1}^{n}\left(x_i\, P_{ci}\right)^{2/3}\ \sum_{i=1}^{n}\left(x_i\, MW_i\right)^{1/2}} \qquad (5.18)$$

The low pressure mixture viscosity is calculated by the formulation of Herning and Zipprer[21] of the form;

$$\eta_o = \frac{\sum_{i=1}^{n}\left(x_i\, \eta_{oi}\sqrt{MW_i}\right)}{\sum_{i=1}^{n}\left(x_i\, \sqrt{MW_i}\right)} \qquad (5.19)$$

where, η_0, MW are as defined above and x_i is the mole fraction of component i in the mixture. Likewise, the mixture reduced density is calculated by Equation (5.16) where the critical density can be computed from Equation (5.20) below;

$$\rho_c = \frac{1}{V_c} = \frac{1}{\sum_{\substack{i=1 \\ i\neq C7+}}^{n}\left(x_i\, V_{ci}\right) + x_{C7+}\left(V_c\right)_{C7+}} \qquad (5.20)$$

where; $(V_c)_{C7+}$ is the critical molar volume of the C7+ plus-fraction calculated from the following expression;

$$V_{cC7+} = 21.573 + 0.015122MW_{C7+} - 27.656SG_{C7+} + 0.070615MW_{C7+}SG_{C7+} \qquad (5.21)$$

The above method is the most popular method for predicting the viscosity of hydrocarbon fluids at reservoir conditions and predominantly used in majority of reservoir flow simulators. The procedure requires that compositions of C1 through C7+ and the molecular weight and specific gravity of the latter must be known.

Extensive evaluation of the LBC method was carried out by Dandekar *et al*[22]. The authors observed that the LBC correlation gives reasonable viscosity predictions for reduced density less than 2.5. The method was then modified to improve its prediction for the dense fluid states as discussed in the following section (Section 5.7.3).

5.7.3 The Modified Lohrenz-Bray-Clark Method (HW1)

Dandekar *et al* [22] evaluated Equation (5.13) and concluded that the above correlation is accurate to within ±20%. for all normal alkanes with carbon number less than 8 (n-Octane) and reduced density less then 2.5. Fluids with molecular weight higher than that of n-Octane and reduced density higher than 2.5, the authors proposed a residual viscosity correlation, Equation (5.22), which relates the reduced viscosity to the molecular weight in addition to the reduced density, as in the following expression;

$$(\eta - \eta_o)\zeta = EXP\left(A + B\rho_r + C\rho_r^2\right) \tag{5.22}$$

where;

$$A = 9.8338 - 0.15568MW + 1.8935x10^{-4}MW^2 \tag{5.23}$$

$$B = -12.150 + 0.10345MW - 1.3971x10^{-4}MW^2 \tag{5.24}$$

$$C = 2.3990 - 1.6355MW + 2.5338x10^{-5}MW^2 \tag{5.25}$$

Mixture critical properties, molecular weight and low pressure gas viscosity are calculated in the same way as for the original LBC. However, the critical volume of the C7+ fraction for the above formulation can be calculated from Equation (5.26), below, which was optimised by matching predicted and measured mixture viscosities;

$$V_{cC7+} = -10.329 + 0.1257MW_{C7+} + 15.461SG_{C7+} - 0.08587MW_{C7+}SG_{C7+} \tag{5.26}$$

The above modified correlation (Equation (5.22)) was used for estimating the viscosities of various hydrocarbon mixtures and found to improve viscosity prediction[23]. However, the improvement in predicting the viscosity of highly branched alkanes was considered

not enough which warrant further investigation. An extensive evaluation was conducted (which is the main objective of this chapter) as discussed in Section 5.7.4 below.

5.7.4 The Modified Residual Viscosity Correlation (HW2)

As mentioned above, the LBC method is the most popular method for predicting fluid viscosity in the petroleum industry and widely used in majority of reservoir flow simulators. However, it was found that the predictive capability of this method deteriorate as the density of fluid increases (i.e., liquid phase). A large amount of data were gathered and evaluated for its internal consistency and accuracy. The JST correlation, Equation (5.13) was modified by incorporating the effect of temperature and molecular weight in its coefficients as will be described later in this section.

Using the modified correlation (HW2) for methane, deviation higher than 20% were observed for reduced density greater than 1.5. As real reservoir fluids contain high concentration of methane, a dedicated correlation for it would improve viscosity prediction for these fluids. Hence, for mixtures containing methane a mixing rule is employed for calculating the overall mixture viscosity.

The modified correlations, referred to as HW2, have been extended for predicting the viscosity of real reservoir fluids. A correlation for the critical volume of the plus-fraction, taken as C7+, has been developed by matching predicted and literature mixture viscosities. The modified correlation (HW2) was then applied to predict the viscosity of various binary hydrocarbon gaseous and liquid mixtures, high pressure-high temperature fluids (with and without water), and variety of real reservoir fluids and compared to that of the CS1 (Section 5.62), CS2 (Section 5.6.3), LBC (Section 5.7.2) and HW1 (Section 5.7.3) viscosity models.

Data Analysis. The development of a reliable correlation for pure components was considered a desirable first step in the evolution of a general correlation for predicting the viscosities of complex hydrocarbon systems. It is also desirable to make use of all available experimental data over a wide range of thermodynamic phase space for as many

fluids as possible for the development of a general correlation. However, the reliability of a developed correlation relies heavily in the accuracy of the experimental data used to develop it.

Literature density and viscosity data on; Nitrogen[24-26], Carbon Dioxide[27-29], Methane[30-33], Ethane[28,31,34], Propane[30.31,35], n-Butane[31,36,37], n-Pentane[31,37-40], n-Hexane[37-44], n-Heptane[39,41,45], n-Octane[37-40,44,46], n-Nonane[45], n-Decane[31,39.47], n-Undecane[45], n-Dodecane[44,46-48], n-Pentadecane[48], n-Hexadecane[43,46], and n-Octadecane[48] at various temperatures were amassed and evaluated for internal consistency and accuracy. For compounds where there exists large amount of data, measured viscosity with an inaccuracy of ±2% were considered to be candidates to use in the development of the new correlation. However, at higher pressure conditions and for compounds where viscosity data are scarce, the above inaccuracy limit was relaxed to ±5%. Table 5.1 gives a summary of fluids (used in developing the modified correlation discussed below) and their temperature and density ranges, and type of viscometers employed in their viscosity measurements along with authors claimed accuracy.

Development of the Modified Correlation. After establishing the desired accuracy limits for the available literature viscosity data, plots of reduced residual viscosity versus reduced density for the above-mentioned compounds were constructed as shown in Figures 5.6 (a) and (b). It is clear from these plots (Figures 5.6 (a) and (b)) that reduced viscosity data for all compounds all collapsed into a single curve, for reduced density less than 2.5 which on-line with what Jossi *et al*[18] had demonstrated in their analysis. However, for higher values of reduced density, a large scatter in the reduced residual viscosity data is evident. The observed scatter (in the reduced residual viscosity data) at higher reduced densities is believed to be due to molecular structural effects as well as temperature effects which have been ignored by Jossi *et al*[18].

As mentioned above (in Section 5.7.3) that Dandekar *et al* [22] did account for the structural effect; however, this alone is believed to be not enough which did not significantly improve their model's predictions for higher reduced density values. As an

initial check in assessing whether the observed scatter is due to the above-mentioned effects, plots of reduced residual viscosity versus reduced temperature at two reduced density values (3.10 and 3.15) were constructed as shown in Figures 5.7 (a) and (b). It is clear from both plots that both the thermal and structural effects should be accounted in order to improve viscosity prediction for dense fluids.

Having identified both effects, a simple model similar to that of JST (Equation (5.13)) was sought for. This was accomplished by relating the coefficients appearing in the JST correlation to the reduced temperature, T_r, and a suitable substance structural property. A number of structural properties such as acentric factor and molecular weight were considered. Preliminary studies showed that molecular weight is the most suitable parameter.

A least-square function was used to regress a total of 2789 viscosity data point to minimise an objective function taken as the sum of square deviation between experimental and calculated values. The ranges of data used for the regression analysis are 0.0 - 0.55 (0.01 - 15 cP) for reduced viscosity, 0.0 - 4.0 for reduced density, and 0.243 - 2.33 for reduced temperature. The correlation, with the coefficient and exponent values below, was found to be the most optimum;

$$\left(\Delta\eta_r + 10^{-4}\right)^{1/4} = \begin{pmatrix} 0.094754 + 0.062016\rho_r - 0.0010273T_r^{-2.0183}MW^{0.44620}\rho_r^2 + \\ 0.00040403T_r^{-2.47063}MW^{0.19188}\rho_r^3 + 0.000086159T_r^{-1.1577}MW^{0.58683}\rho_r^4 \end{pmatrix} \quad (5.27)$$

Comparison of Viscosity Prediction Between the JST and the Modified Correlation, Equation (5.27). The deviation of predicted viscosities from experimental values using the JST correlation (Equation (5.13)) and the above modification (Equation (5.27)) are plotted in Figures 5.8 and 5.9. Comparing Figures 5.8 and 5.9, it can be clearly demonstrated that the deviation of predicted viscosity using both correlations are in the same range for reduced density less than 2.5. For higher reduced densities, the JST correlation is seen to diverge in both direction (relative to 0%) to within ±100%, while the deviation of the modified correlation is within ±20% demonstrating the importance of

including both thermal and structural effects for reliable viscosity prediction for a wide range of thermodynamic phase space. However, for methane viscosities, deviations higher than 20% can be observed using the above proposed correlation. Similar trend was also observed by Assael *et al*[49] at the same reduced density range. van der Gulik *et al*[50] also observed that the viscosity of methane at higher densities did not follow the expected trend, which they attributed to hindered rotation of molecules.

Since real reservoir fluids contains high concentration of methane, it is imperative to develop a separate correlation for it to ensure reliable viscosity prediction for real reservoir fluids. Although there mighe exist a comprehensive correlation for methane, however, to mentian the same consistency with the above correlation (Equation (5.27)), similar procedure was followed. The same least square function was used above for correlating methane viscosity data. The correlation below was found to be optimum;

$$\left(\Delta\eta_r + 10^{-4}\right)^{1/4} = \left(0.10202 + 0.055258\rho_r - 0.011430\rho_r^2 + 0.0047894\rho_r^3 + 0.0000794T_r^{-3.2508}\rho_r^4\right) \quad (5.28)$$

The deviation of the developed correlation for methane was compared to that of JST in Figure 5.10, which clearly improved it viscosity prediction, especially at higher reduced densities.

Viscosity Calculation Procedure. Using the above correlations, Equations (5.27) and (5.28), for calculating the viscosity of various mixtures, a procedure has been developed as explained below;

The procedure employed in calculating mixture viscosity using the above-mentioned equations is similar to that employed by the LBC method. To use Equations (5.27) and (5.28) for mixtures containing Methane, the mixture is split into two components; one being Methane and the other is the lumped pseudo-component. The mixture viscosity is then calculated from the above two equations as follow:

- The Methane reduced residual viscosity is evaluated from Equation (5.28) using the overall mixture reduced density and reduced temperature evaluated from Equations (5.16) and (5.17), respectively.
- The reduced residual viscosity of the second component is evaluated from Equation (5.27), using the overall mixture reduced density, reduced temperature and molecular weight.
- The mixture reduced viscosity is calculated, by the molar average mixing rule, as in Equation (5.29) below:

$$\Delta\eta_r = x_{C1}\Delta\eta_{r,C1} + (1 - x_{C1})\Delta\eta_{r,C2} \tag{5.29}$$

where;

$\Delta\eta_r$: mixture reduced residual viscosity.

$\Delta\eta_{r,C1}$: reduced residual viscosity of methane calculated from Equation (5.28).

$\Delta\eta_{r,C2}$: reduced residual viscosity of lumped component (excluding methane) calculated from Equation (5.27).

x_{C1}: molar composition of methane in the mixture.

- The mixture viscosity can then be obtained after dividing mixture reduced residual viscosity (calculated from Equation (5.29)) by the overall mixture viscosity reducing parameter, ζ, Equation (5.19), and adding the resultant to the overall mixture dilute gas viscosity, Equation (5.20).

5.7.5 Application of the Modified Correlations For Calculating Mixture Viscosities

The procedure described above was employed for a number of binary and multi-component mixtures (synthetic and real) at wide ranges of temperature and pressure, also in the presence of water, and described in the subsequent sections. Table 5.2 gives a summary of those fluids and their temperature, density and pressure ranges.

Binary Mixtures. Literature viscosity and density data[31,50-53] for a number of binary gaseous and liquid mixtures were used to test the modified correlation. The deviations of

the proposed procedure for binary mixture and that of the LBC are plotted in Figures 5.11 through 5.14. It is very clear from those plots (Figures 5.11 through 5.14) that the deviations from the proposed procedure is well within ±5% in most cases (the exception of some few methane/n-Decane data) supporting the reliability of the proposed correlation and the calculation procedure. Furthermore, the correlations were then applied to a number of binary n-alkanes liquid mixtures. Comparing the deviations of the predicted viscosity for these liquid mixtures shown in Figure 5.15, it can be clearly shown that using the modified correlation (HW2) reduced the deviation by more that 50% when compared to those of the LBC. Table 5.3 gives a summary of some statistical measures of the LBC method and its proposed modifications, HW2, along with those for HW1, CS1 and CS2 methods, for the above-tested binary mixtures. The statistical measures listed in Table 5.3 clearly demonstrate the superiority of the proposed modification, HW2.

Multi-components Fluids. To examine the reliability of Equation (5.29) for multi-component fluids, a variety of multi-component fluids were prepared, in conjunctions with the on-going phase behaviour and fluid properties modelling project[54-57]. These fluids range from synthetic 6-components mixtures with and without water to complex real reservoir fluids which are discussed below. The compositional, density and viscosity data of those fluids were taken from the above references[23,54-57].

Synthetic Fluids. Figures 5.16 through 5.19 show the predicted viscosity for the synthetic HPHT gas condensate and volatile oil fluids (with and without water) using LBC, HW1 and HW2 correlations.

For the lower pressures, all the three correlation predicted the same viscosities, however; at higher pressures viscosity predictions from the modified correlation, HW2, is far better than those of the LBC and HW1 correlations. The deviation of predicted viscosities from LBC were reduced by more than 50% when the HW2 correlation is used. More importantly is that the presence of water (which is polar and possesses different bonding than those in hydrocarbons) in hydrocarbon fluids did not effect the predictive capability

of the developed correlation. It is worth pointing out that HW1 correlation does not come into play for reduced density lower than 2.5. For this reason, the predicted viscosities by the LBC and HW1 are not differentiable.

Real Reservoir Fluids. As a continuous assessment on the predictive capability of the developed correlation, HW2, a variety of multi-components gas condensate, volatile oils and near-critical fluids were considered. Pseudo-components and plus-fractions are generally used to describe real reservoir fluids. For viscosity prediction, one needs to calculate the critical properties of these fractions (pseudo-components and plus-fractions) from various correlations. The critical temperature and pressure are calculated using the Twu correlation[58]. For the LBC and HW1 correlations, the critical volume of the lumped fraction is calculated using a dedicated correlation based on the molecular weight and specific gravity of that fraction.

A similar approach was adopted for the HW2 correlation and was used to match measured[16,59] and predicted viscosities. A least square multi-variable regression function was then used to develop a correlation for calculating the critical volume of the lumped fraction, by minimising an objective function taken as the sum of square deviations between predicted and matched critical volumes. The coefficients in the equation below;

$$V_{cC7+} = -6.6458 + 0.1492MW_{C7+} + 8.5467.SG_{C7+} - 0.09921MW_{C7+}SG_{C7+} \qquad (5.30)$$

were found to be the most optimum values. The range of molecular weight and specific gravity of the plus fraction used to optimised the coefficients of Equation (5.30) were 145 - 396 gr.mol^{-1} and 0.7927 - 0.9165, respectively. The percentage average, absolute average and standard deviations of Equation (5.30) are 0.2%, 5% and 7%, respectively.

Using mixture compositional and density data, the viscosities were predicted using the LBC, HW1, CS1, CS2 and HW2 models. The predicted viscosities, by the five models, are compared to the measured ones and plotted with pressure as in Figures 5.20 through 5.26. For the gas condensate GCB98-1 (Figure 5.20), all models predicted the single

phase viscosity very well. However, the predicted viscosity for the saturated liquid from the LBC, CS1 and CS2 model largely deviated from experimental values, while those predicted by the HW1 and HW2 were better. The predicted saturated liquid viscosities by the HW2 correlation were almost overlaying those measured.

For the volatile oils LRA97-1 and LRA97-1 with 14.8% of NCF (Figures 5.21 and 5.22). all models under-predicted both the single phase and saturated liquid viscosities. The LBC method seems to predict the viscosity of the single phase better, while the HW2 method is better in predicting saturated liquid viscosities.

The developed correlation, HW2, was also tested against measured viscosities of the near-critical fluid, NCF (discussed in Chapter 6), and compared to those predicted by the LBC, HW1, CS1 and CS2 models. The predicted viscosities from all models and those measured are plotted with pressure in Figure 5.23. Comparing the predicted viscosity by the various models, the LBC and HW1 models are seen to largely under-predict the viscosity; while CS1 and CS2 are seen to largely over-predicted the same further away from the critical region. The predicted viscosities from the HW2 model are seen to overlay those measured outside the critical viscosity enhancement region (discussed in Chapter 6).

High pressure and temperature viscosity and density data of a gas condensate sample were also used for assessing the reliability of the modified correlation. Figures 5.24 through 5.26 show the measured and predicted viscosities of the above sample. The predicted viscosity by the modified correlation, at all the three temperatures and various pressures, were comparable to the measured data in most of the cases.

The overall statistical measures for the above fluids, for all models, are listed in Table 5.3. The above assessments clearly show that the developed correlation (HW2), is superior to the LBC, HW1, CS1 and CS2 in predicting the viscosity for a variety of synthetic and real reservoir fluids.

Cyclic and Aromatic Fluids. To further asses the reliability and the soundness of the proposed modification for fluids with high concentration of cyclic and aromatic compounds, the developed correlation, Equation (5.29), was applied to predict the viscosity of the binary mixtures of methane/methylcyclohexane and Methane/cis-Decahydronaphthalene at temperatures of 50, 100 and 150 °C.

Figures 5.27 an 5.28 show the deviations of predicted methane/methylcyclohexane and Methane/cis-Decahydronaphthalene viscosity by both the LBC and its recent modification (HW2) from their measured viscosity data. For the methane/methylcyclohexane mixtures (Figure 5.27), the deviation of predicted viscosities by the modified correlation (HW2) is comparable to that of the LBC in most of the cases and better in others. However, for the methane/cis-Decahydronaphthalene mixtures (Figure 5.28), the predicted viscosities by the LBC and HW2 correlations were seen to largely deviate from experimental data for high cis-Decahydronaphthalene (*cis*-DHN) concentration. The predicted viscosities at low *cis*-DHN concentration were comparable to those predicted by the LBC correlation.

5.8 CONCLUSIONS

- The most widely used methods for predicting viscosity in the petroleum industry have been reviewed in Sections 5.4 through 5.7. The residual viscosity method of LBC is the most popular one.
- The JST residual viscosity correlation (Equation (5.13)) has been modified by incorporating the thermal and structural effects, in addition to reduced density. The modified correlation (Equation (5.29)) has been shown to improve viscosity prediction, especially at higher reduced density values.
- The modified correlation (Equation (5.29)) has been used for calculating mixture viscosity for a variety of binary hydrocarbon and carbon dioxide systems and proved to be superior to all tested viscosity prediction methods.

- Viscosity prediction for a variety of multi-components fluids, using the modified correlation, even at high pressure-high temperature conditions, with and without water proved its reliability and superiority to the residual viscosity models (LBC and HW1) and the corresponding viscosity models (CS1 and CS2).
- The modified correlation has been used for calculating mixture viscosity for high pressure-high temperature binary systems of methane/methylcyclohexane and methane/cis-Decahydronaphthanlene. Both the LBC and the modified correlation were comparable for predicting the viscosity of Methane/Methycylclohexane systems. However, both were seen to largely deviate from experimental values for higher cis-Decahydronaphthanlene concentrations.

REFERENCES

[1] Bird, R. B., Stewart, W. E., and Lightfoot, E. N.: Transport Phenomena, Wiley & Sons Inc., New York (1960).

[2] Reid, R. C., Prausnitz, J. M. and Poling, B. E. : The Properties of Gases and Liquids, 4th Edition, McGraw Hill Book Company, New York, (1987).

[3] McCourt, F. R. W. : "Status of Kinetic Theory" in Status and Future Developments in the Study of Transport Properties, Edited by W. A. Wakeham, A. S. Dickinson, F. R. W. McCourt and V. Vesovic, Kluwer Academic Publishers, Netherlands, 117-153, (1992).

[4] Vesovic, V. and Wakeham, W. A. : "Transport Properties of Supercritical Fluids and Fluid Mixtures" Chapter 6 in Supercritical Fluid Technology: Reviews in Modern Theory and Applications, Edited by Bruno, T. J. and Ely, J. F., CRC Press, Florida (USA), 245-289, (1991).

[5] Maitland, G. C., Rigby, M., Smith, E. B. and Wakeham, W. A. : Intermolecular Forces: Their Origin and Determination, Clarendon Press, Oxford, (1981).

[6] Millat, J., Dymond, J. H. and Nieto de Castro, C. A. : Transport Properties of Fluids: Their Correlation, Prediction and Estimation, Cambridge University Press, New York, (1996).

[7] Dymond, J. H. : "Correction to the Enskog Theory for viscosity and thermal conductivity", Physica, **114B**, 267-276, (1987).

[8] Enskog, D. :Kinctische Theoric der Vorgange in massig verdunnten Gases, Almqvist and Wiksell, Uppsala, (1917).

[9] Kay, W. B. : "Density of Hydrocarbon Gases and Vapors", Ind. Eng. Chem. (I & EC), **28**, 1014, (1931).

[10] Mo, K. C. and Gubbins, K. E. : "A Modified Benedict-Webb-Rubin Equation of States for Methane Using Recent Experimental Data", Cryog., **14**, 276, (1974).

[11] Ely, J. F. and Hanley, H. J. M. : "Prediction of the Viscosity and Thermal Conductivity in Hydrocarbon Mixtures- Computer Program, TRAPP", Proceedings of the 60th Annual Convention of Gas Processors Association, 20-29, (March, 1981).

[12] Ely, J. F. and Huber, M. L. : NIST Standard Reference Database 4, Computer program SUPERTRAPP, NIST thermophysical Properties of Hydrocarbon Mixtures, Version 1, (1990).

[13] Tham, M. J. and Gubbins, K. E. : "Correspondence Principle for Transport Properties of Dense Fluids", Ind. Eng. Chem. (I & CE) Fund., **9**, 63-70, (1970).

[14] Pedersen, K. S., Fredensland, Aa., Christensen, P. L. and Thomassen, P.: "Viscosity of Crude Oils", Chem. Eng. Sci., **39**, 1011-1016, (1984).

[15] Pedersen, K. S., and Fredenslund, Aa. : "An Improved Corresponding States Model for the Prediction of Oil and Gas Viscosities and Thermal Conductivities," Chem. Eng. Sci., **42**, 182-186, (1987).

[16] Pedersen, K. S., Fredenslund, Aa., Christensen, P. L. and Thomassen, P. : Properties of Oils and Natural Gases, Contribution in Petroleum Geology and Engineering, Gulf Publishing Company, Houston, Texas (USA), (1989).

[17] Petersen, Aa., K., Knudsen, K. and Fredenslund, Aa. : "Prediction of Viscosities of Hydrocarbon Mixtures," Fluid Phase Equilib., **70**, 293-308, (1991).

[18] Jossi, J. A., Stiel, L. I., and Thodos, G. : "The Viscosity of Pure Substances in the Dense Gaseous and Liquid Phases" AICHEJ, **8**(1), 59-63, (1962).

[19] Abas-zade, A. K., "The law of Heat Conduction of Liquids and Vapors", zh. Eksp. Teor. Fiz., **23**, 60-64, (1952).

[20] Lohrenz, J., Bray, B. G. and Clark, C. R. : "Calculating Viscosities of Reservoir Fluids from Their Compositions", J. Pet. Tech. (JPT), 1171-1176, (Oct., 1964).

[21] Herning, F. and Zipprer, L. :"Calculation of the Viscosity of Technical Gases Mixtures from the Viscosity of Individual Gases" Gas u. Wasserfach. **79**(49), 69. (1936).

[22] Dandekar, A., Danesh, A., Tehrani, D. H. and Todd, A. C. : "A Modified Residual Viscosity Method for Improved Prediction of Dense Phase Viscosities", paper presented at the 7th European Improved Oil Recovery (IOR) Symposium in Moscow, Russia, Oct. 27-29, (1992).

[23] Dandekar, A. : Interfacial Tension and Viscosity of Reservoir Fluids, Ph.D. Thesis, Heriot-Watt University, Edinburgh, Scotland, (1994).

[24] Gracki, J. A., Flynn, G. P, and Ross J. : "Viscosity of Nitrogen, Helium, Hydrogen and Argon from -100 to 25 °C up to 150-250 atm", J. Chem., Phys., **51**(9), 3856-3863, (Nov., 1969).

[25] Zozulya, V. N. and Blagoi, Yu. P. :"Viscosity of Nitrogen Near the Liquid-Vapour Critical Point", Soviet Physics-JETP, **39**(11), 99-105, (Jul., 1974).

[26] Diller, D. E : "Measurements of the Viscosity of Compressed Gaseous and Liquid Nitrogen", Physica, **119A**, 92-100, (1983).

[27] Michels, A., Botzen, A., and Schuurman, W. :"The Viscosity of Carbon Dioxide Between 0 °C and 75 oC and at Pressures up to 2000 Atmospheres", Physica, **23A,** 95-102, (1957).

[28] Iwasaki, H. and Takahashi, M. :"Viscosity of Carbon Dioxide and Ethane", J. Chemical Physics, **74**(3), 1930-1943, (Feb., 1981).

[29] Diller, D. E and Ball, M. J. :"Shear Viscosity Coefficients of Compressed Gaseous and Liquid Carbon Dioxide at Temperatures Between 220 and 320 K and at Pressures to 30 MPa", Int. J. Thermophys., **6**(6), 619-629, (1985).

[30] Giddings J. G., Kao J. T. F. and Kobayashi R. : "Development of a high pressure Capillary Tube Viscometer and its Application to Methane, Propane, and their Mixtures in the Gaseous and Liquid Regions", J. Chem. Phys., **45**(2), (July, 1966).

[31] Lee, A. L: Viscosity of Light Hydrocarbons, Monograph on API Research Project 65, American Petroleum Institute, New York, (1965).

[32] Diller, D. E :"Measurements of the Viscosity of Compressed Gaseous and Liquid Methane ", Physica, **104A,** 417-426, (1980).

[33] van der Gulik, P. S., Mostert, R. and van den Berg, H. R: "The Viscosity of Methane at 25 °C Up to 10 kbar," Physica, **151A**, 153-166, (1988).

[34] Diller, D. E and Saber, J. M. :"Measurements of the Viscosity of Compressed Gaseous and Liquid Ethane ", Physica, **108A,** 143-152, (1981).

[35] Diller, D. E :"Measurements of the Viscosity of Saturated and Compressed Liquid Propane", J. Chem. Eng. Data . **27**, 240-243, (1982).

[36] Diller, D. E and Poolen, L. J. V. : "Measurements of the Viscosity of Saturated and Compressed Liquid Normal Butane and Isobutane", Int. J. Thermophys., **6**(1), 43-62, (1985).

[37] Kiran, E. and Sen, Y. L. : "High-Pressure Viscosity and Density of n-Alkanes", Int. J. Thermophys., **13**(3), 411-442, (1992).

[38] Brazier, D. W. and Freeman, G. R. : "The effects of pressure on the density, dielectric constant, and viscosity of several hydrocarbons and other organic liquids", Cand. J. Chemistry, **47**, 893-899, (1969).

[39] Oliveira, C. M. B. P. and Wakeham, W. A. : "The Viscosity of Five Liquid Hydrocarbon at Pressures up to 250 MPa", Int. J. Thermophys., **13**(5), 774-790, (1992).

[40] Bridgman, P. W. : "The Effect of Pressure on The Viscosity of Forty-Three Pure Liquids", Proc. Amer. Acad. Arts Sci., **61**, 57-94, (1926).

[41] Baylaucq, A., Boned, C., Dauge, P., and Lagourette, B. : "Measurements of the Viscosity and Density of Three Hydrocarbons and the Three Associated Binary Mixtures Versus Pressure and Temperature", Int. J. Thermophys., **18**(1), 3-23, (1997).

[42] Agaev, N. A. and Golubev, I. F. :"The Viscosity of n-Hexane in the Liquid and Gaseous State at High Pressures and Different Temperatures", Dokl. Akad. Nauk USSR, **151**(3), 635-640, (1963).

[43] Dymond, J. H., Young, K. J. and Isadale, J. D.: "Transport Properties of Nonelectrolyte Liquid Mixtures-II. Viscosity Coefficients for n-Hexane + n-Hexadecane System at Temperature from 25 to 100 °C at Pressures Up to the Freezing Pressure or 500 MPa", Int. J. Thermophys., **1**(4), 345-373, (1980).

[44] Dymond, J. H., Robertson, J, and Isadale, J. D.: "Transport Properties of Nonelectrolyte Liquid Mixtures-III. Viscosity Coefficients for n-Octane, n-Dodecane, and Equimolar Mixtures of n-Octane + n-Dodecane and n-Hexane + n-Dodecane from 25 to 100 °C at Pressures Up to the Freezing Pressure or 500 MPa", Int. J. Thermophys., **2**(2), 133-154, (1981).

[45] Assael, M. J. and Papadaki, M. : "Measurements of the Viscosity of n-Heptane, n-Nonane, and n-Undecane at Pressures up to 70 MPa", Int. J. Thermophys., **12**(5), 801 - 810, (1991).

[46] Tanaka, Y, Hosokawa, H., Kubota, H., and Makita, T. : "Viscosity and Density of Binary Mixtures of Cyclohexane with n-Octane, n-Dodecane, and n-Hexadecane Under High Pressures", Int. J. Thermophys., **12**(2), 245-264, (1991).

[47] Knapstad, B., Skjolsvik, P. A., and Oye, H. A.. : "Viscosity of Three Binary Hydrocarbon Mixtures", J. Chem. Eng. Data, **36**, 84-88, (1991).

[48] Hogenboom, D. L, Webb, W. and Dixon, J. A. : "Viscosity of Several Liquid Hydrocarbons as a Function of Temperature, Pressure and Free Volume", J. Chem. phys., **46**(7), 2586 - 2598, (1967).

[49] Assael, M. J., Gallis, Z. A., and Vesovic, V. : "Excess Viscosity of Supercritical Fluids" High Temp. - High Press., **27/28**, 583-594, (1995/6).

[50] Cullick, A. S. and Mathis, M. L. : "Densities and Viscosities of Mixtures of Carbon Dioxide and n-Decane from 310 to 403 K and 7 to 30 MPa", J. Chem. Eng. Data, **29**, 393-396, (1984).

[51] Cooper, E. F. and Asfour, A. A. : "Densities and Kinematic Viscosities of Some C_6-C_{16} n-Alkane Binary Liquid Systems at 293.15 K", J. Chem. Eng. Data, **36**, 265-288, (1991).

[52] Assael, M. J., Karagiannidis, L. and Papadaki, M. :"Measurements of the Viscosity of n-Heptane+n-Undecane Mixtures at Pressures up to 75 MPa", Int. J. Thermophys., **12**(5), 774-790, (1991).

[53] Kovarik, F. S. and Taylor, M. A. :"Viscosity Measurements of High-Pressure CO2/Hydrocarbon Mixtures", paper presented at the 1987 AIChE Annual Meeting, Nov. 15-20, held in New York.

[54] El-Gayed, K. : Viscosity of Petroleum Reservoir Fluids: Measurement and Tuning Predictive Models, M.Phil. Thesis, Heriot-Watt University, Edinburgh, Scotland, (1997).

[55] Reservoir Fluid Studies, Final Report, 1996-1999 Programme, Department of Petroleum Engineering, Heriot-Watt University, Report No.: **PVT/00/1**.

[56] Department of Petroleum Engineering, Heriot-Watt University, EVIDENT Report, Task 1.3 "Data Acquisition on Representative Synthetic Mixtures", The Viscosity and Density of Methane/Methylcyclohexane and Methane/cis-Decahydronaphthanlene Binary Mixtures (from Saturation Pressure Up to 140 Mpa at 50, 100 and 150 °C, (Sep., 1999).

[57] Department of Petroleum Engineering, Heriot-Watt University, EVIDENT Report. Task 1.4 "Data Acquisition on Representative Real Gas Condensate Fluid", The Viscosity and Density of Real Gas Condensate Fluid (from Saturation Pressure Up to 140 Mpa at 50, 100 and 150 °C, (Feb., 2000).

[58] Twu, C. H. :"An Internally Consistent Correlation for Predicting the Critical Properties and Molecular Weights of Petroleum and Coal-Tar Liquids", Fluid Phase Equilib., **16**, 137-150, (1984).

[59] Lawal, A. S. :"Prediction of Vapour and Liquid Viscosities from the Lawal-Lake-Silberberg Equation of State", SPE/DOE 14926, paper presented at the SPE/DOE Fifth Symposium on Enhanced Oil Recovery held in Tulas, OK, April, 20-23, (1986).

Table 5.1 - Summary of Fluids and Their Temperature, Density and Viscosity Ranges Used For Evaluating the JST Viscosity Correlation and Its Modified Correlation (HW2).

Fluid	Reference	N	Experimental Ranges			Viscometer Type/Acc.	
			T_r	ρ_r	η/ cP	Type	Acc./%
Nitrogen	24-26	136	0.71-2.36	0.0-2.50	0.02-0.18	CT, OD, VC	0.5-2.0
Crabon Dioxide	27-29	240	0.72-1.06	0.0-2.54	0.01-0.27	CT, OD, VC	0.1-2.0
Methane	30-33	236	0.52-2.33	0.0-3.50	0.01-0.4	CT, VC, VW	0.5-2.0
Ethane	28,31,34	233	0.33-1.45	0.03-3.18	0.01-1.13	CT, VC, VW	2.0-2.5
Propane	30,31,35	207	0.24-1.11	0.0-3.34	0.01-10.7	CT, VC	1.5-2.0
n-Butane	31,36,37	236	0.33-1.05	0.05-3.27	0.01-2.56	CT, FC, VC, RC	0.5-3.0
n-Pentane	31,37-40	219	0.64-0.95	1.82-3.91	0.06-15.4	CT, FC, FW, RB, VW	0.5-4.0
n-Hexane	37-44	180	0.54-0.88	2.3-3.77	0.10-9.67	FC, FW, RB, VW	0.5-4.0
n-Heptane	39,41,45	147	0.55-0.69	2.61-3.37	0.20-1.8	FC, VW	0.5-2.0
n-Octane	37-40, 44,46	258	0.48-0.79	2.47-3.57	0.20-5.67	FC, FW, VC, RB, VW	0.5-4.0
n-Nonae	44	30	0.51-0.54	2.95-3.20	0.5-1.13	VW	0.5
n-Decane	31,39,47	374	0.44-0.69	2.46-3.49	0.21-5.32	CT, OC, VW	0.5-4.0
n-Undecane	45	25	0.47-0.51	3.03-3.25	0.74-1.84	VW	0.5
n-Dodecane	44,46-48	119	0.45-0.62	2.90-3.64	0.34-10.4	FT, OC, RB	2.0-5.0
n-Pentadecane	48	48	0.44-0.58	2.90-3.54	0.54-10.4	RB	2.0-5.0
n-Hexadecane	43,46	61	0.41-0.52	3.0-3.66	1.20-11.1	FC, VC	2.0
n-Octadecane	48	40	0.45-0.50	2.95-3.57	0.75-11.5	RB	2.0-5.0

Acc. - Accuracy.
CT - Capillary Tube.
FC - Falling Cylinder.
FW - Falling Weight.
OC - Oscillating Cylinder.
OD - Oscillating Disk.
RB - Rolling Ball .
RC - Rotating Cylinder.
VC - Vibrating Crystal.
VW - Vibrating Wire.

Table 5.2 - Summary of Fluids and Their Temperature, Density and Pressure Ranges Used For Testing The LBC, HW1, CS1, CS2 and HW2 Viscosity Methods.

Fluid	Reference	N	Temperature Range		Pressure/Density Range		Conc. CO2
			T/ °C	T_r	P/ psia	ρ_r	mole %
C1/C3	30	313	38-138	0.9-1.8	200-8050	0.0-2.5	-
C1/n-C4	31	63	38-105	1-1.8	200-8000	0.1-2.2	-
C1/n-C10	31	50	38-100	0.6-1.3	1500-15000	0.1-3.1	-
CO2/n-C10	50	70	38-130	0.5-1.4	1000-5000	1.6-3.1	15 - 85
Binary Liquids	51,52	163	20-50	0.4-0.6	15-10450	2.8-3.3	-
5-comp. CO2 Fluids	53	106	38-88	0.5-1.2	1300-2000	0.6-3.2	0 - 99
HPHT MC Synthetic Fluids	55	12	175 & 200	1.9-2.0	7500-20200	1.7-2.8	-
HPHT MC component Real Fluids	23,54,57	80	38-150	0.7-1.6	2000-20060	1.2-3.2	-
HPHT MC Synthetic Fluids with Water	55	12	175 & 200	1.7-1.8	7500-20200	1.7-3.0	5.4-5.7[c]
HPHT C1/MCH	56	100	50-150	1.0-2.0	4000-20207	0.9-2.8	5-33[a]
HPHT C1/cis-DHN	56	67	50-150	1.0-2.0	7000-20120	1.4-2.8	4-26[b]

AD - Average Deviation. AAD - Average Absolute Deviation. SD - Standard Deviation.
HPHT - High Pressure-High Temperature. MC - Multi-component. MCH - Mythylcyclohexane.
DHN - Decahydronaphthalene. a- Concentration of MCH b - Concentration of DHN.
c - Concentration of Water.

Table 5.3 - Summary of Some Statistical Measures For The LBC, HW1, CS1, CS2 and HW2 Methods.

	LBC			HW1			CS1			CS2			HW2 (This Work)		
Fluid	**AD**	**AAD**	**SD**	**AD**	**AAD**	**SD**	**AD**	**AAD**	**SD**	**AD**	**AAD**	**SD**	**AD**	**AAD**	**SD**
C1/C3	-3	4	5	-	-	-	4	5	4	8	8	6	**0**	**1**	**2**
C1/n-C4	-3	4	4	-3	4	4	4	4	4	7	7	5	**-1**	**3**	**4**
C1/n-C10	11	12	9	12	10	5	12	10	6	-18	18	5	**-5**	**5**	**3**
CO2/n-C10	-4	7	6	-3	6	8	30	30	30	5	6	6	**9**	**10**	**6**
Binary Liquids	-19	19	18	-16	16	5	41*	41*	14*	-2*	4*	4*	**2**	**6**	**8**
5-comp. CO2 Fluids	-21	21	14	-17	17	12	**	**	**	**	**	**	**-11**	**13**	**11**
HPHT MC Synthetic Fluids	1	20	28	1	20	28	-6	7	4	4	9	10	**-5**	**13**	**14**
HPHT MC component Real Fluids	-10	20	15	-8	15	10	-25	25	10	-20	20	10	**-7**	**5**	**8**
HPHT MC Synthetic Fluids with Water	14	26	41	14	26	39	-14	15	12	-17	17	16	**11**	**12**	**16**
HPHT C1/MCH	-2	5	6	9	13	21	-1	5	6	1	9	13	**-4**	**5**	**5**
HPHT C1/cis-DHN	-19	19	16	-17	18	18	-25	25	17	-24	25	20	**-22**	**22**	**17**

* - Only 60 Data Points Used Due to insufficient Data in Reference [31] to Carry out Viscosity Prediction.

**- Viscosity Prediction was not Possible Due to non-Convergence Problems.

CS1 - One-reference Fluid Corresponding States, Section 5.6.2. CS2 - Two-reference Fluids Corresponding States, Section 5.6.3.

LBC - Lohrenze-Bray-Clark, Section 5.7.2. HW1 - Modified LBC (Dandekar et al[122]), Section 5.7.3. HW2 - Modified LBC (This work), Section 5.7.4.

Fluid	LBC			HW1			CS1			CS2			HW2 (This Work)		
	AD	AAD	SD	AD	AAD	SD	AD	AAD	SD	AD	AAD	SD	AD	AAD	SD
C1/C3	-3	4	5	-	-	-	4	5	4	8	8	6	**0**	**1**	**2**
C1/n-C4	-3	4	4	-3	4	4	4	4	4	7	7	5	**-1**	**3**	**4**
C1/n-C10	11	12	9	12	10	5	12	10	6	-18	18	5	**-5**	**5**	**3**
CO2/n-C10	-4	7	6	-3	6	8	30	30	30	5	6	6	**9**	**10**	**6**
Binary Liquids	-19	19	18	-16	16	5	41*	41*	14*	-2*	4*	4*	**2**	**6**	**8**
5-comp. CO2 Fluids	-21	21	14	-17	17	12	**	**	**	**	**	**	**-11**	**13**	**11**
HPHT MC Synthetic Fluids	1	20	28	1	20	28	-6	7	4	4	9	10	**-5**	**13**	**14**
HPHT MC component Real Fluids	-10	20	15	-8	15	10	-25	25	10	-20	20	10	**-7**	**5**	**8**
HPHT MC Synthetic Fluids with Water	14	26	41	14	26	39	-14	15	12	-17	17	16	**11**	**12**	**16**
HPHT C1/MCH	-2	5	6	9	13	21	-1	5	6	1	9	13	**-4**	**5**	**5**
HPHT C1/cis-DHN	-19	19	16	-17	18	18	-25	25	17	-24	25	20	**-22**	**22**	**17**

* - Only 60 Data Points Used Due to insufficient Data in Reference [31] to Carry out Viscosity Prediction.

**- Viscosity Prediction was not Possible Due to non-Convergence Problems.

CS1 - One-reference Fluid Corresponding States, Section 5.6.2. CS2 - Two-reference Fluids Corresponding States, Section 5.6.3.

LBC - Lohrenze-Bray-Clark, Section 5.7.2. HW1 - Modified LBC (Dandekar et al[221]), Section 5.7.3. HW2 - Modified LBC (This work), Section 5.7.4.

Fluid	LBC			HW1			CS1			CS2			HW2 (This Work)		
	AD	AAD	SD	AD	AAD	SD	AD	AAD	SD	AD	AAD	SD	AD	AAD	SD
C1/C3	-3	4	5	-	-	-	4	5	4	8	8	6	**0**	**1**	**2**
C1/n-C4	-3	4	4	-3	4	4	4	4	4	7	7	5	**-1**	**3**	**4**
C1/n-C10	11	12	9	12	10	5	12	10	6	-18	18	5	**-5**	**5**	**3**
CO2/n-C10	-4	7	6	-3	6	8	30	30	30	5	6	6	**9**	**10**	**6**
Binary Liquids	-19	19	18	-16	16	5	41*	41*	14*	-2*	4*	4*	**2**	**6**	**8**
5-comp. CO2 Fluids	-21	21	14	-17	17	12	**	**	**	**	**	**	**-11**	**13**	**11**
HPHT MC Synthetic Fluids	1	20	28	1	20	28	-6	7	4	4	9	10	**-5**	**13**	**14**
HPHT MC component Real Fluids	-10	20	15	-8	15	10	-25	25	10	-20	20	10	**-7**	**5**	**8**
HPHT MC Synthetic Fluids with Water	14	26	41	14	26	39	-14	15	12	-17	17	16	**11**	**12**	**16**
HPHT C1/MCH	-2	5	6	9	13	21	-1	5	6	1	9	13	**-4**	**5**	**5**
HPHT C1/cis-DHN	-19	19	16	-17	18	18	-25	25	17	-24	25	20	**-22**	**22**	**17**

* - Only 60 Data Points Used Due to insufficient Data in Reference [31] to Carry out Viscosity Prediction.

**- Viscosity Prediction was not Possible Due to non-Convergence Problems.

CS1 - One-reference Fluid Corresponding States, Section 5.6.2. CS2 - Two-reference Fluids Corresponding States, Section 5.6.3.

LBC - Lohrenze-Bray-Clark, Section 5.7.2. HW1 - Modified LBC (Dandekar et al[122]), Section 5.7.3. HW2 - Modified LBC (This work), Section 5.7.4.

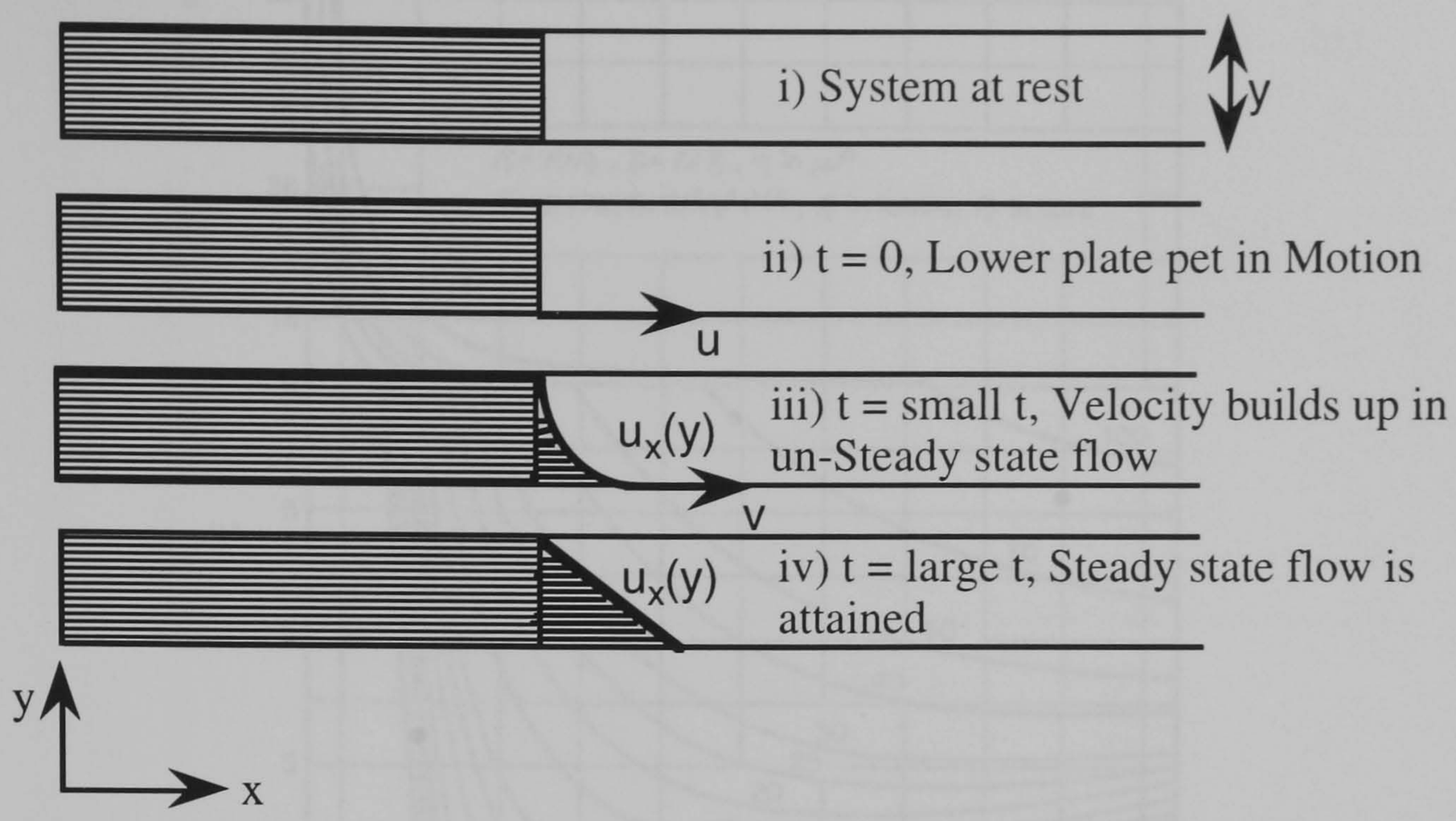

Figure 5.1 - The Transport of Momentum of a Newtonian Fluid Contained Between Two Parallel Plates[1].

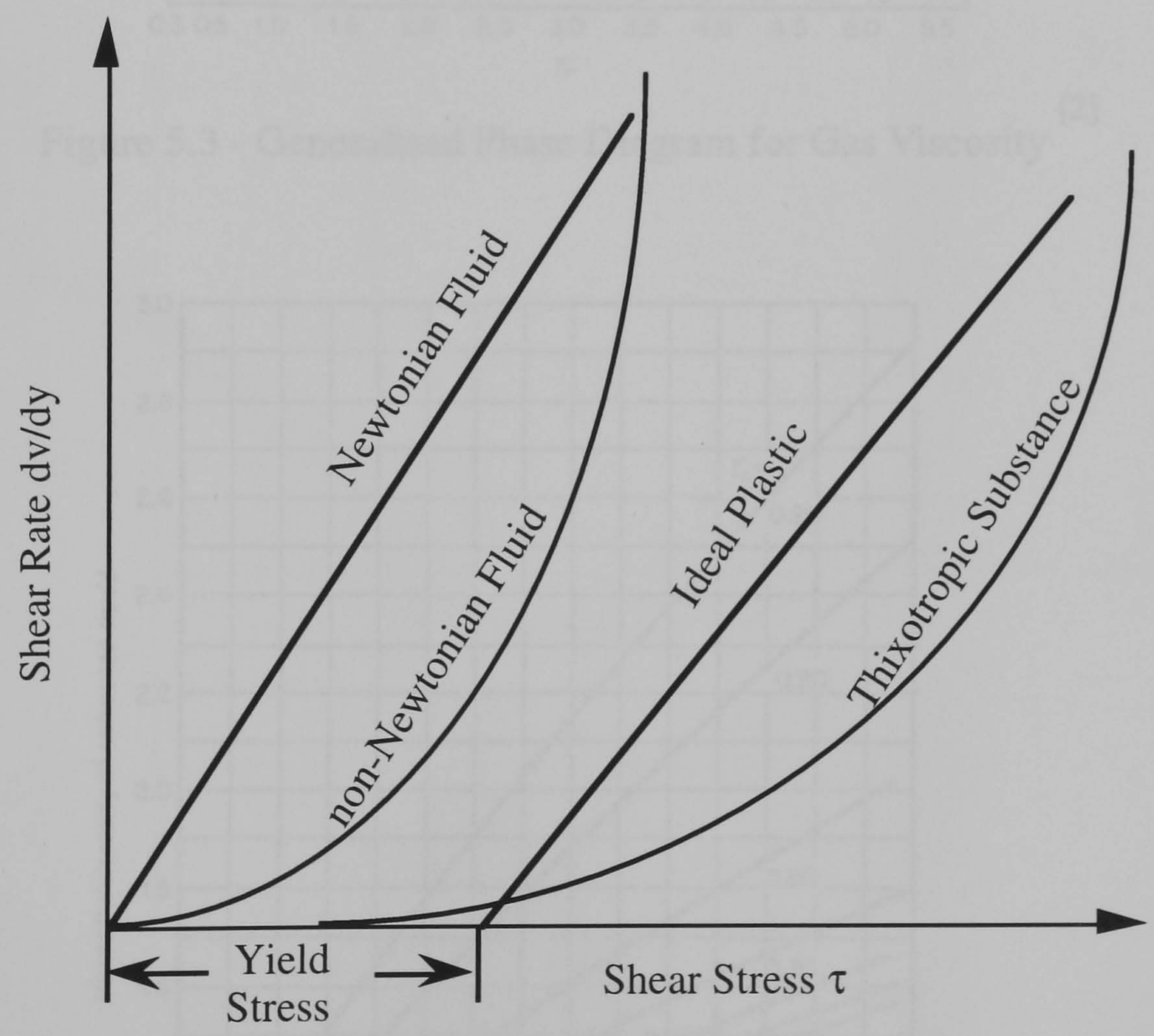

Figure 5.2 - The Relationship Between Shear Stress and Shear Rate for Various Classes of Fluids[1].

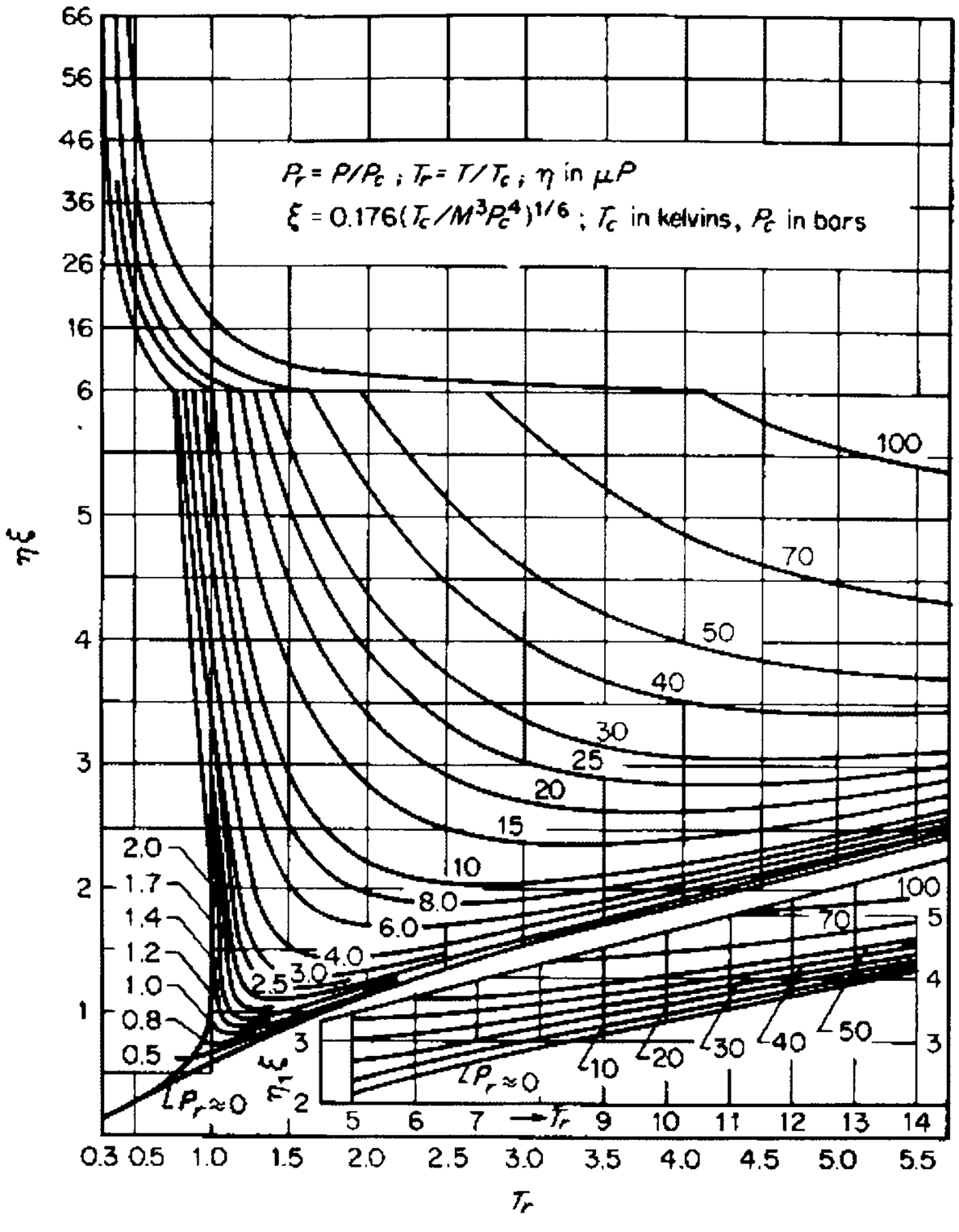

[2]

Figure 5.3 - Generalised Phase Diagram for Gas Viscosity

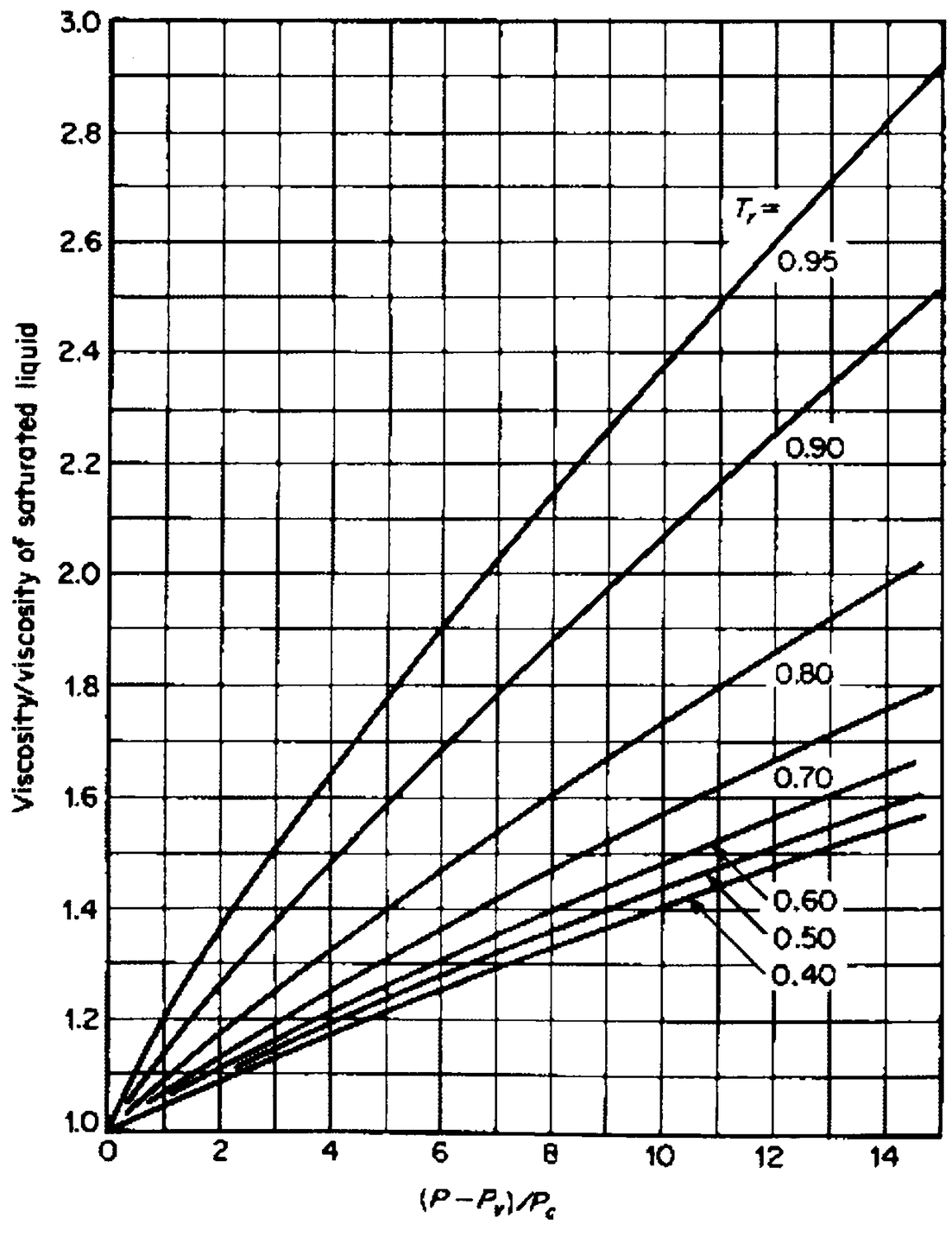

[2]

Figure 5.4 - The Effect of Pressure and Temperature on the Viscosity of Liquid

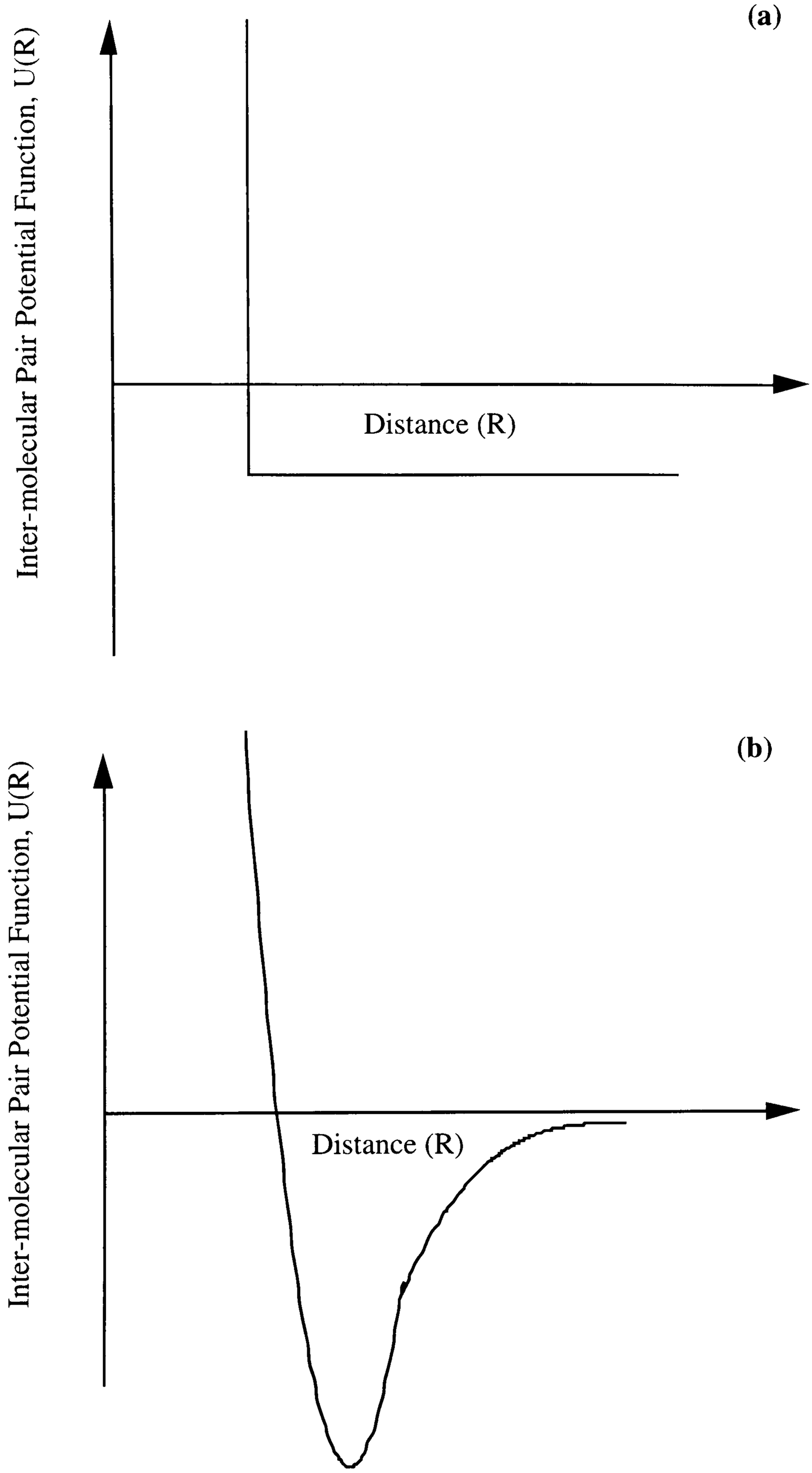

Figure 5.5 - Inter-molecular Pair Potential Curves, (a) van der Waals, (b) Realistic Pair Potential[6].

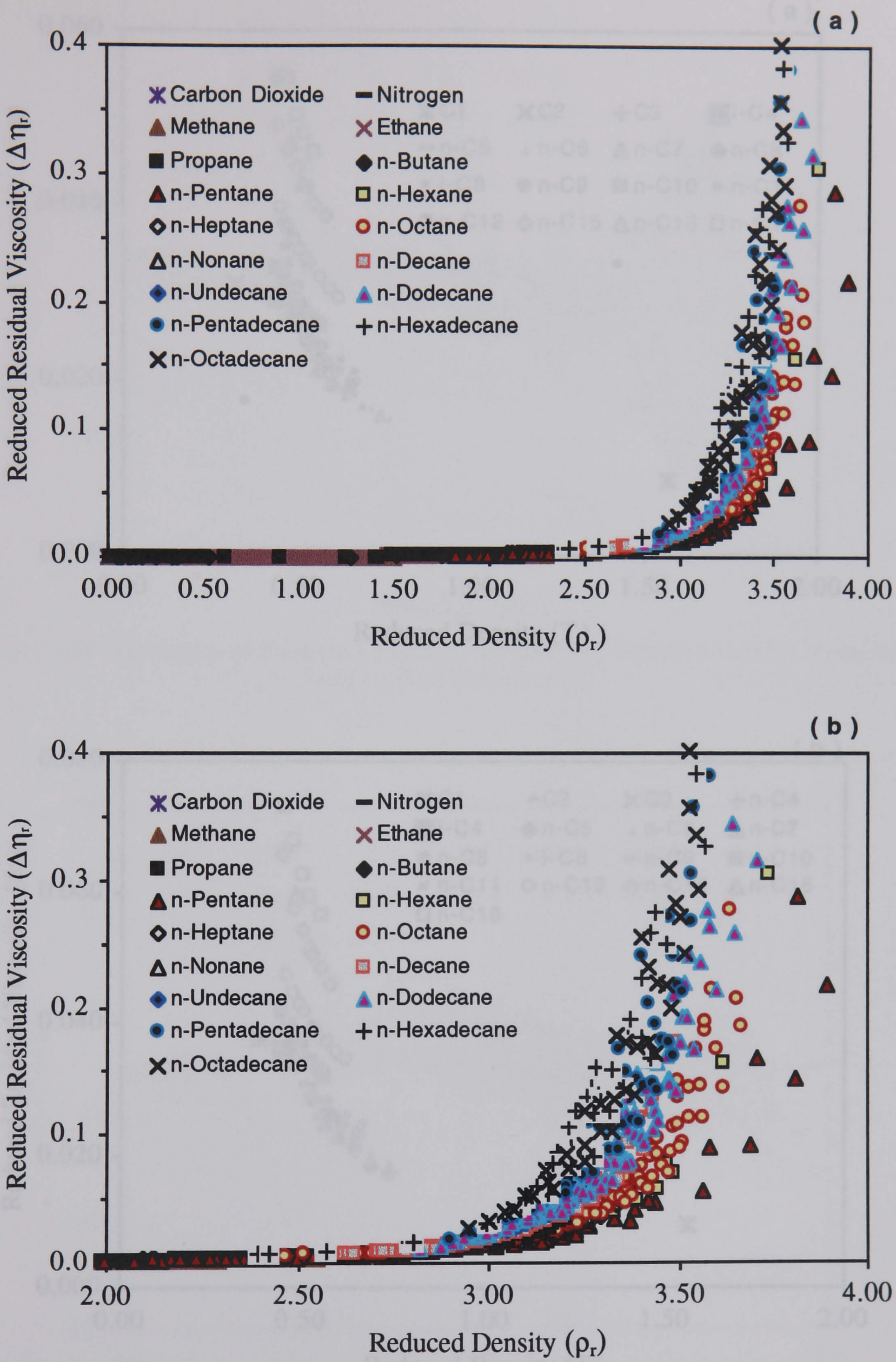

Figure 5.6 - Reduced Residual Viscosity vs. Reduced Density for Various Compounds, (a) Full Reduced Density Range, (b) Reduced Density Range 2.0 to 4.0.

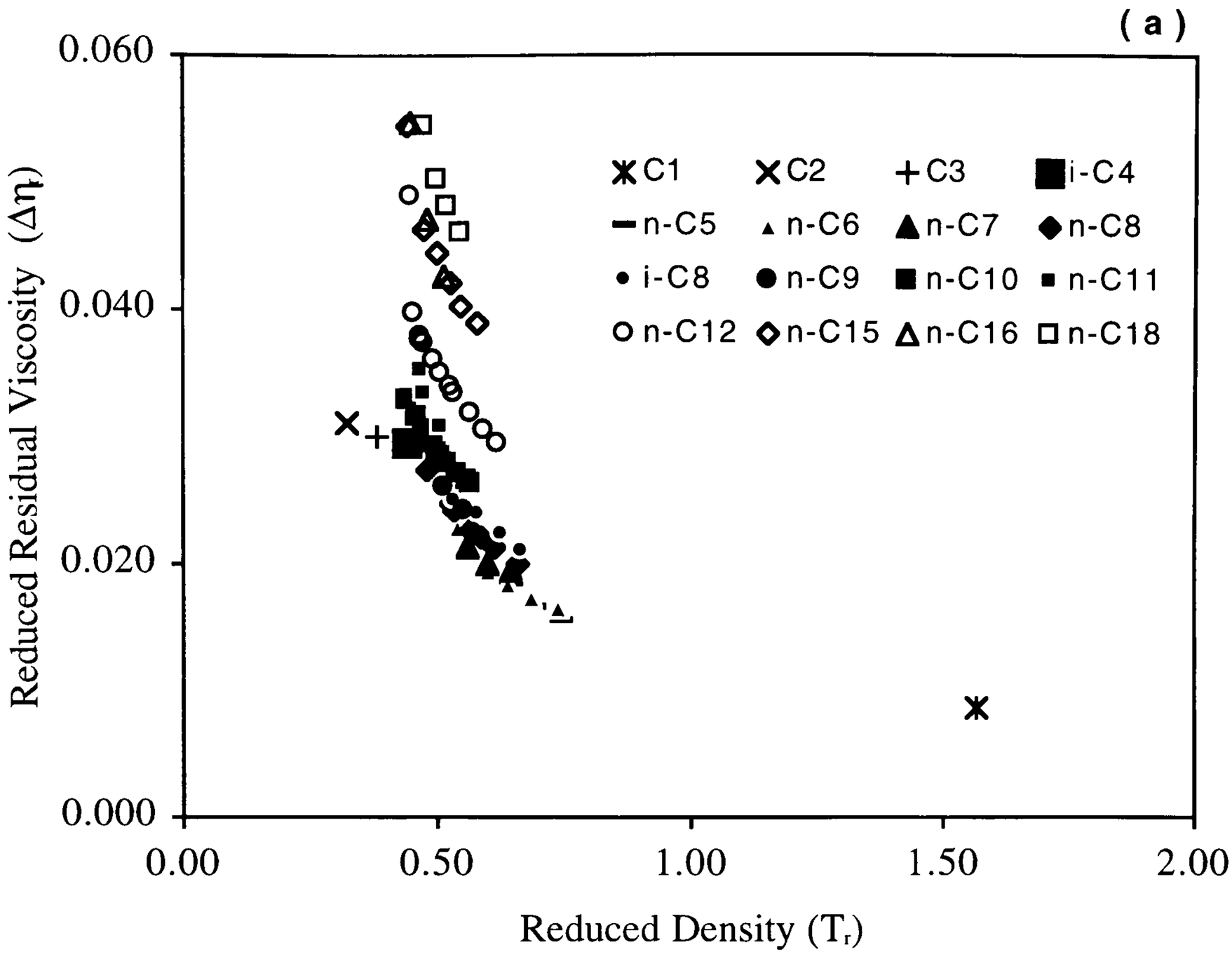

Figure 5.7 - Reduced Residual Viscosity vs. Reduced Temperature at Constant Reduced Density Values, (a) Reduced Density Value of 3.10, (b) Reduced Density Value of 3.15.

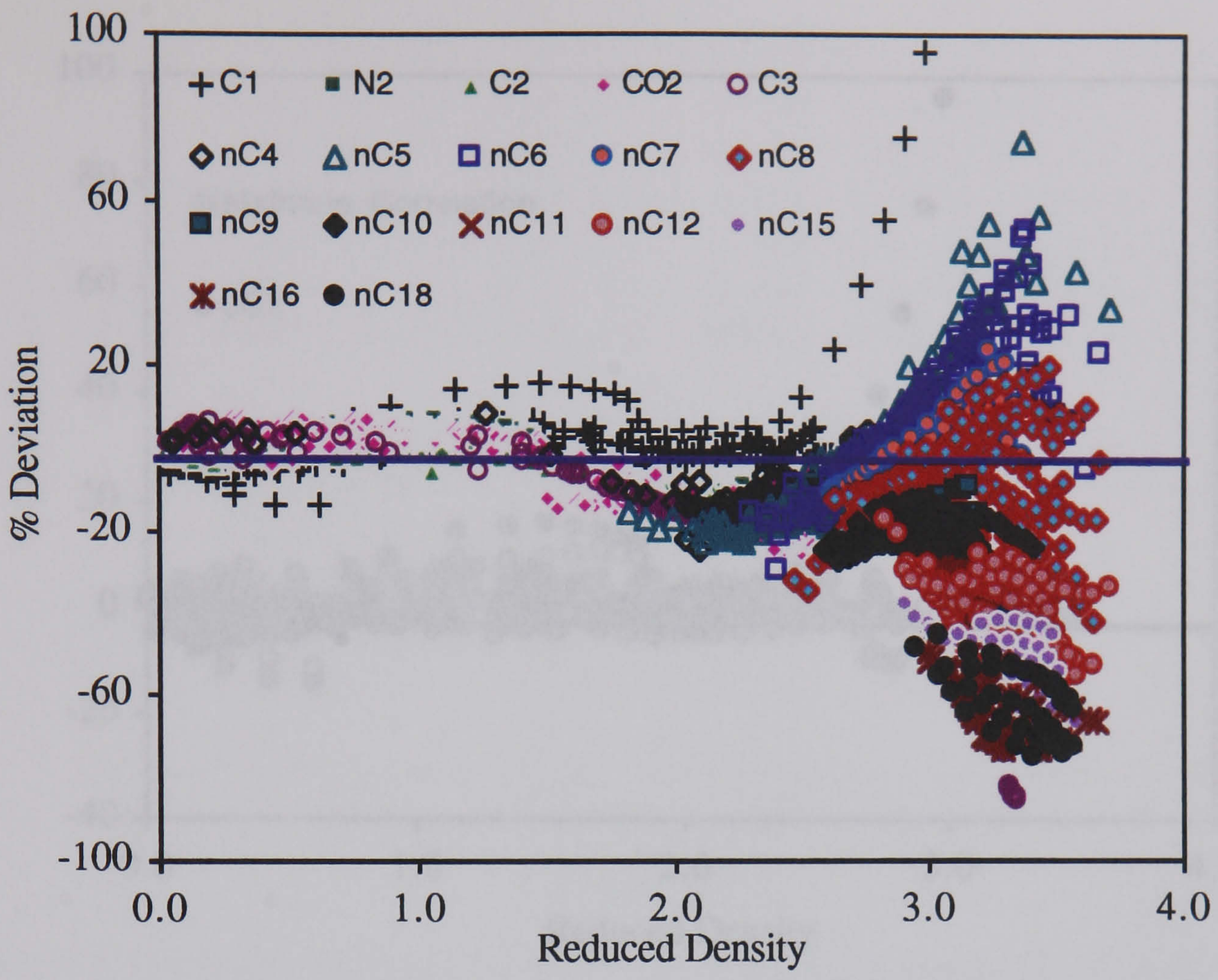

Figure 5.8 - Deviation of Predicted Viscosity by The JST Correlation from Measured Data on Pure Compounds.

Figure 5.9 - Deviation of Predicted Viscosity by The Modified Correlation Equation (5.25), from Measured Data on Pure Compounds.

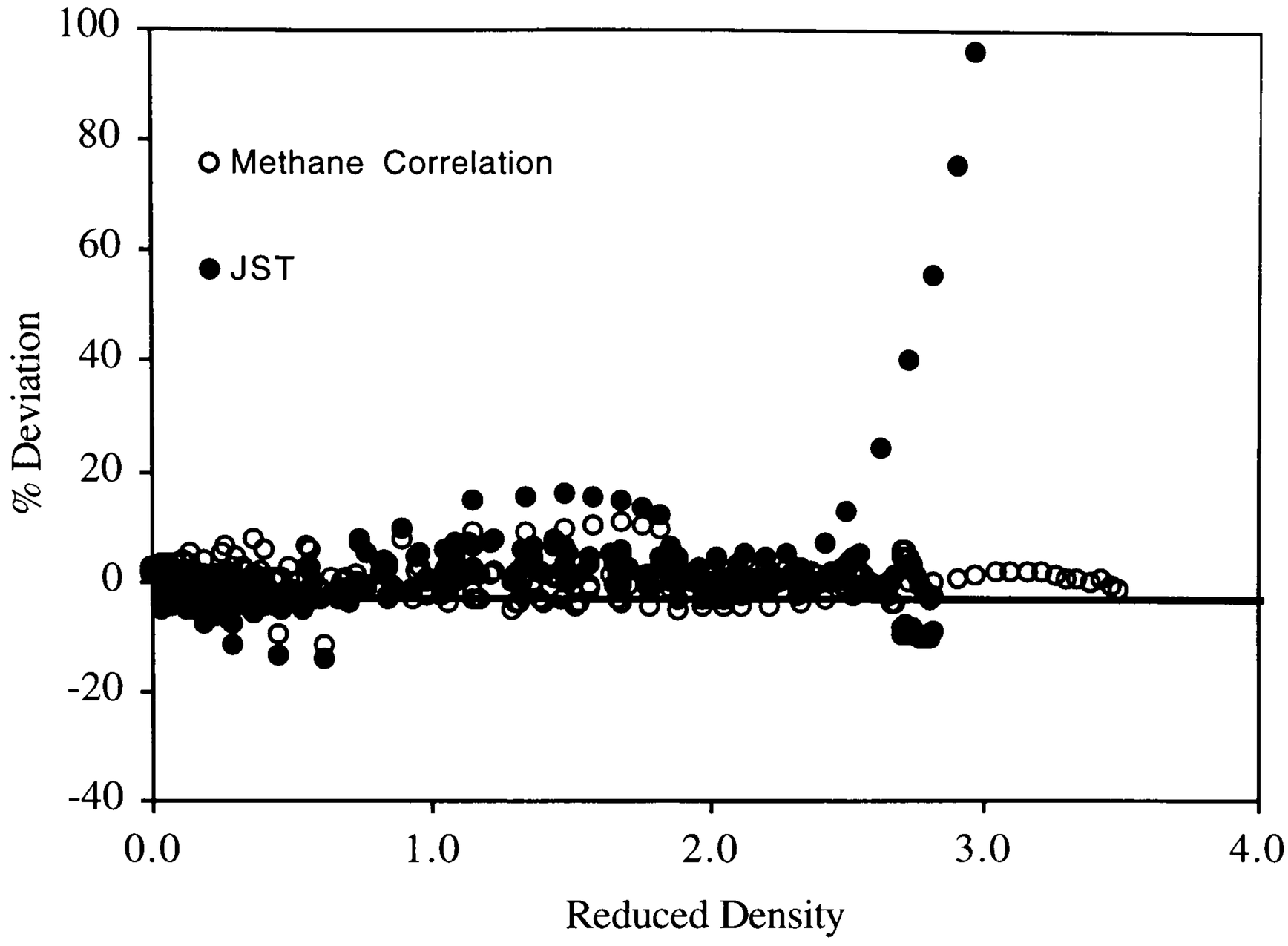

Figure 5.10 - Deviation of Predicted Viscosity by The JST Correlation (Jossi *et al*[24]) and The Modified Methane Correlation, Equation (5.26), from Measured Data.

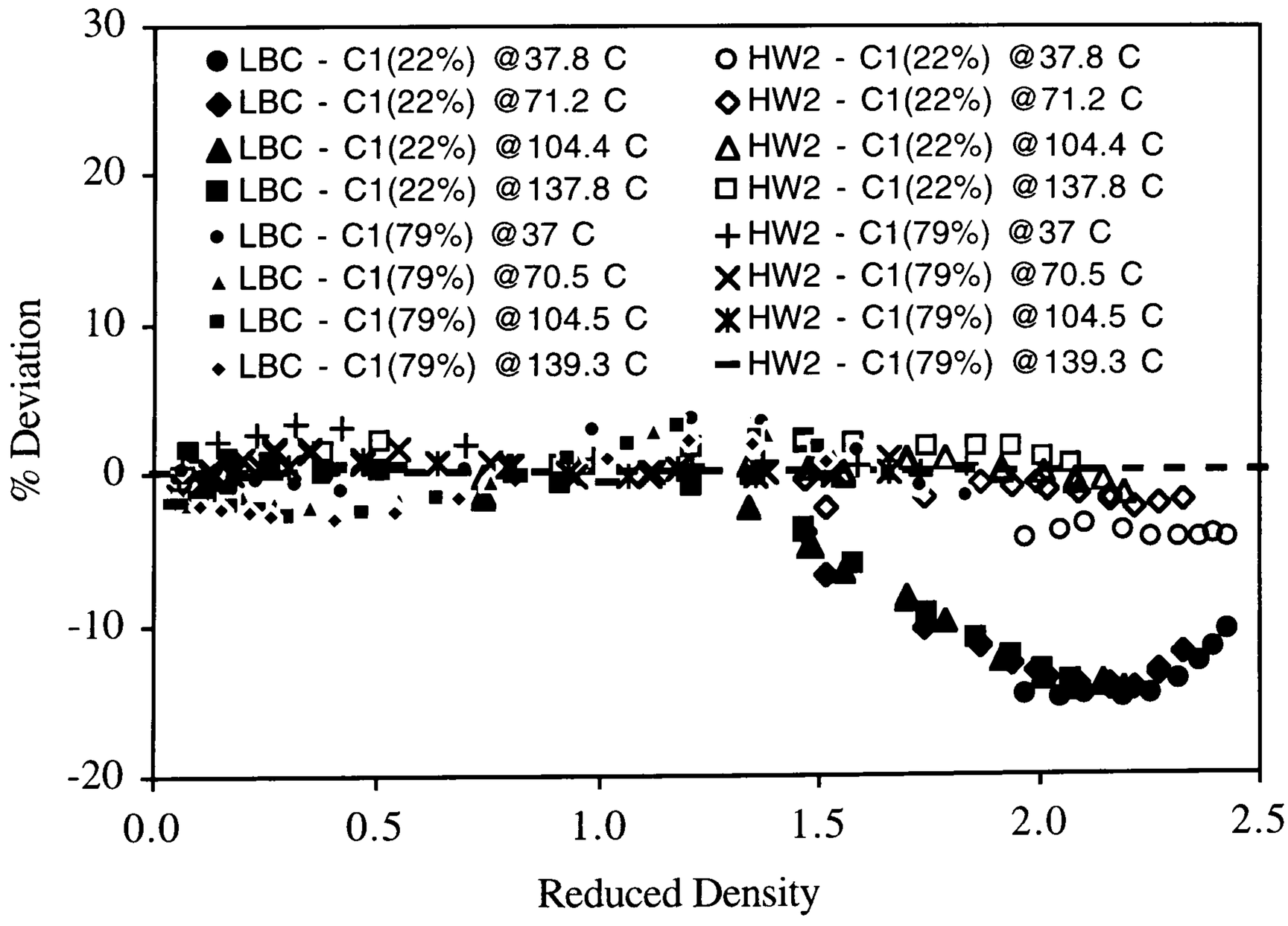

Figure 5.11 - Deviation of Predicted Viscosity by the LBC and HW2 Correlations from Measured Data on Methane/Propane Mixtures (Giddings *et al* [30]).

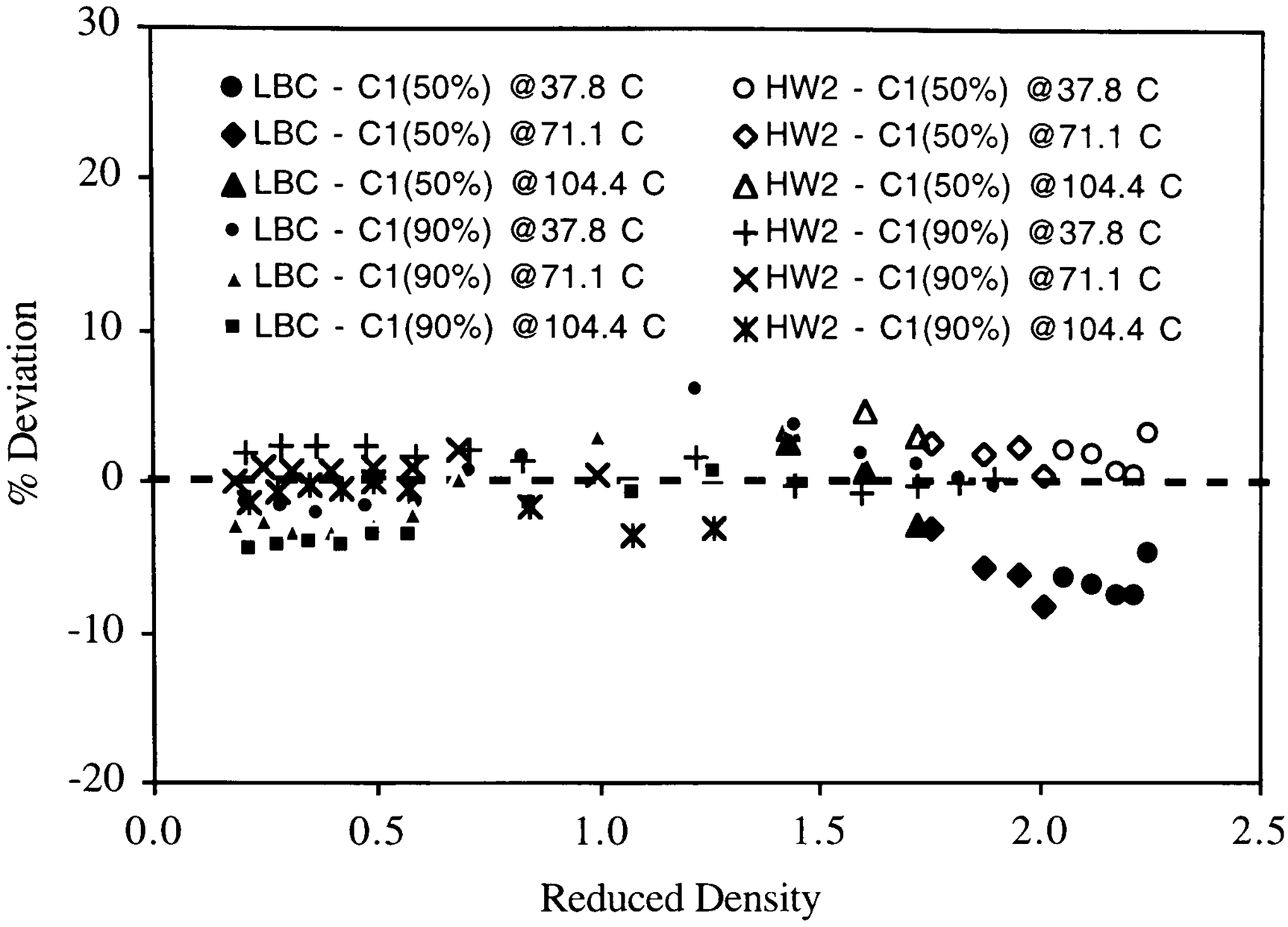

Figure 5.12 - Deviation of Predicted Viscosity by The LBC and HW2 Correlations from Measured Data on Methane/n-Butane Mixtures (Lee[31]).

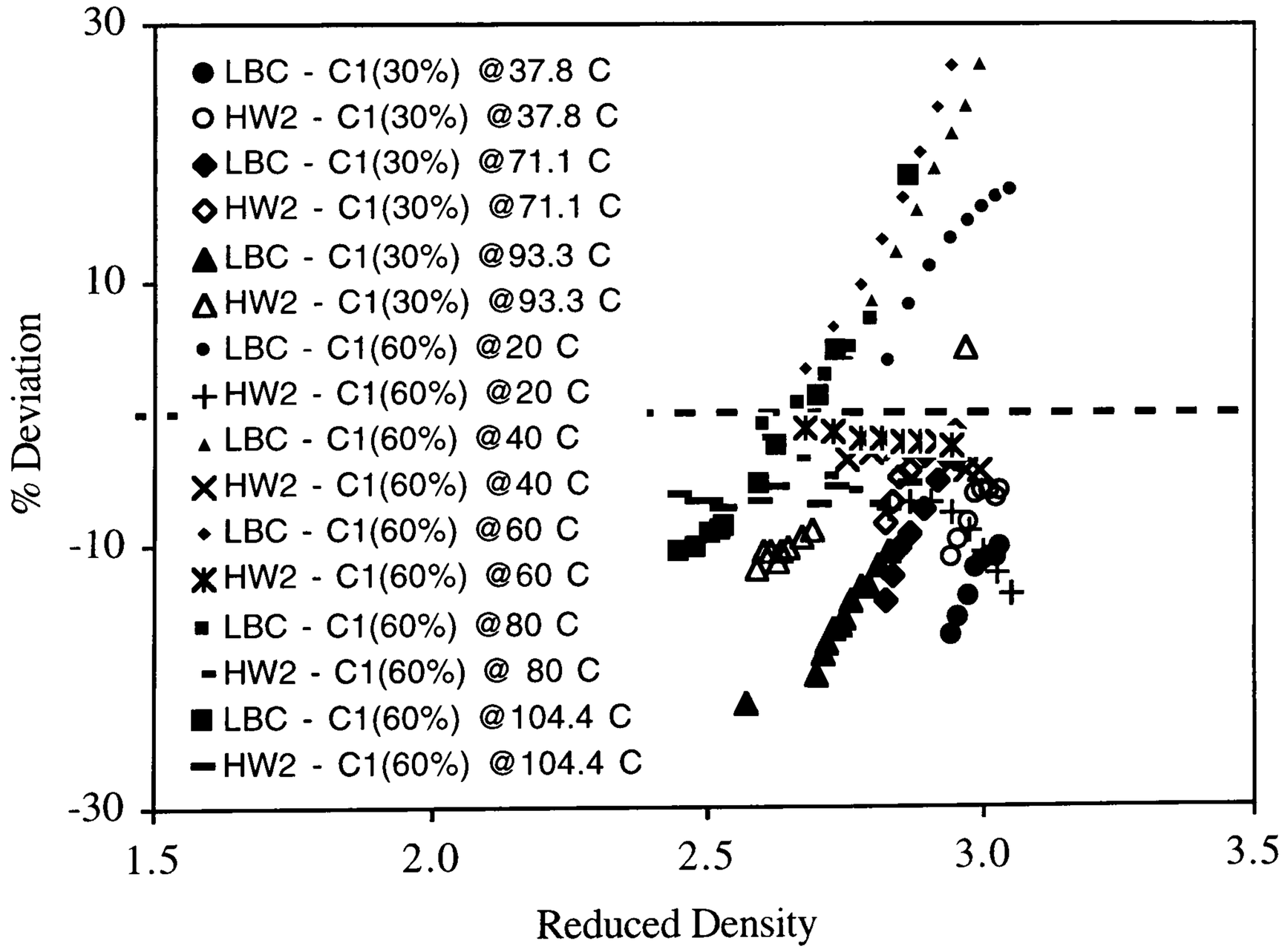

Figure 5.13 - Deviation of Predicted Viscosity by The LBC and HW2 Correlations from Measured Data on Methane/n-Decane Mixtures (Lee[30]).

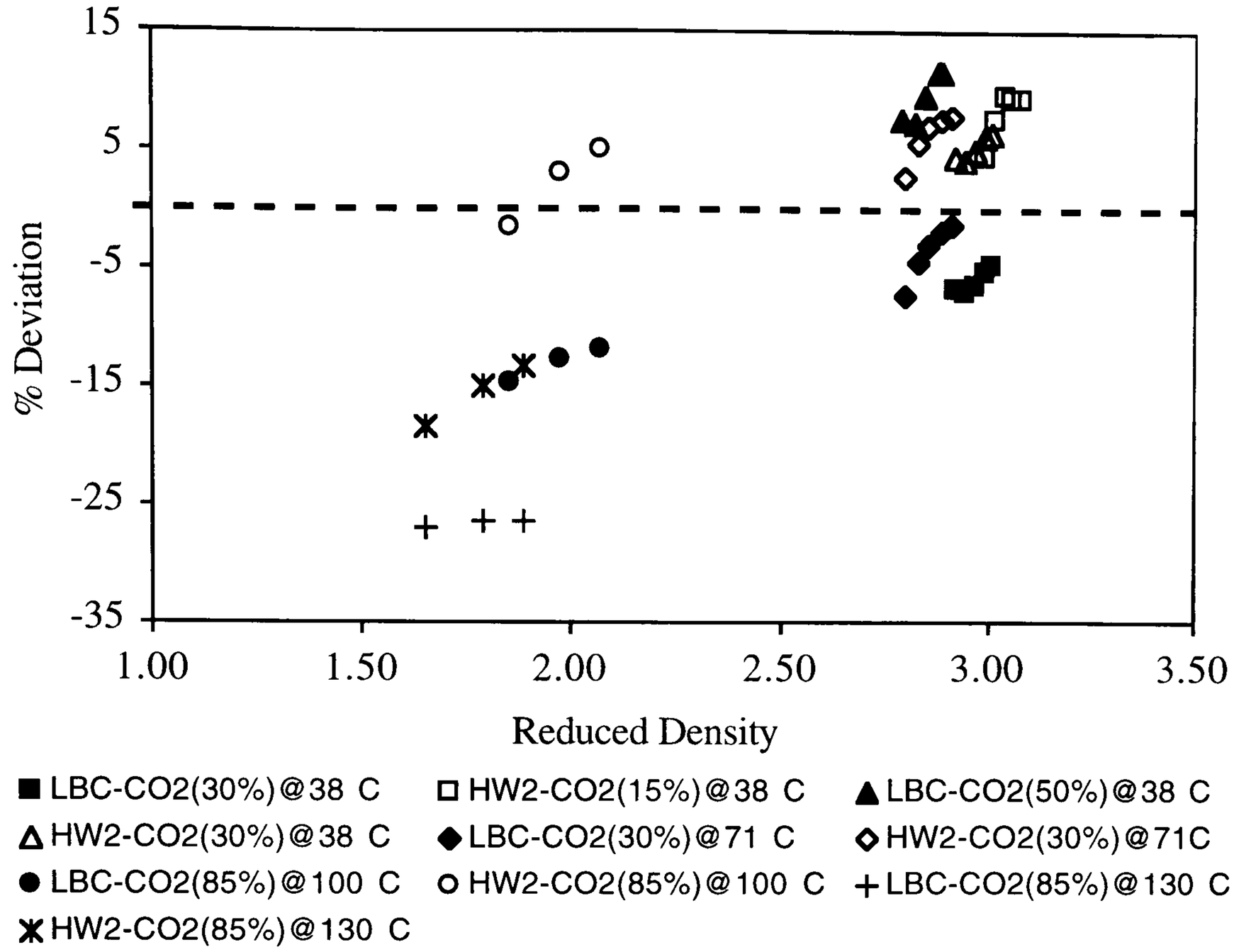

Figure 5.14 - Deviation of Predicted Viscosity by The LBC and HW2 Correlations from Measured Data on Carbon Dioxide/n-Decane Mixtures (Cullick and Mathis[50]).

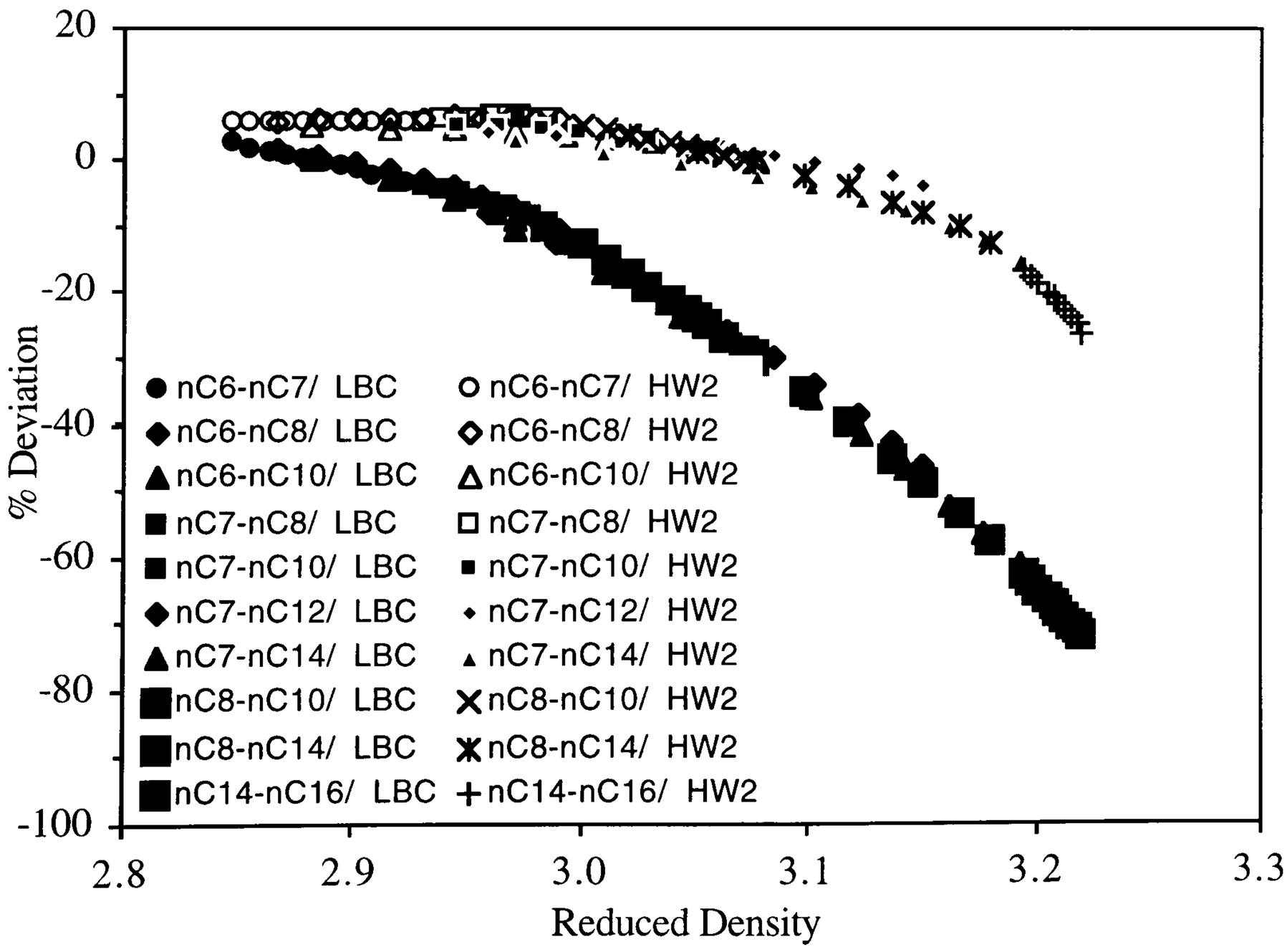

Figure 5.15 - Deviation of Predicted Viscosity by the LBC and HW2 Correlations from Measured Data on Binary Liquid Mixtures (Cooper and Asfour[51], Assael *et al*[52]).

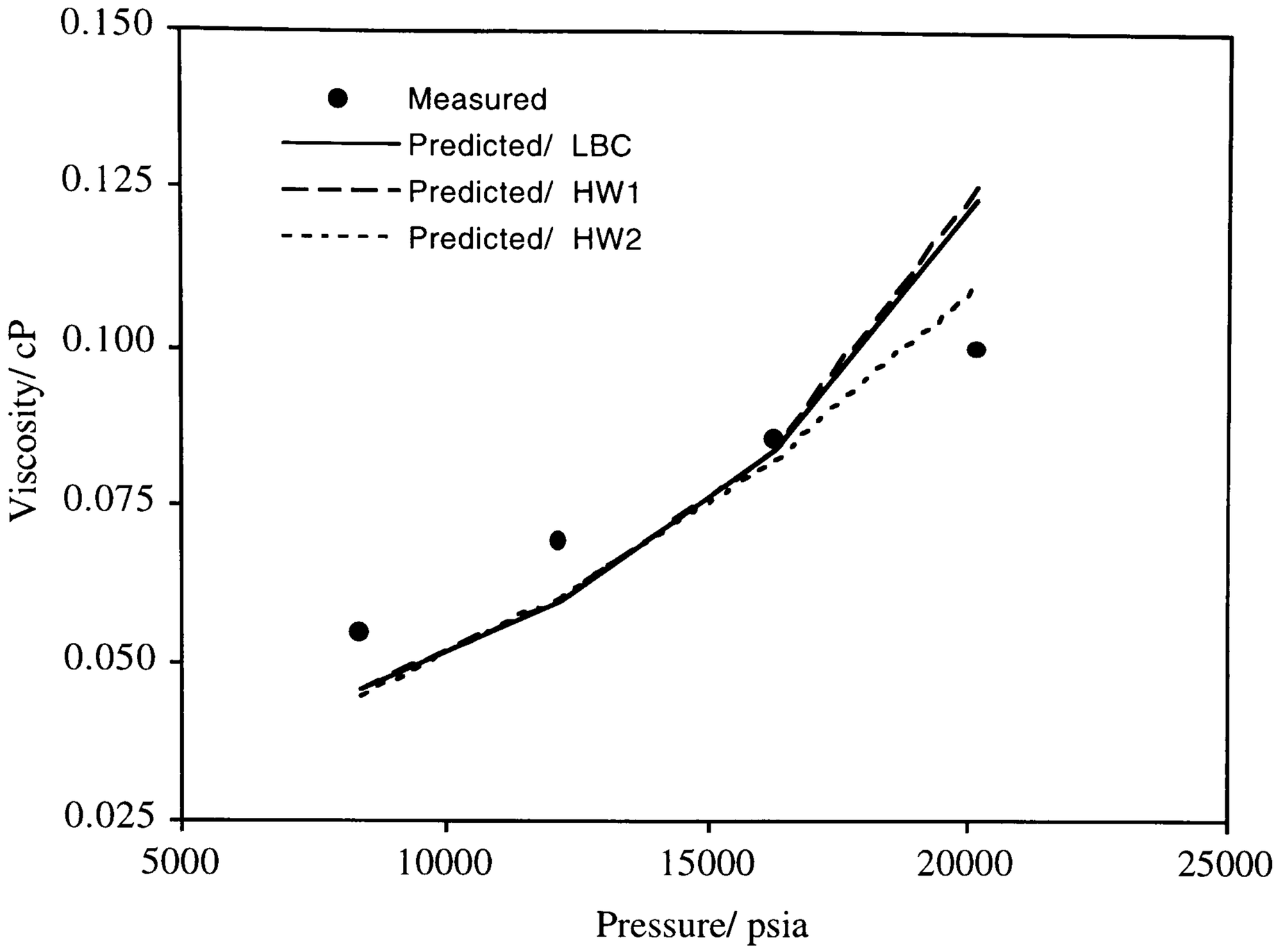

Figure 5.16 - Measured and Predicted Viscosity With Pressure for the Synthetic 6-components Gas Condensate Mixture (Danesh *et al*[55]) at a Temperature of 175 °C, by the LBC, HW1 and HW2 Correlations.

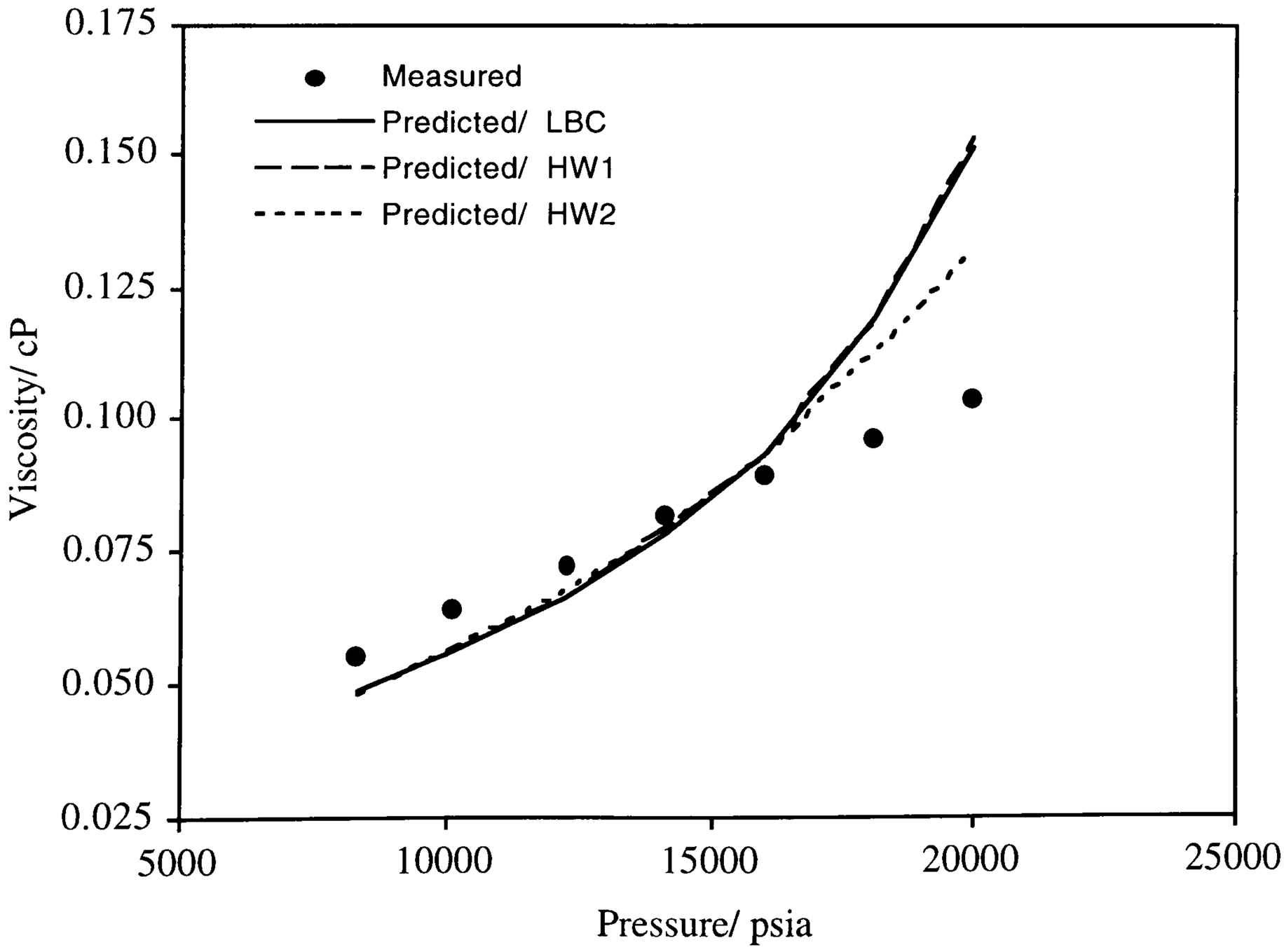

Figure 5.17 - Measured and Predicted Viscosity With Pressure for the Synthetic 6-components Gas Condensate Mixture With 5.71% mole of Water (Danesh *et al*[55]) at a Temperature of 175 °C, by the LBC, HW1 and HW2 Correlations.

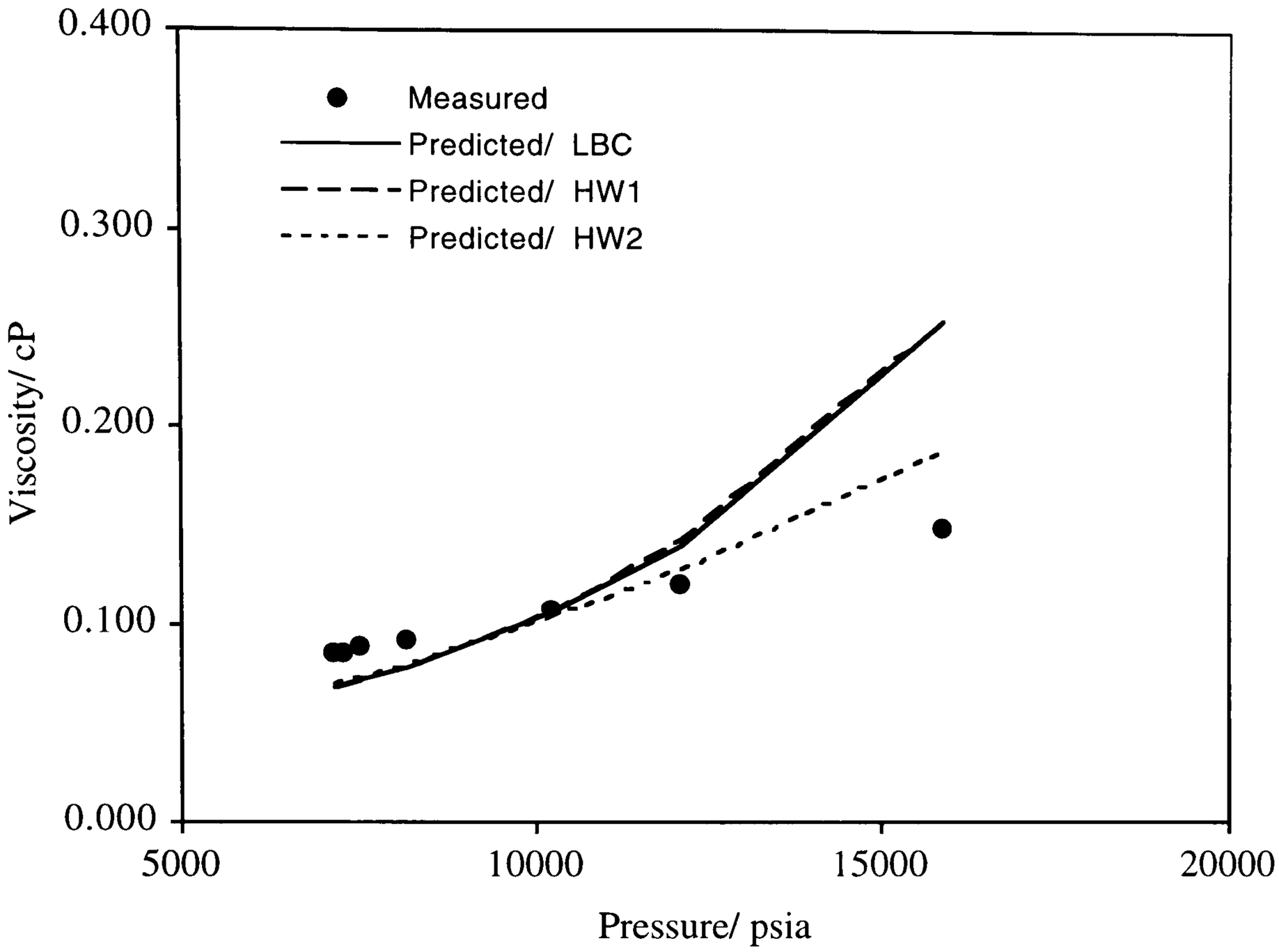

Figure 5.18 - Measured and Predicted Viscosity With Pressure for the Synthetic 6-components Volatile Oil Mixture (Danesh *et al*[55]) at a Temperature of 200 °C, by the LBC, HW1 and HW2 Correlations.

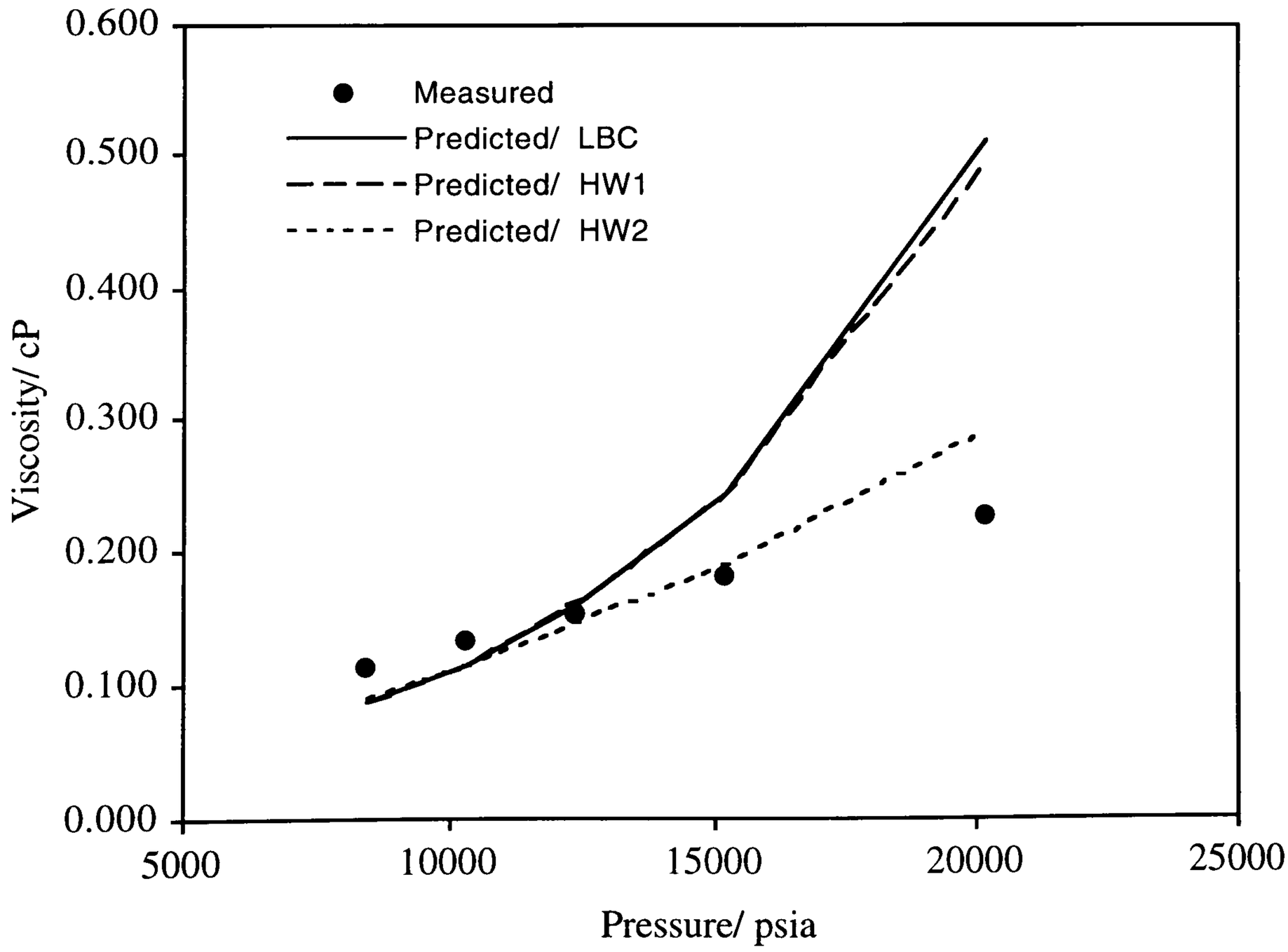

Figure 5.19 - Measured and Predicted Viscosity With Pressure for the Synthetic 6-components Volatile Oil Mixture With 5.40% mole of Water (Danesh *et al*[55]) at a Temperature of 200 °C, by the LBC, HW1 and HW2 Correlations.

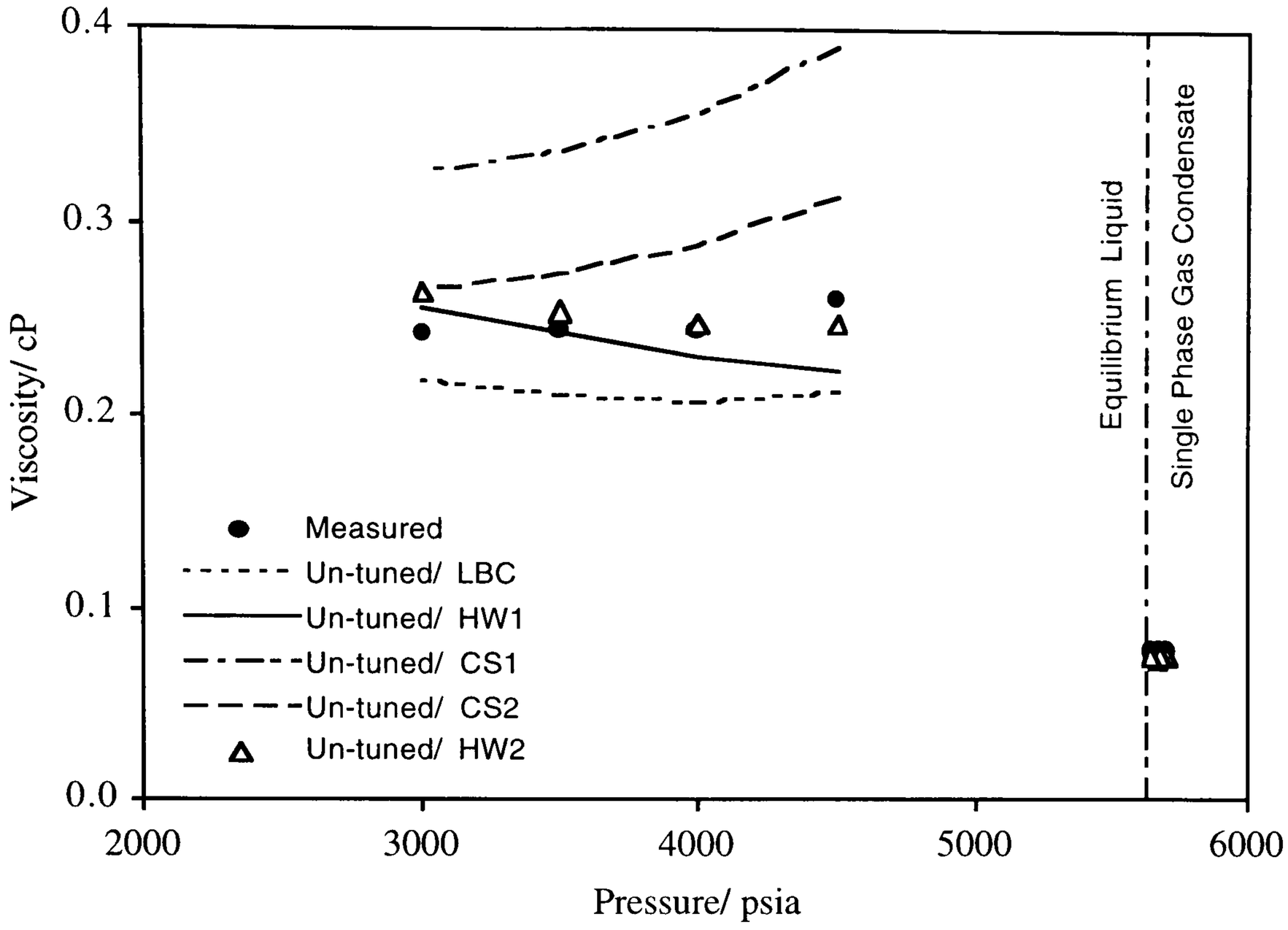

Figure 5.20 - Measured and Predicted Viscosity With Pressure for the Pure Gas Condensate GCB98-1 (Chapter 7, Table 7.15) at a Temperature of 37.8 °C, by the, LBC, HW1 , CS1, CS2 and HW2 Models

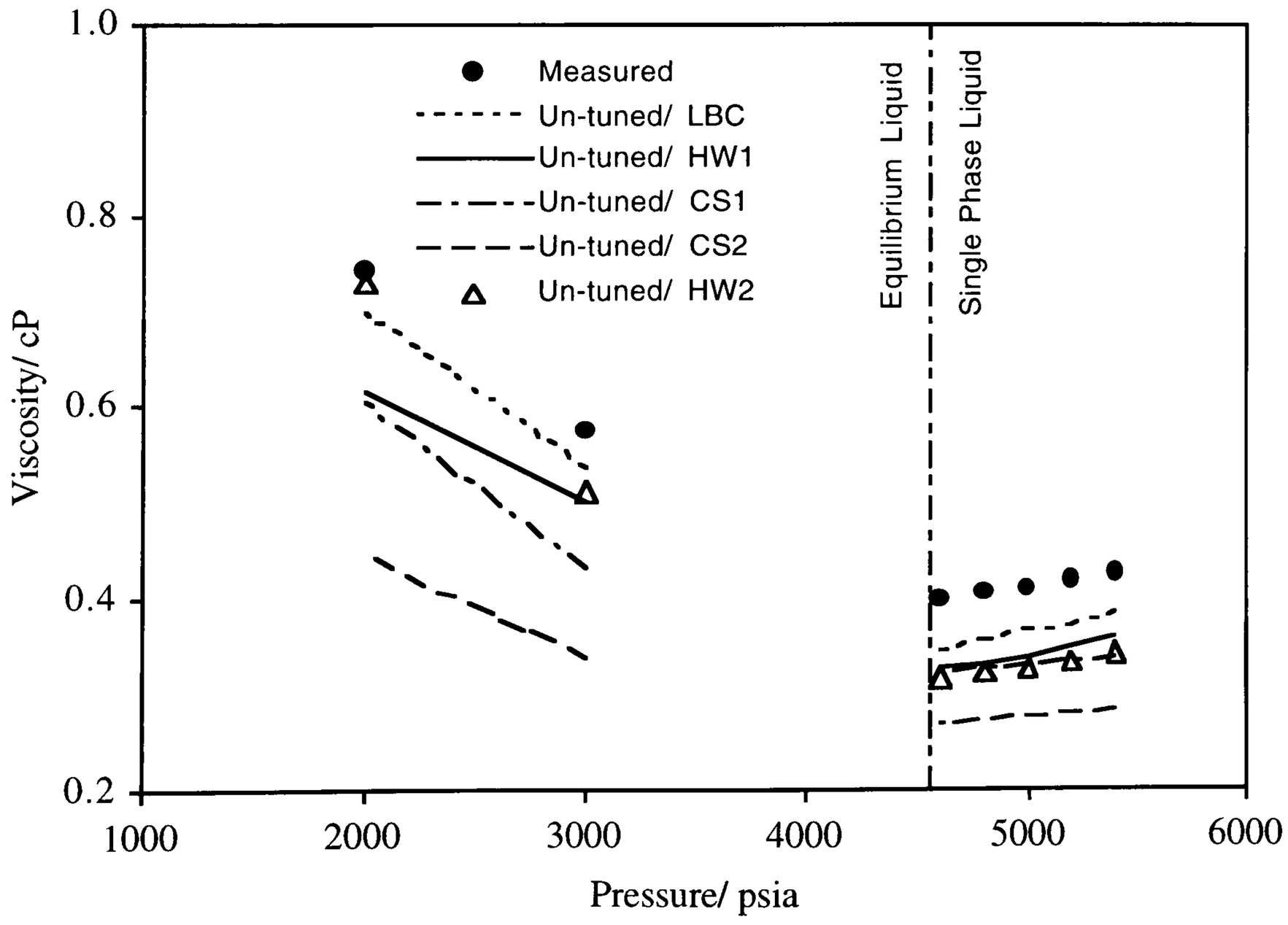

Figure 5.21 - Measured and Predicted Viscosity With Pressure for the Pure Volatile Oil LRA97-1 (Chapter 7, Table 7.13) at a Temperature of 37.8 °C, by the LBC, HW1 , CS1, CS2 and HW2 Models.

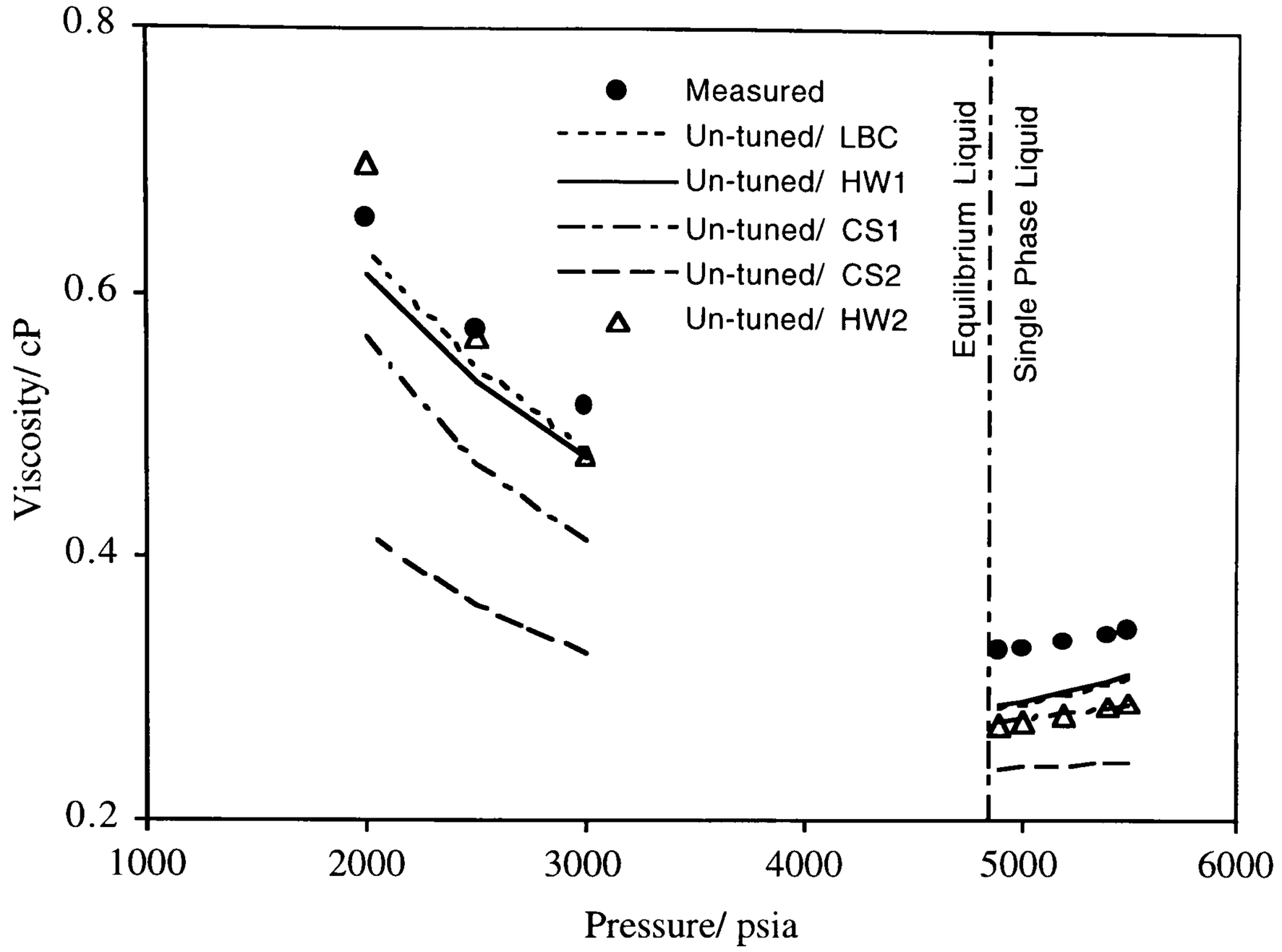

Figure 5.22 - Measured and Predicted Viscosity With Pressure for the Volatile Oil LRA97-1 With 14.8%, by Volume, of NCF (Chapter 6, Table 6.4) at a Temperature of 37.8 °C, by the LBC, HW1 , CS1, CS2 and HW2 Models.

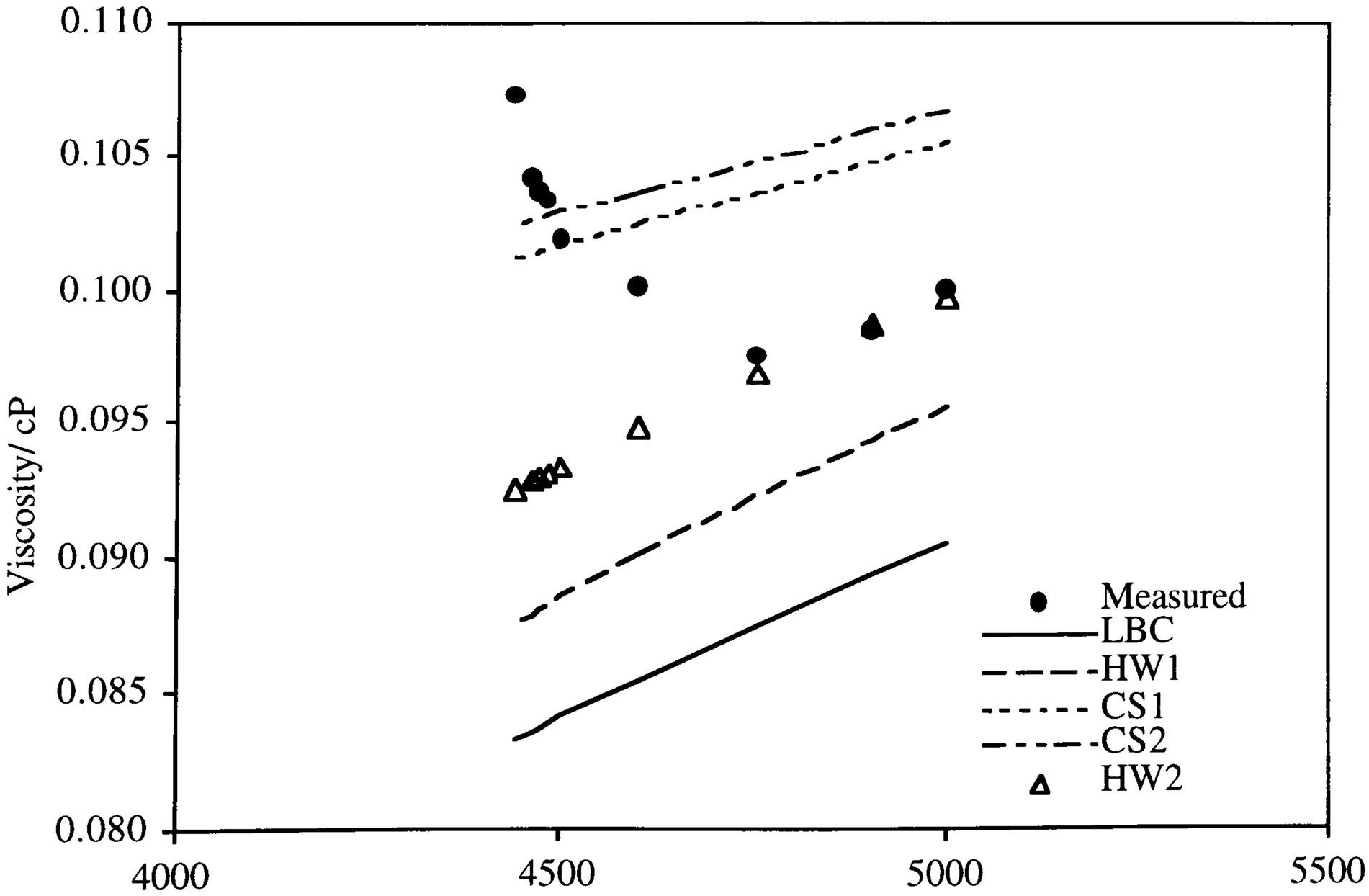

Figure 5.23 - Measured and Predicted Viscosity With Pressure for the Near Critical NCF (Chapter 6, Table 6.4) at a Temperature of 37.8 °C, by the LBC, HW1, CS1, CS2 and HW2 Models.

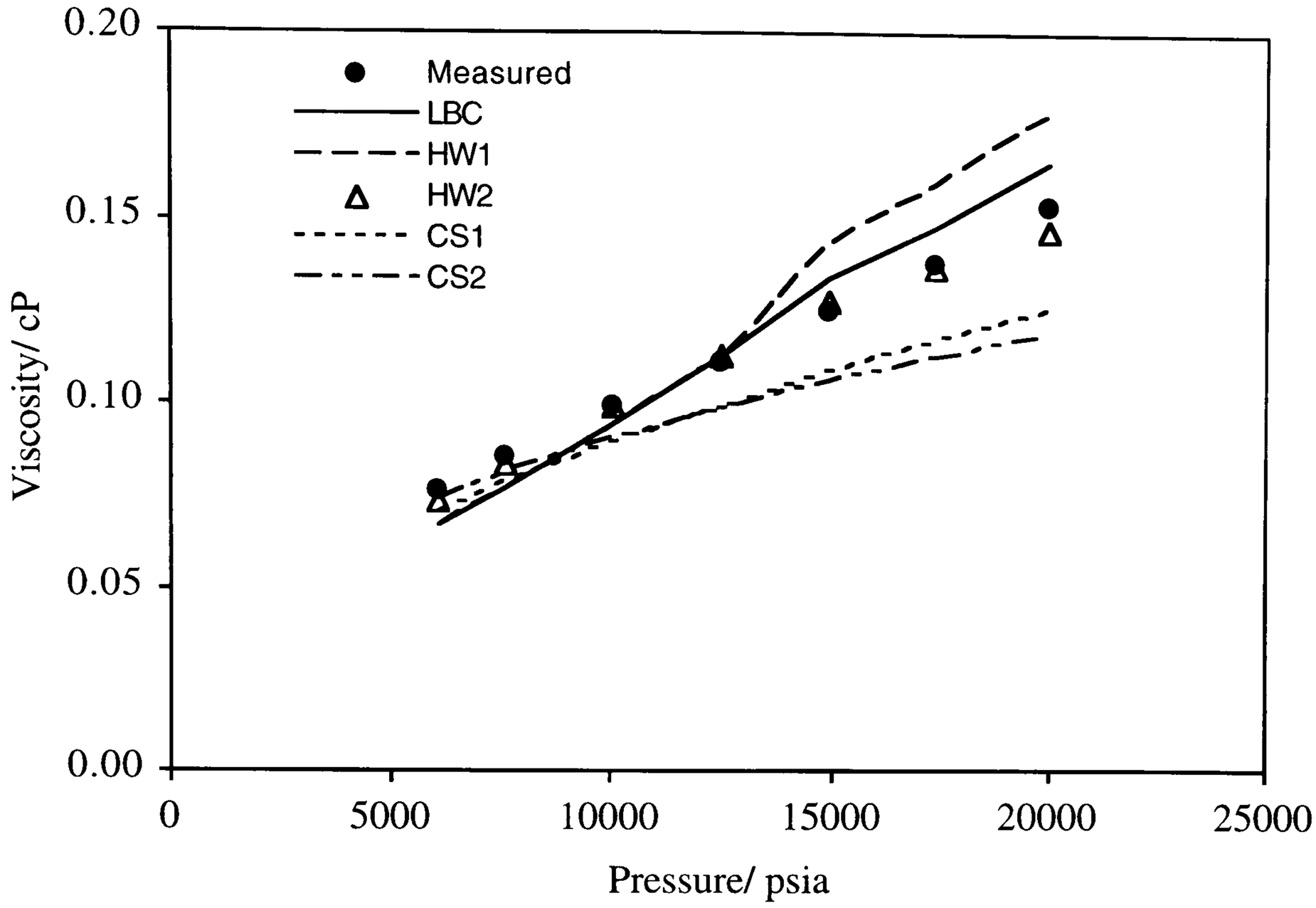

Figure 5.24 - Measured and Predicted Viscosity With Pressure for a Gas Condensate Sample at a Temperature of 50 °C, by the LBC, HW1, CS1, CS2 and HW2 Models[57].

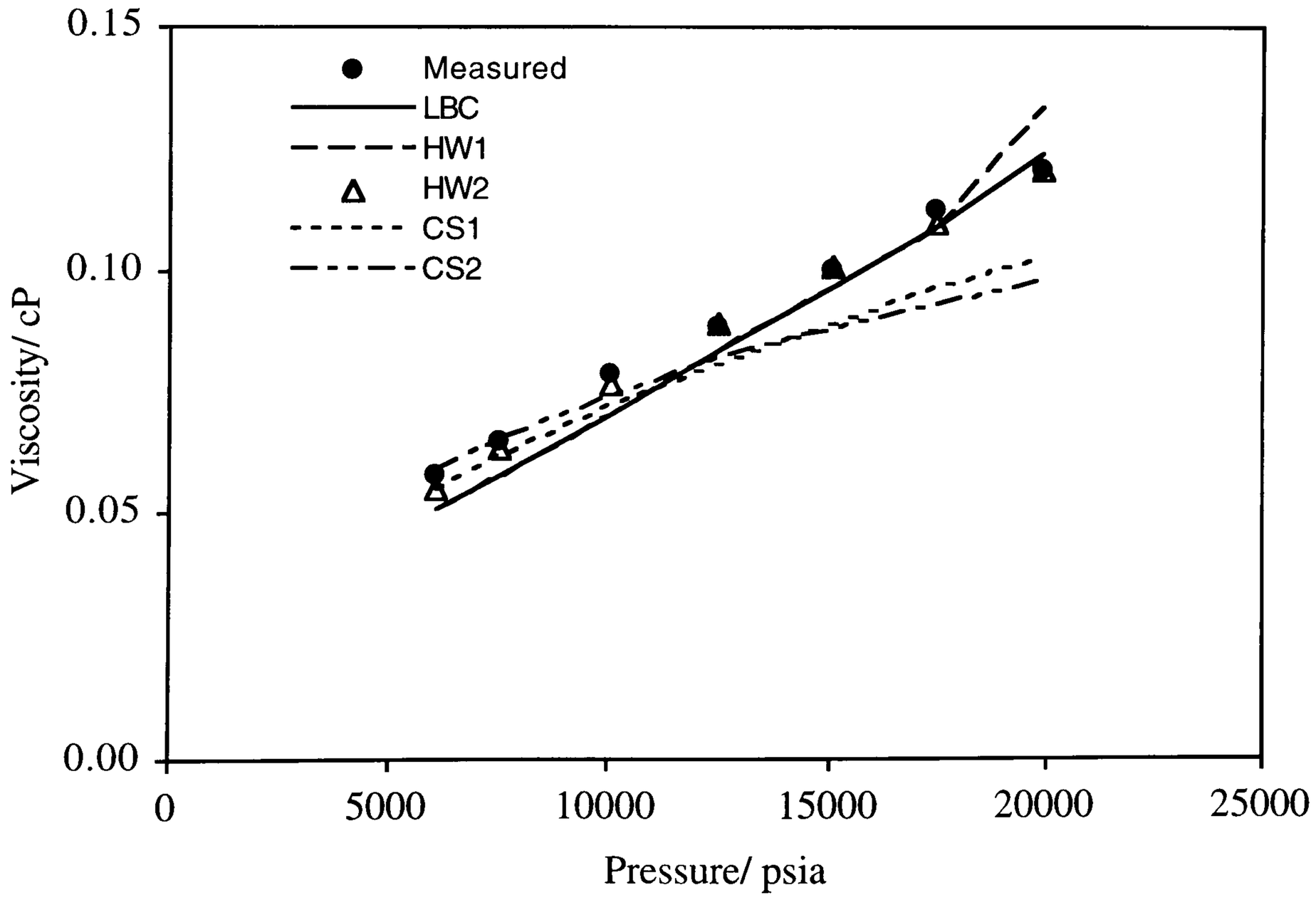

Figure 5.25 - Measured and Predicted Viscosity With Pressure for Gas Condensate Sample at a Temperature of 100 °C, by the LBC, HW1, CS1, CS2 and HW2 Models[57].

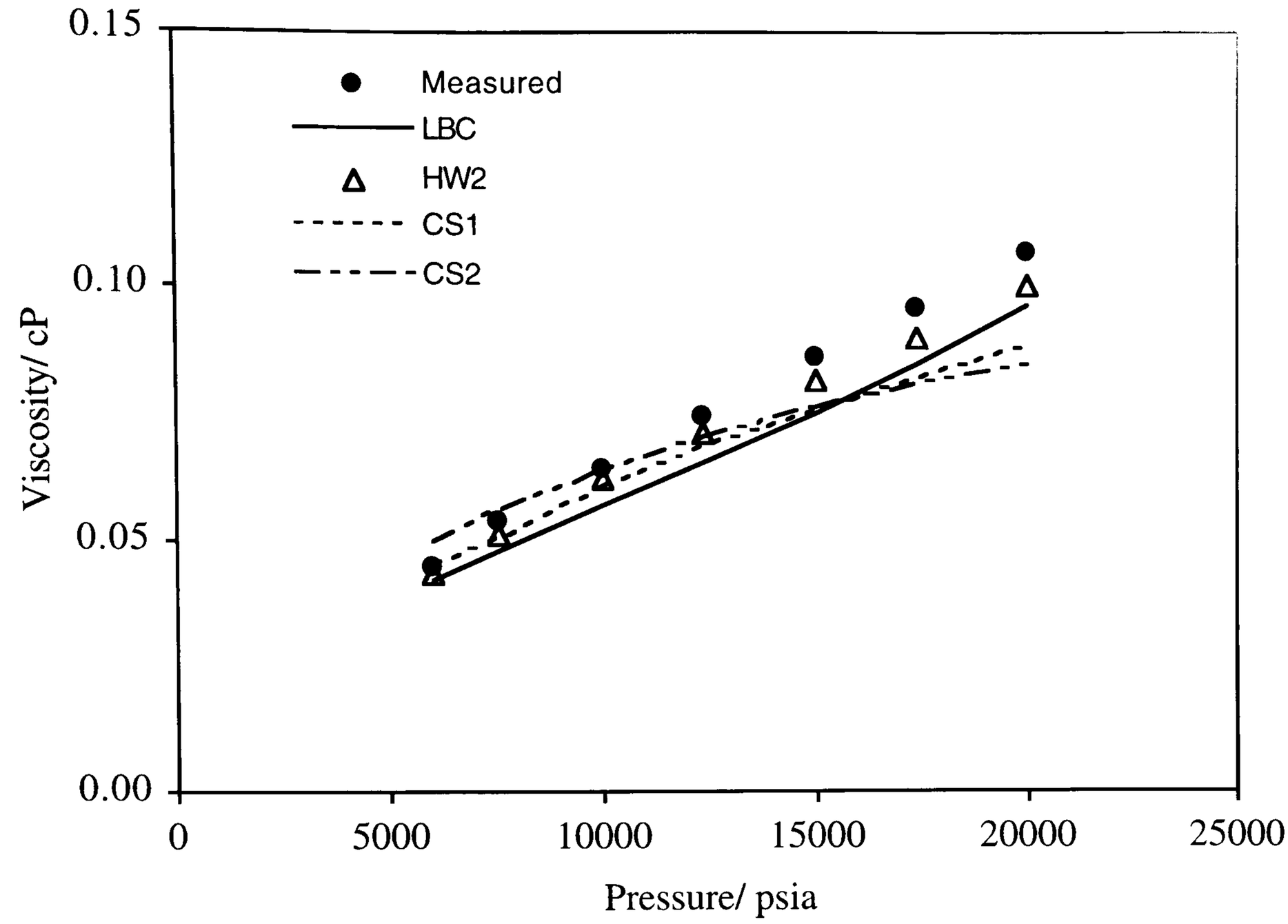

Figure 5.26 - Measured and Predicted Viscosity With Pressure for Gas Condensate Sample at a Temperature of 150 °C, by the LBC, HW1, CS1, CS2 and HW2 Models[57].

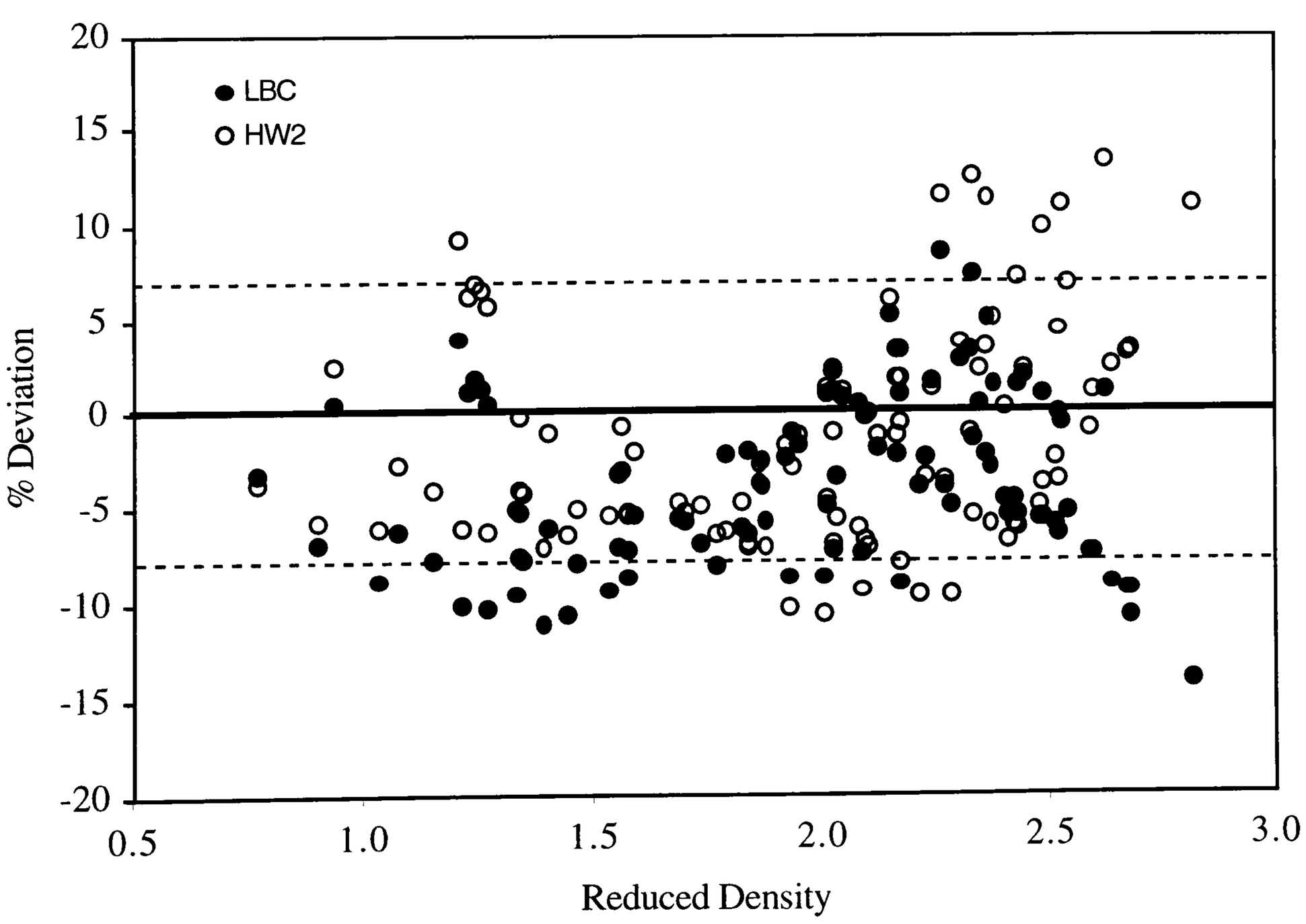

Figure 5.27 - Deviation of Predicted Viscosity by the LBC and HW2 Correlations from Measured Data on Methane/Methylcyclohexane Mixtures[56].

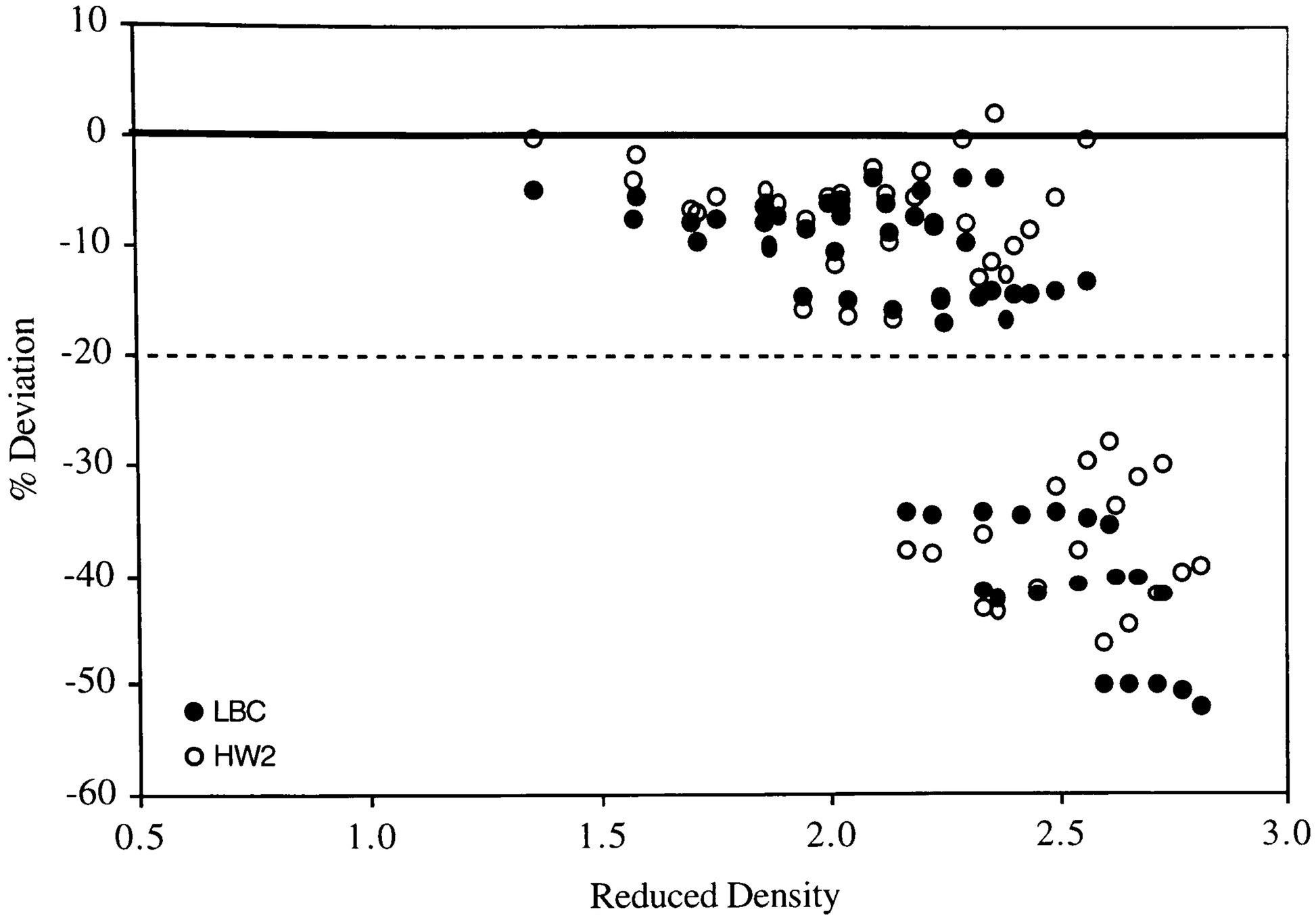

Figure 5.28 - Deviation of Predicted Viscosity by the LBC and HW2 Correlations from Measured Data on Methane/ cis-Decahydronaphthaline Mixtures[56].

CHAPTER 6

ABNORMAL VISCOSITY ENHANCEMENT FOR NEAR-CRITICAL FLUIDS

6.1 OBJECTIVES

The objectives of the research work presented in this chapter are:

- To investigate whether of real reservoir fluids exhibit the same viscosity enhancement (i.e., increase in viscosity) at near critical conditions, similar to those observed for other fluids.
- To investigate whether the viscosity models (residual viscosity models and corresponding states models) which are normally employed for calculating the viscosity of reservoir fluids.
- To develop a correlation, for the critical region, for predicting the near-critical viscosity enhancement of fluids for petroleum engineering application.

6.2 INTRODUCTION

Many thermophysical properties exhibit an anomalous behaviour in the vicinity of the critical point. For instance, the isothermal compressibility, the thermal expansion and specific heat all diverge when approaching the critical point. Anomalous behaviour have also been observed for the thermal conductivity and viscosity of fluids near the critical point[1-4]. The fundamental and most amazing feature of critical phenomena has been the

discovery of critical-point universality; the microscopic structure of fluids becomes unimportant in the vicinity of the critical point. Reliable understanding and description of critical behaviour of fluids and fluid mixtures are needed for many innovative applications such as enhanced oil recovery (e.g., miscible gas injection) and high pressure-high temperature technological processes (e.g., super-critical fluid technology).

Fluid viscosity appears to diverge from the normal trend as the critical point is approached. This critical divergence is believed to be due to compressibility enhancement (i.e., increase in fluid compressibility as the critical point is approached) resulting in a non-linear coupling between the various hydrodynamic modes (mainly viscous and diffusive) of the system. Experimental investigations[5-11] have already established the existence of anomalous viscosity enhancement, for a variety of single- and multi-component fluids, when approaching the critical point. Strumpf *et al*[5] while measuring the viscosity of xenon and ethane through the critical region observed that the viscosities of both substances exhibited an anomalous increase of 15% for xenon and 16% for ethane, relative to their normal viscosity. Zozulya and Blagoi[6] observed an increase of 17% in the normal viscosity while measuring the viscosity of nitrogen at a distance of 0.01 °C from the critical point. Iwasaki and Takahashi[7,8] observed the same anomalous increase for the viscosity of ethylene, carbon dioxide and ethane in the vicinity of their critical regions. Rivkin *et al*[9] observed anomalous increase of 12% for the viscosity of water near the critical region. D'Arrigo *et al*[10] reported viscosity data of the binary system Aniline-cyclohexane at different molar ratios. An anomalous increase of 20% was observed for a critical molar composition of 44.2 % of aniline. The same authors[11] also reported anomalous viscosity data of two ternary mixtures; Water-benzene-ethanol and Water-diethylether-ethanol.

The above experiments demonstrated the existence of universal anomalous viscosity behaviour at near critical conditions for diverse classes of fluids and their mixtures. However, to the best of my knowledge, viscosity enhancement for fluids with phase behaviour similar to real reservoir fluids has not been reported anywhere in the literature.

Unique experimental data of three near critical model fluids (C1/n-C10, C1/n-C8, and C1/n-C8/n-C10) and four real reservoir fluids, namely; NCF, OIL1, GC1 and GC2, close to their critical points are presented in this chapter. Viscosity enhancement in excess of 10% was observed which is significant and should be taken into account in flow simulation of near critical fluids.

Viscosity predictive models of Lohrenz-Bray-Clark (LBC)[12], the modified LBC[13], and the one- and two-reference fluid(s) corresponding state models[14,15] were used for predicting the observed viscosity enhancement. All models were observed to behave unreliably in the vicinity of critical point. To ensure reliable viscosity prediction at such conditions, a simple two-parameter corresponding state viscosity model has been developed (Al-Siyabi *et al*[16]). The methodology employed for developing the model and the comparison between model prediction and the observed viscosity enhancement of the above tested fluids are discussed in the subsequent sections.

6.3 PREDICTION OF VISCOSITY ENHANCEMENT

The principle of critical point universality asserts that diverse systems can all be described by the same type of scaled equation of state near the critical point phase transitions. Various empirical and theoretical attempts, using different mathematical representations, have been implemented to describe the behaviour of viscosity enhancement near the critical point. The two most widely used theoretical approaches to improve understanding of the singular behaviour of transport coefficients in the vicinity of the critical point are the mode-coupling theory[17,18] and the renormalisation-group theory[19,20].

The mode-coupling theory[17,18] originated from the idea that the critical anomalies of transport coefficients result from the non-linear coupling between the hydrodynamic modes of the system; the diffusive decay mode and the transverse viscous mode. Consequently, the theory yields two coupled integral equations for the diffusion, D, and the viscosity, η, in which all other properties of the system are related to. In its simplest

form, the mode-coupling theory[17,18] predicts that the critical viscosity enhancement, $\Delta\eta_c$, will diverge logarithmically as;

$$\eta = \eta_n + \Delta\eta_c = \eta_n\left[1 + \frac{8}{15\pi^2}\ln(q\xi)\right] \tag{6.1}$$

The renormalisation-group theory[19,20] was originally developed to explain the critical behaviour of equilibrium properties, was further extended to deal with dynamic properties. The theory has been used to study the universal aspects of the divergent behaviour of the transport properties. Likewise, the renormalisation-group theory, in its simplest form, predicts that the viscosity, η, will diverge asymptotically as a power law of a multiplicative anomaly;

$$\eta = \eta_n.\Delta\eta_c = \eta_n.(q\xi)^z \tag{6.2}$$

6.4 PRACTICAL EXAMPLES OF NEAR-CRITICAL CONDITIONS IN RESERVOIR ENGINEERING:

Due to the rapid technological advancement in hydrocarbon exploration, drilling and recovery schemes, HPHT reservoirs are now being discovered and exploited in various parts of the world. Reservoir fluids present in these adverse conditions can give rise to peculiar behaviour for volumetric and fluid properties[21]. Moreover, improved oil recovery (IOR) methods are now routinely employed, at early stages of production, for the purposes of maintaining reservoir pressure above the fluid saturation pressure or maximising the sweep efficiency of in-situ hydrocarbons. Due to various environmental constraints, produced gas is normally re-injected back into the reservoir. IOR processes conducted at high pressures and temperatures can result in near critical conditions.

A few examples that are often not fully accounted for in reservoir engineering are briefly discussed. Accurate prediction of the phase behaviour and fluid properties is essential in correctly predicting and managing reservoir performance in such operations.

6.4.1 Compositional Grading

Vertical and lateral compositional grading due to gravity and temperature gradients may exist in a reservoir, especially those of large fluid columns[22]. One might expect that reservoir fluids might have attained mature equilibrium over geological times due to molecular diffusion. However, a complete diffusion process for a column of reservoir fluid may require millions of years for a fluid to attain its homogeneity.

Throughout a fluid column, the pressure and temperature are not uniform. Temperature and pressure gradients of about 0.02-0.03 °C/m (9.76-9.77 °F/ft) and 1.8-8.0 kPa/m (0.08-0.36 psi/ft), respectively, can be expected[22]. Samples collected from different depths can possess vastly different compositions and physical as well as thermodynamic properties. In general, the mixture is expected to get richer in heavier compounds, containing fewer light components, such as methane, with depth which will results in changes in the saturation pressure. The compositional grading can also be very severe, resulting in a column of fluid changing from gas at the top to an oil at the bottom, without any phase boundary, as schematically illustrated in Figure 6.1. Table 6.1 also gives some properties of fluids at different depths for a North Sea reservoir.

Such major changes in compositions and properties can not be ignored as it strongly affect the estimation of reserve and production planning of such reservoirs.

6.4.2 Oil and Gas Displacement in Porous Media

Injection of gas into oil and gas condensate reservoirs to increase hydrocarbon recovery has been a commonly applied technique in various parts of the world. Gas injection can improve hydrocarbon recovery through maintaining the reservoir pressure, displacing oil, or vaporising the intermediate and heavy fractions of the oil[22]. As the injected gas is not primarily in equilibrium with the reservoir oil, the contact between the phases results in mass transfer, hence, changes in the properties of the two phases take place.

The displacement of oil by gas can become a highly efficient process when the properties of the advancing gas and the displaced oil become very similar; that is both phases are in

complete miscibility and the interface between the vapour and liquid phases vanishes. In a multiple-contact miscibility processes, the injected gas (generally free of heavy fractions) enriches the reservoir oil with its intermediate components while it stripes away the heavy components. The reservoir oil in contact with the injected gas becomes lighter as it contacts more gas; while the injected gas enriches with heavier components and thus becomes less similar to the freshly injected gas. As the oil is contacted with additional rich gas, the concentration of its plus fraction decreases lightening the oil in its path toward achieving condensing miscibility.

As forward moving gas becomes richer in heavy fractions, it vaporises less of these compounds whilst losing its intermediates to the oil. It is conceivable that at favourable conditions, the combined vaporisation and condensation process results in a state within the transition zone where the compositional path goes through the critical point achieving miscibility, schematically shown in Figure 6.2

It is very important to account for such changes in composition and fluid properties when modelling such processes.

6.5 TEST FLUIDS AND EXPERIMENTAL RESULTS

6.5.1 Test Fluids

Two binary mixtures of Methane/n-Decane (89.39 mole % Methane : 10.61 mole % n-Decane) and Methane/n-Octane (85.11 mole % Methane : 14.89 mole % n-Octane) were initially prepared to give saturation pressures of 5250 psia and 4018 psia, respectively, which are very close to the critical pressures at the critical temperature of 37.8 °C . A ternary mixture (88.14 mole % Methane : 4.35 mole % n-Octane : 7.51 mole % n-Decane) of the above near critical binary mixtures was also prepared which was found to display the usual near critical luminous colouring as the saturation pressure is approached.

Four near critical real reservoir fluids, namely; NCF, OIL1, GC1, and GC2, were also prepared and tested in this work. The compositional data of the NCF fluid can be found in Table 3.3 of Chapter 3 and those for the OIL1 fluid can be found in Table 4.7 of Chapter 4, where the fluid is referred to as Mix 2. The compositional data of GC1 and GC2 are listed in Table 6.2.

6.5.2 Experimental Results

The viscosity of the above fluids was measured to examine whether they exhibit the same near critical enhancement observed for different classes of fluids. The viscosity data of all tested fluids are tabulated in Tables 6.3 and 6.4. To ensure that the observed behaviour was not an artefact, due to the tube dimension, the measurement for the Methane/n-Decane viscosity was repeated using a capillary tube viscometer with an internal diameter twice that of the original capillary tube, Figure 6.3. The measured viscosity with the larger tube **did** confirm the reality of the observed viscosity enhancement which could be attributed to fluid structural changes as the critical region is approached. However since the objective of using the larger tube was not to quantify the enhancement, it was not fully calibrated. The calibration was done at a single point away from where viscosity enhancement, in the smaller tube, was observed. A value for the internal diameter was derived which was used to calculate the viscosity inside the critical region. Figures 6.4 and 6.5 display the measured viscosity of the tested fluids as a function of pressure at a temperature of 37.8 °C. The results showed that near critical enhancement is universal, however its intensity varied for different fluids. The viscosity of the single phase (gas or liquid) is observed to decrease as pressure is decreased well above the saturation pressure. As the pressure approaches the saturation pressure, the viscosity increases reaching its maximum at the saturation (critical) pressure.

6.6 EVALUATION OF PREDICTIVE MODELS FOR NEAR-CRITICAL FLUIDS

The reliability of predictive techniques[12-15], normally employed in the petroleum industry for viscosity calculation, at near-critical conditions was investigated by comparing their

results with measured values. As expected, none of the models cater for such anomalous enhancement. For example, Figure 6.6 compares the predicted values for C1/n-C8 with measured data. Using the above predictive techniques, even with parameter(s) tuned to conventional data, can lead to unreliable estimation of well or reservoir performance and over- or under-sizing of surface facilities and pipeline systems at such conditions.

As none of the correlations described in Section 6.3 were considered to be readily adopted for real reservoir fluids, a simple model has been developed to estimate the magnitude of viscosity enhancement at near-critical conditions, as described in the Section 6.6, below.

6.7 DEVELOPMENT OF PREDICTIVE MODEL

6.7.1 Methodology

In practice, a description of viscosity in terms of density and temperature, $\eta(\rho,T)$, is often preferred, not only for theoretical reasons, but also because of the accessibility of these variables from routine measurements. In the treatment of properties of near critical fluids, it is advantageous to decompose the property into its normal and critical enhancement components[24]. Viscosity, $\eta\ (\rho,T)$, can be written as the sum of three contributions:

$$\eta\ (\rho,T) = \eta_0(0,T) + \Delta\eta(\rho,T) + \Delta\eta_c(\rho,T) \qquad (6.3)$$

The viscosity data of the pure fluids[5-11], used in the development of the proposed model, have been assessed by several investigators[3,25-27] and believed to be accurate within ±2%. For each substance, the residual viscosity, $\Delta\eta\ (\rho,T)$, as a function of density was first established from the high temperature viscosity data, far away from the critical region, and seen to be very weakly-dependent on temperature, Figures 6.7 through 6.11. Then, the normal viscosity, $\eta_n(\rho,T)$, at any density and temperature of interest was calculated from the relationship:

$$\eta_n(\rho,T) = \Delta\eta(\rho) + \eta_0(0,T) \tag{6.4}$$

The anomalous part of the viscosity was then calculated from the relationship:

$$\Delta\eta_c(\rho,T) = \eta(\rho,T) - \eta_n(\rho,T) \tag{6.5}$$

Several forms of representation of viscosity enhancement were examined. It was observed that a semi-log plot of normalised viscosity enhancement, $\Delta\eta_c/\eta_n$, as a function of the reduced scaled density, $\Delta\rho_r = (\rho-\rho_c)/\rho_c$, of pure compounds almost gives a linear relationship, as shown in Figures 6.12 through 6.16. Furthermore, it was assumed that the two-parameter corresponding states principle is valid, and the coefficients, of the semi-logarithmic functional form, of each isotherm were correlated with the reduced scaled temperature, ΔT_r, as;

$$\frac{\Delta\eta_c(\rho_r,T_r)}{\eta_n(\rho_r,T_r)} = -A(\ln\Delta\rho) - B \tag{6.6}$$

Figure 6.17 shows that the coefficients A and B can be satisfactorily correlated with the reduced scaled temperature for different compounds, demonstrating the reliability of the above assumption. According to Figure 6.17, the coefficients are almost equal. From the above analysis, the final form of the proposed model for the enhancement term is obtained as,

$$\frac{\Delta\eta_c(\rho_r,T_r)}{\eta_n(\rho_r,T_r)} = [0.008\ln\Delta T_r + 0.03][\ln\Delta\rho_r + 1] \tag{6.7}$$

The above developed model, Equation (6.7), was used to re-calculate the observed viscosity enhancement for pure components, as shown in Figure 6.18. Figure 6.18

clearly shows that the model is universal and can be used to predict viscosity enhancement with reasonable accuracy.

6.7.2 Capability of the Developed Model.

The viscosity of the following mixtures C1/n-C10, C1/n-C8, C1/n-C8/n-C10, NCF, OIL1, GC1, and GC2, were measured inside and outside their critical regions. For the purpose of comparing the measured and predicted viscosity enhancements, the normal viscosities of the above mentioned fluids as predicted by conventional methods[12-15] were first estimated. The conventional models are often tuned to experimental data initially for improved reliability. The models are normally tuned by slight adjustment of critical properties or molecular weight of the fluid components. For reservoir fluid mixtures, adjustment of the above influential properties are customarily applied to the plus fraction (normally taken as C7+). For each fluid mixture, the model which yielded the overall minimum deviation for the viscosities outside the critical region were then used for calculating normal viscosities inside the critical region.

Figure 6.19 through 6.25 show the results of applying the above empirical model, Equation (6.7), to the tested fluids. In general, the model shows good agreement with experimental data, especially close to the critical points. Deviations of the model prediction from experimental data seem to increase as the reduced scaled density moves further away from the critical region.

For simple fluids, reduced temperature and reduced density or pressure is usually sufficient in correlating a state property. However, to generalise a correlation to different classes of fluids, a third parameter (e.g., molecular weight, acentric factor) is normally needed. For this work, the disappearance of critical enhancement, $\Delta\eta_c=0$, for pure components was established from the plots of normalised viscosity enhancement versus reduced scaled density shown in Figure 6.12 through 6.16. The calculated reduced scaled density, marking the disappearance of viscosity enhancement, was then plotted as a function of molecular weight shown in Figure 6.26. Figure 6.26 shows that there is no

obvious trend between the disappearance of viscosity enhancement with fluids molecular weight. As far as the corresponding state principle is concerned, the disappearance of viscosity enhancement for simple fluids (N2, CO2, C2H6 and C2H4) should occur at the same reduced scaled density. The scattering in the calculated values, shown in Figure 6.26, could be due to errors introduced to the calculated critical enhancement from the assumption that residual viscosity is independent of temperature. This assumption could be significant in establishing the normal viscosity, which in turn is used to calculate the viscosity enhancement, especially for those fluids showing weak viscosity enhancement.

6.8 CONCLUSIONS

- The measurement of viscosity of several near critical mixtures, representative to those discovered for HPHT reservoirs and IOR processes, exhibited viscosity enhancement near the critical region (Figures 6.4 and 6.5), similar to those of pure compounds reported in the literature. Viscosity enhancement in excess of 10% was observed which is significant and should be taken into account in flow simulation at such conditions.
- The developed correlation (Equation (6.7)), for the critical region, successfully predicted the near critical viscosity enhancement of all tested fluids. Deviations were observed to increase further away from the critical point.
- The deviation of model predictions from experimental data for real fluids was investigated by including the molecular weight as the third corresponding state parameter (Figure 6.26). No obvious trend between the disappearance of viscosity enhancement with the component molecular weight can be seen.

REFERENCES

[1] Sengers, A. L., Hocken, R. and Sengers, J. V. : "Critical-Point Universality and Fluids", Physics Today, 42-51, (Dec., 1977).

[2] Sengers, J. V. : "Critical Behaviour of Fluids: Concepts and Applications", in Supercritical Fluids: Fundamentals for Application, edited by E. Kiran and J. M. H. Levelt Sengers, Kluwer Press, Dordrecht, 3-38, (1994).

[3] Sengers, J. V. : "Transport Properties of Gases and Binary Liquids Near the Critical State", Transport Phenomena, J. Kestine, ed., AIP Conference Proceedings No. **1**, 229-277, (1973).

[4] Kieselev, S. B. and Kulikov, V. D. : "Thermodynamic and Transport Properties of Fluids and Fluid Mixtures in the Extended Critical Region", Int. J. Thermophys., **18**(5), 1143-1182, (1997).

[5] Strumpf, H. J., Collings, A. F. and Pings, C. J. : "Viscosity of Xenon and Ethane in the Critical Region", J. Chem. Phys., **60**(8), 1309-1323, (April, 1974).

[6] Zozulya, V. N. and Blagoi, Yu. P. : "Viscosity of Nitrogen Near the Liquid-Vapour Critical Point", Soviet Physics-JETP, **39**(11), 99-105, (Jul., 1974).

[7] Iwasaki, H. and Takahashi, M. : "Viscosity of Ethylene", Proceedings of the 4th International Conference on High Pressure, Kyoto, 523-529, (1974).

[8] Iwasaki, H. and Takahashi, M. : "Viscosity of Carbon Dioxide and Ethane", J. Chem. Phys., **74**(3), 1930-1943, (Feb., 1981).

[9] Rivkin, S. L., Levin, A. Ja, Izrailevsky, L. B. and Kharitonov, K. G. : "Experimental Investigation of Viscosity of Light Water near the Critical Point and of Heavy Water in Liquid Phase and in Supercritical Region", Proceedings of the 8th International Conference on the Properties of Water & Steam, Paris, 153-162, (1975).

[10] D'Arrigo, G., Mistura, L., and Tartaglia, P. : "Concentration and Temperature Dependence of Viscosity in the Critical Mixing Region of Aniline-Cyclohexane", J. Chem. Phys., **66**(1), 80-84 (1977).

[11] D'Arrigo, G., Mistura, L. and Tartaglia, P. : "Shear Viscosity in Ternary Liquid Systems Near a Plait Point", J. Chem. Phys., **66**(1), 74-79 (1977).

[12] Lohrenz, J., Bray, B. G. and Clark, C. R. : "Calculating Viscosities of Reservoir Fluids from Their Compositions", JPT, 1171-1176, (Oct., 1964).

[13] Dandekar, A., Danesh, A., Tehrani, D. H. and Todd, A. C. : "A Modified Residual Viscosity Method for Improved Prediction of Dense Phase Viscosities", Presented at the 7th European Improved Oil Recovery (IOR) Symposium in Moscow, Russia, Oct. 27-29, (1992).

[14] Pedersen, K. S, and Fredenslund, Aa. : "An Improved Corresponding States Model for the Prediction of Oil and Gas Viscosities and Thermal Conductivities", Chem. Eng. Sci., **42**, 182-186, (1987).

[15] Petersen, Aa. K., Knudsen, K. and Fredenslund, A. : "Prediction of Viscosities of Hydrocarbon Mixtures," Fluid Phase Equilib., **70**, 293-308, (1991).

[16] Al-Siyabi, Z. K., Danesh, A., Tohidi, B. and Todd, A. C. : "Abnormal Viscosity Behaviour of Near Critical Fluids, Experimental Data and Modelling", paper No. 57 presented at the 10th Improved Oil Recovery Symposium held in Brighton, UK, Aug. 18-21, (1999).

[17] Kawasaki, K. : "Mode-Coupling and Critical Dynamics", in Phase Transitions and Critical Phenomena, C. Domb and M. S. Green, eds. (Academic Press, New York, **5A**, 165-403, (1976)

[18] Perl, P. and Ferrell, R. A. : "Decoupled Mode Theory of Critical Viscosity and Diffusion in the Binary-Liquid Phase Transition," Phys. Rev., **6A**, 2358-2369, (1972).

[19] Wilson, K. G. and Fisher, M. E. : "Renormalisation group theory", Phys. Rev. Lett., **28**, 248 (1972).

[20] Hohenberg, P. C. and Halperin, B. I. : "Theory of Dynamic Critical Phenomena". Rev. Mod. Phys., **49**(3), 435-479, (1977).

[21] Ungerer, P., Moracchini, G., Jensen, M., de Hemptinne, J. C., Sportisse, M., Batut, C. and Dhima, A. : "Characterization of High Temperature-High Pressure Reservoir Fluids", Progress on HP-HT Fields, Aberdeen, April ,1996.

[22] Danesh, A. : PVT and Phase Behaviour of Petroleum Reservoir Fluids, Elsevier Science B. V., The Netherlands (1998).

[23] Reservoir Fluid Studies, Final Report, 1996-1999 Programme, Department of Petroleum Engineering, Heriot-Watt University, Report No.: **PVT/00/1**.

[24] Vesovic, V. and Wakeham, W. A. : "Transport Properties of Supercritical Fluids and Fluid Mixtures", Chapter 6 in Supercritical Fluid Technology: Reviews in Modern Theory and Applications, CRC Press Inc., Boca Raton, Florida, 245-289, (1991).

[25] Stephen, K. and Krauss, R. : "Viscosity and Thermal Conductivity of Nitrogen for a wide range of Fluid States," J. Phys. Chem. Ref. Data, **16**(4), 993-1023, (1987).

[26] Vesovic, V., Wakeham, W. A., Olchowy, G. A., Sengers, J. V., Watson, J. T. R. and Millat, J. : "The Transport Properties of Carbon Dioxide", J. Phys. Chem. Ref. Data, **19**(3), 763-808, (1990).

[27] Hendl, S., Millat, J., Vogel, E., Vesovic, V., Wakeham, W. A., Leuttmer-Strathmann, J., Sengers, J. V., and Assael, M. J. : "The Transport Properties of Ethane. I. Viscosity", Int. J. Thermophys., **15**(1), 1-31, (1994).

Table 6.1 - Properties of Fluids at Different Depths in a North Sea Reservoir[22].

Fluid Properties	Well 1	Well 2C	Well 2B	Well 2A
Depth/ m	3136	3156	3181	3217
Reservoir Pressure/ psia	6517	6511	6441	6577
Reservoir Temperature/ C	111	106.6	107.7	108.8
Density at Res. Press./ g/cc	0.4004	0.5308	0.5577	0.5734
Saturation Pressure/ psia	5656	5482	5410	4786
Saturation Point	Dew Point	Dew Point	Bubble Point	Bubble Point
Density at Sat. Press./ g/cc	0.3974	0.5030	0.5400	0.5462
Separator Pressure/ psia	6.5	1.6	1.7	1.2
Separator Temperature/ psia	12.2	34.9	37.7	17.7
Separator GOR/ m^{-3}/m^{-3}	1005.0	611.0	390.0	304.0
Tank Oil Specific Gravity	0.7877	0.8170	0.8254	0.8185

Table 6.2 - Calculated Molar Compositions of GC1 and GC2 Fluids.

Comp.	(GC1) | (GC2)		
	MW |	Mole/ %	
C1	16.04	70.45	70.32
C2	30.07	11.54	11.38
C3	44.10	4.66	4.69
i-C4	58.12	0.80	0.82
n-C4	58.12	1.69	1.72
i-C5	72.15	0.60	0.61
n-C5	72.15	0.77	0.80
C6	88.5	0.91	0.74
C7	92.0	1.35	1.04
C8	103	1.32	1.08
C9	116	0.73	0.72
C10	131	0.54	0.53
C11	147	0.39	0.41
C12	161	0.31	0.30
C13	173	0.27	0.39
C14	186	1.63	0.73
C15	203	0.22	0.93
C16	215	0.79	0.78
C17	229	0.14	0.62
C18	246	0.14	0.44
C19	258	0.11	0.27
C20+	384	0.64	0.68

Table 6.3 - Measured Viscosity Data, in cP, for the Binary Methane / n-Octane, Methane / n-Decane Fluids and Their Mixture at 37.8 °C.

Pressure (psia)	C1 / n-C8	C1 / n-C10	C1 / n-C8 / n-C10
5500	0.0790	0.0799	0.0788
5450	-	0.0789	-
5400	-	0.0778	-
5350	-	0.0793	-
5300	-	0.0825	0.0763
5275	-	0.0839	-
5265	-	0.0849	-
5255	-	0.0857	-
5100	-	-	0.0745
5000	0.0753	-	0.0756
4900	-	-	0.0769
4875	-	-	0.0776
4850	-	-	0.0785
4500	0.0715	-	-
4200	0.0708	-	-
4100	0.0720	-	-
4050	0.0735	-	-
4030	0.0742	-	-
4025	0.0748	-	-

Table 6.4 - Measured Viscosity Data, in cP, for the Multi-component Fluids NCF, OIL1, GC1 and GC2 at 37.8 °C.

Pressure/ (psia)	NCF	OIL1	GC1	GC2
5700	-	-	-	0.1075
5500	-	0.1397	0.0944	0.1041
5400	-	0.1362	-	0.1056
5350	-	0.1348	-	-
5300	-	0.1337	0.0929	0.1067
5200	-	0.1343	-	-
5150	-	-	0.0920	-
5100	-	0.1359	-	0.1096
5060	-	-	-	0.1124
5000	0.0999	0.1391	0.0918	-
4950	-	0.1417	-	-
4925	-	0.1448	-	-
4900	0.0984	-	0.0925	-
4850	-	-	0.0929	-
4800	-	-	0.0940	-
4780	-	-	0.0956	-
4750	0.0974	-	-	-
4600	0.1000	-	-	-
4500	0.1019	-	-	-
4480	0.1033	-	-	-
4460	0.1042	-	-	-
4440	0.1072	-	0.0956	-

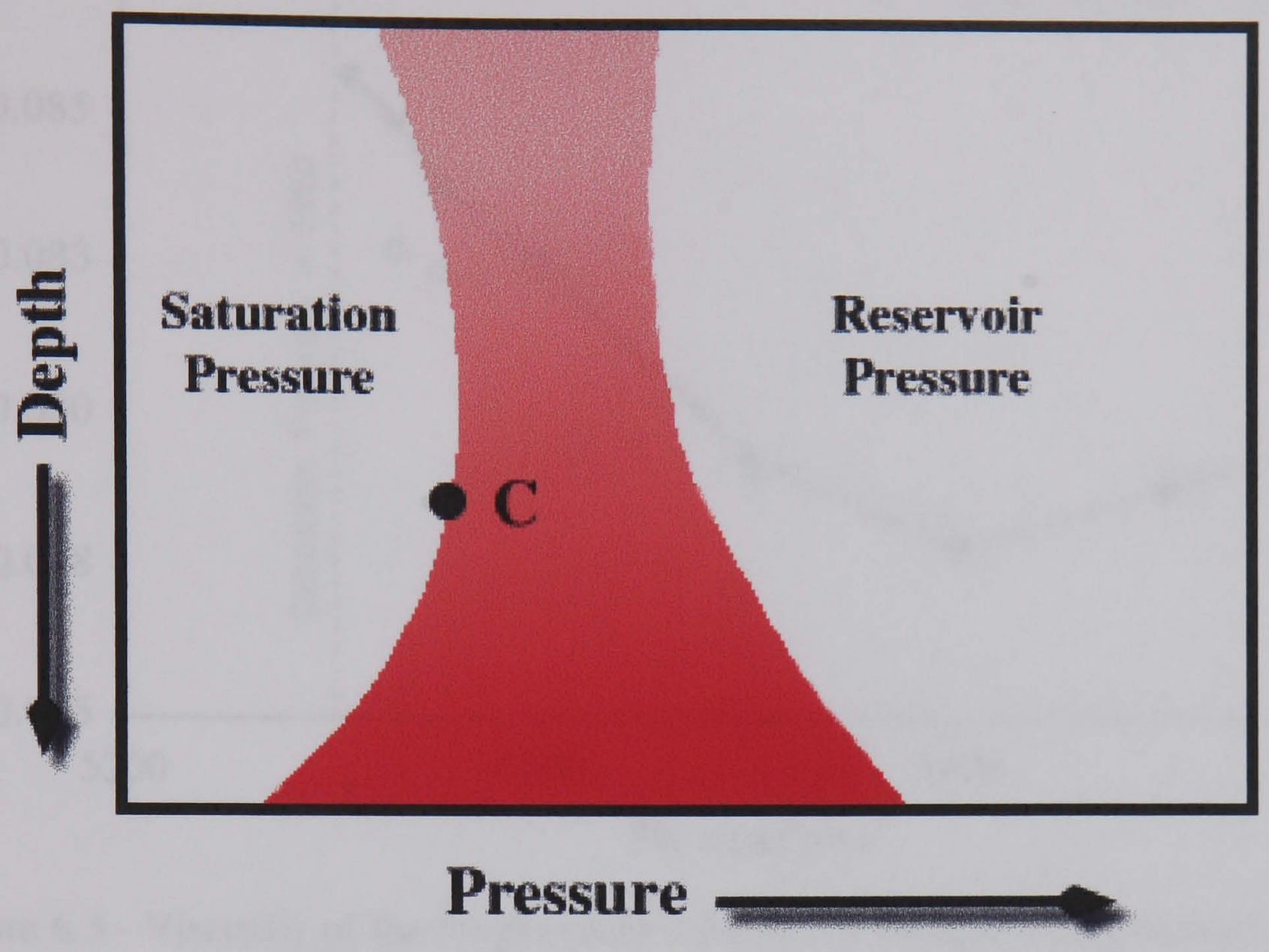

Figure 6.1 – Phase Variation in Reservoirs with Compositional Grading.

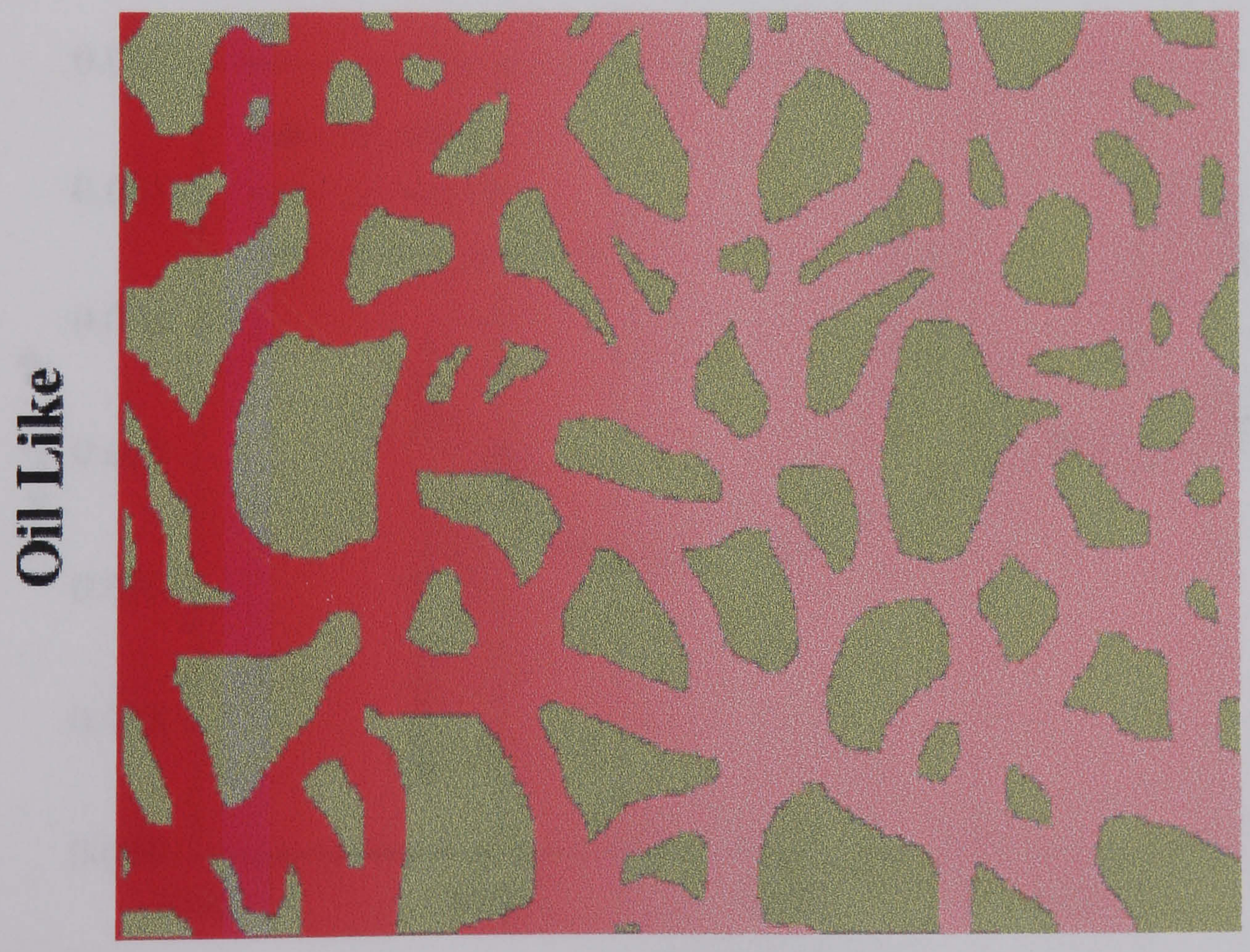

Figure 6.2 – Phase Variation in Reservoirs During Gas Injection Displacement Process in Porous Media.

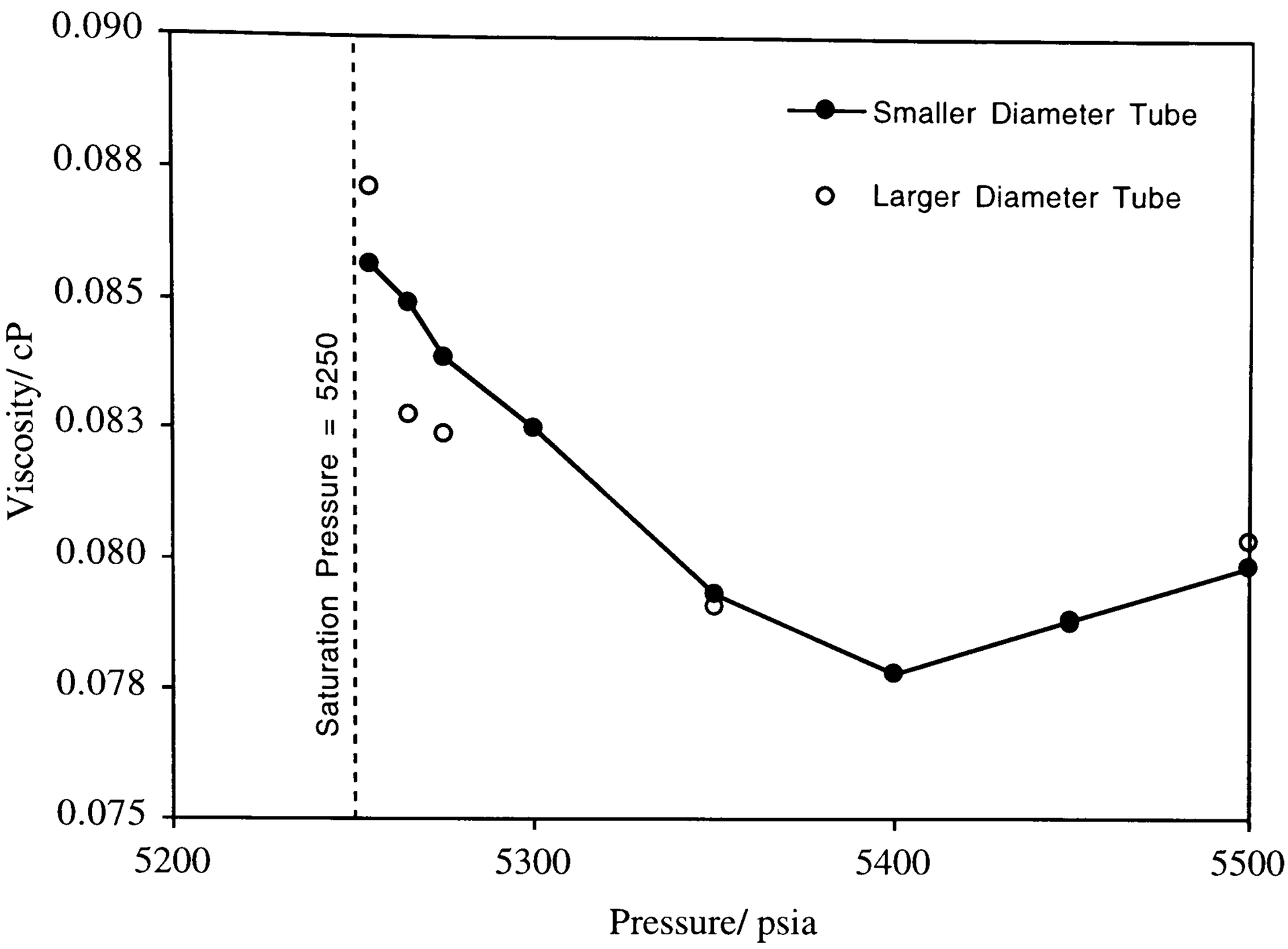

Figure 6.3 - Viscosity of the Single-phase Methane/n-Decane Using Smaller and Larger Diameter Tubes at a Temperature of 37.8 oC

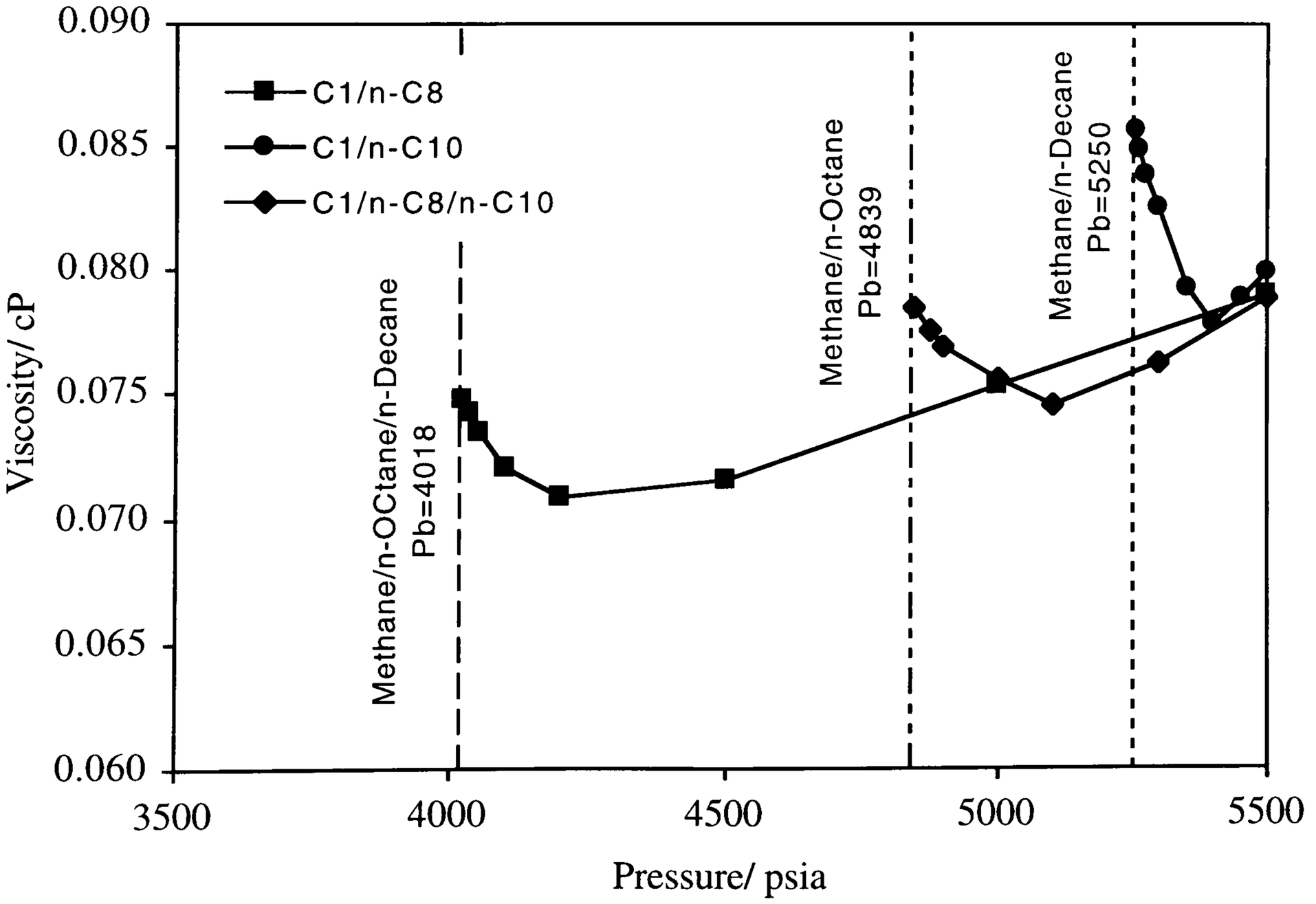

Figure 6.4 - Viscosity of Single-phase Methane/n-Octane, Methane/n-Decane, and Methane/n-Octane/n-Decane Mixtures at a Temperature of 37.8 oC

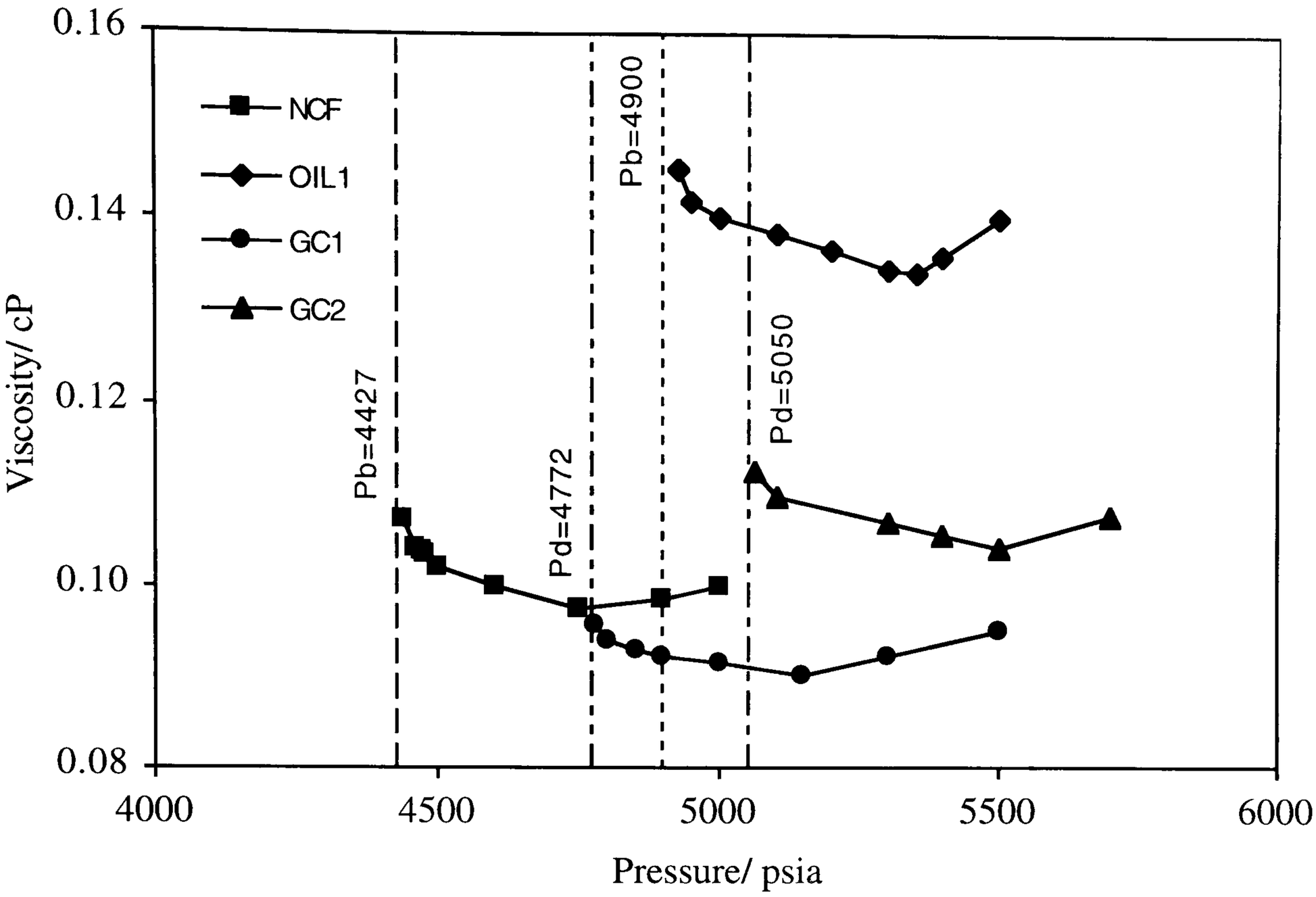

Figure 6.5 - Viscosity of Single-phase NCF, OIL1, GC1, GC2 Fluids at 37.8 oC

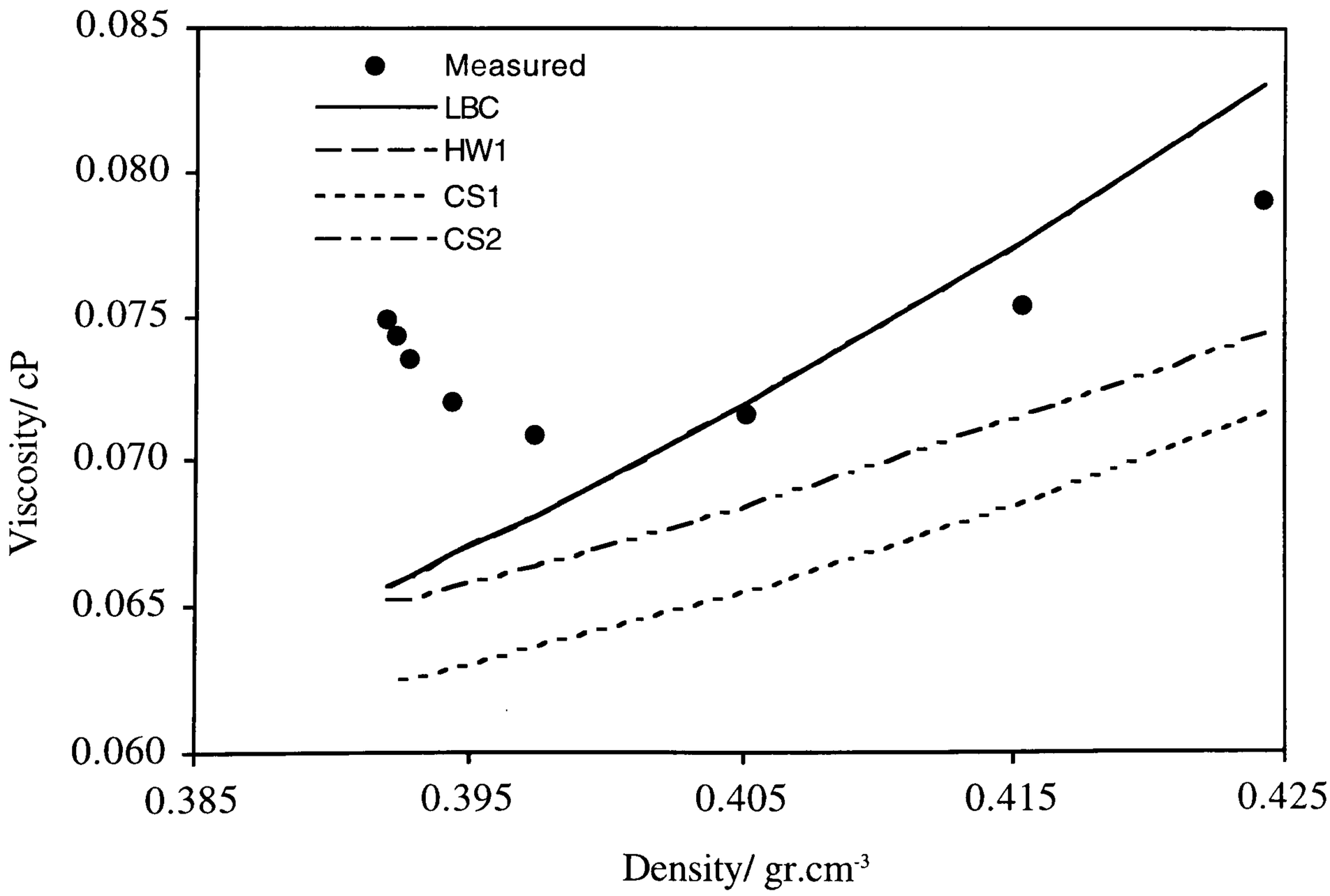

Figure 6.6 - Measured and Predicted Single-phase Viscosity of the Methane/n-Octane Mixture at 37.8 oC.

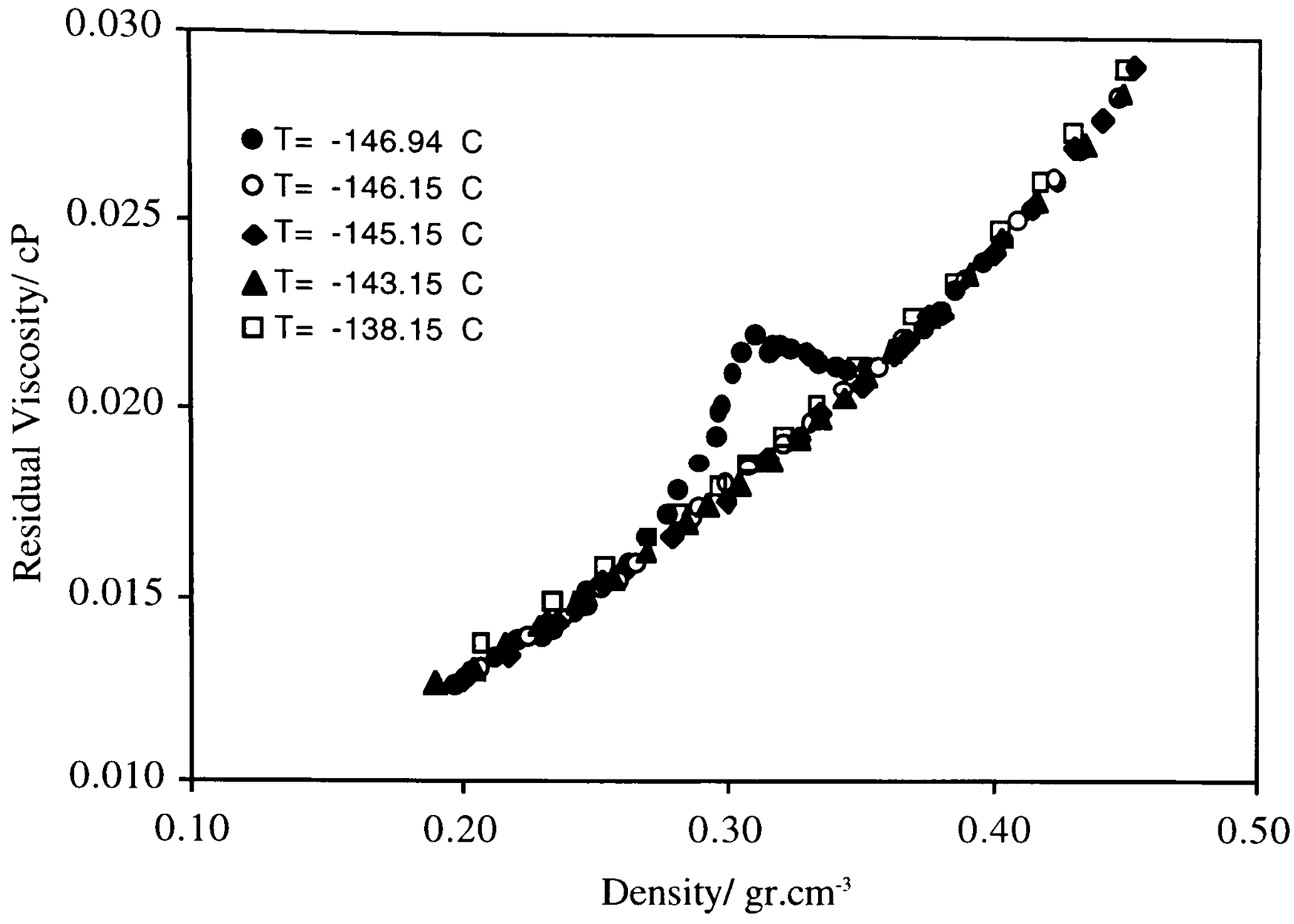

Figure 6.7 - Residual Viscosity vs. Density of Nitrogen.

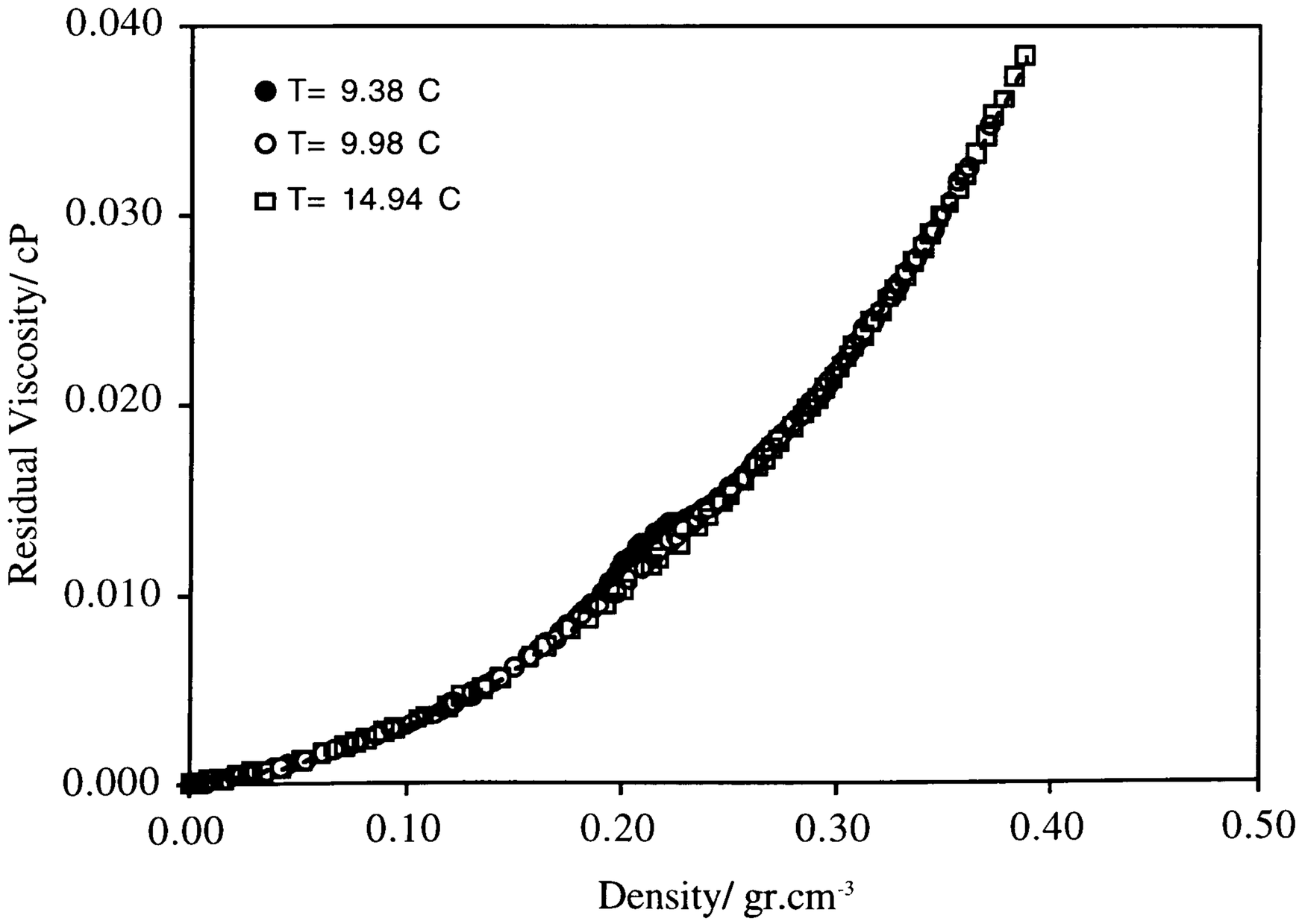

Figure 6.8 - Residual Viscosity vs. Density of Ethylene.

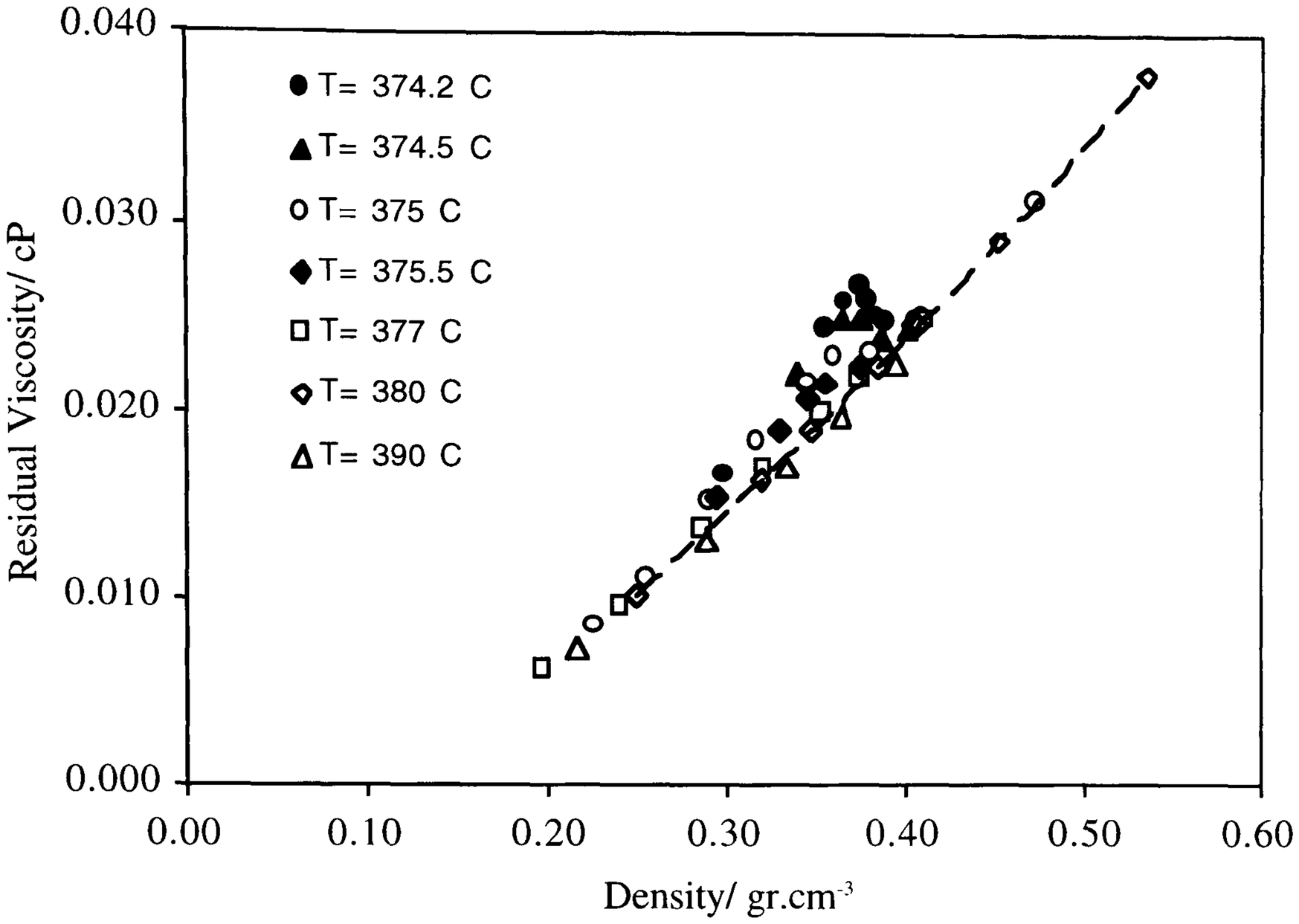

Figure 6.9 - Residual Viscosity vs. Density of Water.

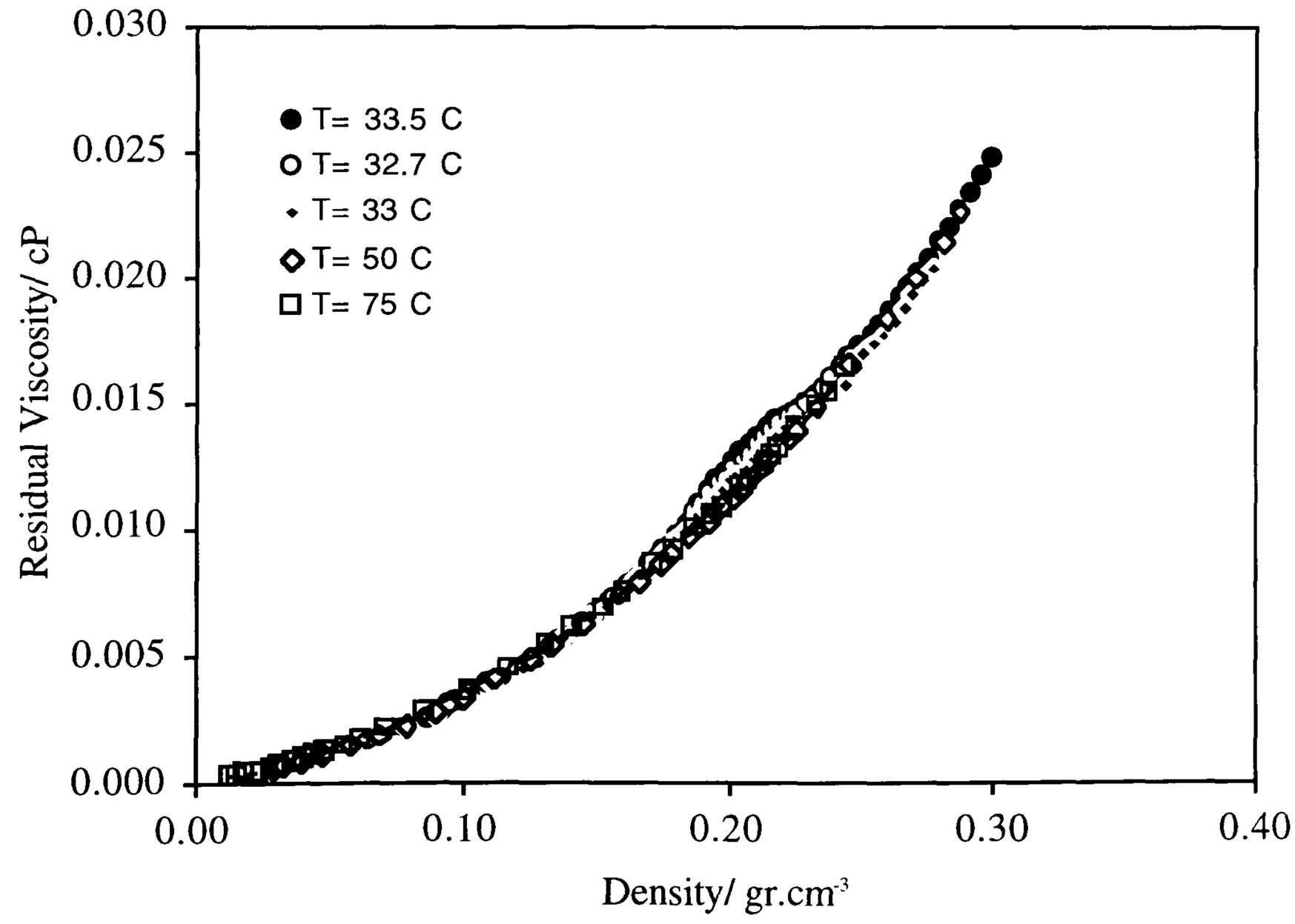

Figure 6.10 - Residual Viscosity vs. Density of Carbon Dioxide.

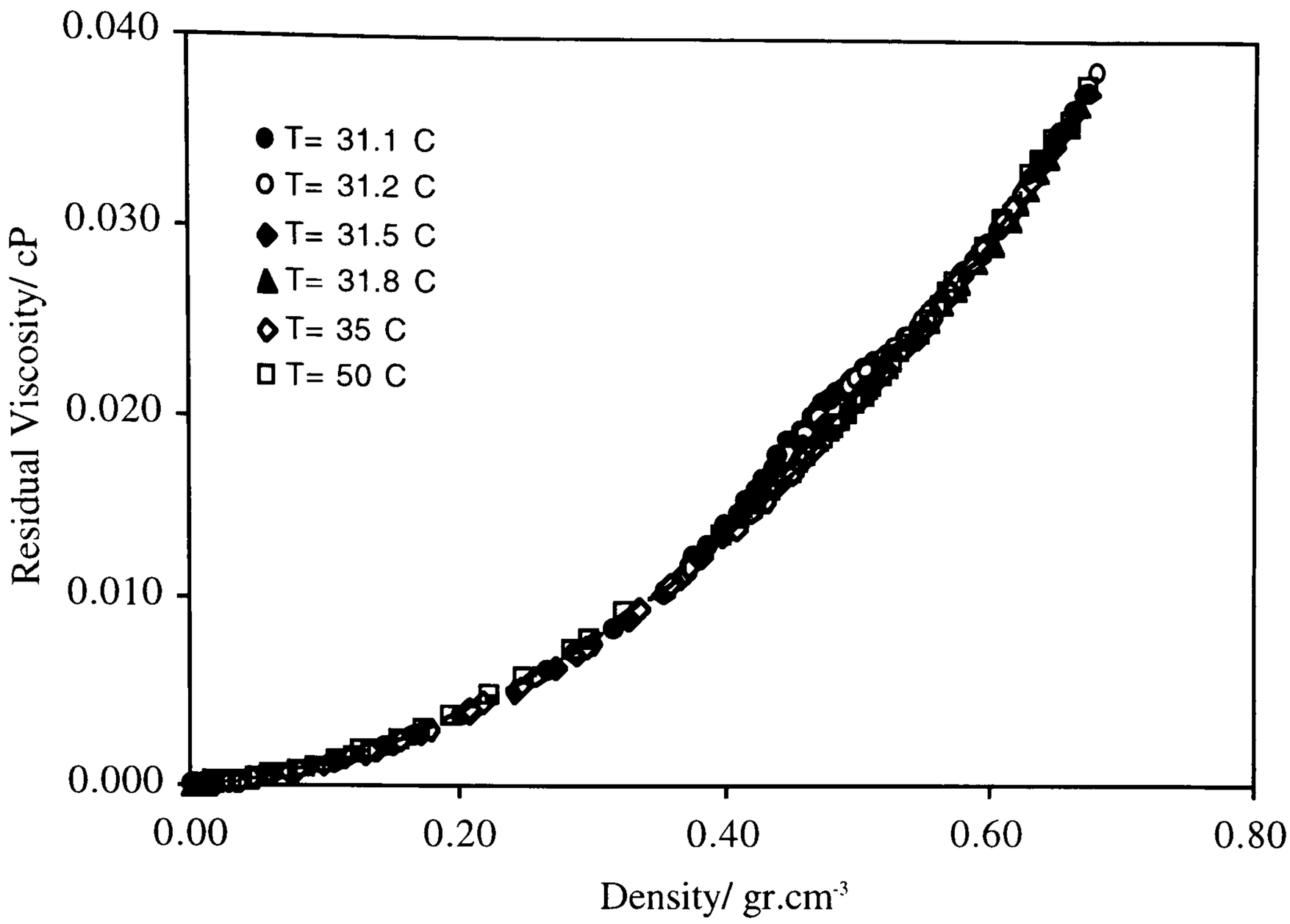

Figure 6.11 - Residual Viscosity vs. Density of Ethane.

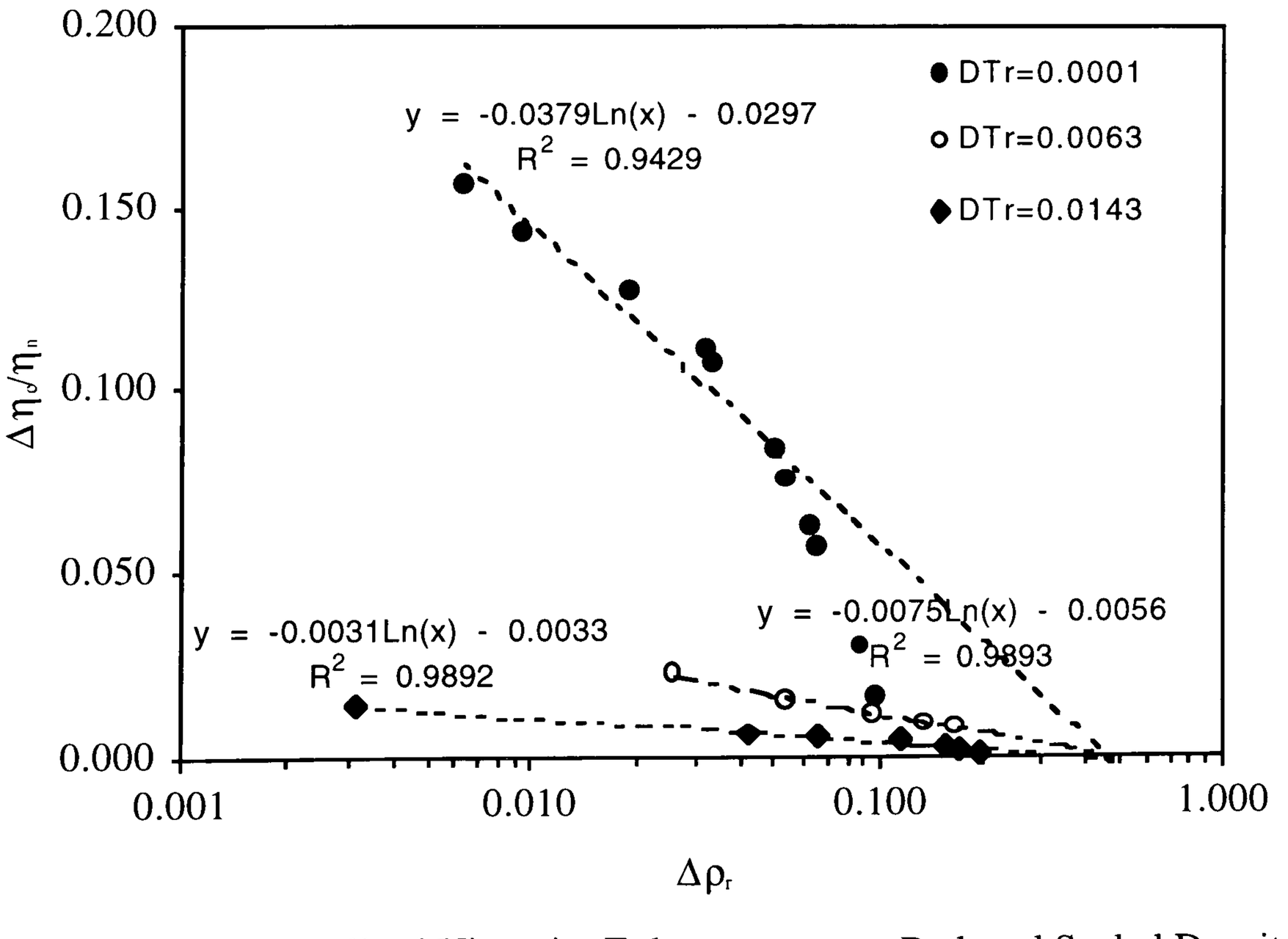

Figure 6.12 - Normalised Viscosity Enhancement vs. Reduced Scaled Density of Nitrogen.

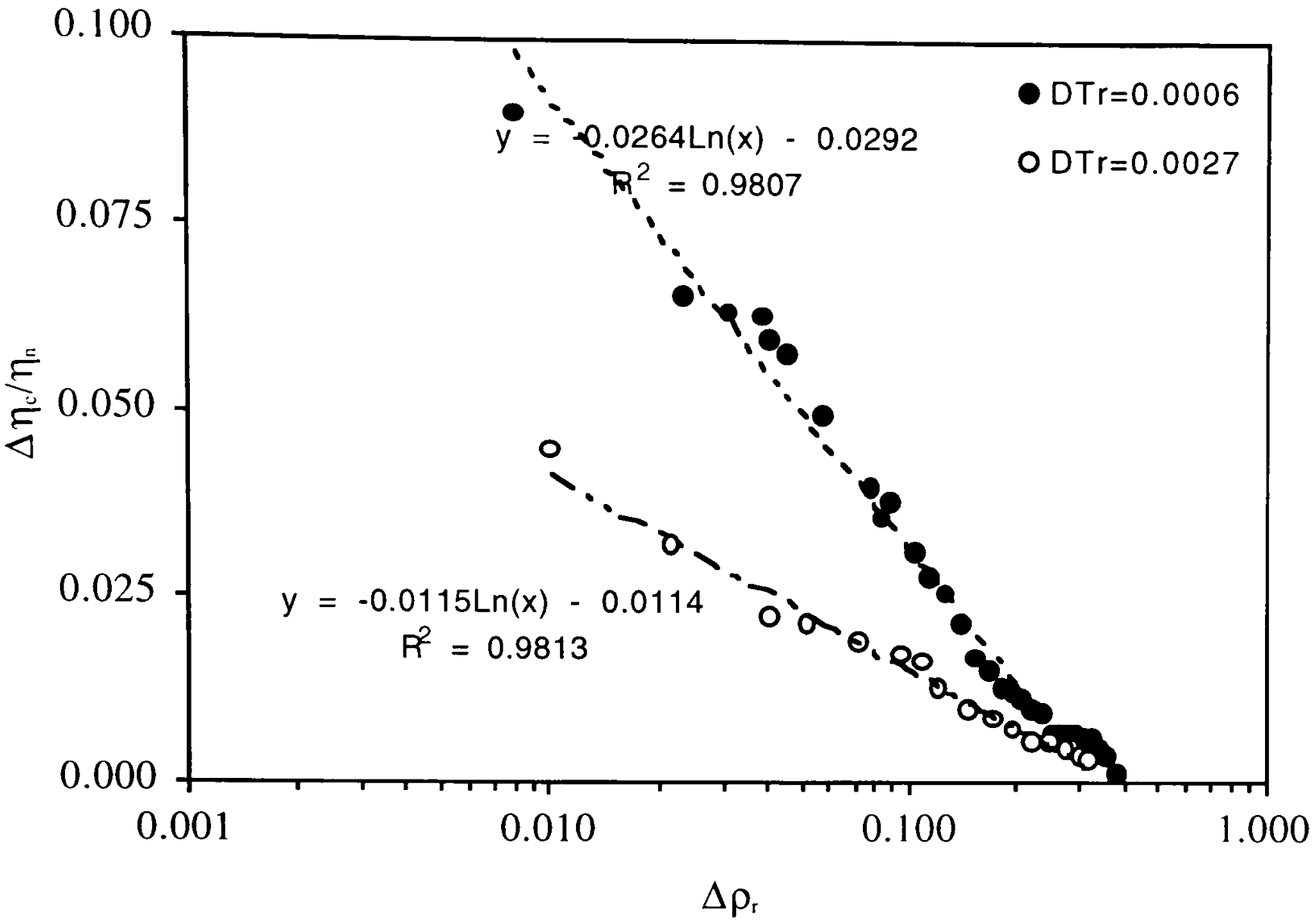

Figure 6.13 - Normalised Viscosity Enhancement vs. Reduced Scaled Density of Ethylene.

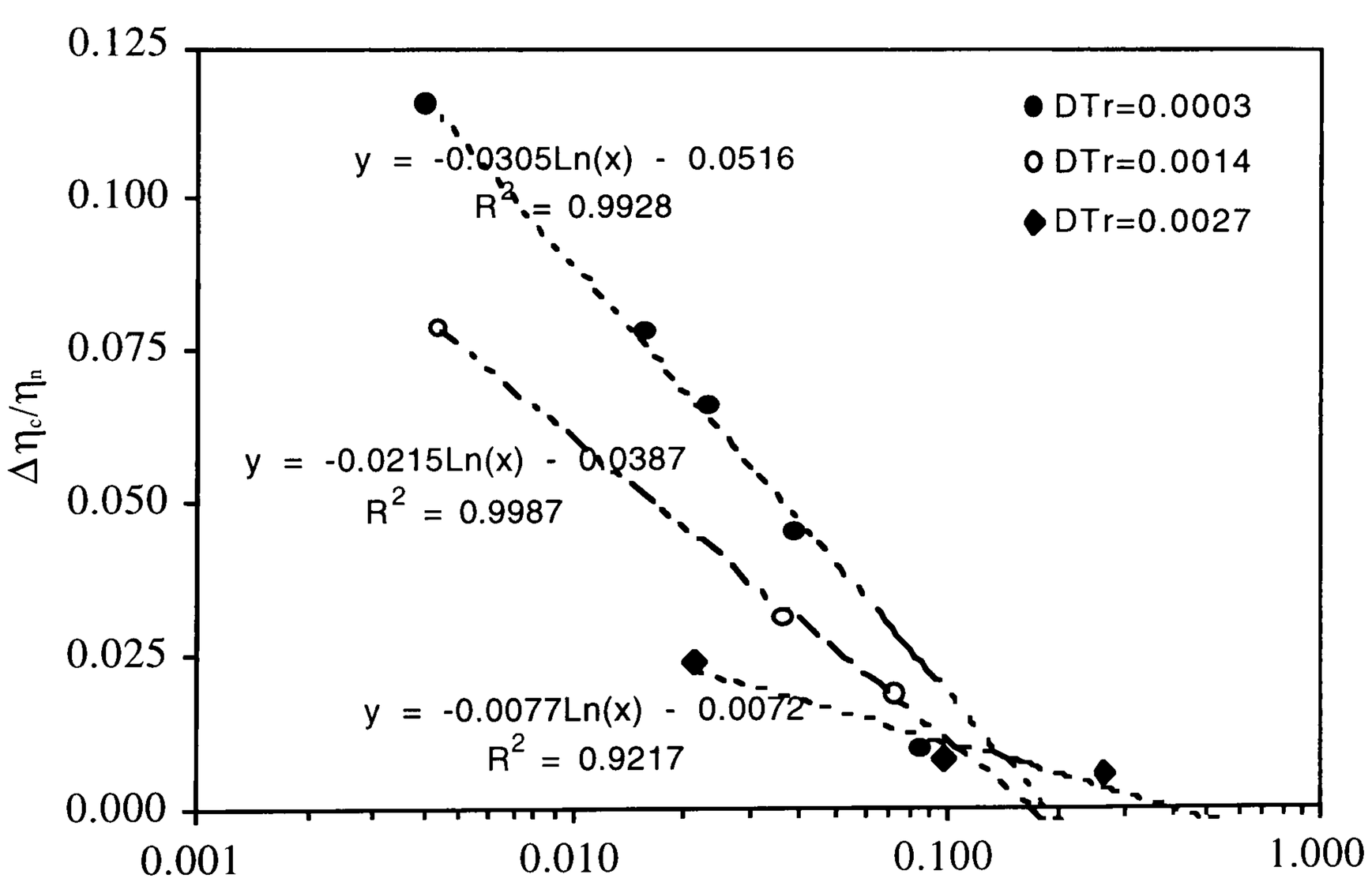

Figure 6.14 - Normalised Viscosity Enhancement vs. Reduced Scaled Density of Water.

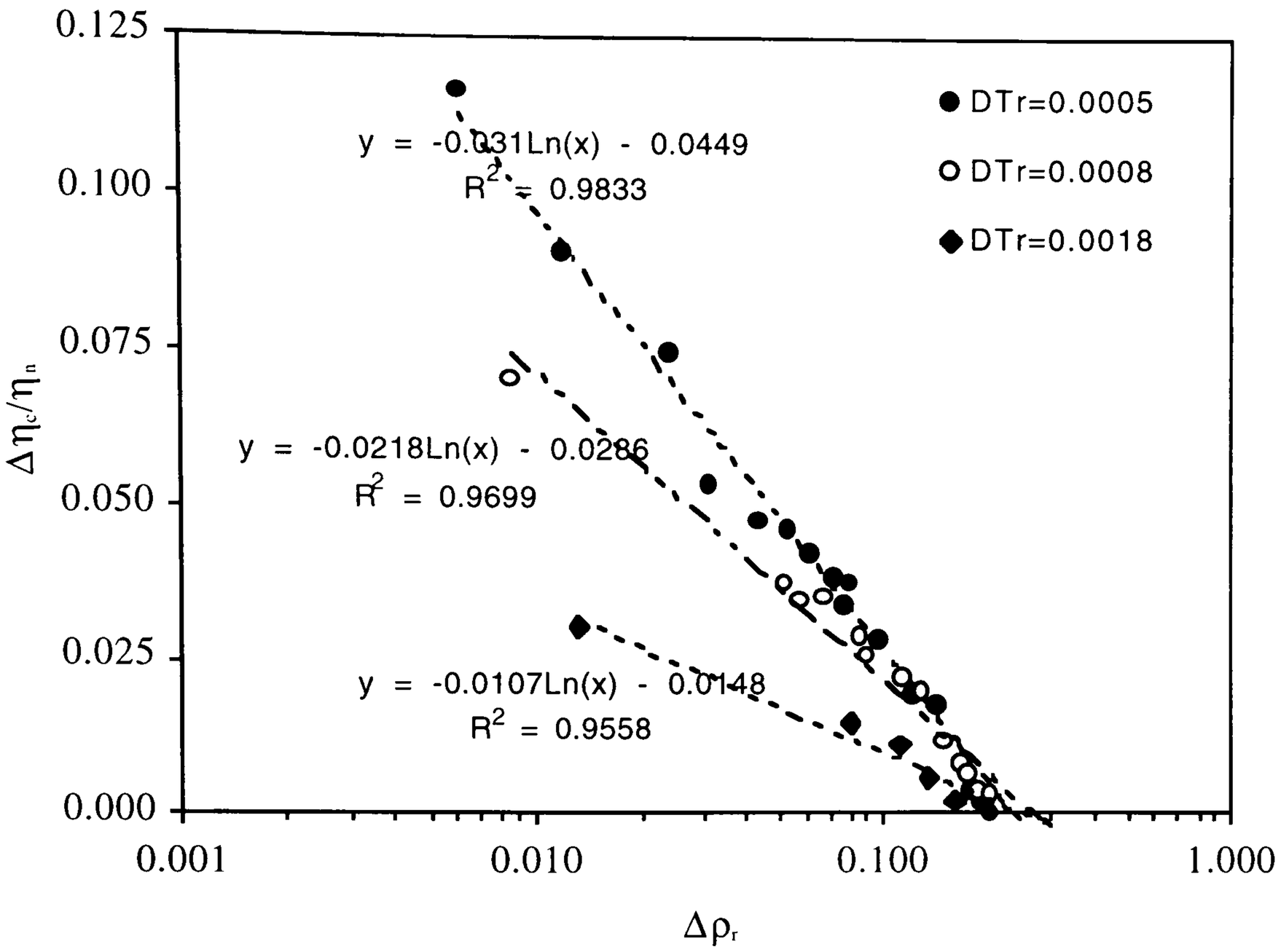

Figure 6.15 - Normalised Viscosity Enhancement vs. Reduced Scaled Density of Carbon Dioxide.

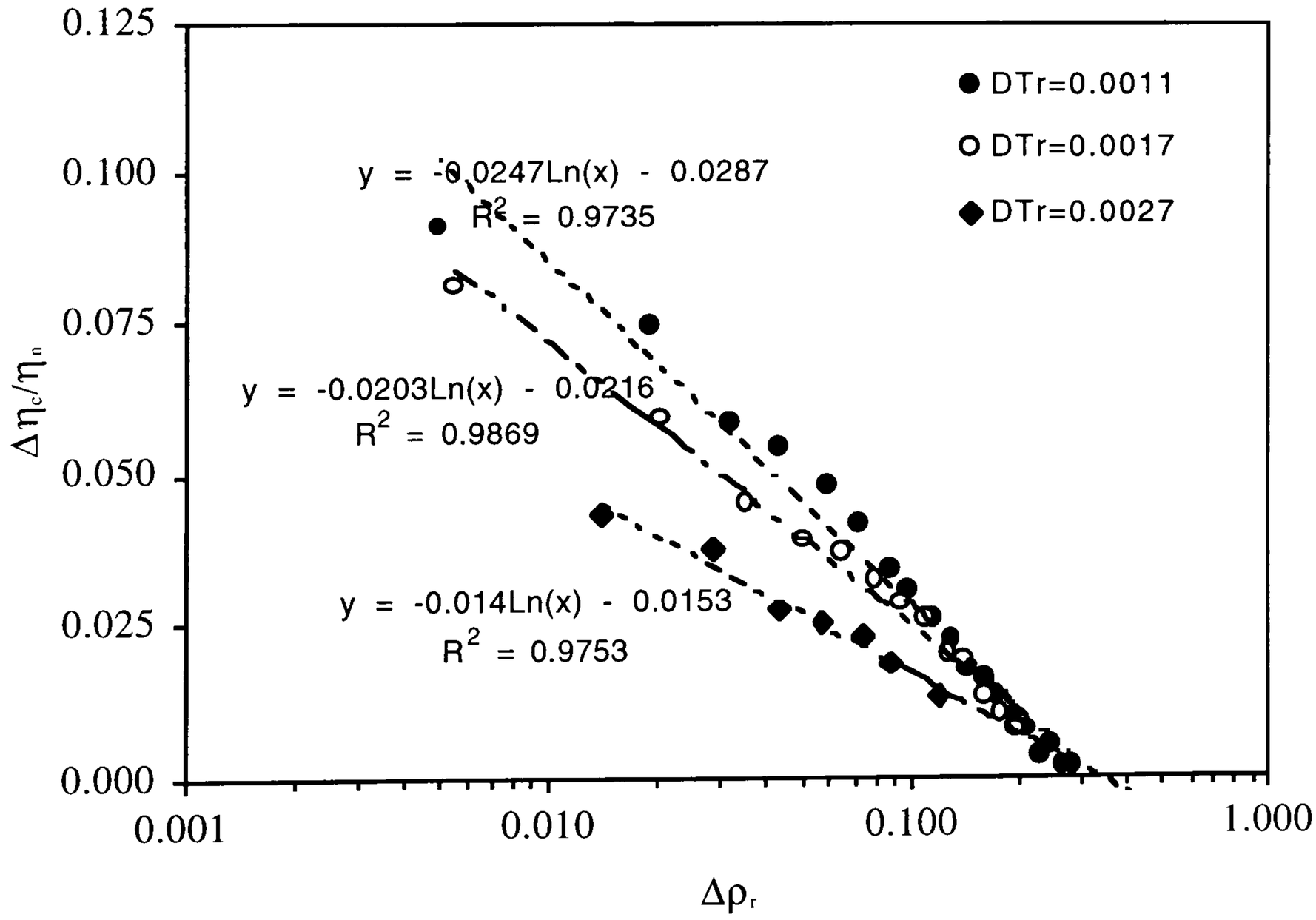

Figure 6.16 - Normalised Viscosity Enhancement vs. Reduced Scaled Density of Ethane.

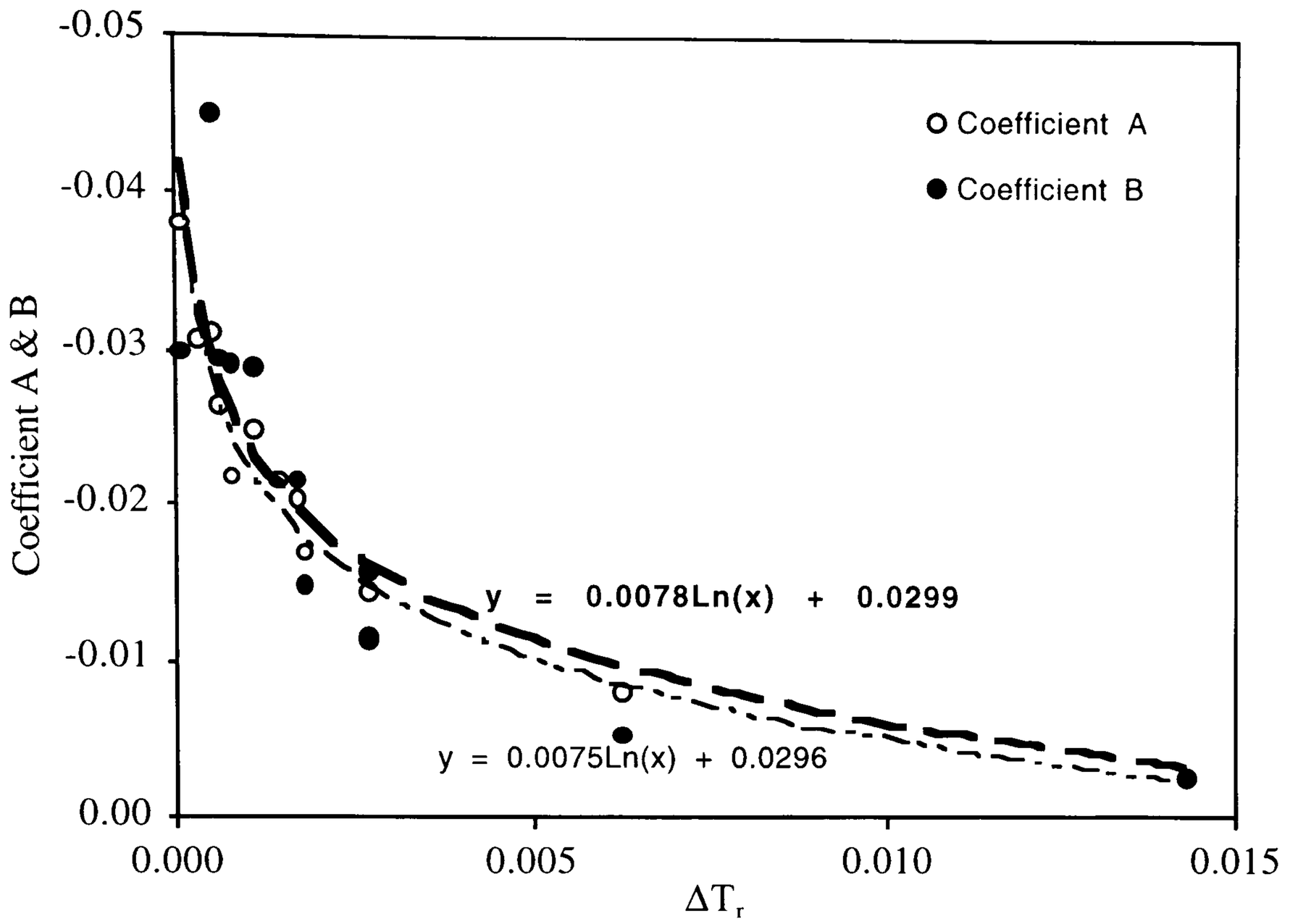

Figure 6.17 - Relationship of A & B Coefficients with Reduced Scaled Temperature, ΔT_r.

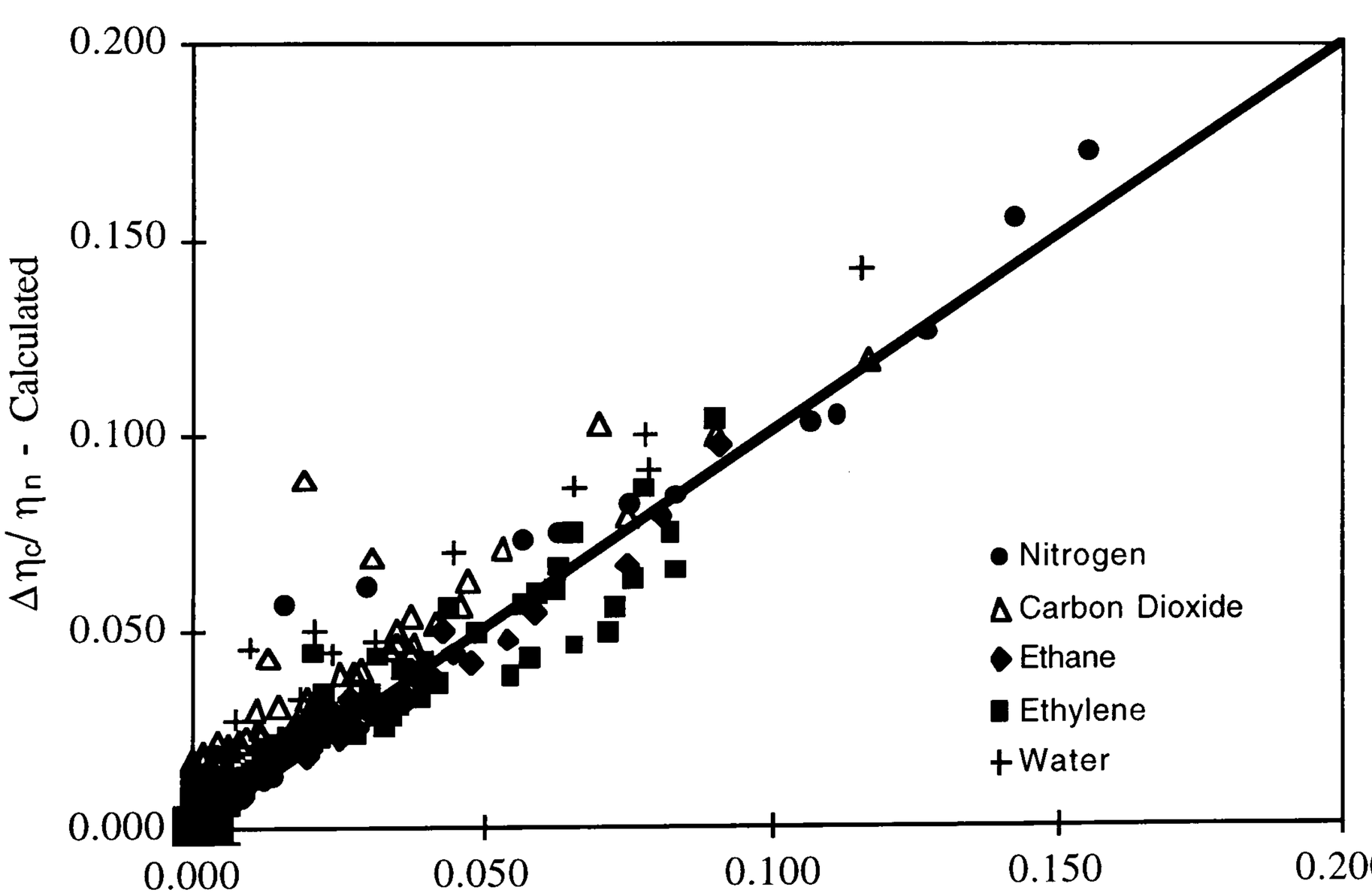

Figure 6.18 - Prediction of Pure Component Near-Critical Viscosity Enhancement.

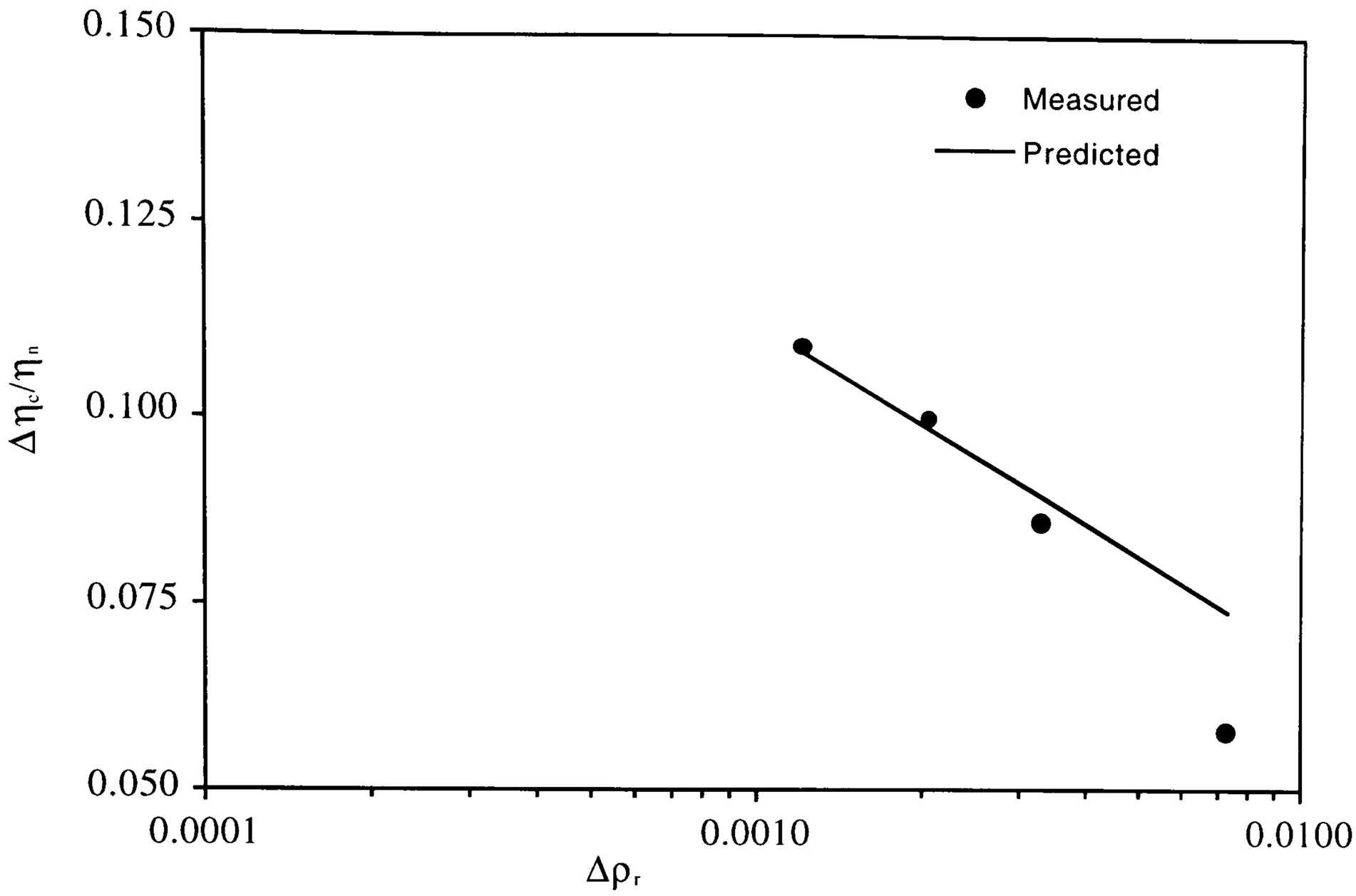

Figure 6.19 - Comparison of Experimental and Predicted Normalised Viscosity Enhancement of Methane/n-Octane.

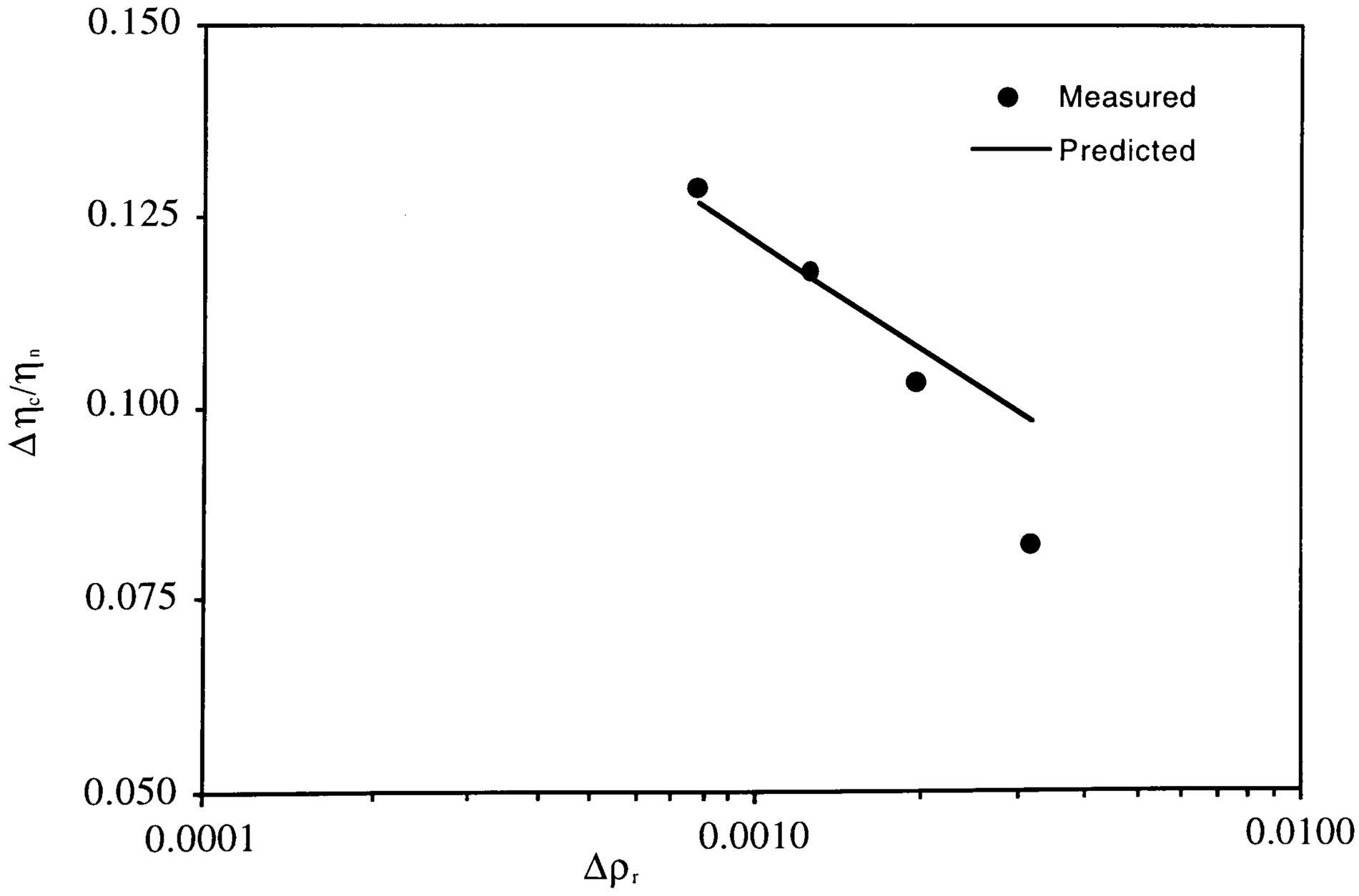

Figure 6.20 - Comparison of Experimental and Predicted Normalised Viscosity Enhancement of Methane/n-Decane.

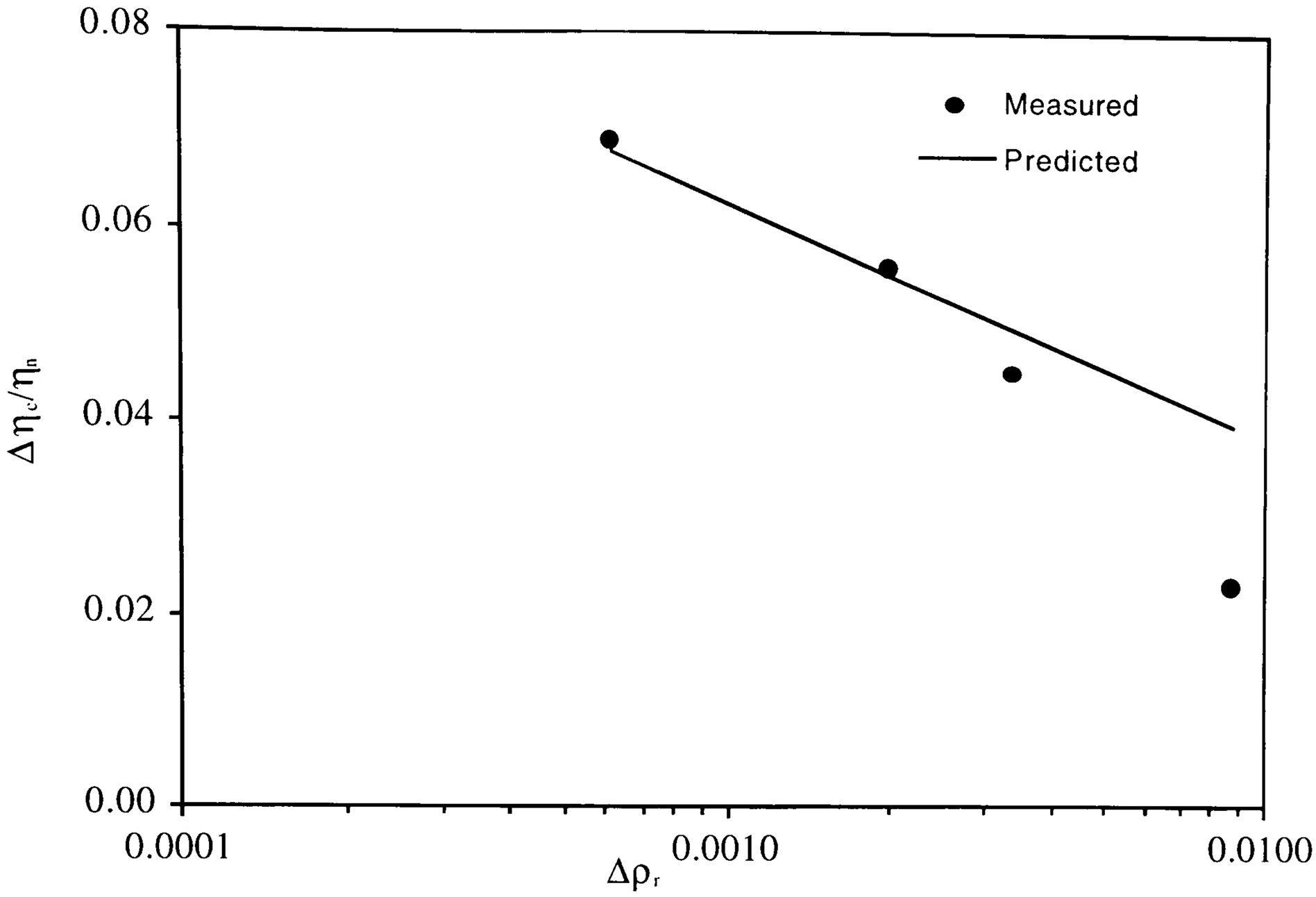

Figure 6.21 - Comparison of Experimental and Predicted Normalised Viscosity Enhancement of Methane/n-Octane/n-Decane.

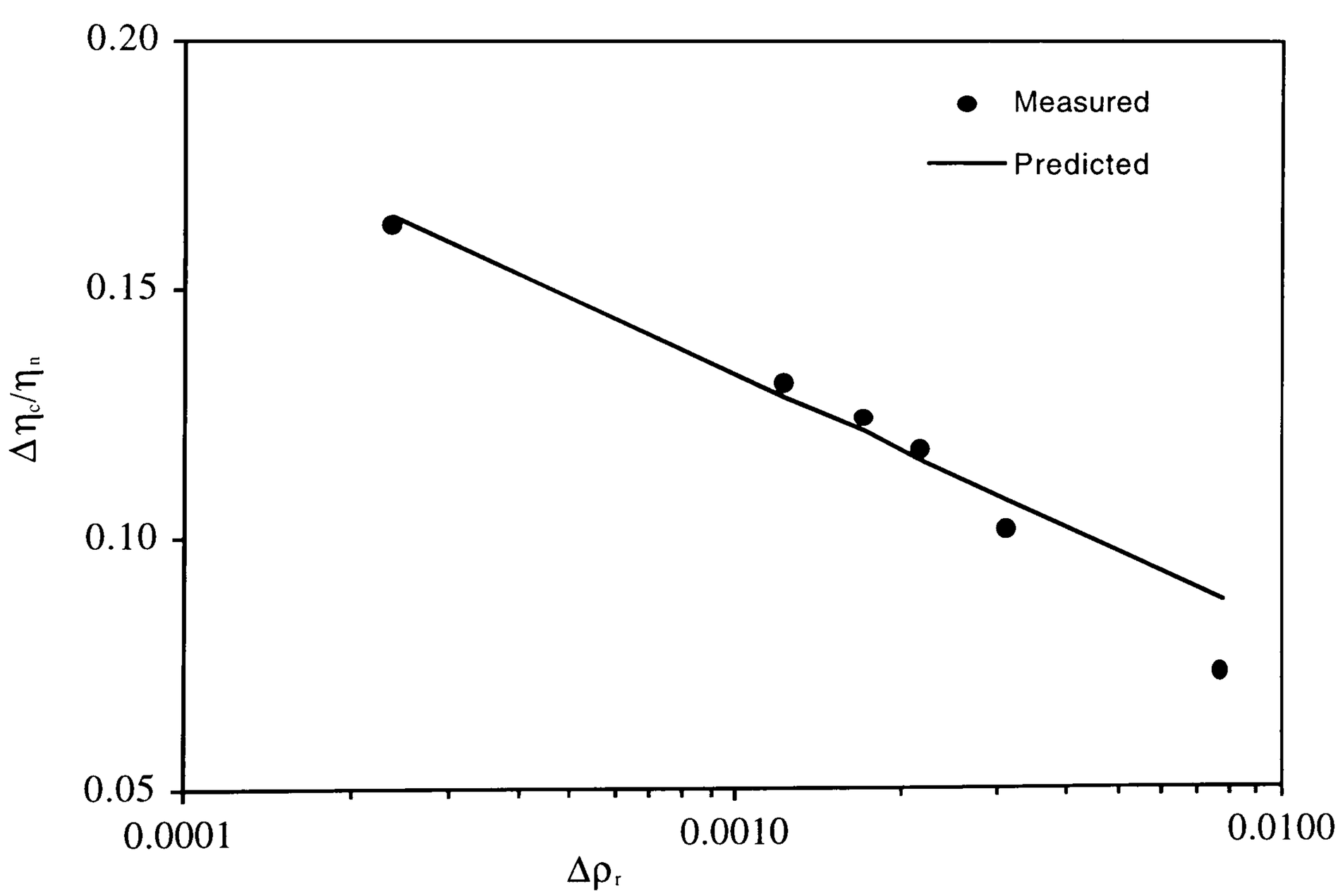

Figure 6.22 - Comparison of Experimental and Predicted Normalised Viscosity Enhancement of the Near-Critical NCF Fluid.

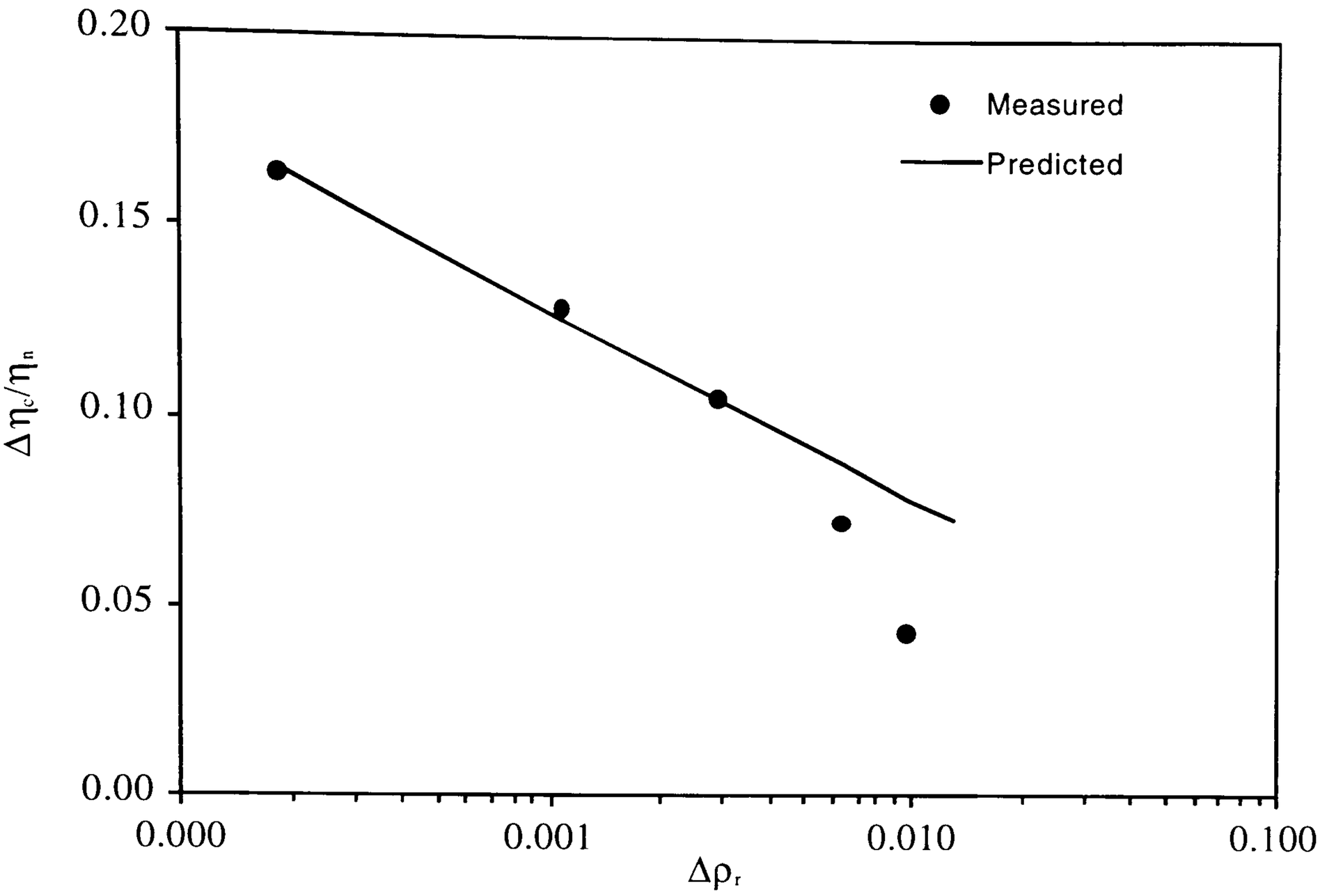

Figure 6.23 - Comparison of Experimental and Predicted Normalised Viscosity Enhancement of the Near-Critical OIL1 Mixture.

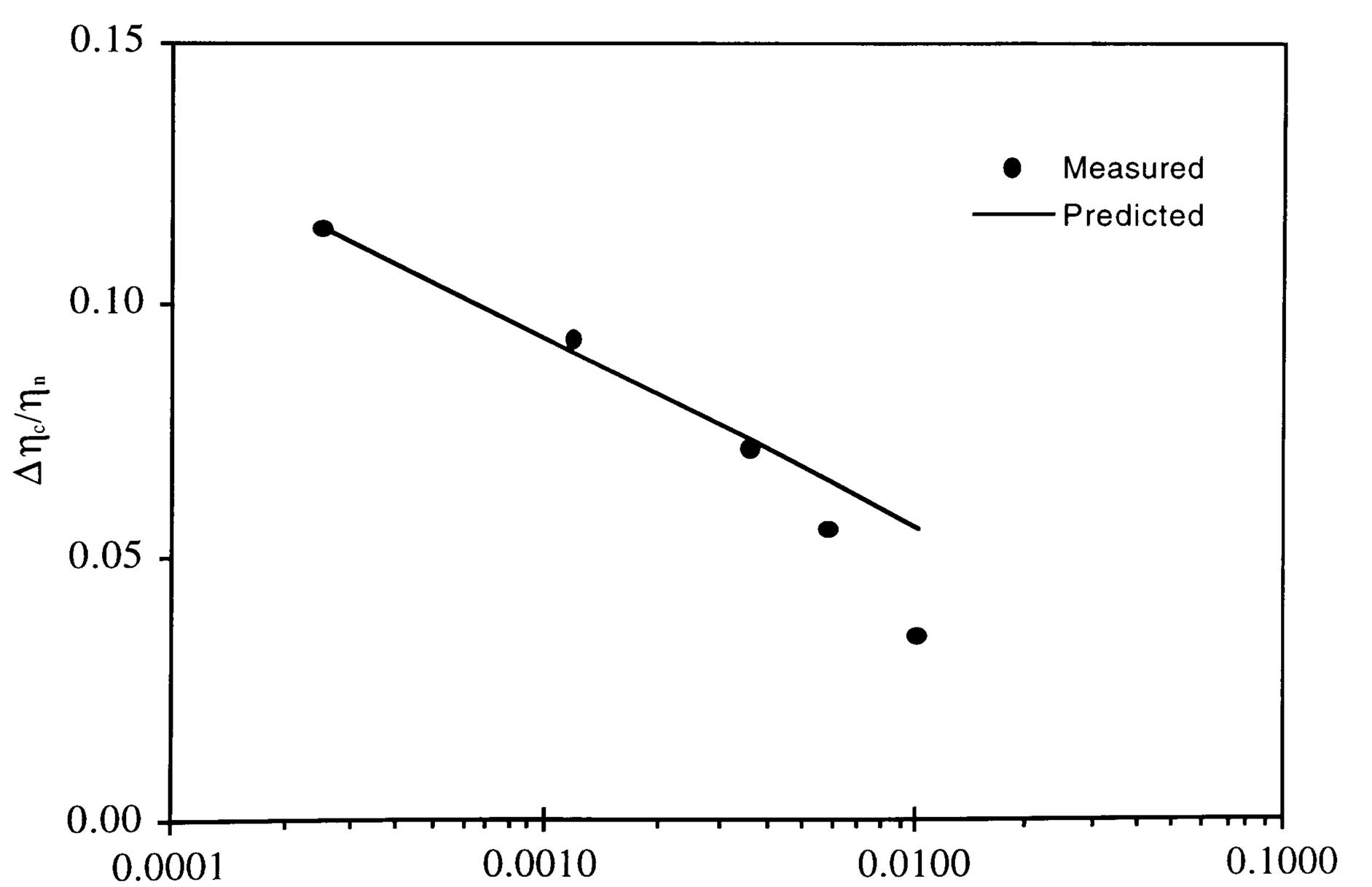

Figure 6.24 - Comparison of Experimental and Predicted Normalised Viscosity Enhancement of the Near-Critical GC1 Mixture.

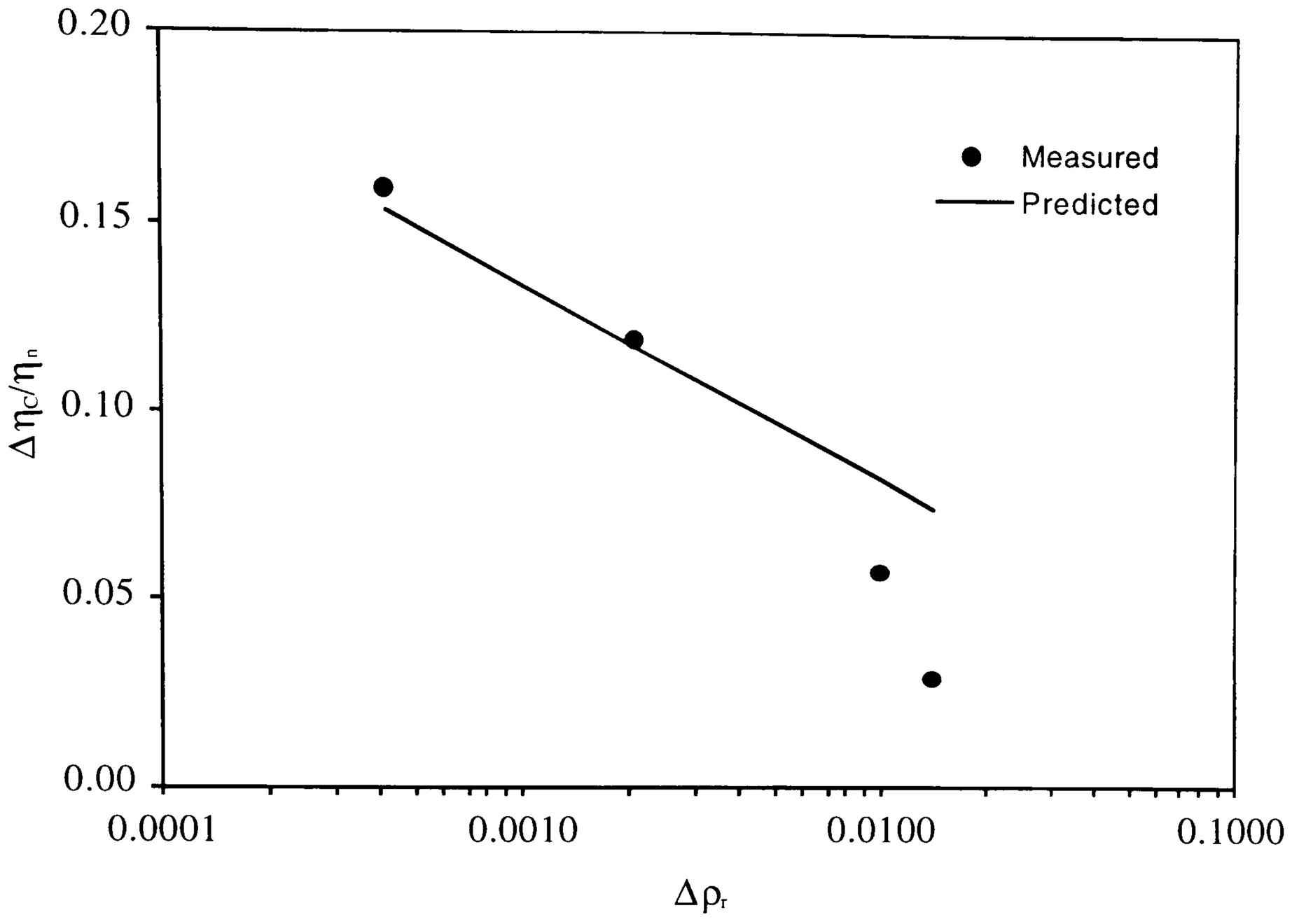

Figure 6.25 - Comparison of Experimental and Predicted Normalised Viscosity Enhancement of the Near-Critical GC2 Mixture.

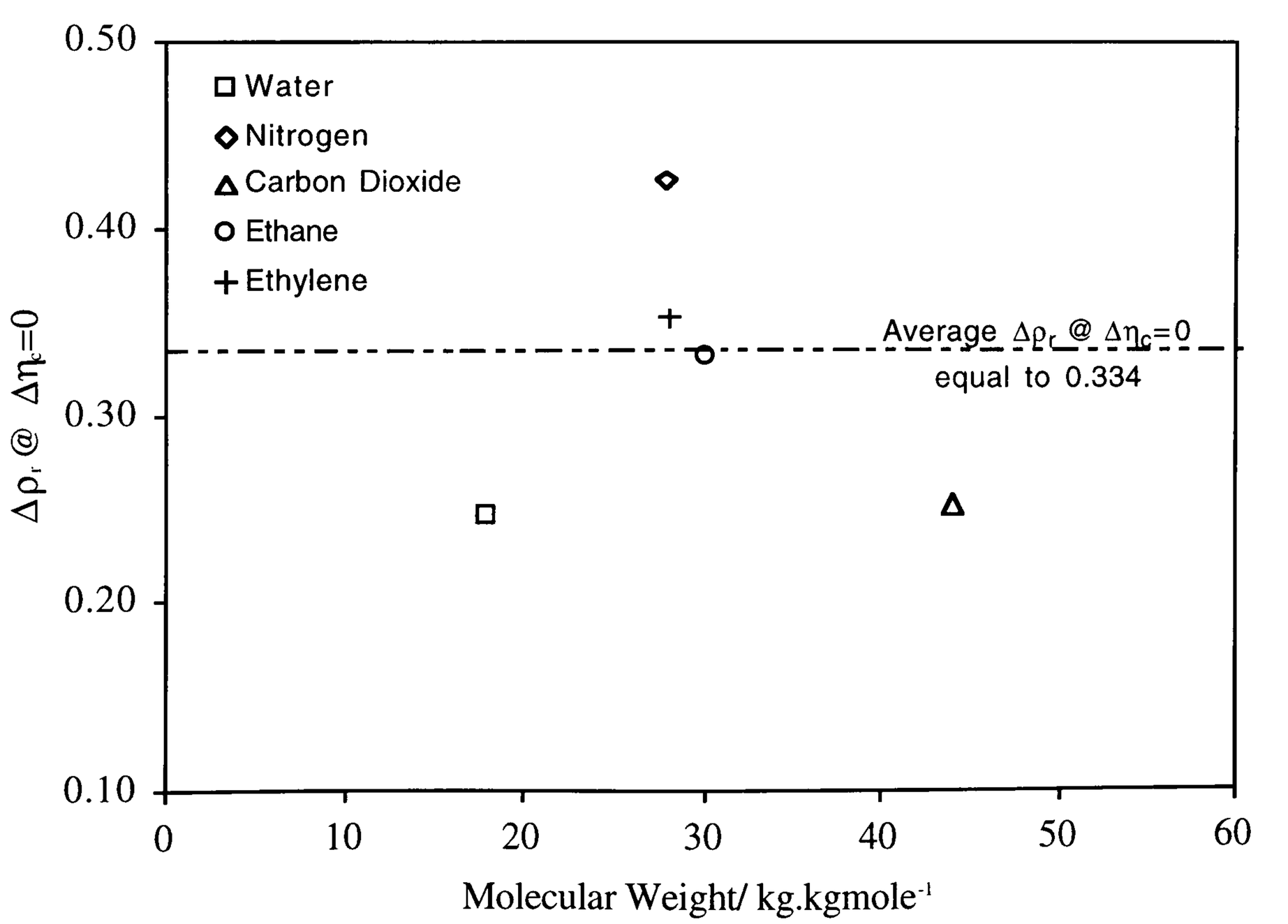

Figure 6.26 - Plot of the Intercept of the Normalised Viscosity Enhancement -Reduced Scaled Density Line With the x-axis vs. the Molecular Weight of Pure Components.

CHAPTER 7

CONTAMINATION OF RESERVOIR FLUIDS WITH OIL-BASED MUD FILTRATES

7.1 OBJECTIVES

The main objective of the contamination study presented in this chapter is:

- To develop a methodology whereby the viscosity and interfacial tension of the original (un-contaminated) reservoir fluid can be retrieved from contaminated reservoir fluid samples with oil-based drilling mud filtrate.

7.2 INTRODUCTION

Any fluid produced from a reservoir can provide valuable information on its phase behaviour and flow characteristics in the reservoir. Oil-based drilling muds are widely used drilling fluids which are known to minimise drilling-induced damages to hydrocarbon bearing formation. These drilling muds range from simple synthetic to natural multi-component fluids.

Downhole sampling tools like Modular Dynamic Tester (MDT) are widely used to sample different types of reservoir fluids. Reservoir fluid samples obtained, using those tools, are often contaminated with mud filtrate, particularly oil-based which is completely miscible with reservoir fluid and affects its properties. Obtaining a mud-free reservoir fluid sample

is often challenging and a time consuming operation. Therefore; it is important to be able to retrieve the properties of the original fluid from contaminated samples using some predictive tools.

The impact of contamination (using synthetic and natural oil-based mud filtrates) on the interfacial tension (IFT) and viscosity of several gas condensate and volatile oil samples, and procedures of determining the properties of the original (un-contaminated) reservoir fluid from contaminated samples are discussed in Sections 7.3 and 7.4. The procedure to determine the properties of the original fluid involves three steps. First, the level of contamination in the sample is calculated and the original composition is retrieved. Next, the contaminated samples are tested to generate the required data to tune the predictive compositional models. Finally, the retrieved model parameters and composition are used to determine the properties of the original fluid.

To develop the above methodology, a number of volatile oil and gas condensate samples have been purposely contaminated with mud filtrate at different levels. The samples, original and contaminated, have been fully characterised and tested experimentally at the reservoir and surface conditions. The contamination level was increased incrementally in the tests to the extent of converting the gas condensate samples to volatile oil systems. Conclusions arrived to from the above study will be presented in Section 7.5.

7.3 EFFECT OF MUD-FILTRATE CONTAMINATION ON THE INTERFACIAL TENSION OF RESERVOIR FLUID

The properties of the original reservoir fluid are essential in the design of process facilities as well as reservoir management. Despite advances in downhole sampling tools, obtaining a mud-free reservoir fluid sample still remains a challenge. To retrieve the properties of the original fluid, from contaminated samples, predictive tools[1-4] are often used.

A number of volatile oil and gas condensate samples were subjected to different contamination studies. In the first study, fluid samples were contaminated with a two-component drilling mud filtrate known as DMF-3; while in the second contamination study, samples were contaminated with a multi-component natural drilling fluid known as DMF-1 at various contamination levels. The compositional data of the above drilling mud filtrates are listed in Tables 7.1 and 7.2. Experimental interfacial tension data of multi-component volatile oil LRA97-1 and gas condensate fluids GCB98-1 and GCB98-2 in their original state as well as their contaminated samples will be presented in this section.

To retrieve the IFT of the original fluids, the original Weinaug-Katz model[1] was tuned, to all contaminated samples, by adjusting the parachor value of their plus-fractions. This is based on the view that these fractions have solid-like compounds associated with them and hence will not follow the same correlation for calculating parachors as other compounds. The un-tuned and tuned predicted results of the contaminated and un-contaminated samples are presented and compared with experimental data. The predicted IFT of the original (un-contaminated) reservoir fluids using retrieved parachors and those obtained from the tuned Weinaug-Katz model will be compared to experimental data and discussed in this section.

7.3.1 Experimental Results

Interfacial tension measurements between equilibrated vapour and liquid phases were performed using both pendant drop and meniscus height techniques. The procedures for interfacial tension measurements are described in Chapter 2. All the interfacial tension (IFT) measurements, presented here, were taken during CCE experiments at reservoir and surface temperatures and various equilibrium pressures. The effects of the addition of contaminants (DMF-3 and DMF-1) on the measured interfacial tension data of the above-mentioned fluids are described below.

Volatile Oil Fluids:

LRA97-1 Fluid. The LRA97-1 fluid was subjected to DMF-3 contamination at a temperature of 37.8 °C and 5.08 vol% and 19.92 vol%, on the basis of stock tank liquid

volume (STLV), contamination levels. The single phase compositional data of these samples are listed in Table 7.3.

Due to the inky colour of the liquid phase, it was not possible to accurately locate the base of the vapour-liquid interface, hence the height of the meniscus could not be accurately determined. Therefore, interfacial tension measurement by the meniscus height technique was not possible and the pendant drop method was the only method available. The interfacial tension data of the volatile oil LRA97-1 in its pure form and with 5.08% and 19.92% of the contaminant DMF-3 are listed in Table 7.4, also graphically shown in Figures 7.1 (a) and (b). The interfacial tension can be seen to slightly increase with the volumetric addition of DMF-3 to the pure oil LRA97-1. The difference is gradually increasing toward the lower pressure conditions, Figure 7.1(b).

Gas Condensate Fluids:

GCB98-1 Fluid (Contamination With DMF-3). Interfacial tension of the original gas-condensate GCB98-1 fluid and with 5 vol%, 15 vol% and 30 vol%, on the basis of STLV, of DMF-3 were measured by both the meniscus height and pendant drop techniques at a temperature of 37.8 °C. The single phase compositional data of these samples are listed in Table 7.5.

Figures 7.2 (a) and (b) present the results of these interfacial tension measurements. The data are, also, tabulated in Table 7.6. The measured IFT data by both techniques are in excellent agreement which is less than ±2% in most cases. It is interesting to note that the addition of DMF-3 produced two different effects throughout the investigated pressure range. The IFT between the equilibrated liquid and vapour phases is seen to decrease with increasing DMF-3 contamination at higher equilibrium pressures; while it is seen to increase with increasing DMF-3 contamination for lower equilibrium pressures. The decrement in measured IFT at higher pressure conditions was found to be well above experimental uncertainty of ±5%. Therefore, these opposing effects could be attributed to the presence of asphaltic and/or surfactant compounds within the drilling mud filtrate which

become volatile at higher pressures and temperatures and known to decrease interfacial tension. The solubility of asphaltic compounds were seen to cause much more significant effects at higher pressure than when they precipitate at lower pressure conditions. To clarify these effects, the addition of DMF-3 to the pure GCB98-1 decreased the measured interfacial tension from -13% to -86% by increasing DMF-3 from 5% to 30%, respectively. On the other hand, increasing DMF-3 by the same amounts, increased IFT from 5 to 27% at lower equilibrium pressures.

GCB98-2 Fluid (Contamination With DMF-3). GCB98-2 fluid was contaminated with 20 vol%, 49 vol%, 51 vol% and 55 vol%, by STLV, of DMF-3. Table 7.7 lists he single compositional data of the above samples.

Interfacial tension measurements of the above contaminated GCB98-2 samples were conducted at a reservoir temperature of 100 °C using the meniscus height technique. The results of these measurements are tabulated in Table 7.8 and shown in Figures 7.3 (a) and (b). The contaminated sample with 20% and 49% of DMF-3 displayed phase behaviour characteristics similar to those for gas-condensate fluids; while those of 51% and 55% contamination levels showed phase behaviour characteristics similar to those of volatile oils.

Similarly, the addition of DMF-3 to the original GCB98-2 resulted in two different effects in the measured IFTs, similar to those observed for GCB98-1/DMF-3 samples at 37.8 °C. For the same reasons as above, the IFT was observed to decrease for equilibrium pressures higher than 4000 psia and increases thereafter as DMF-3 contamination level increases. For the oil samples, although the measured IFT was lower than the those of the original fluid, the IFT was observed to increase with increasing DMF-3 throughout the whole pressure range.

GCB98-2 Fluid (Contamination With DMF-1). GCB98-2 was also contaminated with various proportions of DMF-1 mud filtrate at both reservoir and surface temperatures.

The single phase compositional data and the results of interfacial tension measurements of the fluid GCB98-2 in its pure form and its contaminated samples with 15 vol%, 30 vol%, 45 vol%, 50 vol%, 56 vol% and 70 vol%, by STLV, of DMF-1 at 100 °C and 37.8 °C are tabulated in Tables 7.9 through 7.11, respectively.

Figures 7.4 (a) and (b) present the variation of IFT (of the un-contaminated GCB98-2 and with 15 vol%, 30 vol%, 50 vol%, 56 vol% and 70 vol%) with pressure at 100 °C. The contaminated samples with 15%, 30% and 50% of DMF-1 displayed phase behaviour characteristics similar to those for gas-condensate fluids; while those of 56% and 70% contamination levels showed phase behaviour characteristics similar to those of volatile oils.

As for the DMF-3 contamination studies, the addition of 15%, 30% and 50% of DMF-1 to the original GCB98-2 resulted in two different effects in measured IFTs. For the same reasons stated above, the IFT was observed to increase for equilibrium pressures lower than 4000 psia and increases thereafter as DMF-1 contamination level increases. For the 70% DMF-1 contaminated samples, the measured IFT was higher than those of other samples throughout the whole pressure range. The IFT of the 56% contaminated sample, although it is higher than other contaminated samples, it is still lower than those of the un-contaminated GCB98-2 sample at high equilibrium pressures.

It is also worth mentioning that the measured IFTs of the 50% contaminated sample were higher than those of the 56% contaminated sample (volatile oil), despite the fact that both samples are very close to the critical concentration of the GCB98-2. A possible reason for such behaviour could be that the 56% contaminated sample was much closer to the critical concentration than that of the 50% contaminated sample.

The GCB98-2 fluid was also contaminated with DMF-1 at three contamination levels of 15 vol%, 30 vol%, and 45 vol%, by STLV, at separator conditions of 37.8 °C. Interfacial tension measurements of the original fluid and its contaminated samples were conducted

using both the meniscus height and pendant drop techniques at a temperature of 37.8 °C. The results of these measurements are tabulated in Table 7.11 and shown in Figures 7.5 (a) and (b). All samples displayed phase behaviour characteristics similar to those for gas-condensate fluids.

Similar to the above observation, the measured IFT was observed to increase at lower equilibrium pressures, while it decreases for higher equilibrium pressures as DMF-1 contamination level increases. The exception here is that the IFT for the 45% contaminated sample at 4000 psia increases which could be attributed to the dominant effects of heavier compounds at this lower temperature than those of the aspheltic ones.

7.3.2 Predicting the Interfacial Tension of the Original Fluids

As far as IFT modelling is concerned, the only difference between the two contamination studies is the selection of the plus-fraction. The choice of plus-fraction for any contamination study is constrained by two factors. These factors are; **(i)** the effect of mud filtrate contamination must be seen on the properties (e.g., molecular weight, specific gravity ..etc.) of the plus fraction, and **(ii)** the availability of more extended analysis for the tested fluid, to ensure appropriate characterisation and to reduce heavy tuning to the predictive model.

In general due to significant changes of the carbon group properties in equilibrated phases of volatile reservoir fluids below the saturation pressure, it is advisable to avoid using groups containing a wide range of components. Hence, it is expected to obtain a more reliable prediction of IFT by describing the plus-fraction with as many as single carbon number (SCN) groups as practicable. However, the heavy end has been described by C7+ in the contamination studies using DMF-3. This has justified changing the properties of the plus-fraction due to contamination, and its extrapolation to the zero contamination level for the original fluid.

As previously mentioned, the original Weinaug-Katz model (Section 4.3, Chapter 4) was applied in this study, once with calculated parachors for SCN groups and plus-fraction, using Equation (4.8), and once with tuned parachors. The predicted un-tuned results show that Weinaug-Katz model under-predicts the IFT of reservoir fluids, especially at low IFT conditions. This in turn necessitates the need for tuning the model. For all contaminated samples, the model was tuned to all measured IFTs. Average parachor values for the plus-fraction were calculated which were then used to the predict samples IFT at any condition of interest. As an example, Figures 7.6 through 7.8 show comparisons between the measured and predicted IFT data for the contaminated GCB98-1 samples. As can be seen, from Figures 7.6 through 7.8, the tuned model improved the predicted results. Table 7.12 lists the absolute and average deviations of predicted IFTs, for all tested fluids, from the un-tuned and tuned Weinaug-Katz model.

To retrieve the IFT of the original fluids, plots of the tuned plus-fraction parachors against level of contamination were constructed. Figure 7.9 gives an example of those plots. The tuned plus-fraction parachor values, of all tested fluids, were seen to behave linearly with contamination level. This feature facilitated extrapolation to 0% contamination level, whereby the required plus-fraction parachor values for the un-contaminated fluids were retrieved.

Using the retrieved parachor values, the IFTs of the original fluids were predicted and compared to those obtained by tuning the IFTs of the original fluids, as shown in Figures 7.10 through 7.14. As can be seen from those plots (Figures 7.10 through 7.14) the difference between the two predictions (tuned and extrapolated) is insignificant and the observed deviation were believed to be due to model being inconsistent in predicting the IFT of reservoir fluids (i.e., the model was seen to under-predict low IFT conditions while it over-predicts the same at high IFT conditions[5]). The absolute and average deviations of predicted IFTs using the retrieved parachors are listed in Table 7.12 which are comparable to those calculated using the tuned values. It is worth mentioning that due to the fact that component's parachor is independent of temperature, the established parachor relationship

for the same DMF-1 contamination study at 100 °C was used to calculate the parachor values of the plus-fractions of the GCB98-2 samples at 37.8 °C which is needed to predict their IFTs. This procedure has resulted in large deviations when predicting the IFT of the un-contaminated GCB98-2 fluid at 37.8 °C as shown in Figure 7.14.

7.4 EFFECT OF MUD-FILTRATE CONTAMINATION ON THE VISCOSITY OF RESERVOIR FLUID

Experimental viscosity data of single phase and saturated liquid and vapour phases of multi-components volatile oil LRA97-1, and gas condensate GCB98-1 and GCB98-2 in their original states as well as their contaminated samples are presented in this section. The un-tuned and tuned predicted results, by the Lohrenz *et al* (LBC)[6], Dandekar *et al* (HW1)[7] and the one- and two reference fluid(s) corresponding state (CS1[8] and CS2[9]) models of the contaminated and un-contaminated samples are also presented and compared with experimental data in this section.

7.4.1 Experimental Results

Viscosity measurements of the single phase and saturated liquid and vapour phases were conducted using a capillary tube viscometer, hosted inside the VLE facility, at a temperature of 37.8 °C. Viscometer details and test procedures are described in detail in Chapter 2. The effects of the addition of DMF-3 and DMF-1 on the measured viscosity of the original fluids are described below. The compositional data of DMF-3, DMF-1, the single phase of the LRA97-1, GCB98-1 and GCB98-2 fluids and their contaminated samples are listed in Tables 7.1, 7.2, 7.3, 7.5 and 7.9, respectively.

Volatile Oil Fluids:

LRA97-1 Fluid. The volatile oil LRA97-1 fluid was contaminated with 5.08 vol% and 19.92 vol% of DMF-3 (based on STLV) at a temperature of 37.8 °C. The viscosity data of the single phase and saturated liquid and vapour phases of the original LRA97-1 and its contaminated samples are listed in Table 7.13, and shown in Figures 7.15 through 7.17.

As expected, the viscosity of the single phase can be clearly seen to increase with the volumetric addition of DMF-3 to the original LRA97-1. However, the viscosity of the saturated liquid and vapour phases is observed to slightly decrease with the addition of DMF-3. The decrease in equilibrium phases viscosity could probably be attributed to the presence of alkenes in the DMF-3 filtrate, which in turn could change the overall force-fields between molecules.

The low pressure viscosity measurements that were performed on the stabilised oils during these tests are presented in Figure 7.18 and also tabulated in Table 7.14. The viscosity of the stabilised oil can also be seen to decrease with increasing amounts of DMF-3 which is similar to that observed for the saturated liquids.

Gas Condensate Fluids:

GCB98-1 Fluid (Contamination With DMF-3). Viscosity measurements of the single phase gas and saturated liquid of the original gas condensate GCB98-1 fluid and with 5%, 15% and 30% (based on STLV) of DMF-3 were measured by capillary tube viscometer at a temperature of 37.8 °C. The saturated vapour viscosity could not be measured, except for the 2000 psia equilibrium pressure of the 30% DMF-3 contaminated sample, due to continuous drop of liquid droplets as it passes through the viscometer tube. The results of these measurements are shown in Figures 7.19 and 7.20 and also tabulated in Table 7.15. The viscosity of the single phase gas of the original GCB98-1 was seen to gradually increase with the volumetric addition of DMF-3, where a much more pronounced increase observed for the 30% DMF-3 contaminated sample. However, this increase on the single phase viscosity was much less compared to that seen on the previously studied volatile oil LRA97-1. It is worth noting that the addition of 30% DMF-3 to the un-contaminated gas-condensate GCB98-1 resulted in a near-critical mixture at a temperature of 37.8 °C. An enhancement in the viscosity can be clearly seen as the pressure approaches the saturation pressure of 4772 psia.

Depending on the prevailing composition below the saturation point, the saturated liquid viscosity, shown in Figure 7.20, is seen to display two opposing trends with increasing DMF-3 contamination. For saturation pressures of 3000 psia and higher, liquid viscosity was seen to decrease with increasing amount of DMF-3 contamination, similarly to what had been observed for the volatile oil LRA97-1. Liquid viscosity for saturation pressures below 3000 psia is seen to reverse the above trend with increasing DMF-3 contamination.

GCB98-2 Fluid (Contamination With DMF-1). During the testing of the gas condensate GCB98-2 in its original (un-contaminated) form and with 15%, 30%, and 45% of DMF-1 , the viscosity of the single phase gas and saturated liquid and vapour phases were measured. Figures 7.21 through 7.23 present the results of these measurements. Table 7.16 also lists these measurements. Figure 7.21 shows that the viscosity of single phase gas increases with increasing amounts of DMF-1 contamination. The increase in viscosity is much more pronounced at higher contamination levels. Viscosity enhancement observed for the 45% contaminated sample is an indication that the sample is a near critical mixture. For such mixtures, an enhancement in viscosity has been observed as pressure approaches the saturation pressure.

The saturated liquid viscosity, shown in Figure 7.22, is seen to behave similar to that of GCB98-1, with increasing amounts of DMF-1 contamination. The viscosity of the saturated vapour, Figure 7.23, is observed to decrease as DMF-1 contamination increases.

7.4.2 Predicting the Viscosity of the Original Fluids

The petroleum industry uses several methods for predicting the viscosity of petroleum fluids, ranging from mathematically rigorous to completely empirical. The most widely used predictive models are the residual viscosity model known as the LBC method[6] (Section 5.7.2, Chapter 5) and those based on the principle of corresponding states[8,9] (Sections 5.6.2 and 5.6.3, Chapter 5). In addition to the above, the in-house developed residual viscosity model, referred to as HW1[7] (Section 5.7.3, Chapter 5) is used in this

study. For more detail discussion of the above methods, the reader should refer to Chapter 5.

Tuning of the viscosity predictive models by adjusting parameters which are known to be less accurate has become a common practice in petroleum industry, for use in reservoir flow simulators. Reservoir fluids are composed of numerous individual hydrocarbon components and have to be characterised by a limited number of groups often referred to as pseudo-components. The properties of these pseudo-components such as critical properties are required for viscosity calculations. Since critical properties are often difficult to measure experimentally, they are usually determined from different correlations. As a result of using these inaccurate correlations for real reservoir fluids, they often lead to poor predictions.

The main objective of the following tuning process is to investigate whether the viscosity of the original reservoir fluid can be accurately predicted from tuned models of the contaminated samples. The critical properties of the plus-fraction, which are required for viscosity prediction, were calculated from Twu's correlation[10]. Different viscosity models showed more dependency on the critical properties and molecular weight of pseudo-components (single- and multi-carbon cuts). Sensitivity analyses were performed on the effects of these properties on the predicted fluid viscosity, where limits have been set to control their adjustment[11]. Table 7.17 lists those influential properties for LBC, HW1, CS1 and CS2 viscosity models and their tuning limits. The predicted results using the above-mentioned models are described below.

Volatile Oil Fluids:

LRA97-1 Fluid. Figures 7.24 through 7.26 show a comparison between measured and predicted (un-tuned) single phase and saturated liquid viscosity for the original LRA97-1 fluid and with 5.08% and 19.92% of DMF-3. Generally, all predictive models reasonably predicted the saturated vapour viscosity of all the three samples with an average deviation of less than 5%. However, single phase and saturated liquid viscosities were poorly

predicted. In general, the residual viscosity models (LBC & HW1) were much better in their predictions than those of the corresponding states ones (CS1 & CS2).

Following the poor prediction of single phase and saturated liquid viscosity, it is necessary to tune the viscosity models by adjusting the properties of the plus-fraction. For the residual viscosity models (LBC & HW1), the critical volume of the C7+ fraction was adjusted whereas for the corresponding states ones (CS1 & CS2), the adjusted property is the critical temperature of the plus fraction. An average tuning (or multiplying) factor was derived, for all of the samples, using all single and saturated liquid phases viscosity data. Figures 7.27 and 7.28 show the predicted single phase and saturated liquid viscosity of the LRA97-1 with 5.08% and 19.92% of DMF-3 obtained from the above adjustment procedure. As can be seen in the above figures, adjusting the plus-fraction critical properties significantly improved prediction of the mixture viscosities for the LBC and HW1 models. While for those of CS1 and CS2 the adjustment limit of 10% was exhausted, yet predictions were poor in some cases. Table 7.18 lists the multiplying factors required to match measured viscosities, while retaining the previously set limits.

To investigate the possibility of retrieving the viscosity of the original LRA97-1 fluid, the multiplying factors, listed in Table 7.18, were plotted against the level of DMF-3 contamination, as shown in Figure 7.29. Although two contamination levels were available for this particular fluid, however a linear relationship has been observed when modelling the phase behaviour of this fluid where more than two contamination levels were available[12]. This behaviour in turn facilitates linear extrapolation of the multiplying factors needed for predicting the viscosity of the original LRA97-1 fluid. Multiplying factors of 1.016, 1.022 and 1.105, for the LBC HW1 and CS1 models, respectively, were found to correspond to 0% contamination level which are in good agreement to those obtained by adjusting the critical properties of the plus-fraction to measured viscosity of the original fluid. The corresponding state model (CS2) was not used in the above extrapolation procedure because of its failure in modelling the viscosity of these oil samples.

Using the above (extrapolated and adjusted) multiplying factors, the viscosity of the original LRA97-1 fluid was predicted and compared. Figure 7.30 shows that the difference between the two predictions is insignificant.

Gas Condensate Fluids (GCB98-1 and GCB98-2):

As mentioned above, the gas condensate GCB98-1 was contaminated with DMF-3 whereas the GCB98-2 was contaminated with DMF-1 at various contamination levels.

During the prediction of the single phase and saturated liquid and vapour viscosities, the un-tuned models were observed to behave differently for each fluid phase. All models predicted the vapour viscosity with reasonable accuracy. The corresponding states ones (CS1 & CS2) models reasonably predicted the single phase condensate viscosity with deviation of less than 5%. The residual viscosity models (LBC and HW1) reasonably predicted the saturated liquid viscosities, especially those close to saturation pressures.

The tuning exercise previously employed for the volatile oil LRA97-1 was repeated here to ensure reliable viscosity prediction from all models. The possibility of retrieving the viscosity of the original GCB98-1 and GCB98-2 was investigated in a similar way to that employed for the LRA97-1. Using the extrapolated and adjusted multiplying factors, the viscosity of the original GCB98-1 and GCB98-2 fluids were predicted and compared with the measured data, as shown in Figures 7.31 and 7.32. It can be seen in Figures 7.31 and 7.32 that the difference between the two predictions is insignificant and that errors seen in viscosity prediction are mostly due to the deficiencies of the models.

To assess the overall performance and the reliability of the above employed methods for predicting fluid viscosity, the overall average deviations for the single phase oil , single phase condensate and saturated liquid and vapour phase, of all tested fluids, are listed in Tables 7.19 through 7.22. The overall deviation tables show that the un-tuned viscosity models poorly predicted the single phase oil viscosities, while they reliably predicted the viscosities of the saturated vapour. The un-tuned corresponding states (CS1 and CS2)

models performed very well for predicting the viscosities of the single phase condensate, while the residual viscosity (LBC and HW1) models predicted the viscosity of the saturated liquids with reasonable accuracy.

The deviations of predicted viscosity of the original fluids using the tuned and extrapolated C7+ critical properties are in very close agreement. This in turn demonstrated the reliability of the method used in retrieving the viscosity of un-contaminated reservoir fluids from contaminated samples.

7.5 CONCLUSIONS

From the above studies, the following conclusions can be made:

- A methodology (Sections 7.3.2 and 7.4.2) has been developed to retrieve the interfacial tension and viscosity of the original (un-contaminated) reservoir fluid from contaminated samples with oil-based drilling mud filtrate.
- The interfacial tension of the un-contaminated fluid can be predicted, with reasonable accuracy, by extrapolating the parachor value of the plus-fraction, obtained from tuned models of the contaminated samples, to 0% contamination (Figures 7.10 through 7.14).
- The overall deviations (Tables 7.19 through 7.22) show that the un-tuned viscosity models poorly predicted the single phase oil viscosities, while they reliably predicted the viscosities of the saturated vapour. The un-tuned one- and two-reference fluid(s) corresponding states models (Sections 5.6.2 and 5.6.3, respectively) performed very well for predicting the viscosities of the single phase condensate, while residual viscosity models (LBC, Section 5.7.2, and HW1, Section 5.7.3) predicted the viscosity of the saturated liquids with reasonable accuracy.
- The deviations of predicted viscosity of the original single and saturated fluid phases using the tuned and extrapolated C7+ critical properties are in very close agreement (Figures 7.30 through 7.32). This in turn demonstrated the reliability of the

methodology employed in retrieving the viscosity of un-contaminated reservoir fluids from contaminated samples

REFERENCES

[1] Weinaug, C. F. and Katz, D. L.: "Surface Tension of Methane - Propane Mixtures", Ind. Eng. Chem. (I & EC), **35**(2), 239-246, (1943).

[2] Hough, E. W. and Stegemeier, G. L. :"Correlation of Surface and Interfacial Tension of Light Hydrocarbons in The Critical Region", Soc. Pet. Eng. J. (SPEJ), 259-263, (Dec., 1961).

[3] Lee, S. T. and Chien, M. C. H. : "A New Multicomponent Surface Tension Correlation Based on Scaling Theory", paper SPE 12643 presented at the SPE/DOE Enhanced Oil Recovery Symposium, Tulsa, Oklahoma, (1984).

[4] Hugill, J. A. and Welsenes, Van, A. J. : "Surface Tension: A Simple Correlation for Natural Gas + Condensate Systems", Fluid Phase Equilib., **29**, 383-390, (1986).

[5] Dandekar, A. : Interfacial Tension and Viscosity of Reservoir Fluids, Ph.D. Thesis, Heriot-Watt University, Edinburgh, Scotland, (1994).

[6] Lohrenz, J., Bray, B. G. and Clark, C. R. : "Calculating Viscosities of Reservoir Fluids from Their Compositions", J. Pet. Tech. (JPT), 1171 - 1176, (Oct., 1964).

[7] Dandekar, A., Danesh, A., Tehrani, D. H and Todd, A. C :"A Modified Residual Viscosity Method for Improved Prediction of Dense Phase Viscosities", Presented at the 7th European Improved Oil Recovery (IOR) Symposium in Moscow, Russia, Oct. 27-29, (1992).

[8] Pedersen, K. S, and Fredenslund, Aa. : "An Improved Corresponding States Model for the Prediction of Oil and Gas Viscosities and Thermal Conductivities," Chem. Eng. Sci., **42**, 182-186, (1987).

[9] Petersen, Aa., Knudsen, K. and Fredenslund, Aa. : "Prediction of Viscosities of Hydrocarbon Mixtures," Fluid Phase Equilib., **70**, 293-308, (1991).

[10] Twu, C. H : "An internally Consistent Correlation for Predicting the Critical Properties and Molecular Weights of Petroleum and Coal-Tar Liquids", Fluid Phase Equilib., **16**, 137-150, (1984).

[11] El-Gayed, K. : Viscosity of Petroleum Reservoir Fluids: Measurement and Tuning Predictive Models, M.Phil. Thesis, Heriot-Watt University, Edinburgh, Scotland, (1997).

[12] Gozalpour, F. : Integrated Phase Behaviour Modelling of Petroleum Fluids for Compositional Simulation of Reservoir-Surface Processes, Ph.D. Thesis, Heriot-Watt University, Edinburgh, Scotland, (1998).

Table 7.1 - Measured Molar Compositions of the Drilling Mud Filtrate DMF-3.

Comp.	Mole / %
C14	69.0
C16	31.0

Table 7.2 - Measured Molar Compositions of the Drilling Mud Filtrate DMF-1.

Comp.	MW*	Mole / %
C11	147	0.04
C12	161	0.17
C13	175	1.75
C14	190	13.38
C15	206	27.60
C16	222	20.13
C17	237	16.84
C18	251	9.26
C19	263	5.47
C20	275	2.65
C21	291	1.32
C22	300	0.70
C23	312	0.39
C24	324	0.17
C25	337	0.07
C26	349	0.03
C27	360	0.02
C28	372	0.01
C29	382	0.005
C30	394	0.002
C31+	445	0.002

* - Generalised

Table 7.3 - Measured and Calculated Single Phase Compositions of LRA97-1 Fluid and Its contaminated Samples with 5.08% and 19.92% of DMF-3 on Stock Tank Liquid Volume (STLV) Basis.

Comp.	MW	Mole / %		
		0%	5.08*%	19.92*%
C1	16.04	55.92	54.79	50.98
C2	30.07	9.88	9.68	9.01
C3	44.10	5.67	5.56	5.17
i-C4	58.12	1.18	1.16	1.08
n-C4	58.12	2.03	1.99	1.85
i-C5	72.15	1.10	1.08	1.00
n-C5	72.15	1.92	1.88	1.75
C6	88	1.54	1.51	1.40
C7	92	2.16	2.12	1.97
C8	103	2.69	2.64	2.45
C9	117	1.99	1.95	1.81
C10	132	1.70	1.67	1.55
C11	147	1.30	1.27	1.19
C12	161	0.95	0.93	0.87
C13	174	1.22	1.20	1.11
C14	**189**	**0.86**	**2.24**	**6.87**
C15	199	0.87	0.85	0.79
C16	**218**	**0.68**	**1.29**	**3.36**
C17	231	0.50	0.49	0.46
C18	249	0.57	0.56	0.52
C19	257	0.60	0.59	0.55
C20+	460	4.69	4.60	4.28

* - Calculated

Table 7.4 - Measured Interfacial Tension Data, in $mN.m^{-1}$, of the LRA97-1 Fluid and Its Contaminated Samples With DMF-3 at a Temperature of 37.8 °C.

Pressure/ psia	DMF-3 Contamination Level		
	0%	5.08%	19.92%
14.7	24.7*	25.9*	27.8*
1000	-	-	12.2
1250	-	9.77	-
1500	-	-	7.70
2000	4.71	4.90	5.44
2500	2.89	-	-
3000	1.80	1.95	-
3500	1.21	-	-

* - IFT of the 3000 psia Stabilised Liquid and its Vapour.

Table 7.5 - Measured and Calculated Single Phase Compositions of GCB98-1 Fluid and Its contaminated Samples with 5%, 15% and 30% of DMF-3 on STLV Basis.

Comp.	MW	Mole / %			
		0%	5*%	15*%	30*%
C1	16.04	71.87	71.69	71.28	70.45
C2	30.07	11.78	11.75	11.68	11.54
C3	44.10	4.75	4.74	4.71	4.66
i-C4	58.12	0.81	0.81	0.80	0.80
n-C4	58.12	1.72	1.72	1.71	1.69
i-C5	72.15	0.62	0.61	0.61	0.60
n-C5	72.15	0.78	0.78	0.78	0.77
C6	88.5	0.93	0.93	0.92	0.91
C7	92	1.38	1.37	1.37	1.35
C8	103	1.35	1.34	1.33	1.32
C9	116	0.75	0.74	0.74	0.73
C10	131	0.55	0.55	0.54	0.54
C11	147	0.40	0.40	0.40	0.39
C12	161	0.32	0.32	0.32	0.31
C13	173	0.27	0.27	0.27	0.27
C14	**186**	**0.27**	**0.44**	**0.84**	**1.63**
C15	203	0.23	0.23	0.23	0.22
C16	**215**	**0.18**	**0.26**	**0.43**	**0.79**
C17	229	0.14	0.14	0.14	0.14
C18	246	0.14	0.14	0.14	0.14
C19	258	0.12	0.12	0.11	0.11
C20+	384	0.65	0.65	0.65	0.64

* - Calculated

Table 7.6 - Measured Interfacial Tension Data, in $mN.m^{-1}$, of the GCB98-1 Fluid and Its Contaminated Samples With DMF-3 at a Temperature of 37.8 °C.

Pressure/ psia	DMF-3 Contamination Level			
	0%	5%	15%	30%
14.7	22.8*	23.1*	23.8*	24.1*
2000	-	-	-	3.71
2500	-	1.68	2.04	-
3000	0.911	0.966	1.01	1.16
3500	0.514	0.550	-	0.513
4000	0.342	0.303	0.260	-
4500	0.190	-	-	0.047

* - IFT of the 3000 psia Stabilised Liquid and its Vapour.

Table 7.7 - Measured and Calculated Single Phase Compositions of GCB98-2 Fluid and Its contaminated Samples with 20%, 49%, 51% and 55% of DMF-3 on STLV Basis.

Comp.	MW	Mole / %				
		0%	20*%	49*%	51*%	55*%
C1	16.04	72.48	71.75	69.75	69.53	69.04
C2	30.07	11.73	11.61	11.29	11.25	11.17
C3	44.10	4.84	4.79	4.66	4.64	4.61
i-C4	58.12	0.84	0.84	0.81	0.81	0.80
n-C4	58.12	1.78	1.76	1.71	1.70	1.69
i-C5	72.15	0.63	0.62	0.61	0.60	0.60
n-C5	72.15	0.83	0.82	0.80	0.79	0.79
C6	88.5	0.76	0.75	0.73	0.73	0.73
C7	92	1.07	1.06	1.03	1.03	1.02
C8	103	1.12	1.11	1.08	1.07	1.06
C9	116	0.75	0.74	0.72	0.72	0.71
C10	131	0.54	0.54	0.52	0.52	0.52
C11	147	0.42	0.41	0.40	0.40	0.40
C12	161	0.30	0.30	0.29	0.29	0.29
C13	173	0.32	0.32	0.31	0.31	0.31
C14	**186**	**0.28**	**0.98**	**2.87**	**3.08**	**3.55**
C15	203	0.22	0.22	0.22	0.22	0.21
C16	**215**	**0.17**	**0.48**	**1.33**	**1.42**	**1.63**
C17	229	0.12	0.12	0.11	0.11	0.11
C18	246	0.14	0.13	0.13	0.13	0.13
C19	258	0.13	0.13	0.12	0.12	0.12
C20+	384	0.54	0.53	0.52	0.52	0.52

* - Calculated

Table 7.8 - Measured Interfacial Tension Data, in $mN.m^{-1}$, of the GCB98-2 Fluid and Its Contaminated Samples With DMF-3 at 100 °C.

	DMF-3 Contamination Level					
Pressure/ psia	**0%**	**20%**	**40%**	**49%**	**51%**	**55%**
5150	-	0.007	-	-	-	-
5100	-	0.012	-	-	-	-
5000	-	0.023	-	-	-	-
4900	-	0.043	*	*	*	*
4800	0.241	0.065	*	*	*	*
4500	0.380	0.177	0.102	0.094	0.122	0.145
4000	0.718	0.530	0.548	0.621	0.605	0.670
3500	1.25	1.13	1.28	1.33	1.48	1.45
3000	2.06	2.09	2.33	2.48	2.61	2.68
2500	3.27	3.47	3.87	3.90	4.15	4.27
2000	4.85	5.13	5.55	5.88	6.09	6.12
1000	9.87	10.5	10.5	11.4	-	11.4

* Meniscus too Small to Measure

Table 7.9 - Measured Single Phase Compositions of GCB98-2 Fluid and Its contaminated Samples with 15%, 30%, 45%, 50%, 56% and 70% of DMF-3 on STLV Basis.

Comp.	MW	Mole / %					
		15%	30%	45%	50%	56%	70%
C1	16.04	72.00	71.33	70.32	69.87	69.18	66.64
C2	30.07	11.65	11.54	11.38	11.31	11.20	10.78
C3	44.10	4.81	4.76	4.69	4.67	4.62	4.45
i-C4	58.12	0.84	0.83	0.82	0.81	0.81	0.78
n-C4	58.12	1.76	1.75	1.72	1.71	1.69	1.63
i-C5	72.15	0.63	0.62	0.61	0.61	0.60	0.58
n-C5	72.15	0.82	0.81	0.80	0.80	0.79	0.76
C6	88.5	0.76	0.75	0.74	0.73	0.73	0.70
C7	92	1.07	1.06	1.04	1.03	1.02	0.98
C8	103	1.11	1.10	1.08	1.07	1.06	1.02
C9	116	0.74	0.73	0.72	0.72	0.71	0.68
C10	131	0.54	0.53	0.52	0.52	0.51	0.49
C11	**147**	**0.42**	**0.41**	**0.41**	**0.40**	**0.40**	**0.39**
C12	**161**	**0.30**	**0.30**	**0.30**	**0.30**	**0.29**	**0.29**
C13	**173**	**0.34**	**0.36**	**0.39**	**0.37**	**0.38**	**0.43**
C14	**186**	**0.38**	**0.52**	**0.73**	**0.76**	**0.88**	**1.34**
C15	**203**	**0.38**	**0.60**	**0.93**	**1.22**	**1.47**	**2.43**
C16	**215**	**0.30**	**0.49**	**0.78**	**0.89**	**1.08**	**1.78**
C17	**229**	**0.23**	**0.39**	**0.62**	**0.72**	**0.88**	**1.47**
C18	**246**	**0.20**	**0.30**	**0.44**	**0.47**	**0.55**	**0.87**
C19	**258**	**0.16**	**0.21**	**0.27**	**0.32**	**0.37**	**0.56**
C20+	**384**	**0.57**	**0.61**	**0.68**	**0.69**	**0.78**	**0.95**

Table 7.10 - Measured Interfacial Tension Data, in $mN.m^{-1}$, of the GCB98-2 Fluid and Its Contaminated Samples With DMF-1 at 100 °C.

	DMF-1 Contamination Level					
Pressure/ psia	**0%**	**15%**	**30%**	**50%**	**56%**	**70%**
5000	0.171	0.060	-	-	0.066	0.193
4900	-	-	0.044	0.049	0.105	0.255
4800	0.241	0.120	0.069	0.083	0.152	0.330
4500	0.380	0.252	0.210	0.249	0.348	0.615
4000	0.718	0.604	0.601	0.773	0.886	1.30
3500	1.25	1.18	1.29	1.65	1.72	2.29
3000	2.06	2.04	2.30	2.88	2.83	3.52
2500	3.27	3.24	3.70	4.51	4.26	4.98
2000	4.85	4.96	5.49	6.55	5.95	6.71
1000	9.87	9.92	10.5	12.0	10.3	10.8

Table 7.11 - Measured Interfacial Tension Data, in $mN.m^{-1}$, of the GCB98-2 Fluid and Its Contaminated Samples With DMF-1 at 37.8 °C.

Pressure/ psia	DMF-1 Contamination Level			
	0%	**15%**	**30%**	**45%**
4000	0.348	0.324	0.309	0.461
3000	0.979	1.04	1.14	1.53
2500	1.78	1.92	2.21	2.30
14.7	23.0*	24.4*	23.8*	22.4*

* IFT of the 3000 psia Stabilised Liquid and its Vapour.

Table 7.12 - Deviations of Predicted Interfacial Tension Data of All Tested Fluids.

Prediction Mode	LRA97-1 Samples		GCB98-1 Samples		GCB98-2 Samples	
	AD	AAD	AD	AAD	AD	AAD
Un-tuned / %	-17	17	-62	62	-50	50
Tuned / %	1	10	1	21	-5	19
Extrapolated / % (Original Fluids)	2	13	-11	13	2	15

$$AD = \sum_{i=1}^{N}\left(\left(IFT_{pred.} - IFT_{\exp.}\right)/IFT_{\exp.}\right)/N \quad , AAD = \sum_{i=1}^{N}\left|\left(\left(IFT_{pred.} - IFT_{\exp.}\right)/IFT_{\exp.}\right)\right|/N$$

Table 7.13 - Measured Viscosity, in cP, of Single Phase and Saturated Liquid and Vapour Phases of the LRA97-1 Fluid and Its Contaminated Samples with DMF-3 at 37.8 °C.

Pressure/ (psia)	DMF-3 Contamination Level					
	0%		**5.08%**		**19.92%**	
	Gas	Liquid	Gas	Liquid	Gas	Liquid
5400		0.426		-		-
5200		0.419		0.445		-
5000		0.409		0.438		0.558
4800		0.404		0.432		-
4600		0.399		-		-
4500		-		0.422		0.538
4300		-		0.416		-
4000		-				0.521
3500		-				0.497
3425		-				0.493
3000*	0.030	0.575		0.557	-	-
2000*	0.019	0.742	0.019	0.728	0.018	0.718
1500*	-	-	-	-	0.016	0.848
1250*	-	-	0.015	0.975	-	-
1000*	-	-		-	0.013	1.025

* - Two-phase Region.

Table 7.14 - Measured Viscosity, in cP, of The Stabilised Liquid of the LRA97-1 Fluid and Its Contaminated Samples with DMF-3 at 37.8 °C.

Pressure/ (psia)	DMF-3 Contamination Level		
	0%	**5.08%**	**19.92%**
200	2.72	2.32	2.28
500	2.95	2.64	2.29
1000	3.07	2.77	2.41

Table 7.15 - Measured Viscosity, in cP, of Single Phase and Saturated Liquid and Vapour Phases of the GCB98-1 Fluid and Its Contaminated Samples with DMF-3 at 37.8 °C.

Pressure/ (psia)	DMF-3 Contamination Level							
	0%		**5%**		**15%**		**30%**	
	Gas	Liquid	Gas	Liquid	Gas	Liquid	Gas	Liquid
5700	0.078	-	0.080	-	-	-	-	-
5675	0.078	-	-	-	-	-	-	-
5650	0.077	-	-	-	-	-	-	-
5600	-	-	0.078	-	-	-	-	-
5500	-	-	0.077	-	0.082	-	0.094	-
5400	-	-	-	-	0.080	-	-	-
5300	-	-	-	-	-	-	0.093	-
5200	-	-	-	-	0.080	-	-	-
5150	-	-	-	-	-	-	0.092	-
5000	-	-	-	-	-	-	0.092	-
4900	-	-	-	-	-	-	0.093	-
4850	-	-	-	-	-	-	0.093	-
4800	-	-	-	-	-	-	0.094	-
4780	-	-	-	-	-	-	0.096	-
4500*	-	0.261	-	-	-	-	-	0.148
4000*	-	0.245	-	0.232	-	0.206	-	-
3500*	-	0.245	-	-	-	-	-	-
3000*	-	0.244	-	0.231	-	0.241		0.233
2500*	-	-	-	0.239	-	0.246	-	-
2000*	-	-	-	-	-	-	0.018	0.300

* - Two-phase Region.

Table 7.16 - Measured Viscosity, in cP, of Single Phase and Saturated Liquid and Vapour Phases of the GCB98-2 Fluid and Its Contaminated Samples with DMF-1 at 37.8 °C.

Pressure/ (psia)	DMF-1 Contamination Level							
	0%		15%		30%		45%	
	Gas	Liquid	Gas	Liquid	Gas	Liquid	Gas	Liquid
5700	0.077	-	0.081	-	0.089	-	0.108	-
5675	0.077	-	-	-	-	-	-	-
5650	0.077	-	-	-	-	-	-	-
5550	-	-	0.080	-	-	-	-	-
5500	-	-	-	-	0.089	-	0.104	-
5400	-	-	-	-	-	-	0.106	-
5300	-	-	0.079	-	0.088	-	0.107	-
5100	-	-	-	-	0.087	-	0.110	-
5060	-	-	-	-	-	-	0.112	-
4000*	-	0.2393	-	0.215	-	0.2008	-	0.215
3000*	-	0.2380	-	0.243	0.032	0.2488	0.030	0.273
2500*	-	0.2376	0.027	0.255	0.026	0.2742	0.023	0.308

* - Two-phase Region.

Table 7.17 - The Most Influential Tuning Properties For Different Viscosity Methods and Their Tuning Limits.

Method	Tuning Property	Tuning Limit/ %
LBC	V_c	5
HW1	V_c	5
CS1	T_c	10
CS2	T_c	10

Table 7.18 - Multiplying Factors for the Adjusted C7+ Critical Properties of the Original LRA97-1 Fluid and Its Contaminated Samples with DMF-3 at 37.8 °C.

Model	Adjusted Parameter	Multiplying Factors For Different DMF-3 Contamination Levels			
		5.08%	19.92%	0%	
LBC	Vc	1.015	1.011	1.016[1]	1.012
HW1	Vc	1.020	1.015	1.022[1]	1.022
CS1	Tc	1.090	1.048	1.105[1]	1.090
CS2	Tc	1.100	1.100	-	1.100

[1] Extrapolated from Figure 7.28.

Table 7.19 - Absolute and Average Deviations of Predicted Viscosity of the Single Phase Volatile Oil of All Tested Fluids at 37.8 °C.

Viscosity Prediction	LBC		HW1		CS1		CS2	
	AD	AAD	AD	AAD	AD	AAD	AD	AAD
Un-tuned	-11	11	-14	14	-18	18	-33	12
Tuned	-1	2	0	1	-1	1	-16	8
Extrapolated	1	2	-3	4	-3	4	*	*

* - No extrapolation was made for CS2 model because of its poor predictions.

$$AD = \sum_{i=1}^{N}\left(\left(IFT_{pred.} - IFT_{\exp.}\right)/IFT_{\exp.}\right)\Big/N \quad , AAD = \sum_{i=1}^{N}\left|\left(\left(IFT_{pred.} - IFT_{\exp.}\right)/IFT_{\exp.}\right)\right|\Big/N$$

Table 7.20 - Absolute and Average Deviations of Predicted Viscosity of the Single Phase Gas Condensate of All Tested Fluids at 37.8 °C.

Viscosity Prediction	LBC		HW1		CS1		CS2	
	AD	AAD	AD	AAD	AD	AAD	AD	AAD
Un-tuned	-13	13	-13	13	-3	3	1	3
Tuned	-8	8	-8	8	-9	9	0	1
Extrapolated	-8	8	-8	8	-10	10	-5	5

Table 7.21 - Absolute and Average Deviations of Predicted Viscosity of the Saturated Liquid of All Tested Fluids at 37.8 °C.

Viscosity Prediction	LBC		HW1		CS1		CS2	
	AD	AAD	AD	AAD	AD	AAD	AD	AAD
Un-tuned	-8	9	2	11	16	15	-5	13
Tuned	6	7	7	10	10	10	-3	4
Extrapolated	8	9	6	11	9	9	-5	8

Table 7.22 - Absolute and Average Deviations of Predicted Viscosity of the Saturated Vapour of All Tested Fluids at 37.8 °C.

Viscosity Prediction	LBC		HW1		CS1		CS2	
	AD	AAD	AD	AAD	AD	AAD	AD	AAD
Un-tuned	-2	4	-2	4	-5	5	-3	5
Tuned	*		*		*		*	
Extrapolated	*		*		*		*	

* - Tuning Did not Effect the Predicted Vapour Viscosities.

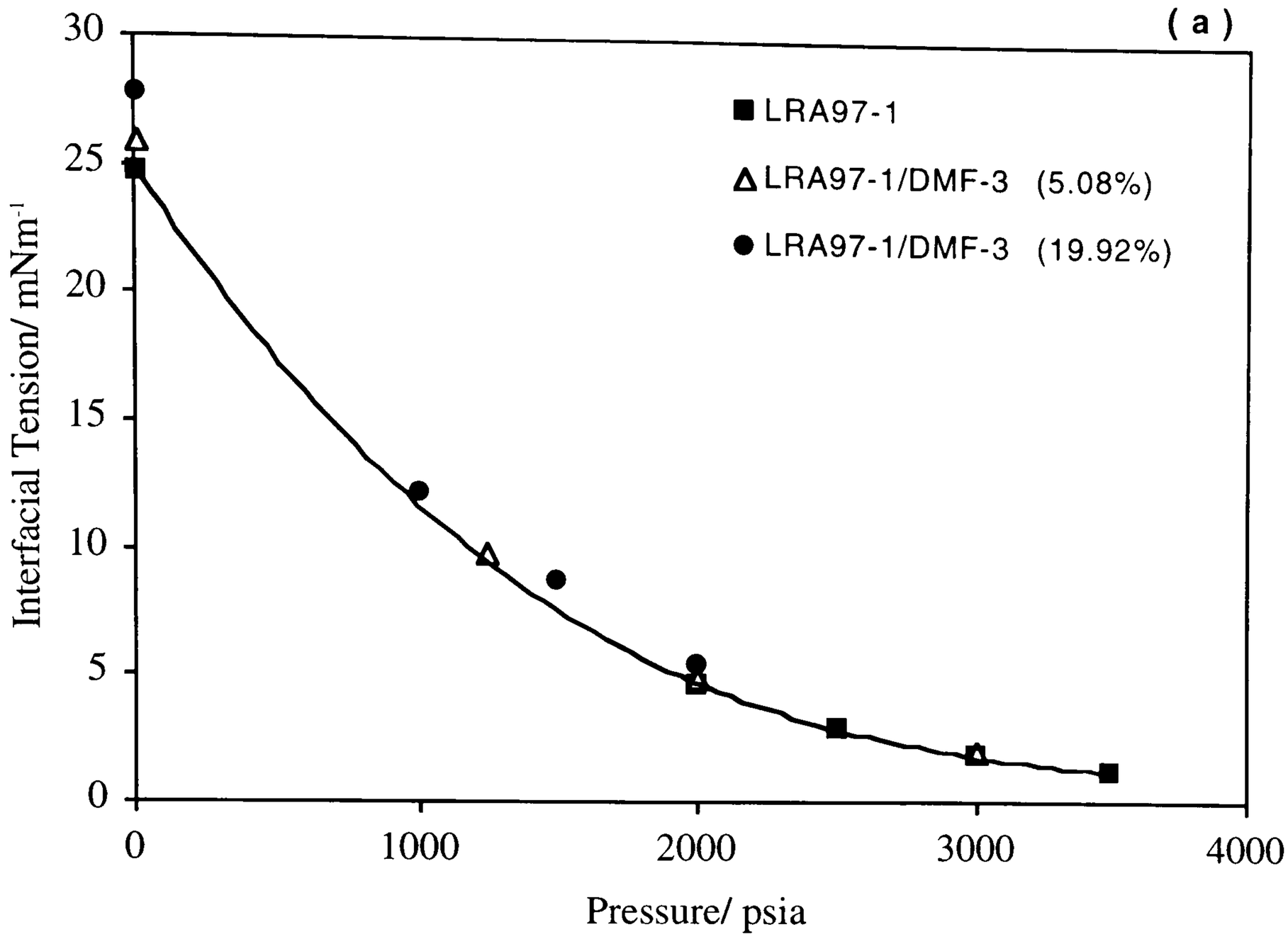

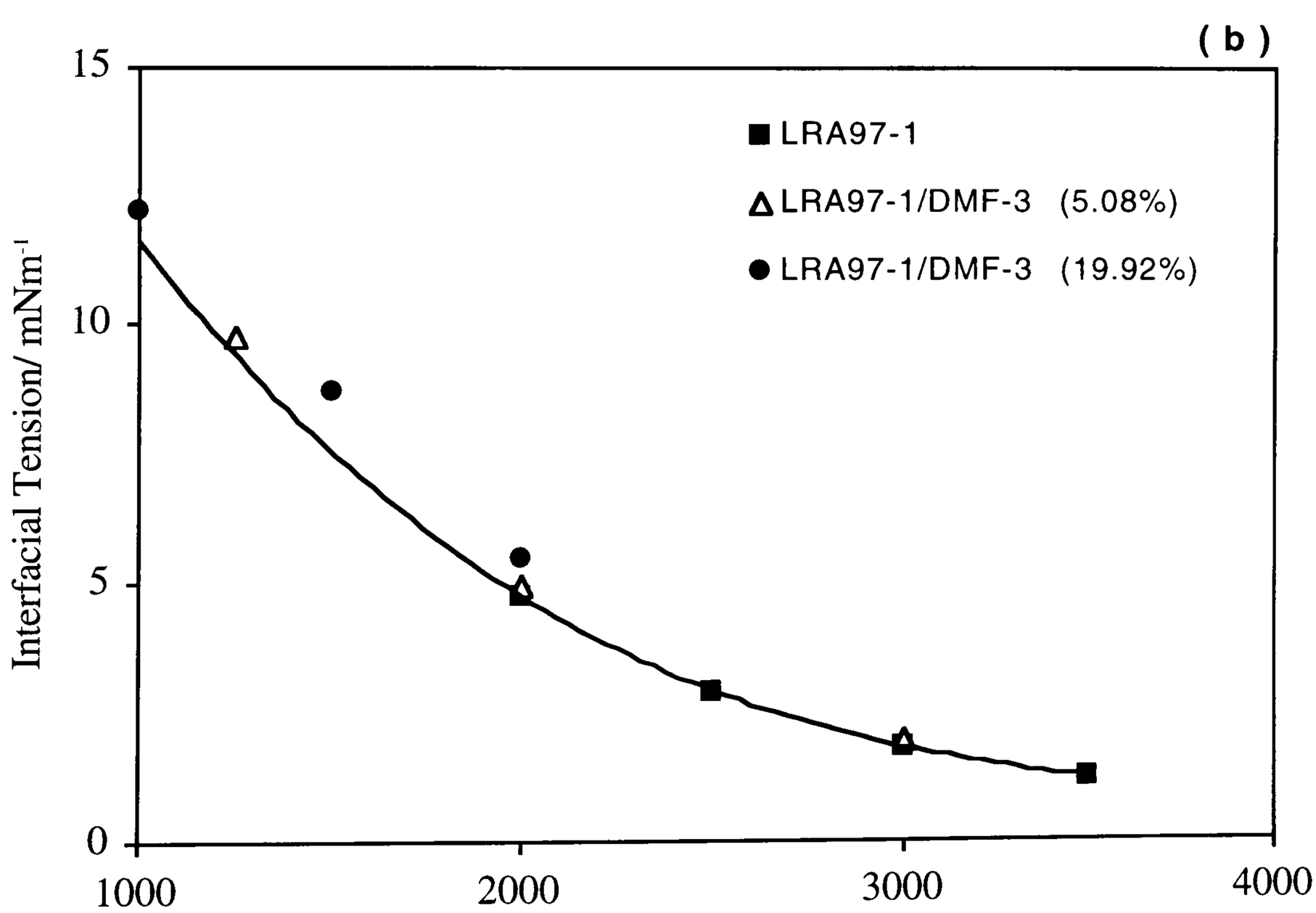

Figure 7.1 - Variation of Interfacial Tension With Pressure of the LRA97-1 Fluid With Various Volumes of DMF-3 Contamination at 37.8 °C, **(a)** Full Pressure Range, and **(b)** Pressure up to 1000 psia.

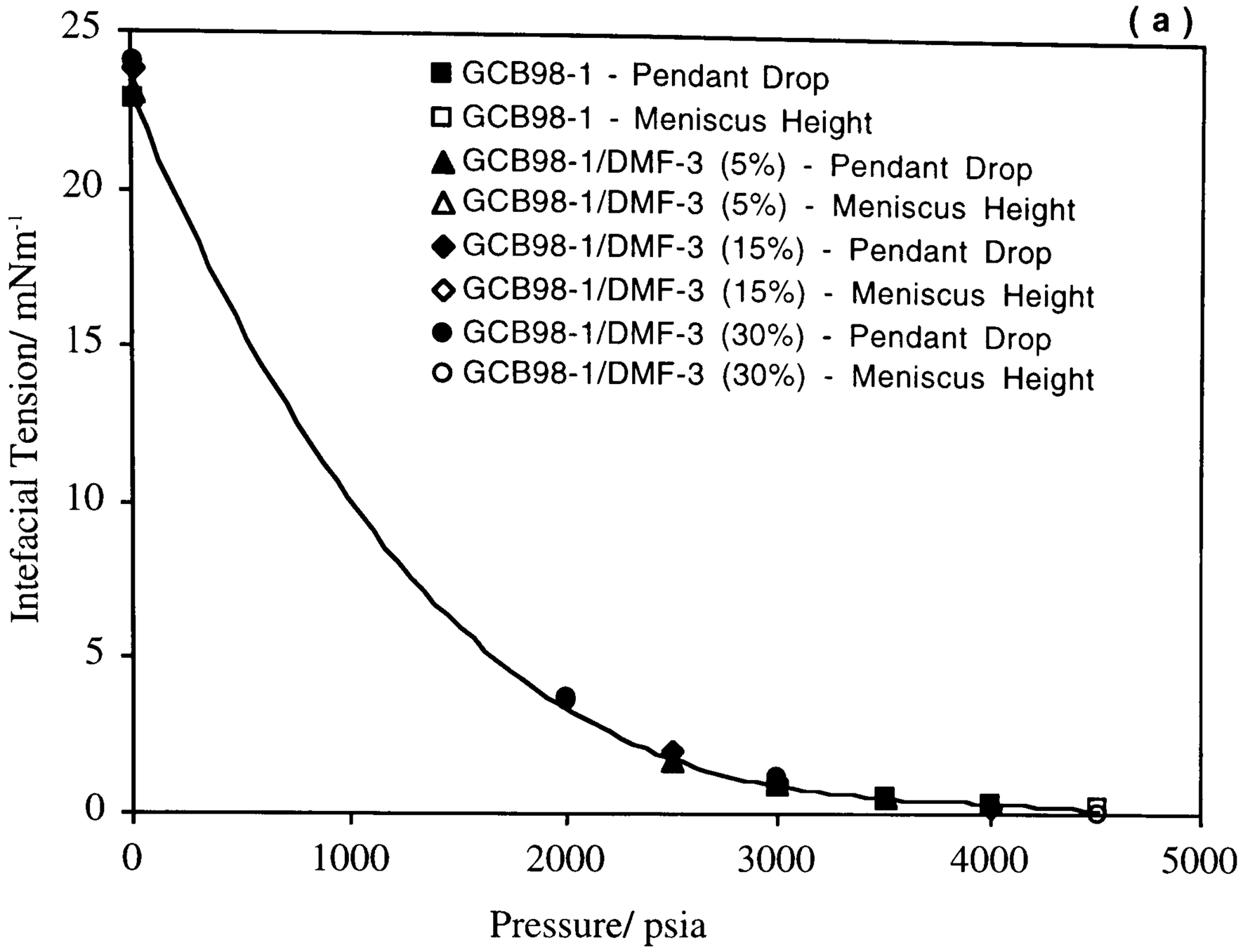

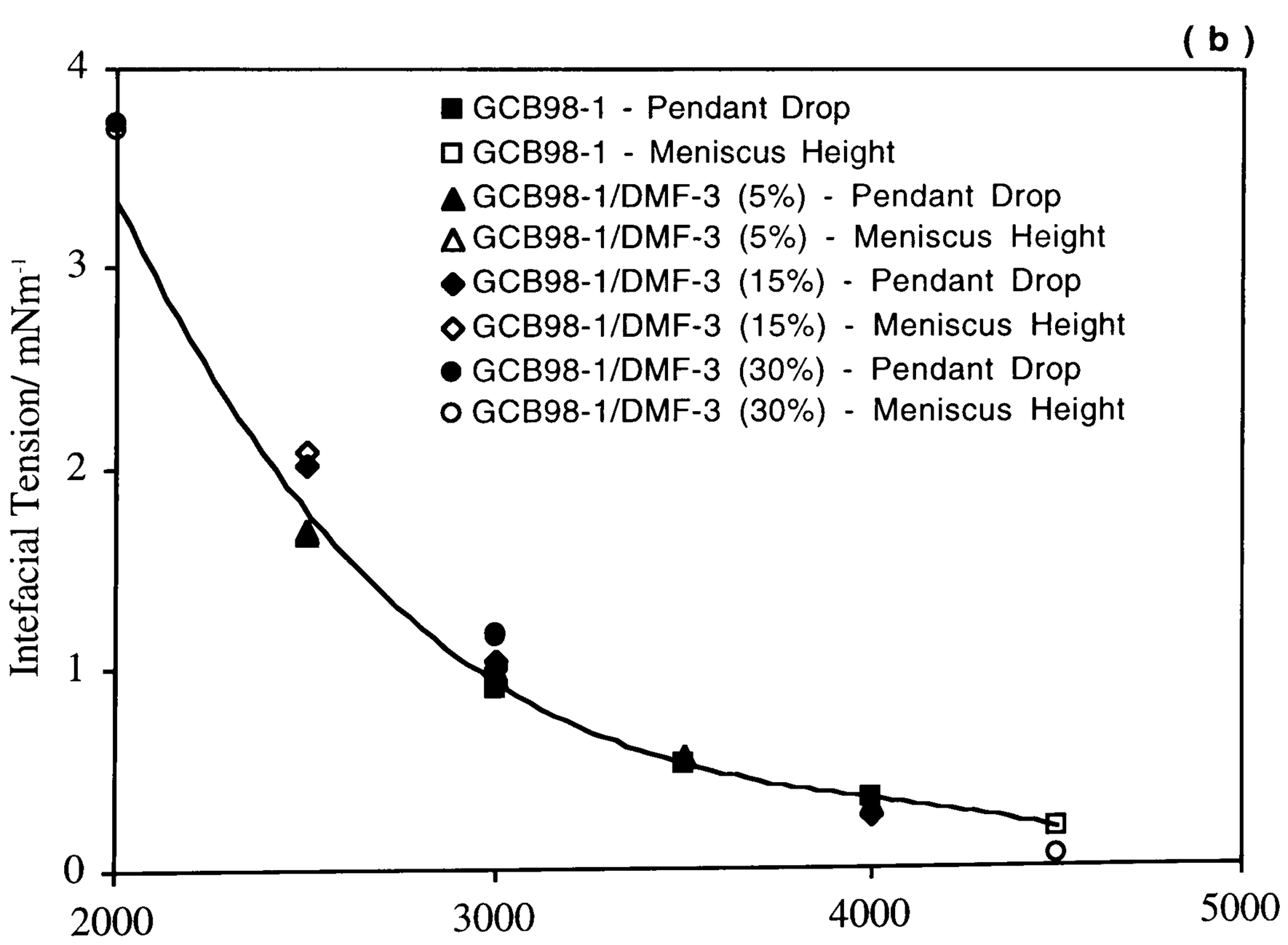

Figure 7.2 - Variation of Interfacial Tension With Pressure of the GCB98-1 Fluid With Various Volumes of DMF-3 Contamination at 37.8 °C, (**a**) Full Pressure Range, and (**b**) Pressure up to 2000 psia.

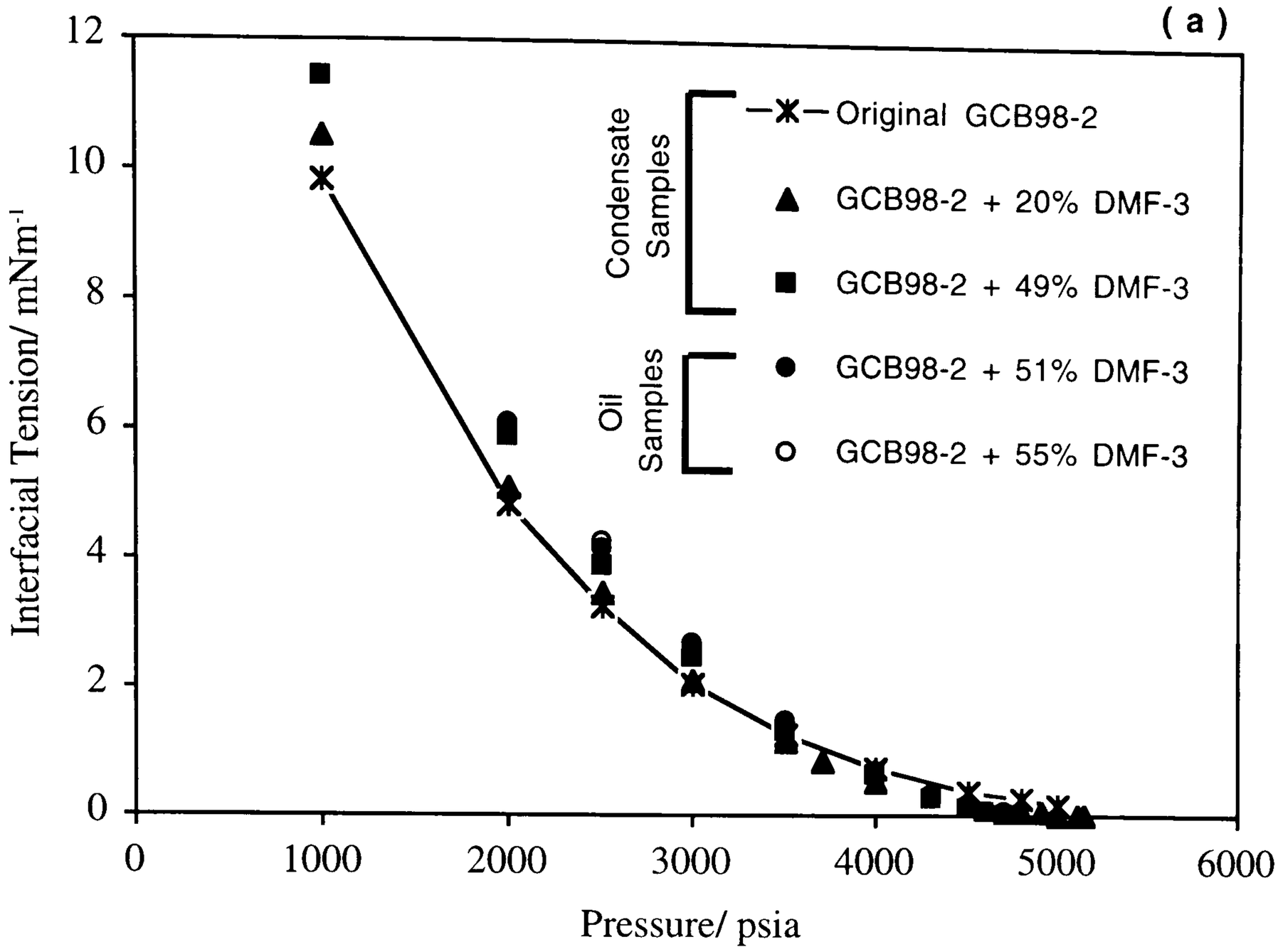

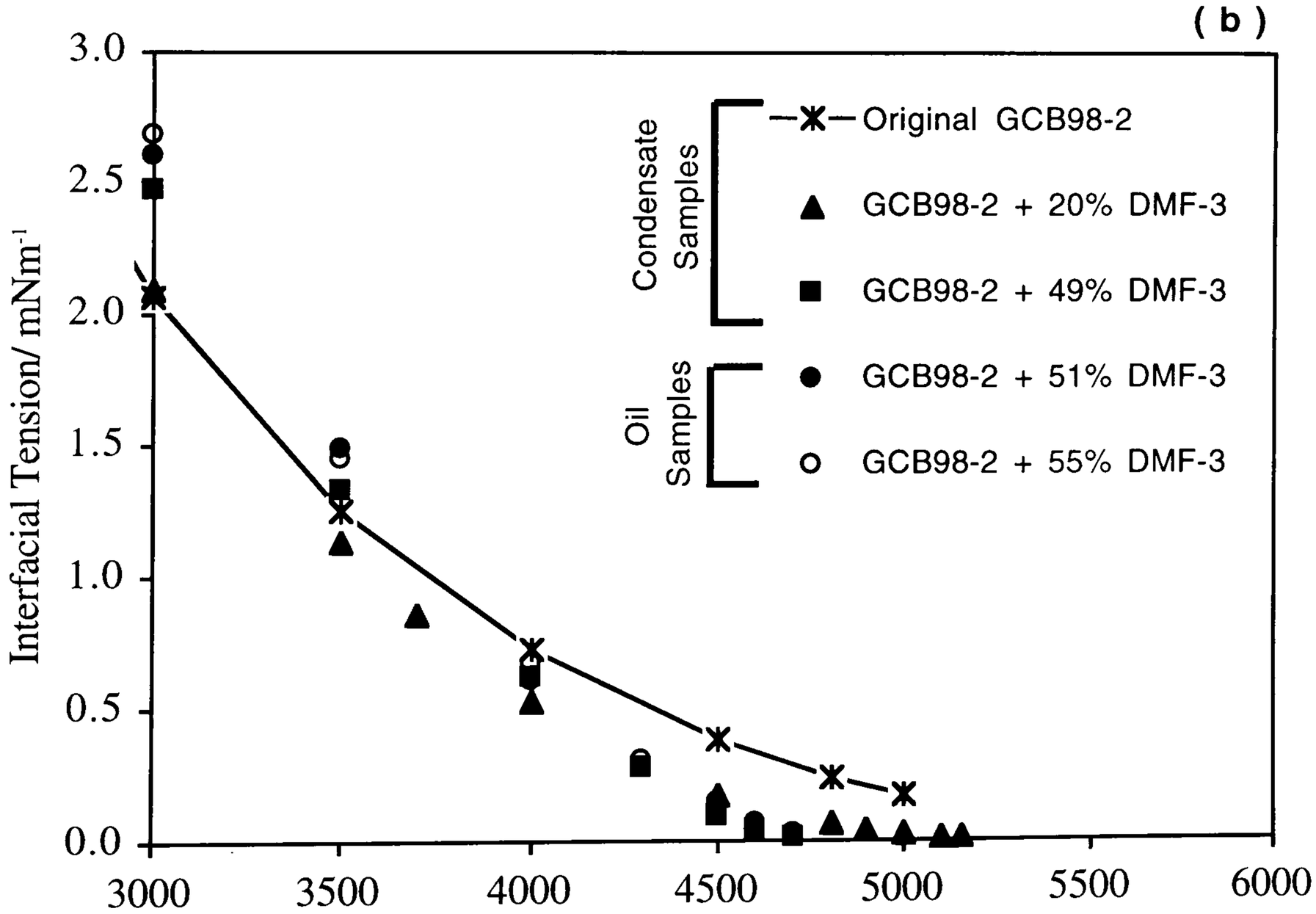

Figure 7.3 - Variation of Interfacial Tension With Pressure of the GCB98-2 Fluid With Various Volumes of DMF-3 Contamination at 100 °C, (**a**) Full Pressure Range, and (**b**) Pressure up to 3000 psia.

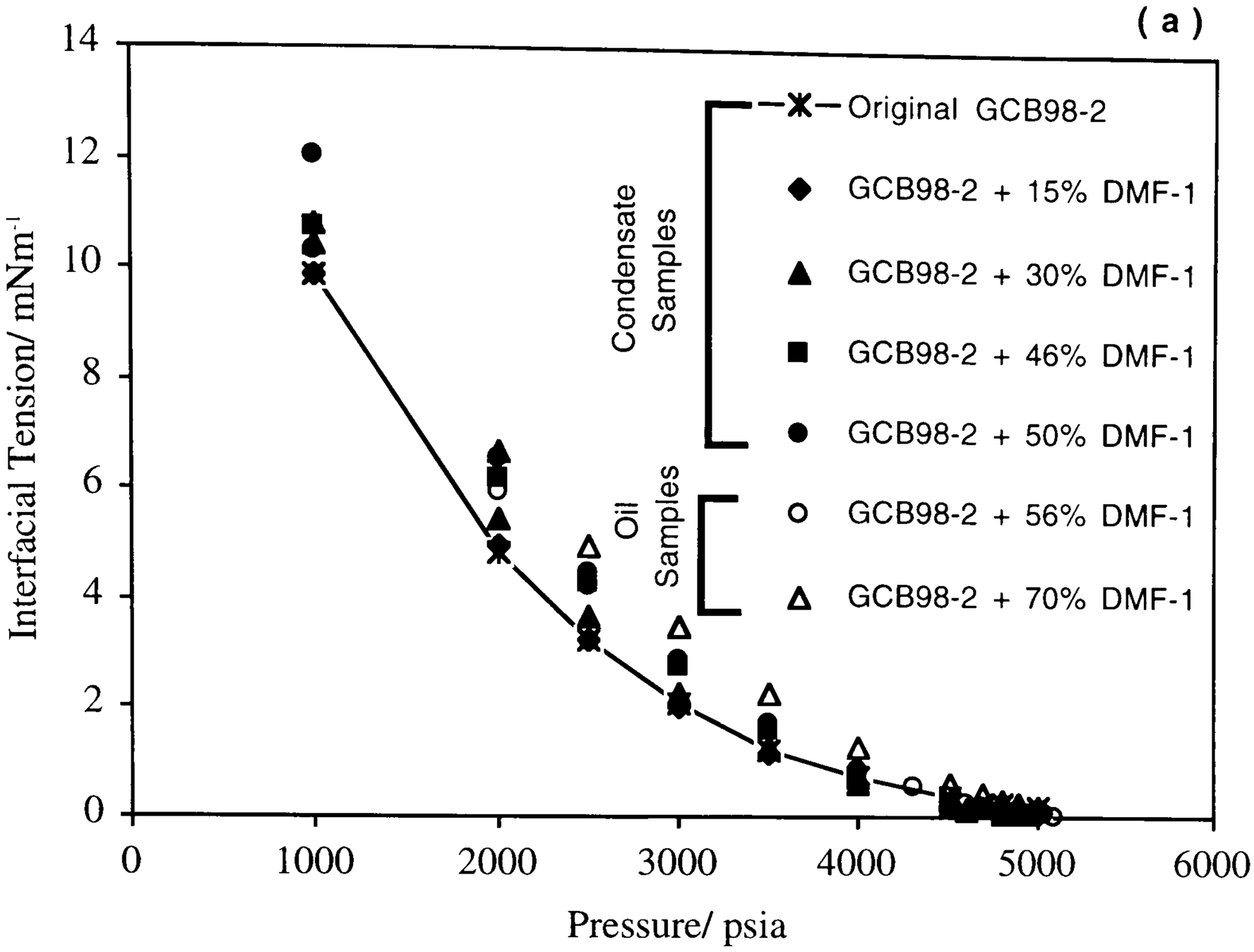

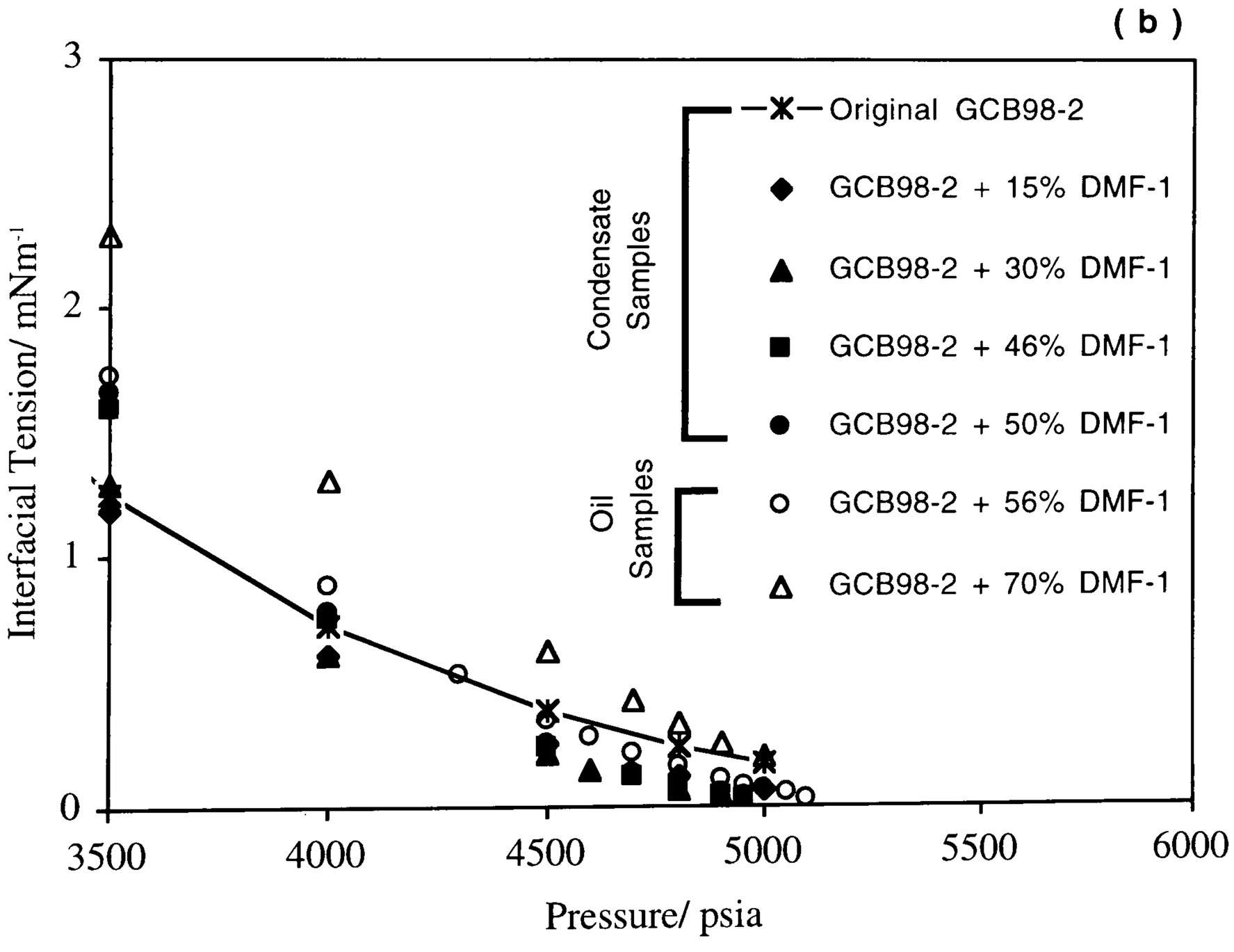

Figure 7.4 - Variation of Interfacial Tension With Pressure of the GCB98-2 Fluid With Various Volumes of DMF-1 Contamination at 100 °C, (**a**) Full Pressure Range, and (**b**) Pressure up to 3500 psia.

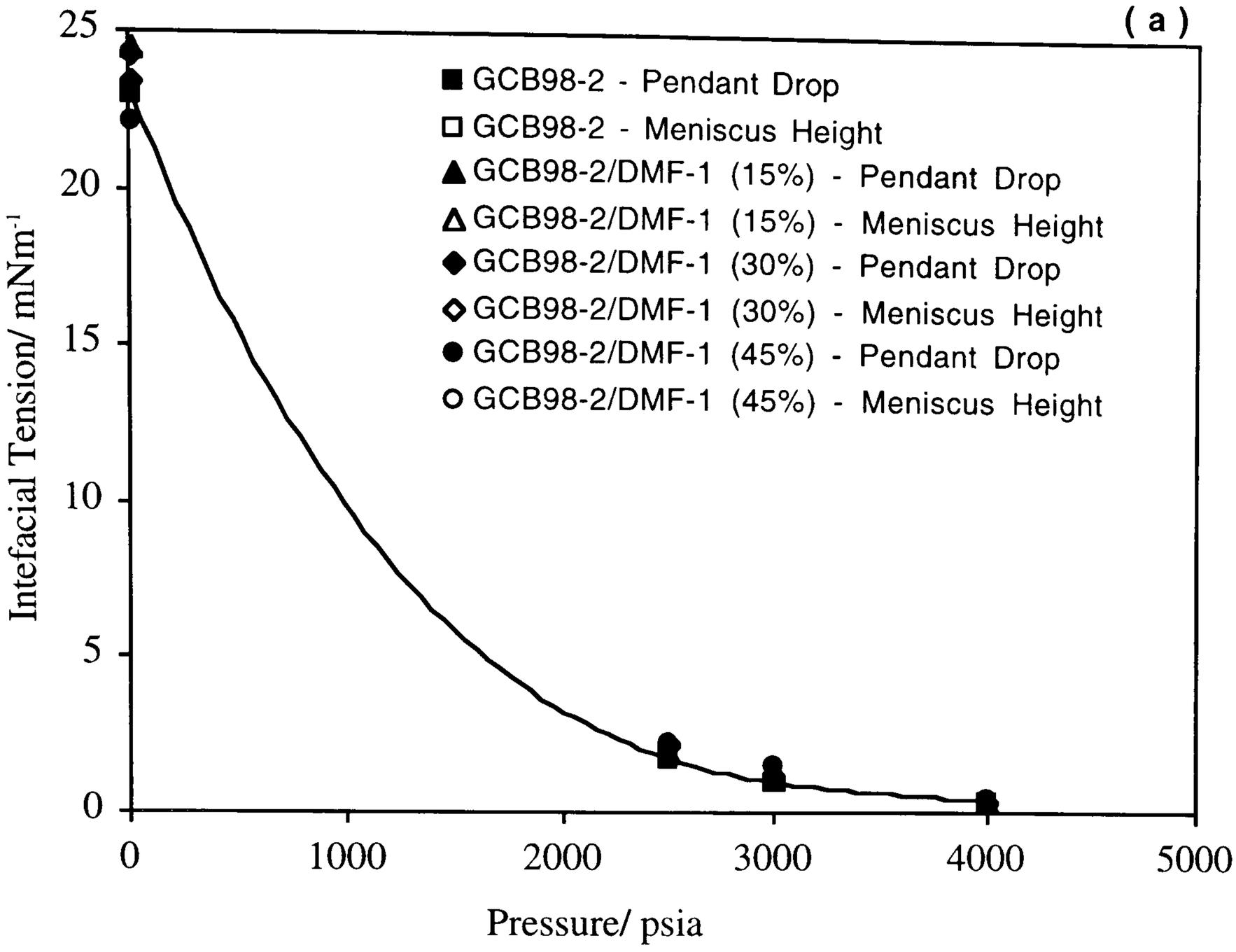

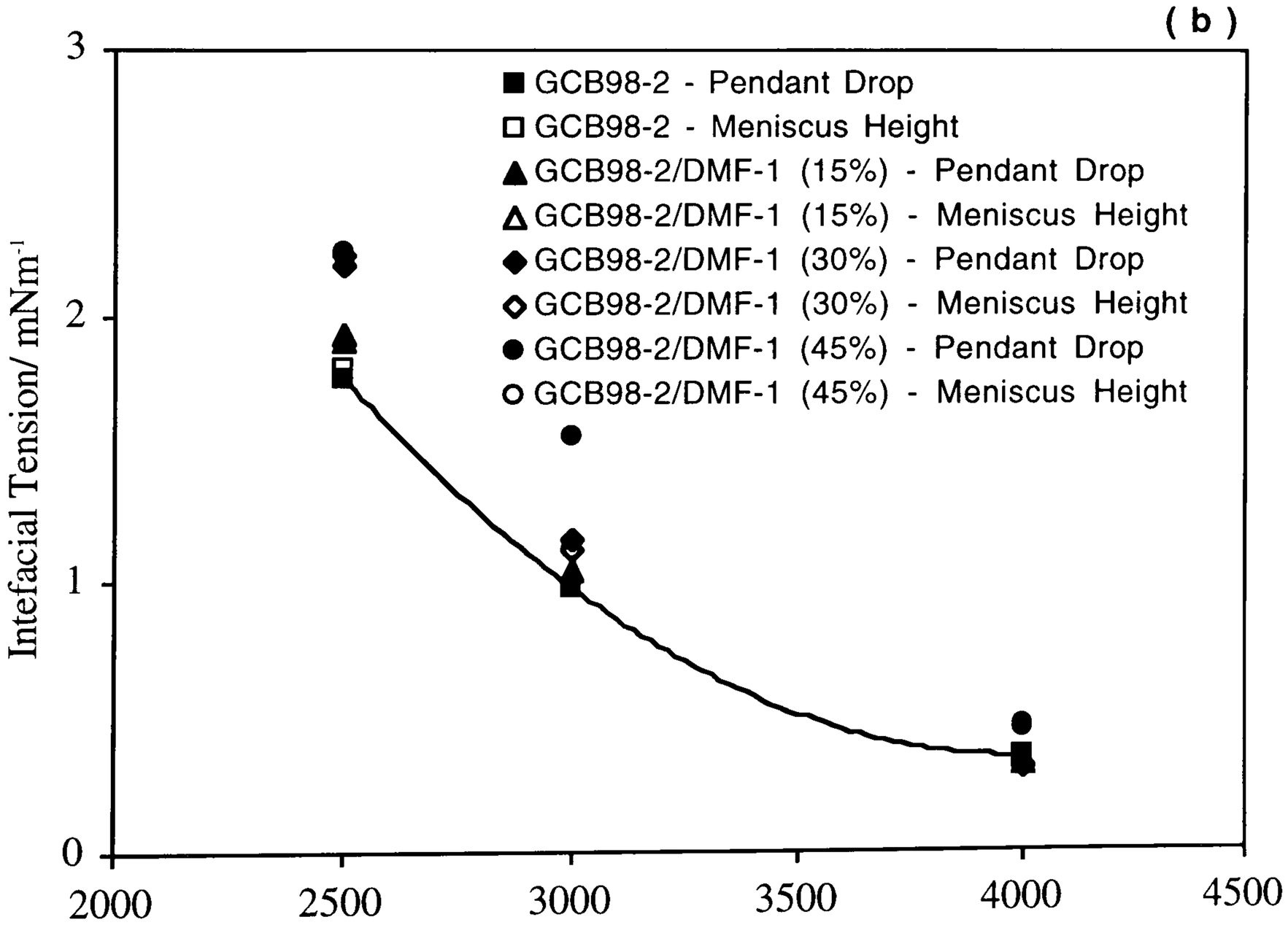

Figure 7.5 - Variation of Interfacial Tension With Pressure of the GCB98-2 Fluid With Various Volumes of DMF-1 Contamination at 37.8 °C, (**a**) Full Pressure Range, and (**b**) Pressure up to 2000 psia.

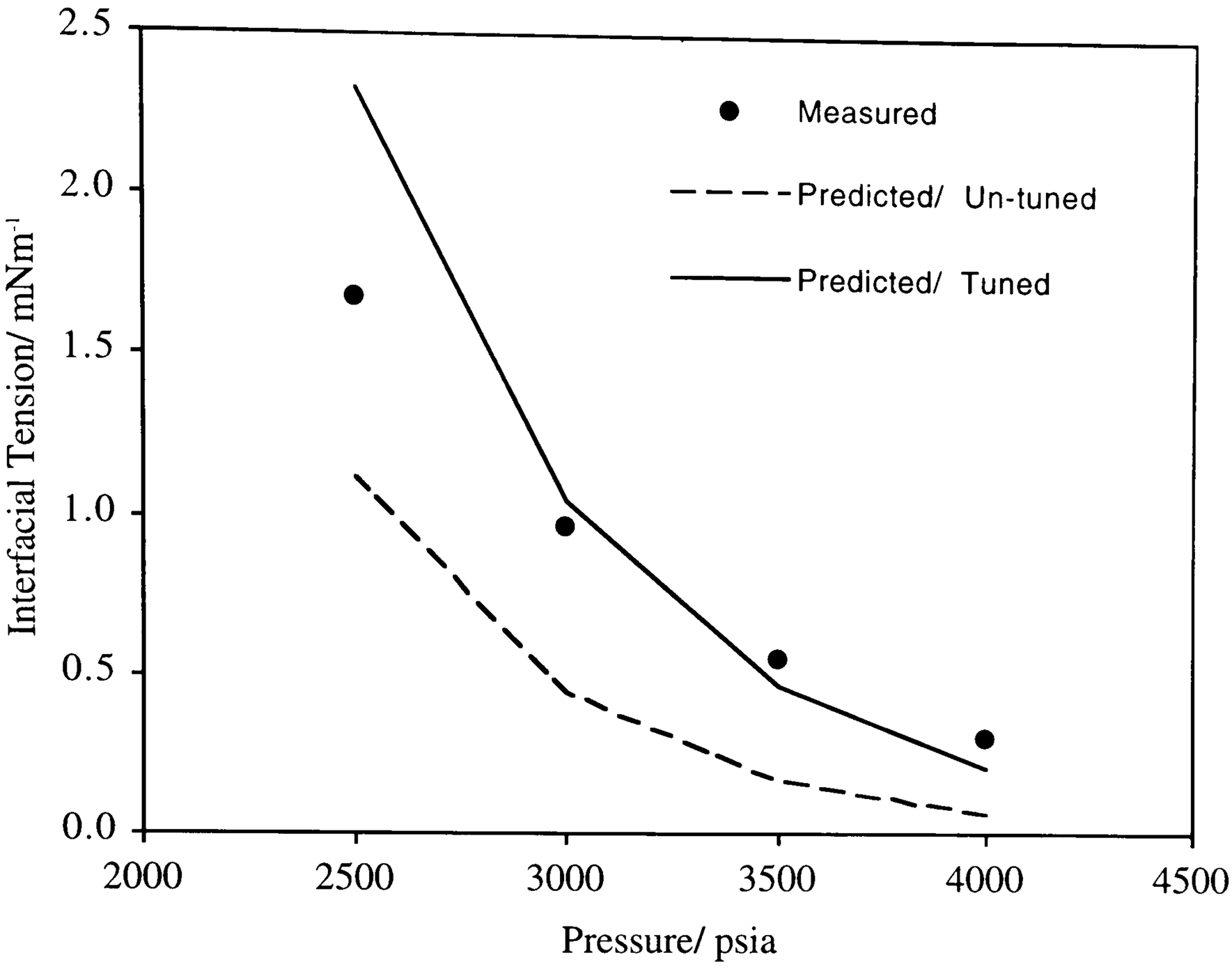

Figure 7.6 - Experimental and Predicted Interfacial Tension of the GCB98-1 Fluid With 5% DMF-3 Contamination at 37.8 °C.

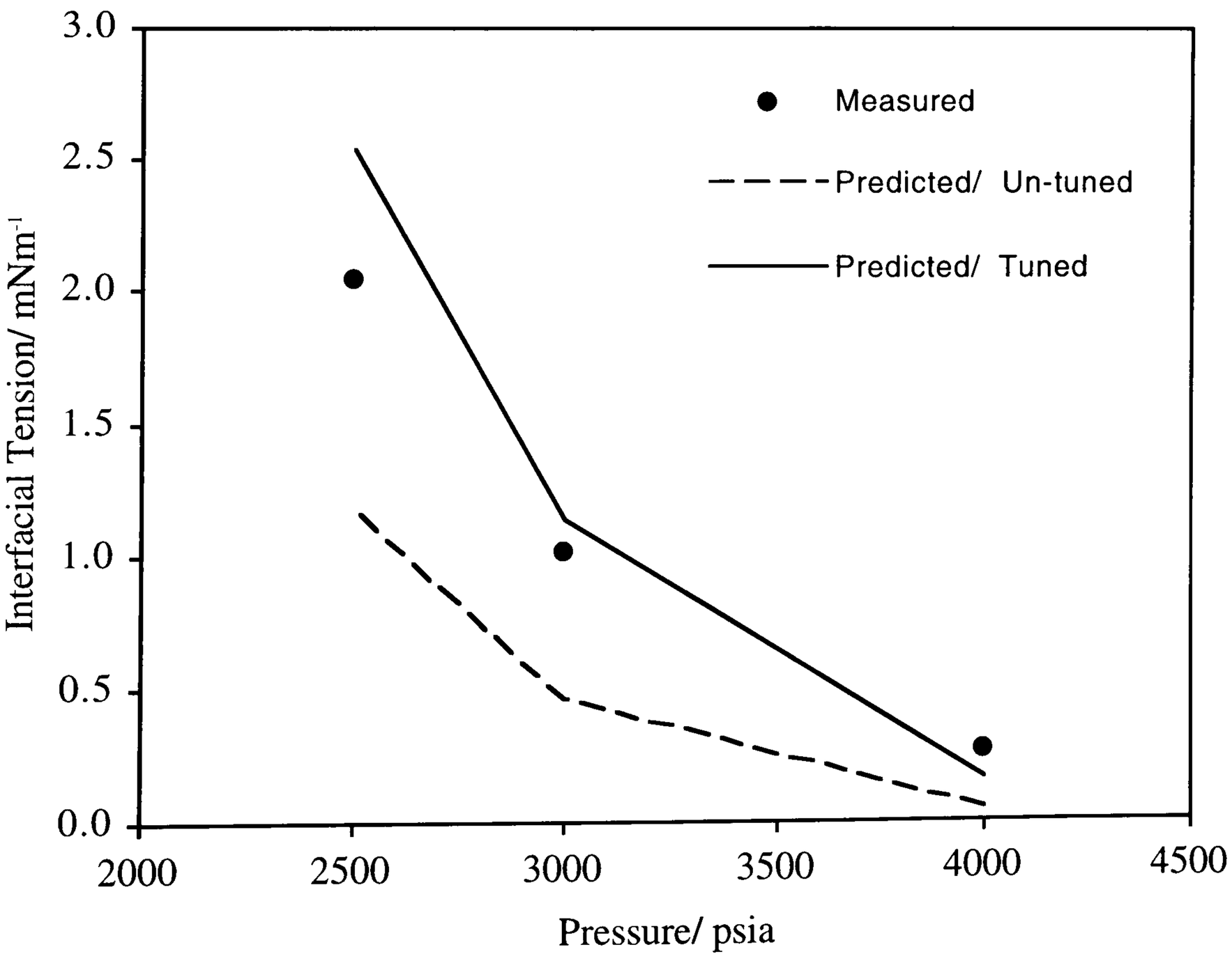

Figure 7.7 - Experimental and Predicted Interfacial Tension of the GCB98-1 Fluid With 15% DMF-3 Contamination at 37.8 °C.

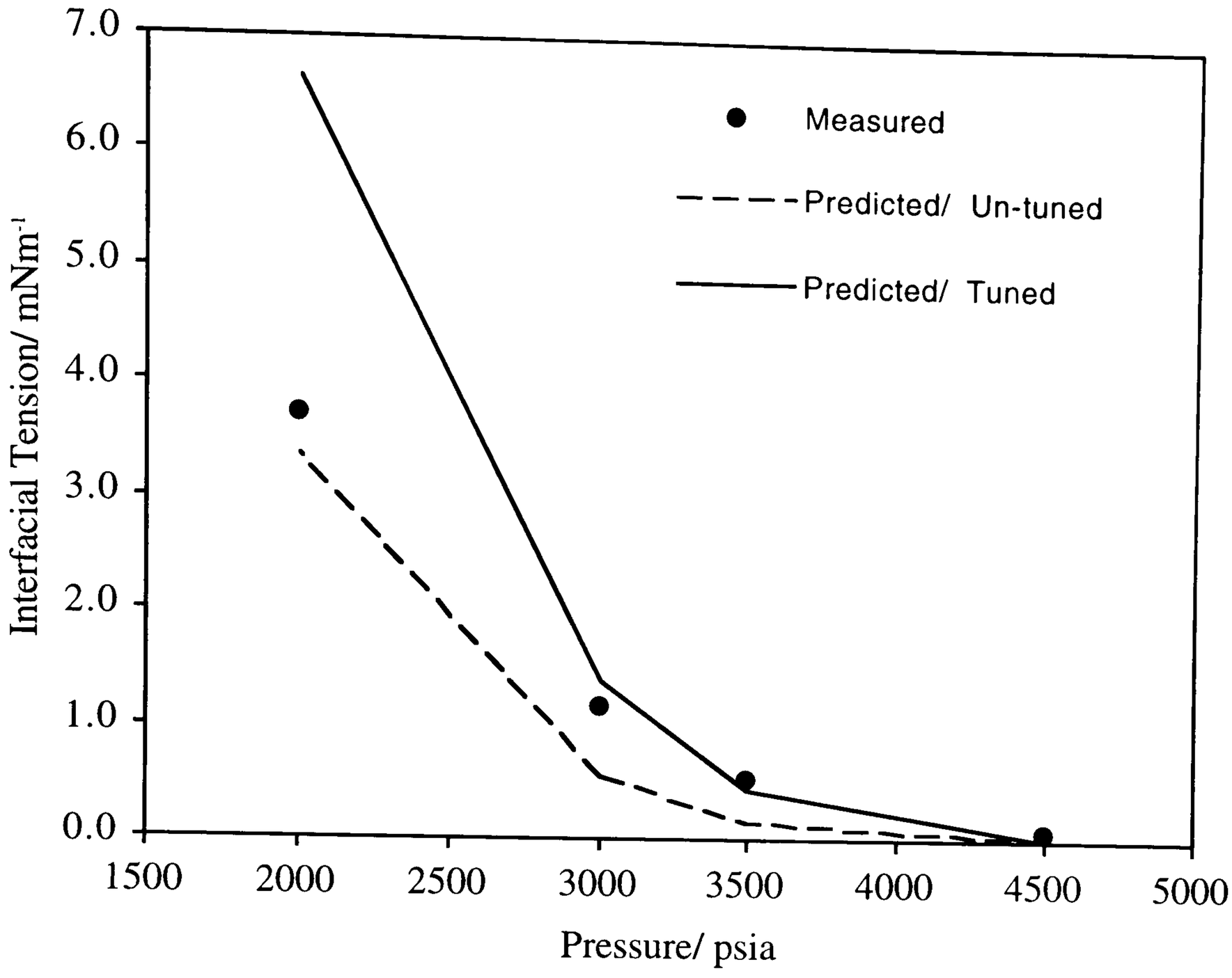

Figure 7.8 - Experimental and Predicted Interfacial Tension of the GCB98-1 Fluid With 30% DMF-3 Contamination at 37.8 °C.

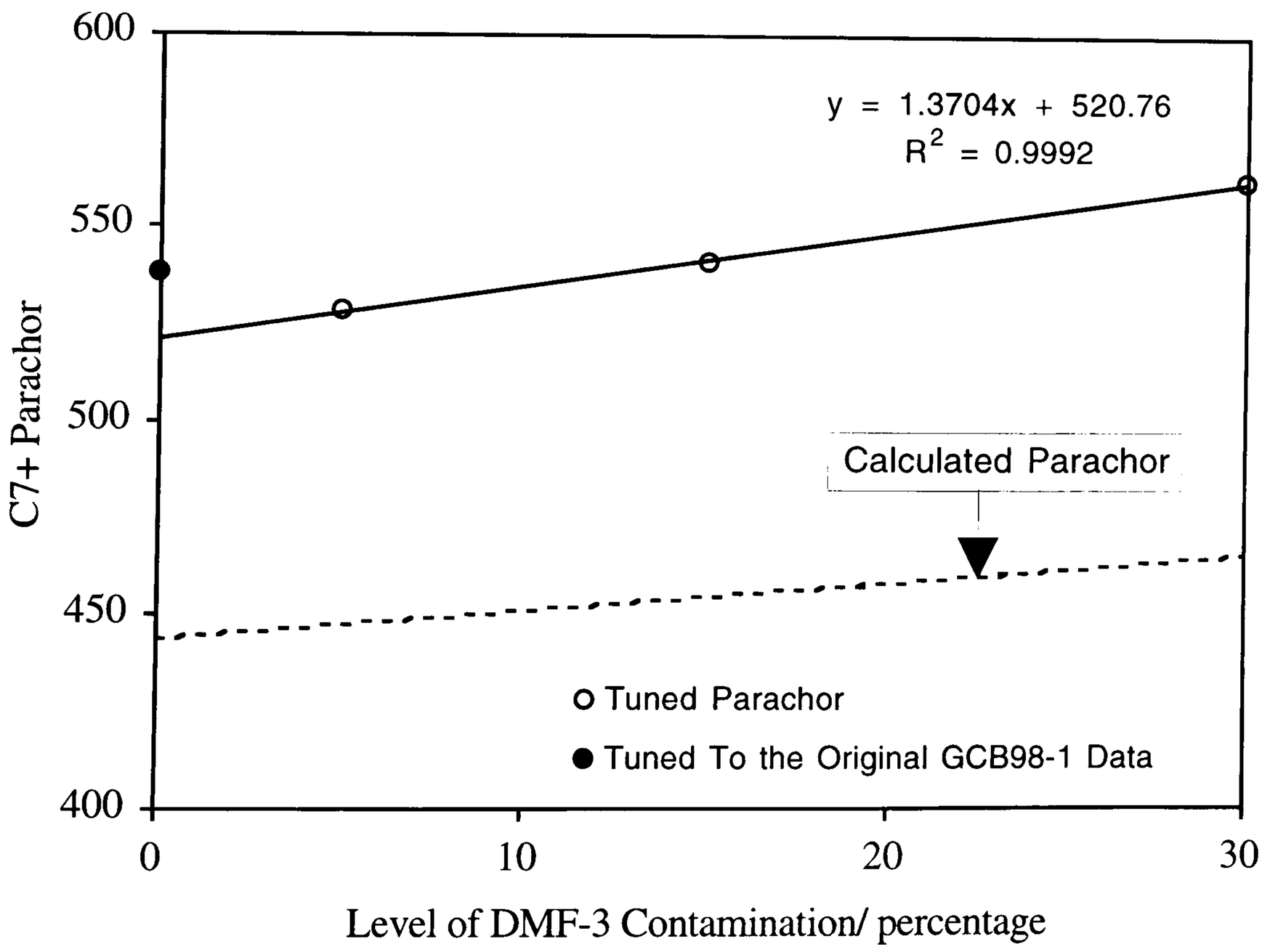

Figure 7.9 - Tuned C7+ Parachor versus % Level of DMF-3 Contamination for the Contaminated GCB98-1 Samples at 37.8 °C.

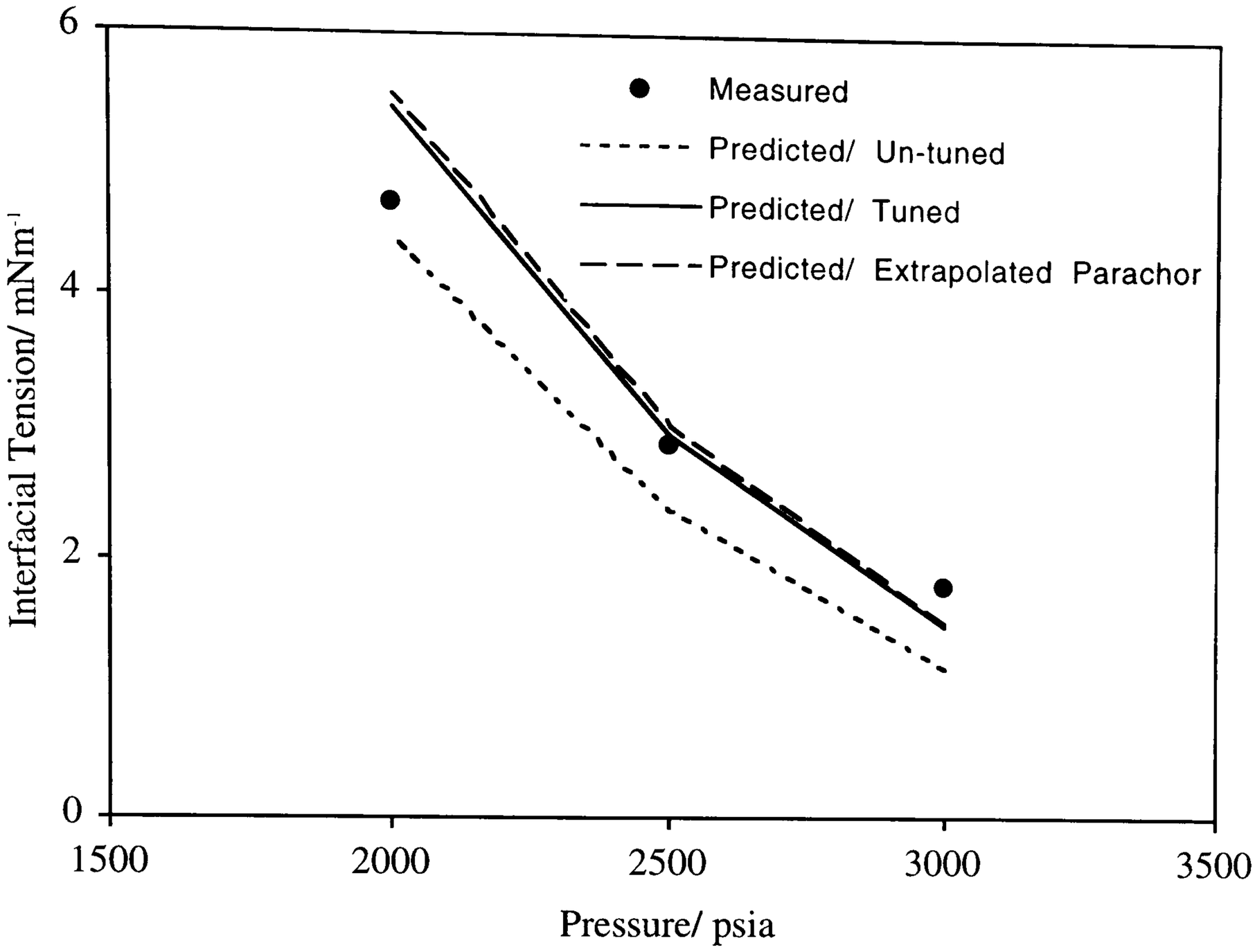

Figure 7.10 - Experimental and Predicted Interfacial Tension of the Original LRA97-1 Fluid at 37.8 °C.

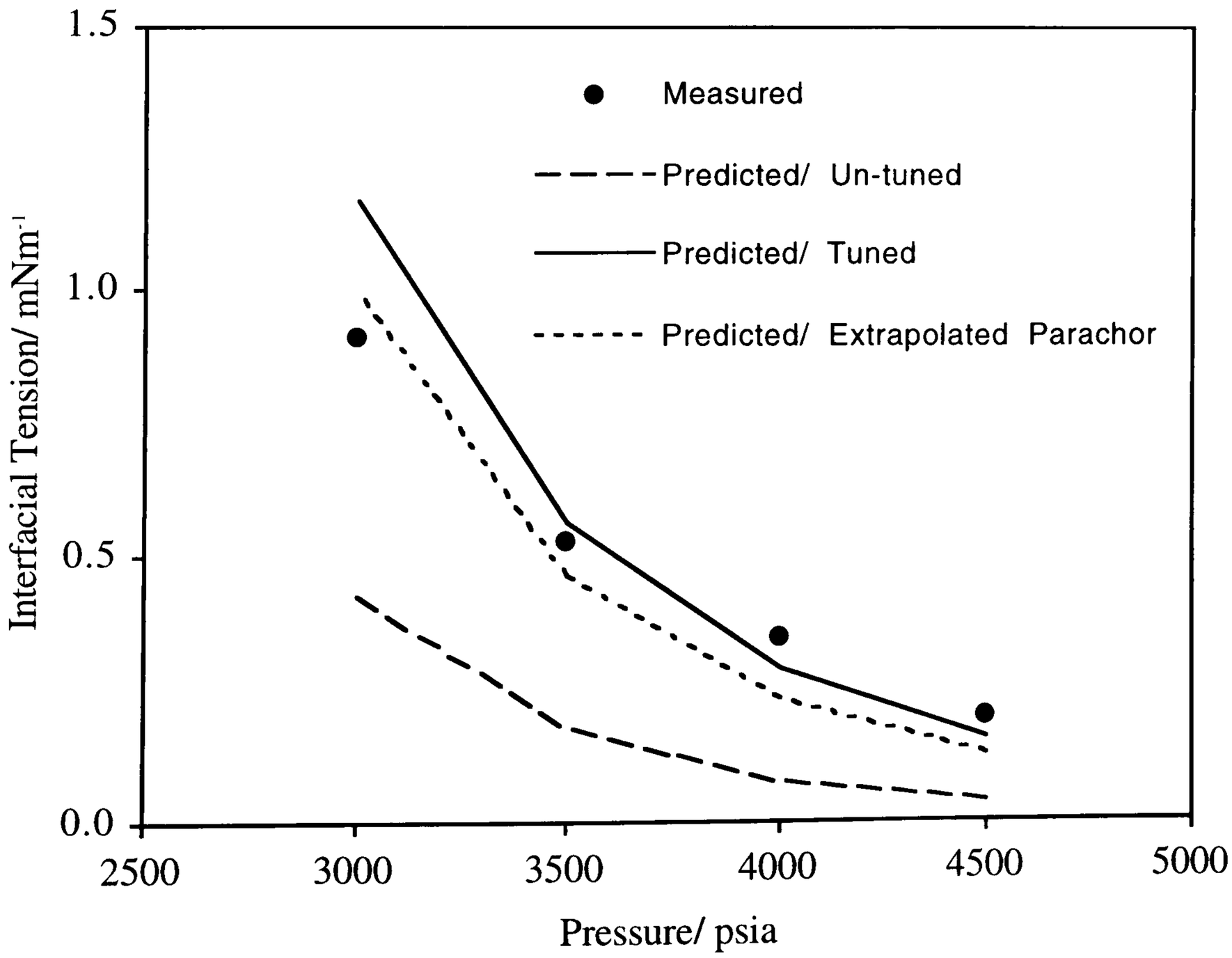

Figure 7.11 - Experimental and Predicted Interfacial Tension of the Original GCB98-1 Fluid at 37.8 °C.

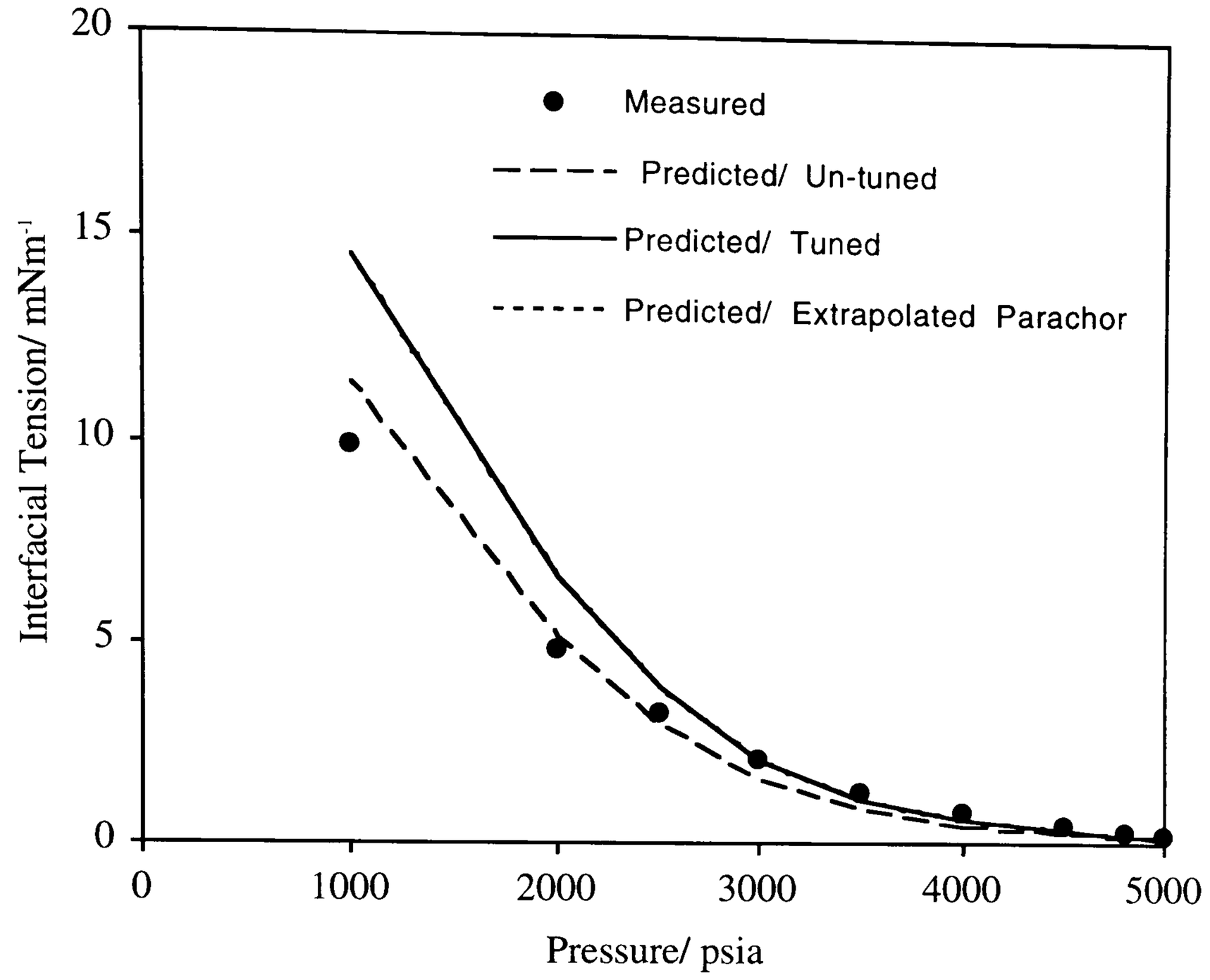

Figure 7.12 - Experimental and Predicted Interfacial Tension of the Original GCB98-2 Fluid at 100 °C (DMF-3 Contamination Study).

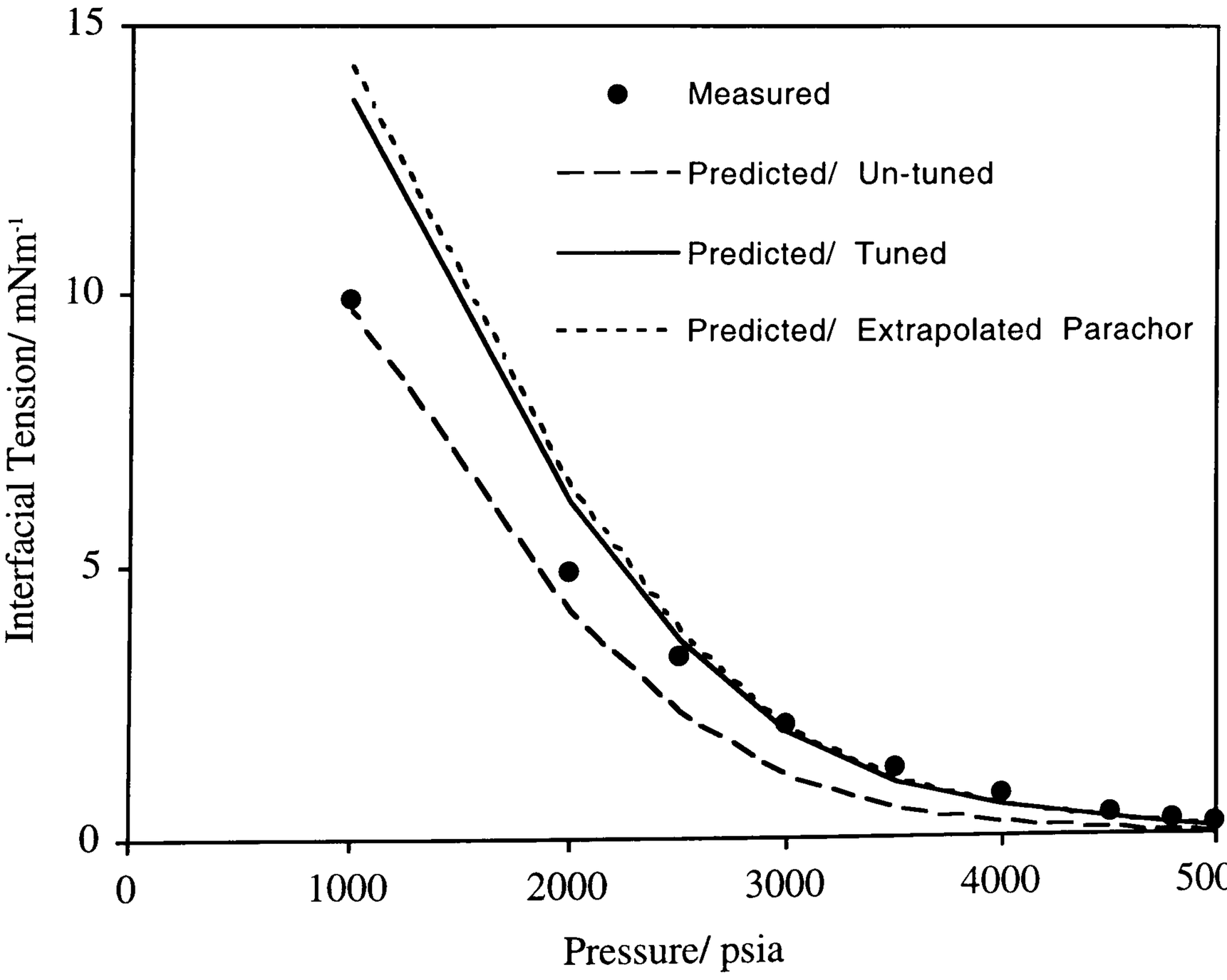

Figure 7.13 - Experimental and Predicted Interfacial Tension of the Original GCB98-2 Fluid at 100 °C (DMF-1 Contamination Study).

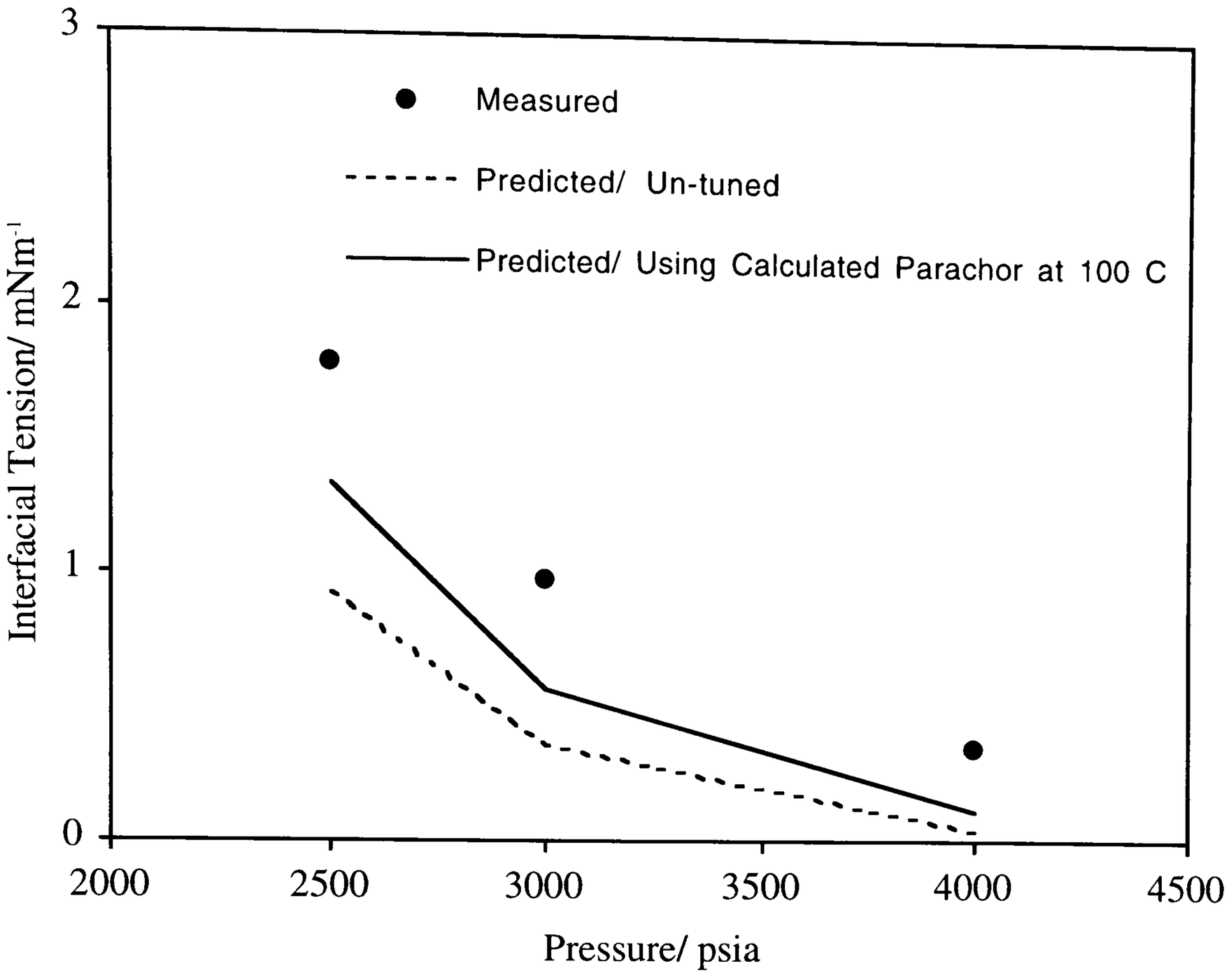

Figure 7.14 - Experimental and Predicted Interfacial Tension (DMF-1 Contamination Study) of the Original GCB98-2 Fluid at 37.8 °C.

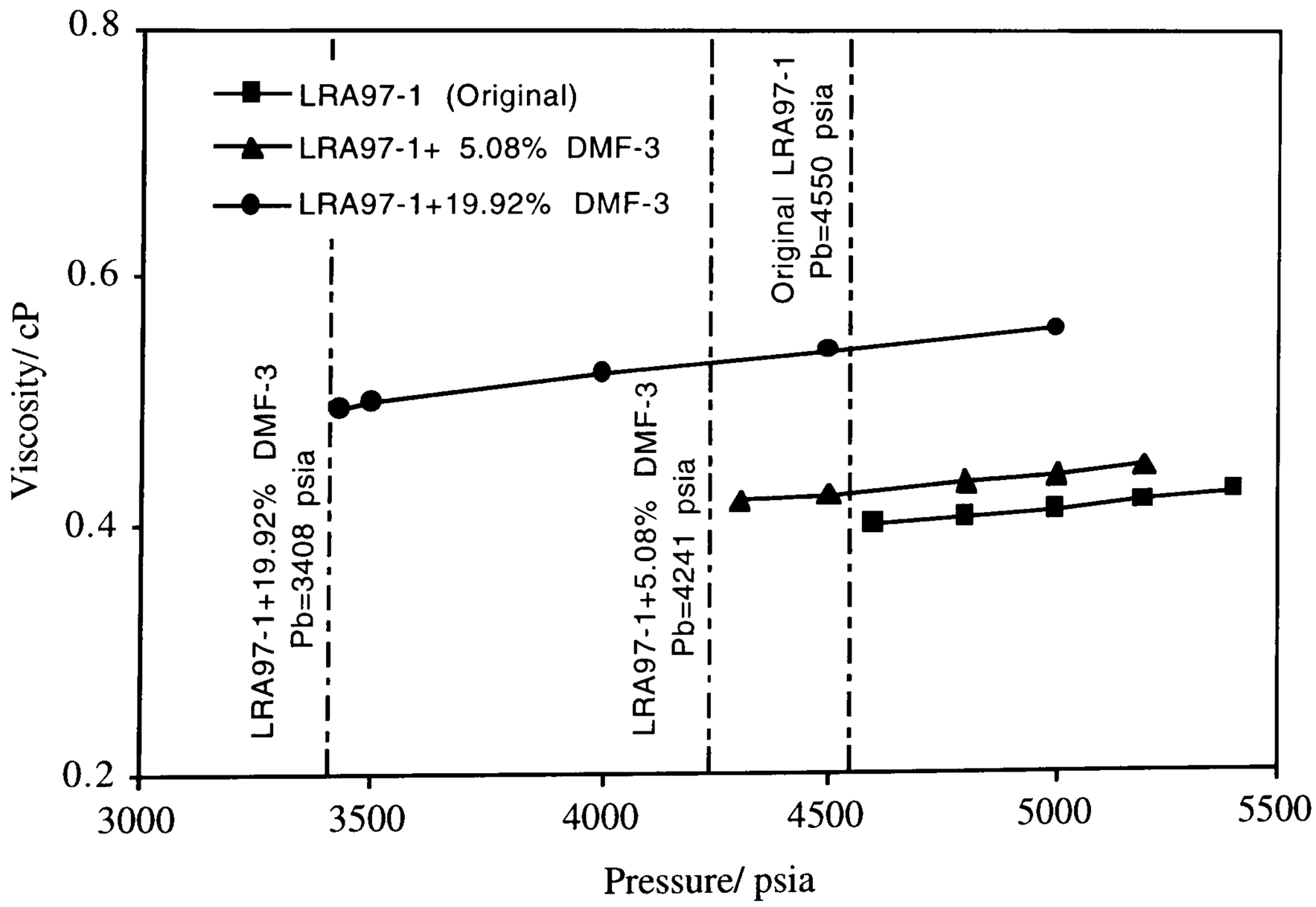

Figure 7.15 - Variation in Single Phase Viscosity With Pressure for the Volatile Oil LRA97-1 With Various Volumes of DMF-3 Contamination at 37.8 °C.

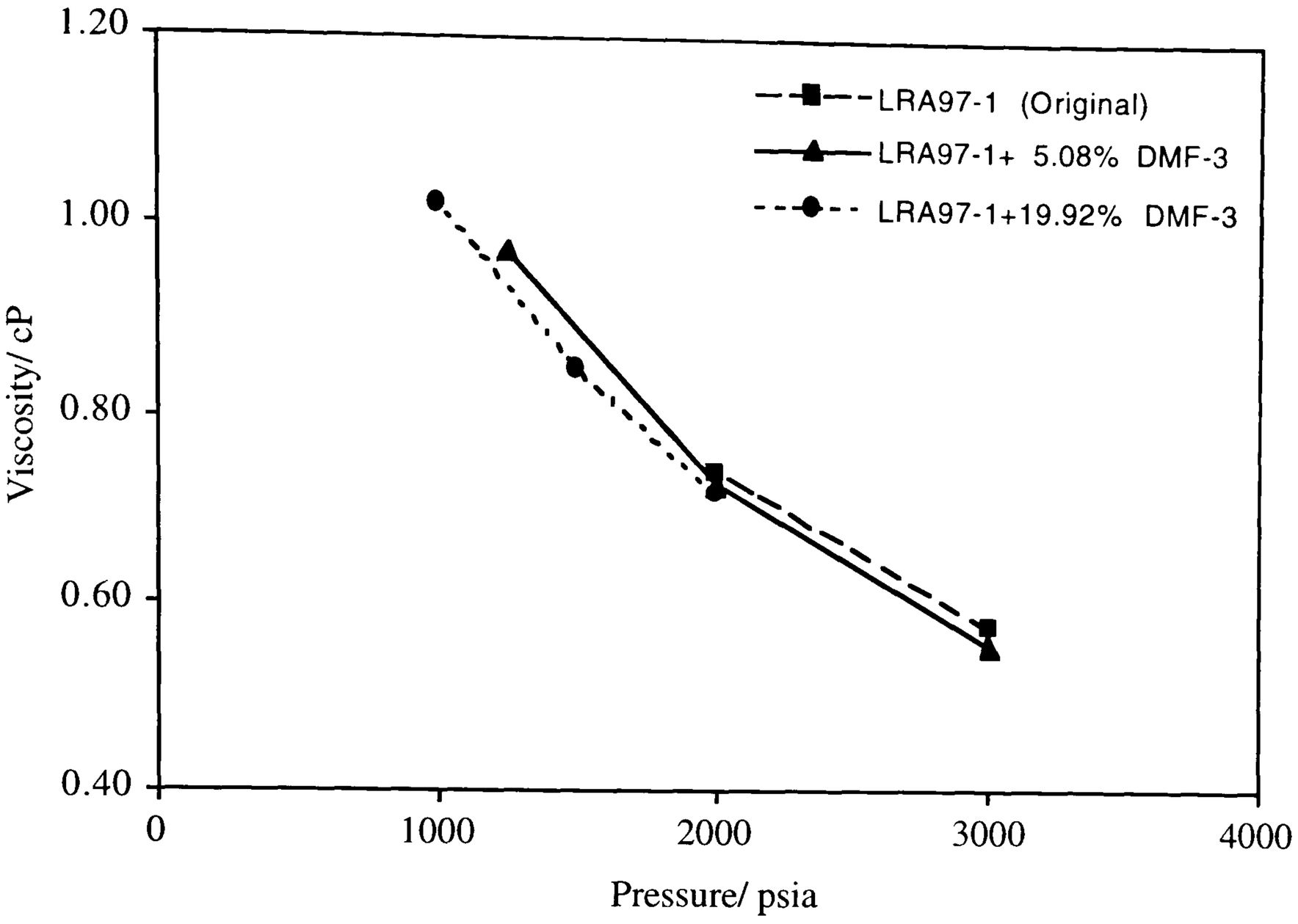

Figure 7.16 - Variation in Saturated Liquid Viscosity with Pressure for the Volatile Oil LRA97-1 with Various Volumes of DMF-3 Contamination at 37.8 °C.

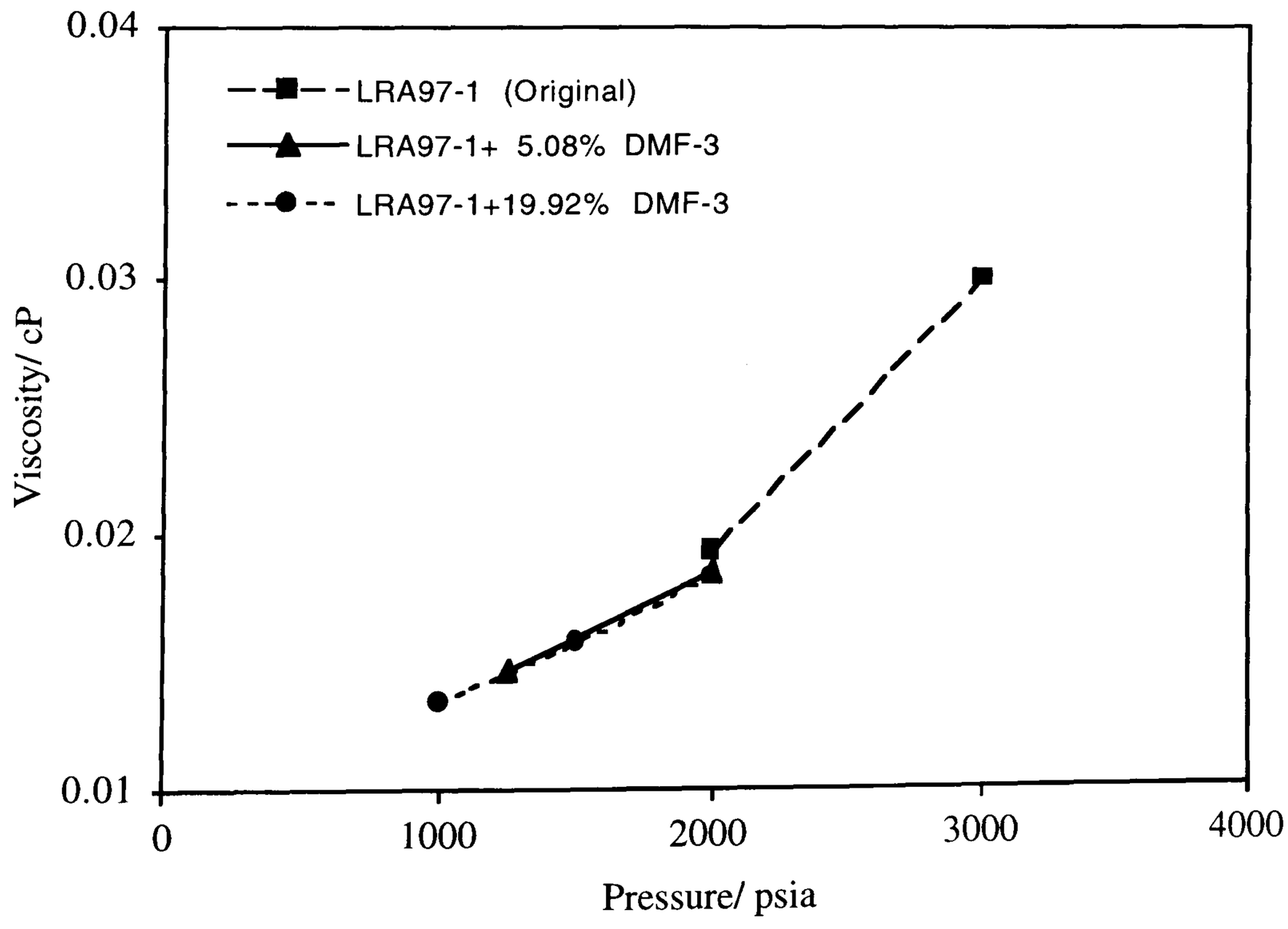

Figure 7.17 - Variation in Saturated Vapour Viscosity with Pressure for the Volatile Oil LRA97-1 with Various Volumes of DMF-3 Contamination at 37.8 °C.

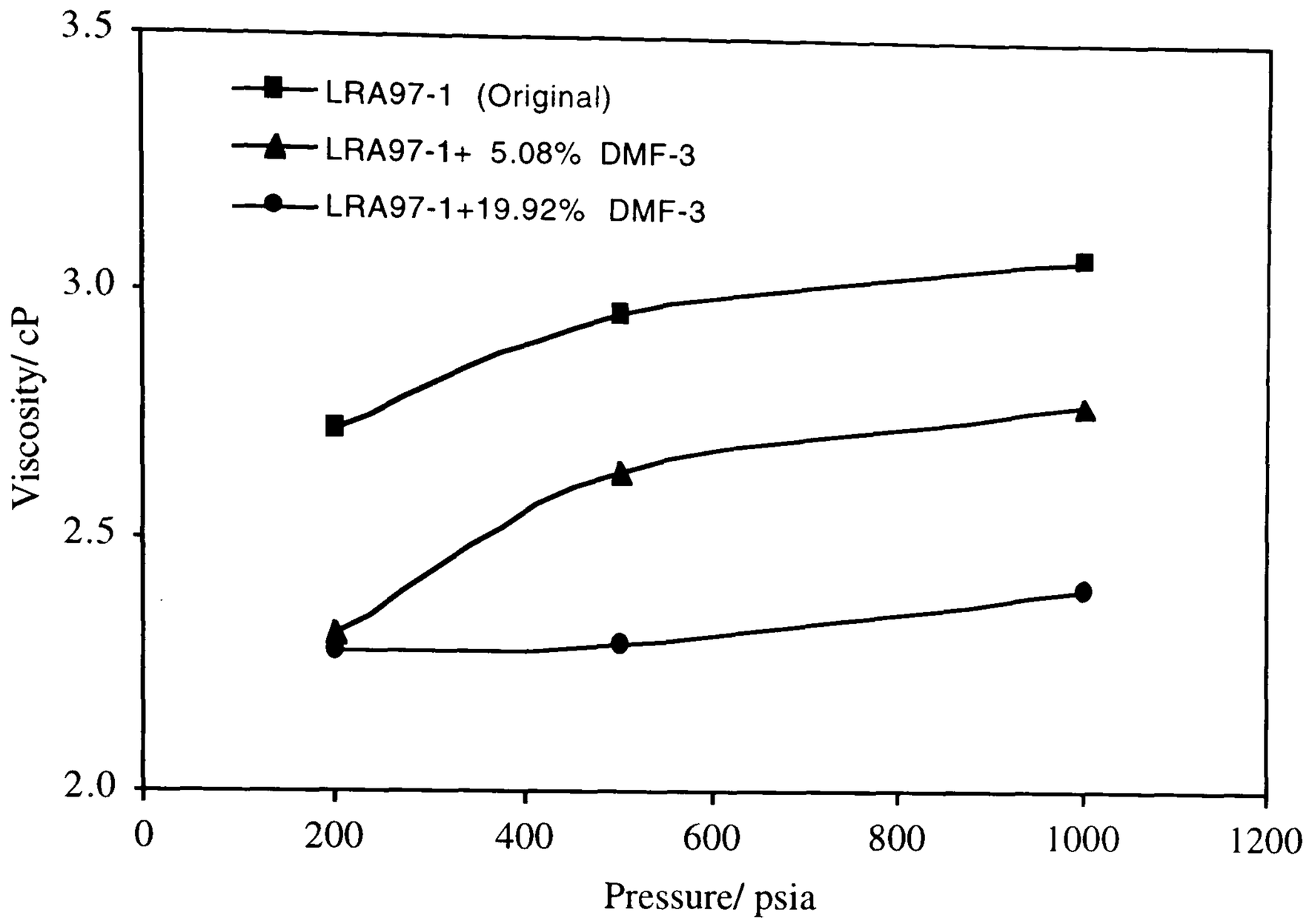

Figure 7.18 - Variation in Stabilised Liquid Viscosity with Pressure for the Volatile Oil LRA97-1 with Various Volumes of DMF-3 Contamination at 37.8 °C.

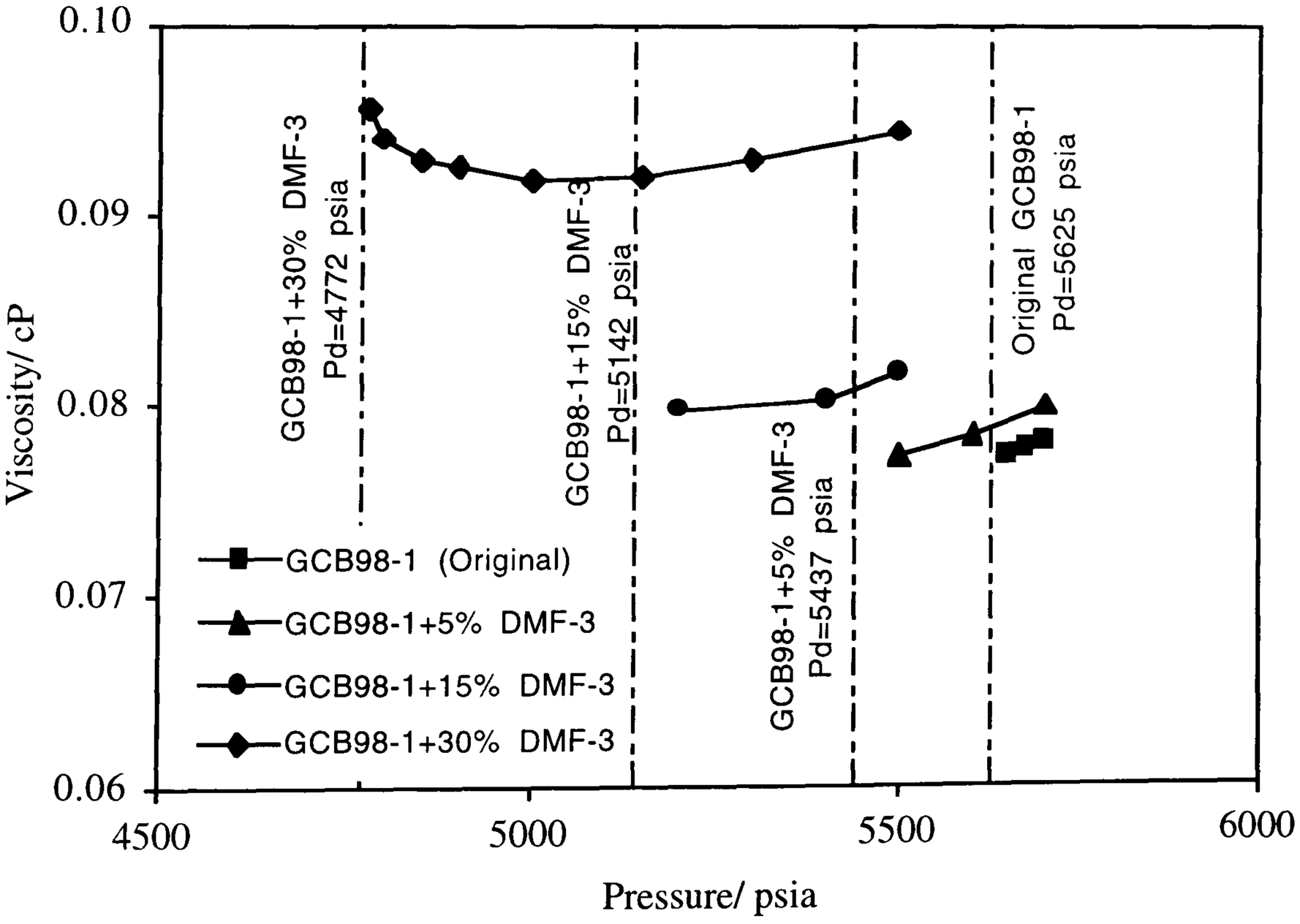

Figure 7.19 - Variation in Single Phase Viscosity With Pressure for the Gas-Condensate GCB98-1 With Various Volumes of DMF-3 Contamination at 37.8 °C.

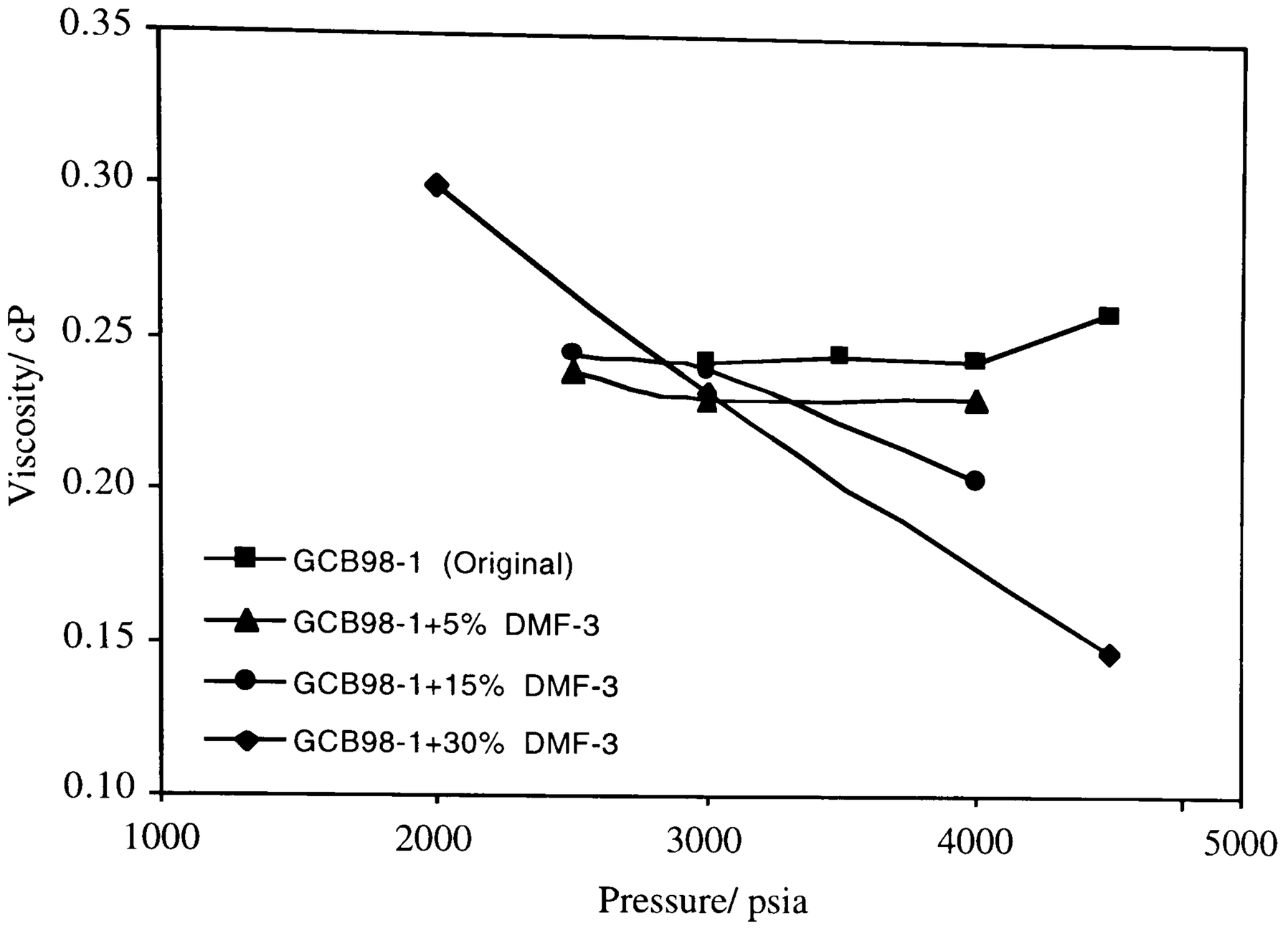

Figure 7.20 - Variation in Saturated Liquid Viscosity with Pressure for the Gas-Condensate GCB98-1 with Various Volumes of DMF-3 Contamination at 37.8 °C.

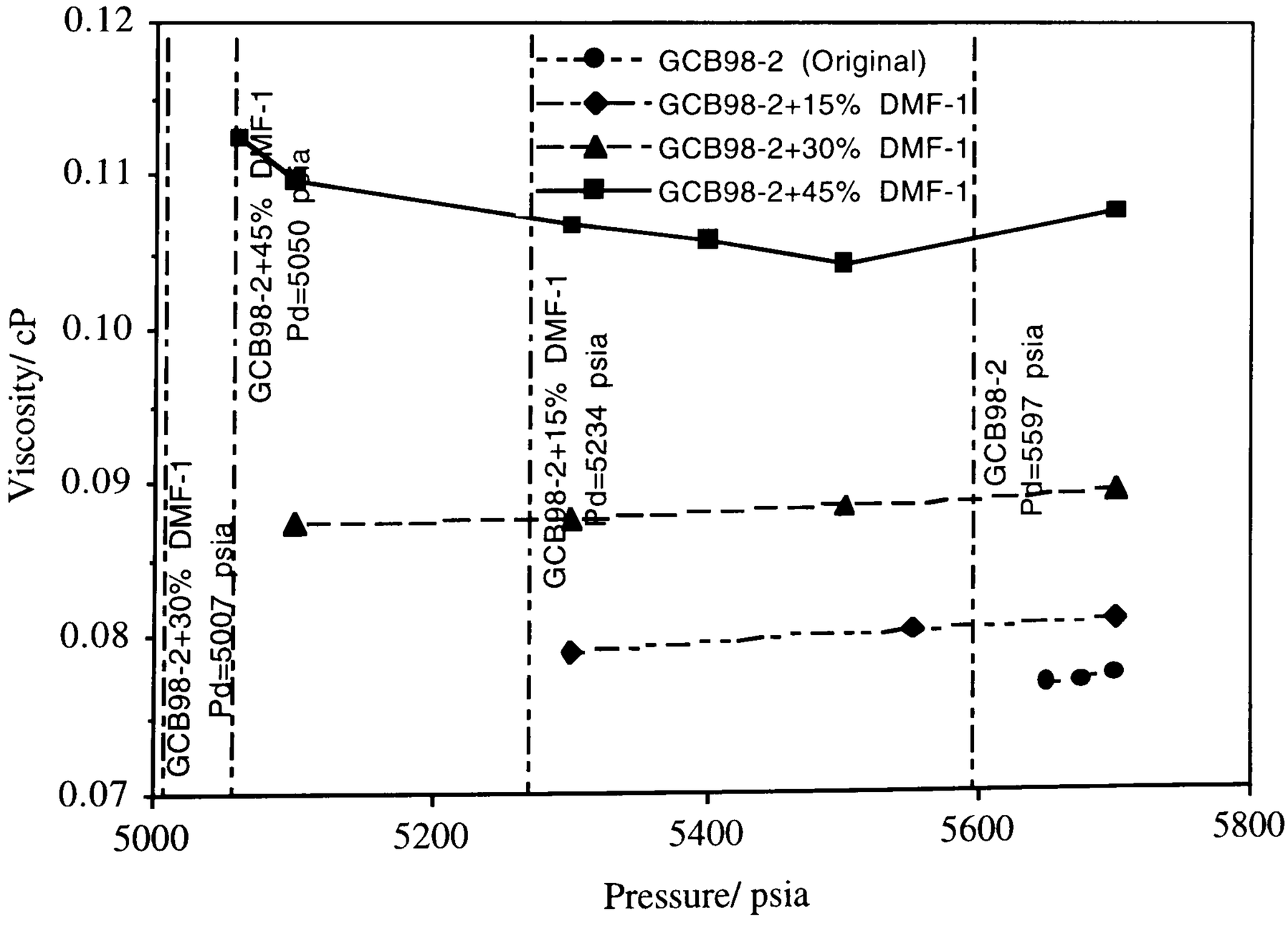

Figure 7.21 - Variation in Single Phase Viscosity with Pressure for the Gas-Condensate GCB98-2 with Various Volumes of DMF-1 Contamination at 37.8 °C.

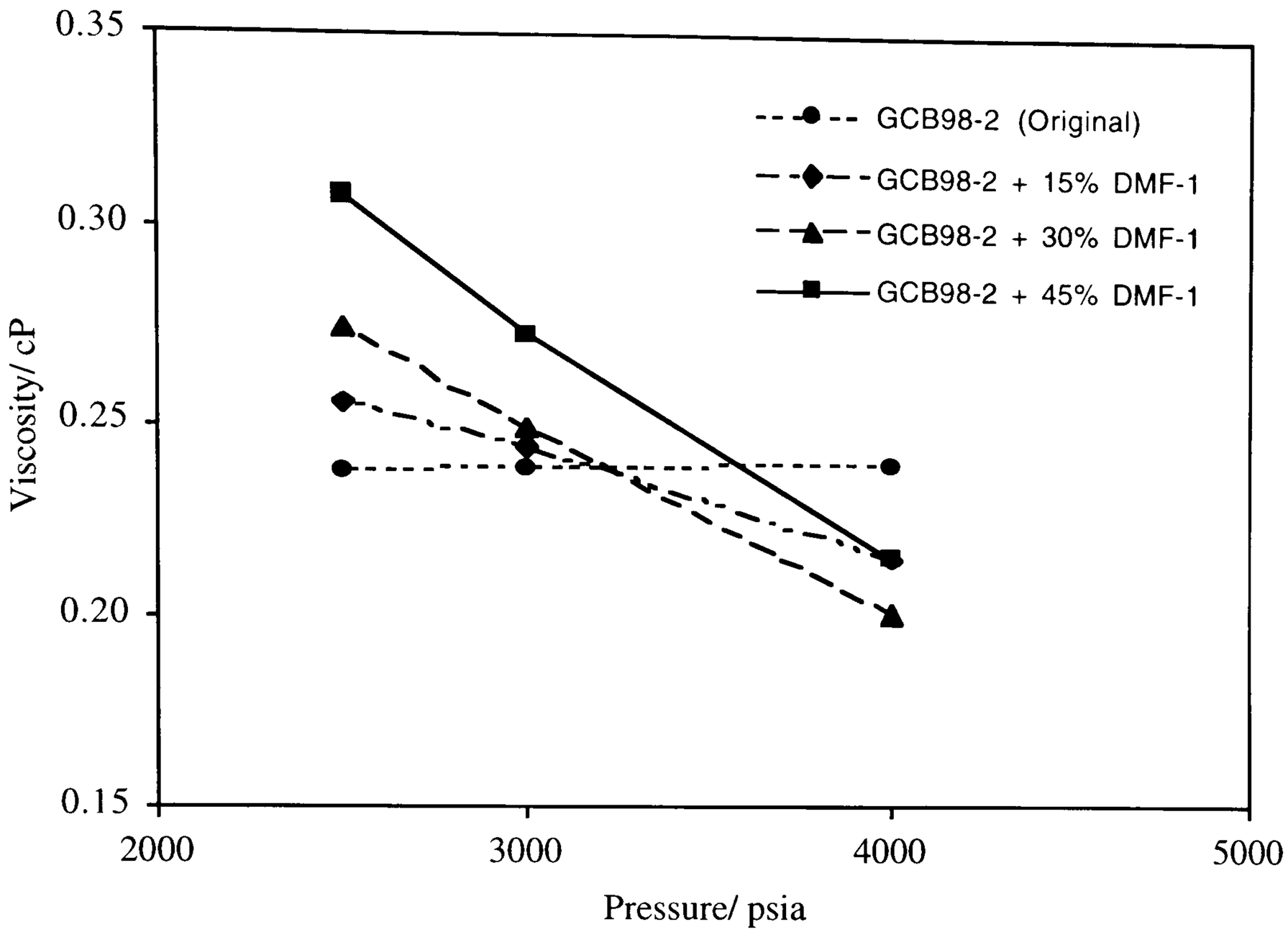

Figure 7.22 - Variation in Saturated Liquid Viscosity with Pressure for the Gas-Condensate GCB98-2 with Various Volumes of DMF-1 Contamination at 37.8 °C.

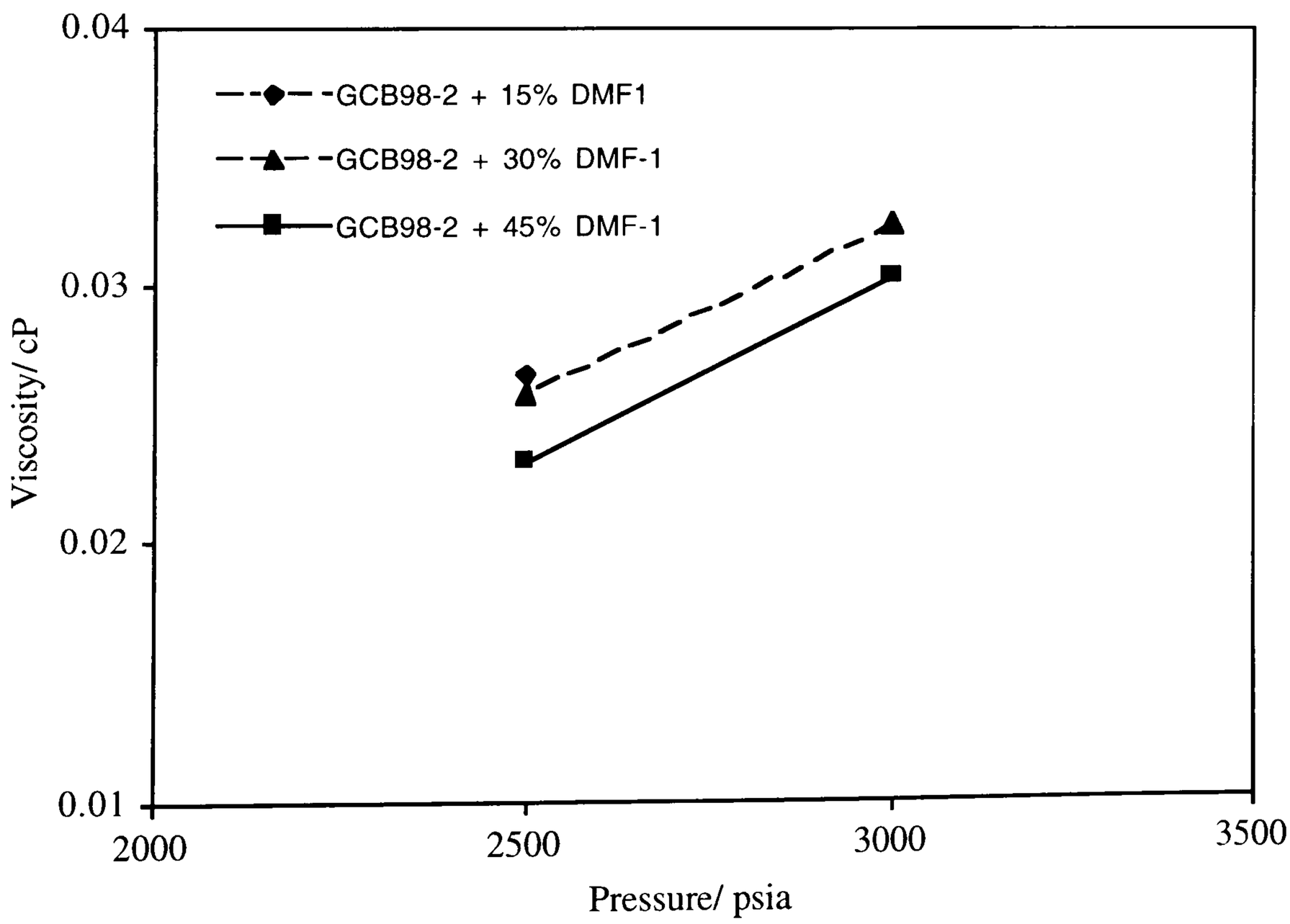

Figure 7.23 - Variation in Saturated Vapour Viscosity with Pressure for the Gas-Condensate GCB98-2 with Various Volumes of DMF-1 Contamination at 37.8 °C.

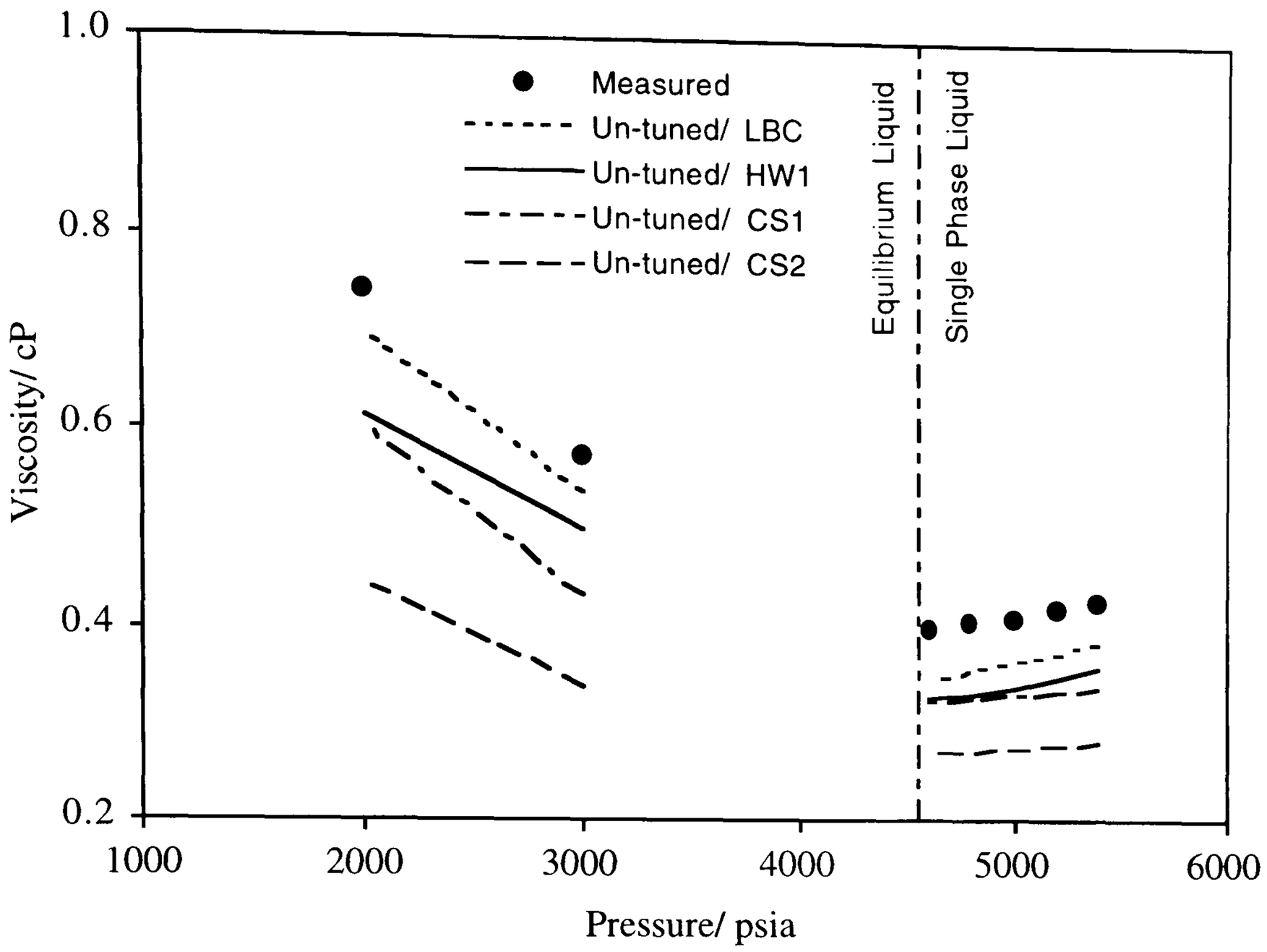

Figure 7.24 - Experimental and Predicted Viscosities Versus Pressure of the Original Volatile Oil LRA97-1 at 37.8 °C, Without Adjusting C7+ Properties.

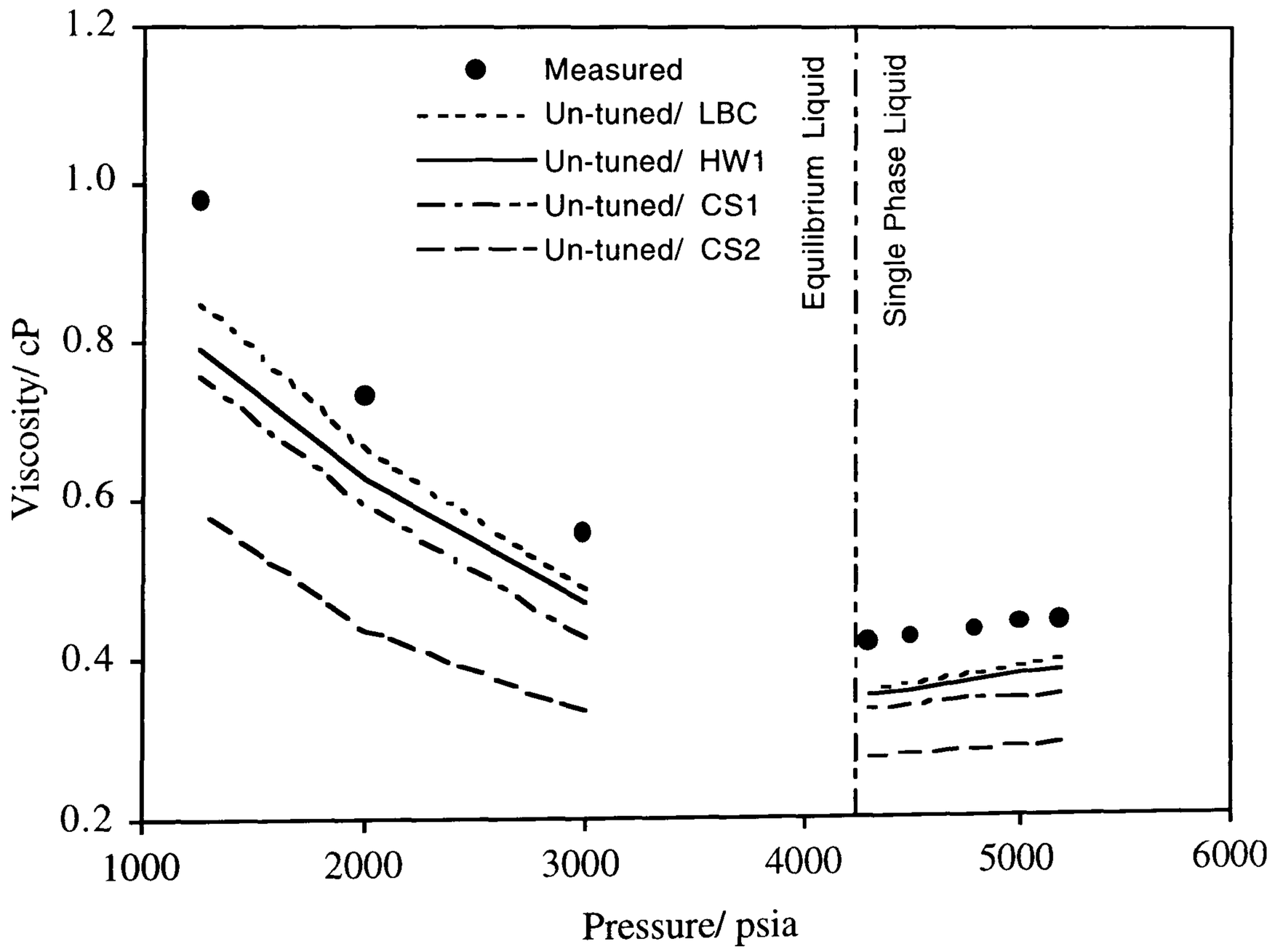

Figure 7.25 - Experimental and Predicted Viscosities Versus Pressure of the Volatile Oil LRA97-1 With 5.08% of DMF-3 at 37.8 °C, Without Adjusting C7+ Properties.

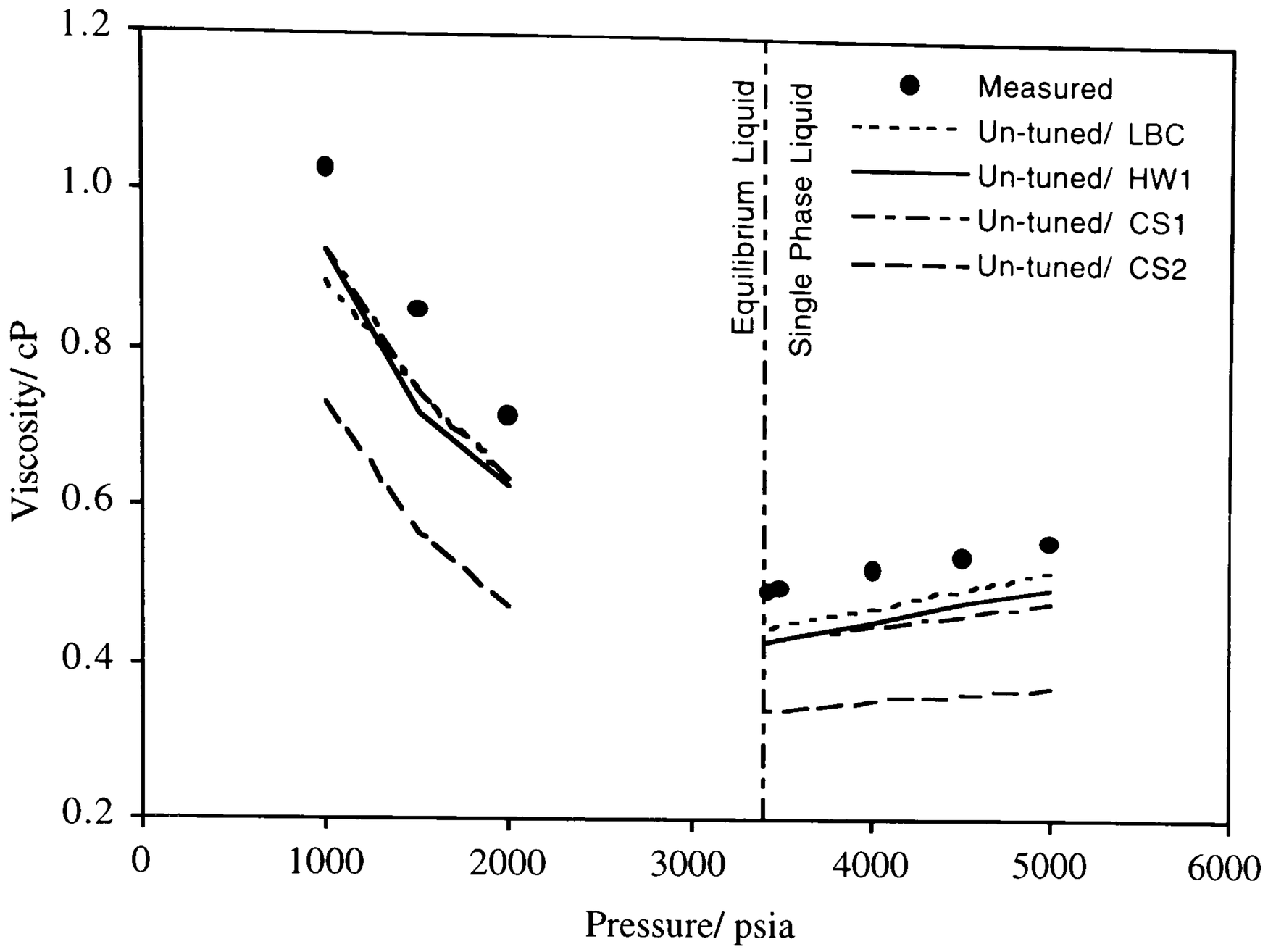

Figure 7.26 - Experimental and Predicted Viscosities Versus Pressure of the Volatile Oil LRA97-1 With 19.92% of DMF-3 at 37.8 °C, Without Adjusting C7+ Properties.

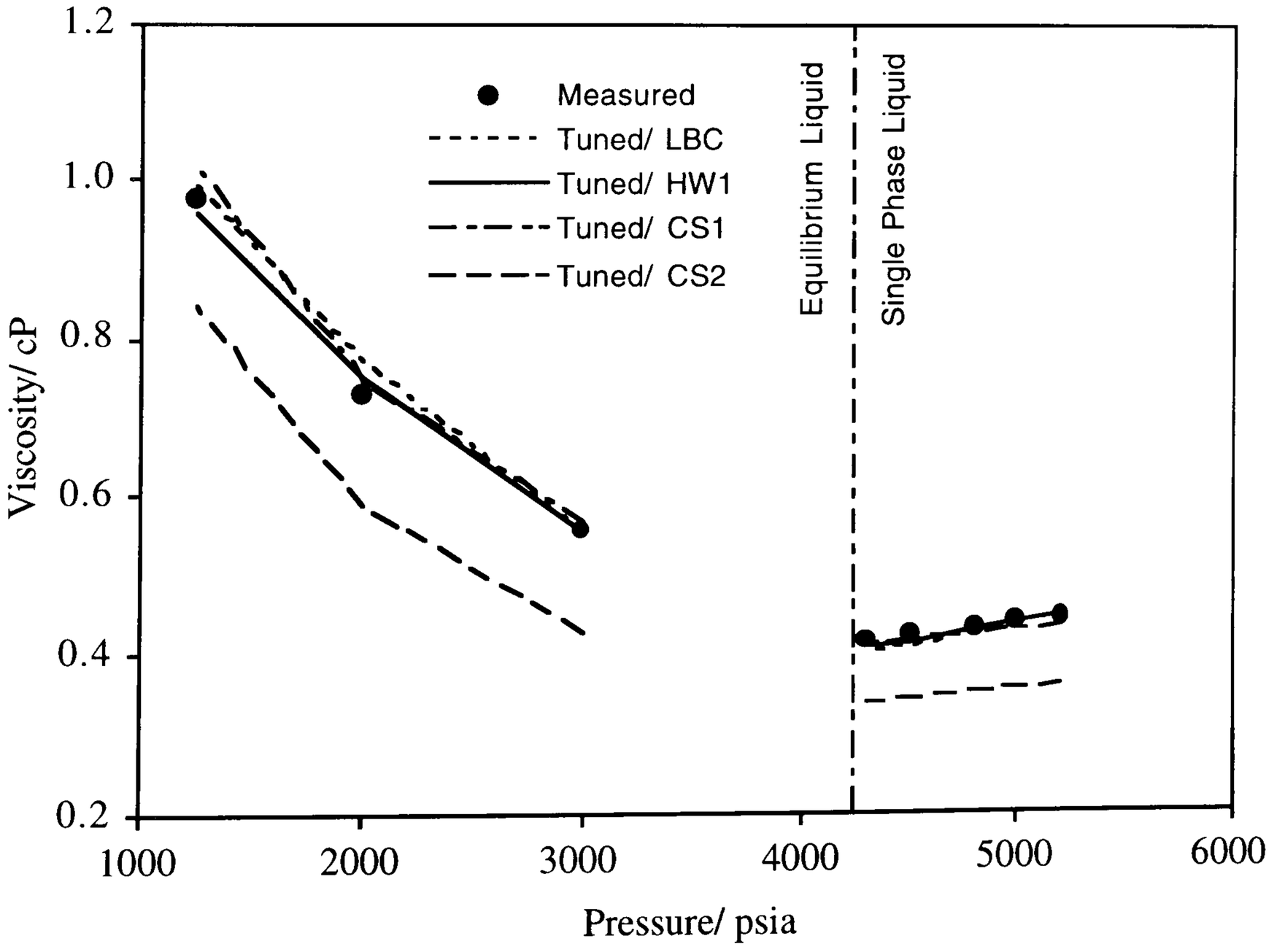

Figure 7.27 - Experimental and Predicted Viscosities Versus Pressure of the Volatile Oil LRA97-1 With 5.08% of DMF-3 at 37.8 °C, With Adjusted C7+ Properties.

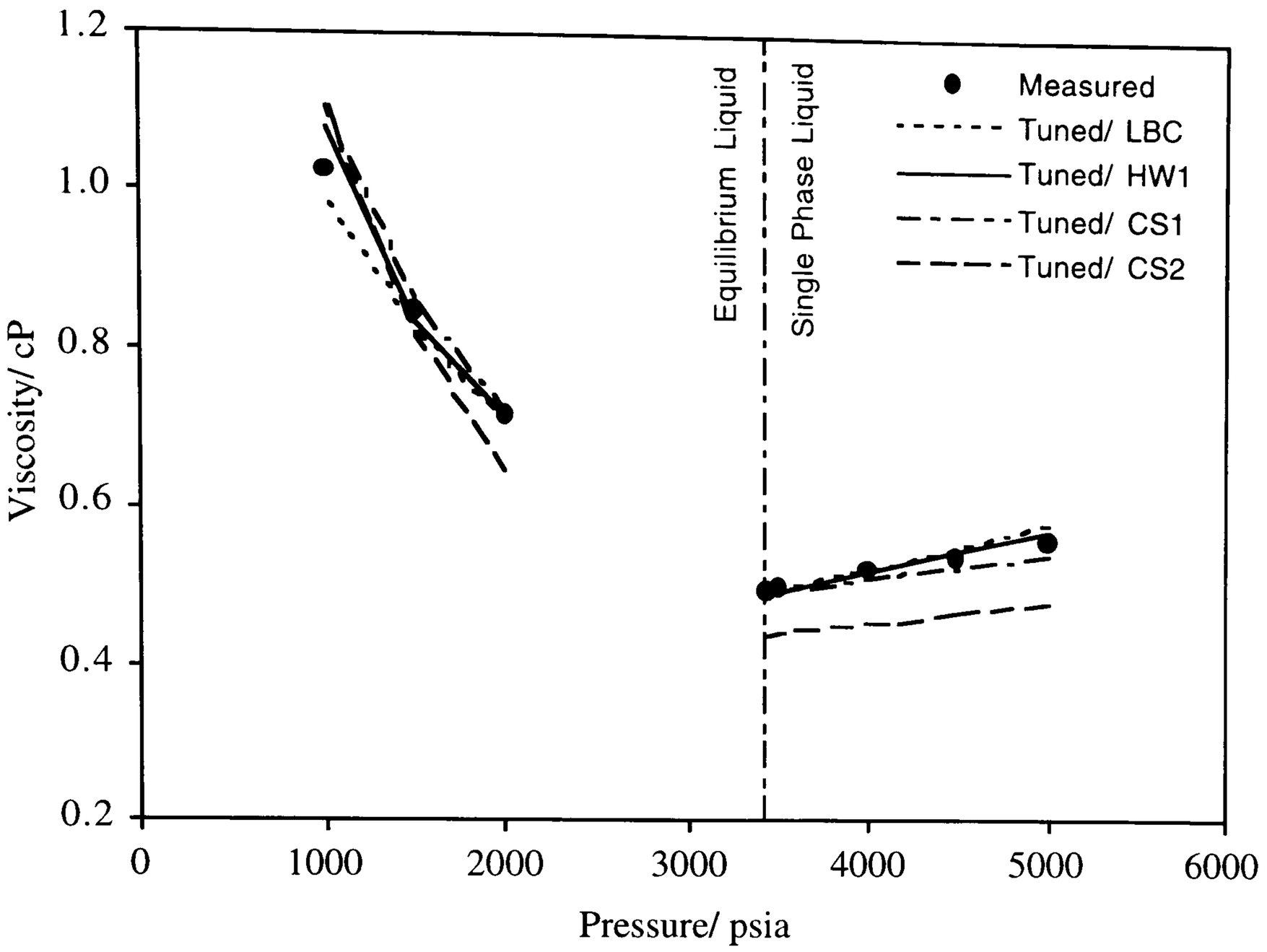

Figure 7.28 - Experimental and Predicted Viscosities Versus Pressure of the Volatile Oil LRA97-1 With 19.92% of DMF-3 at 37.8 °C, With Adjusted C7+ Properties.

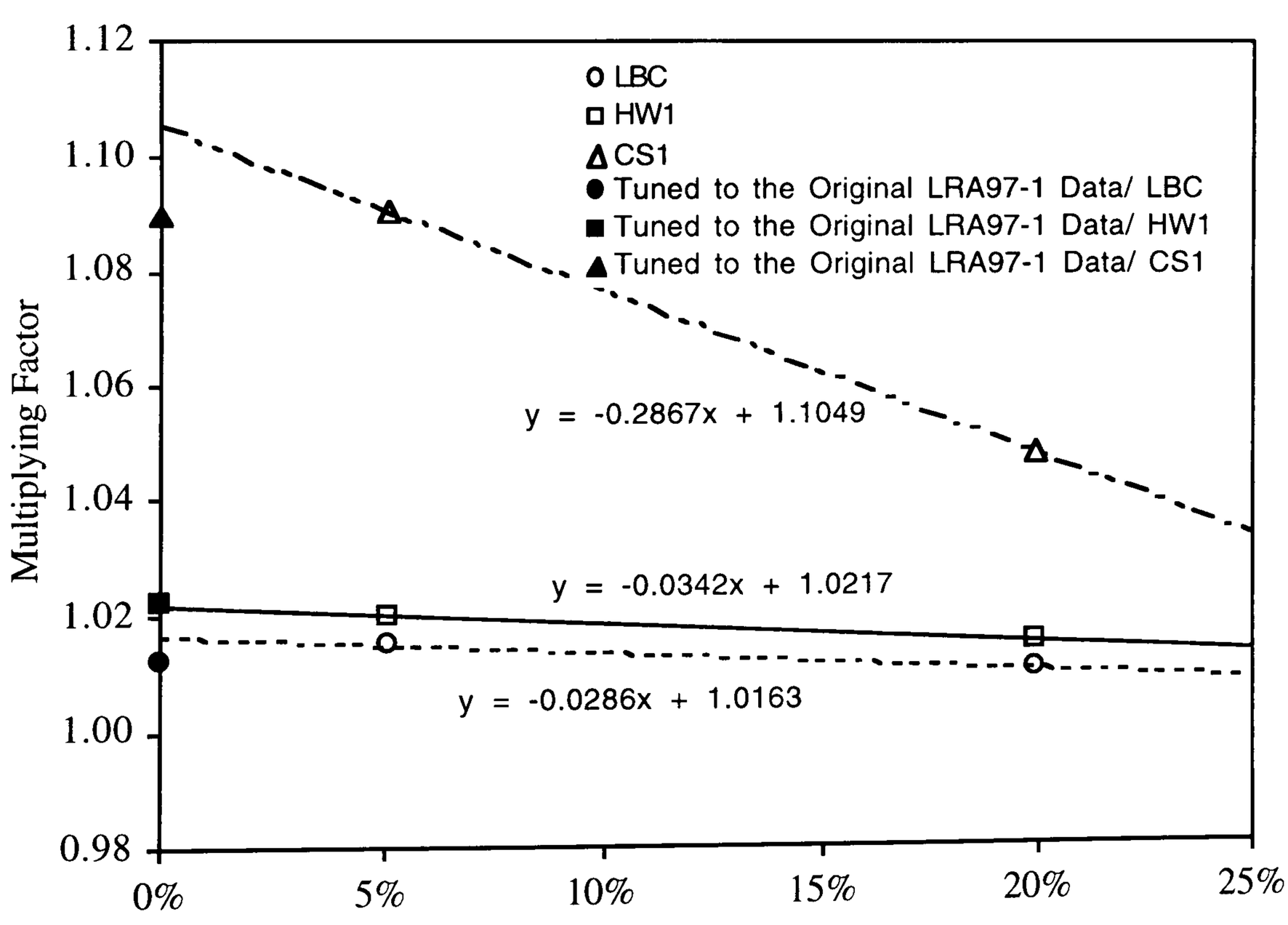

Figure 7.29 - Multiplying Factors for the Adjusted C7+ Properties of LRA97-1 Samples Versus % Level of DMF-3 Contamination.

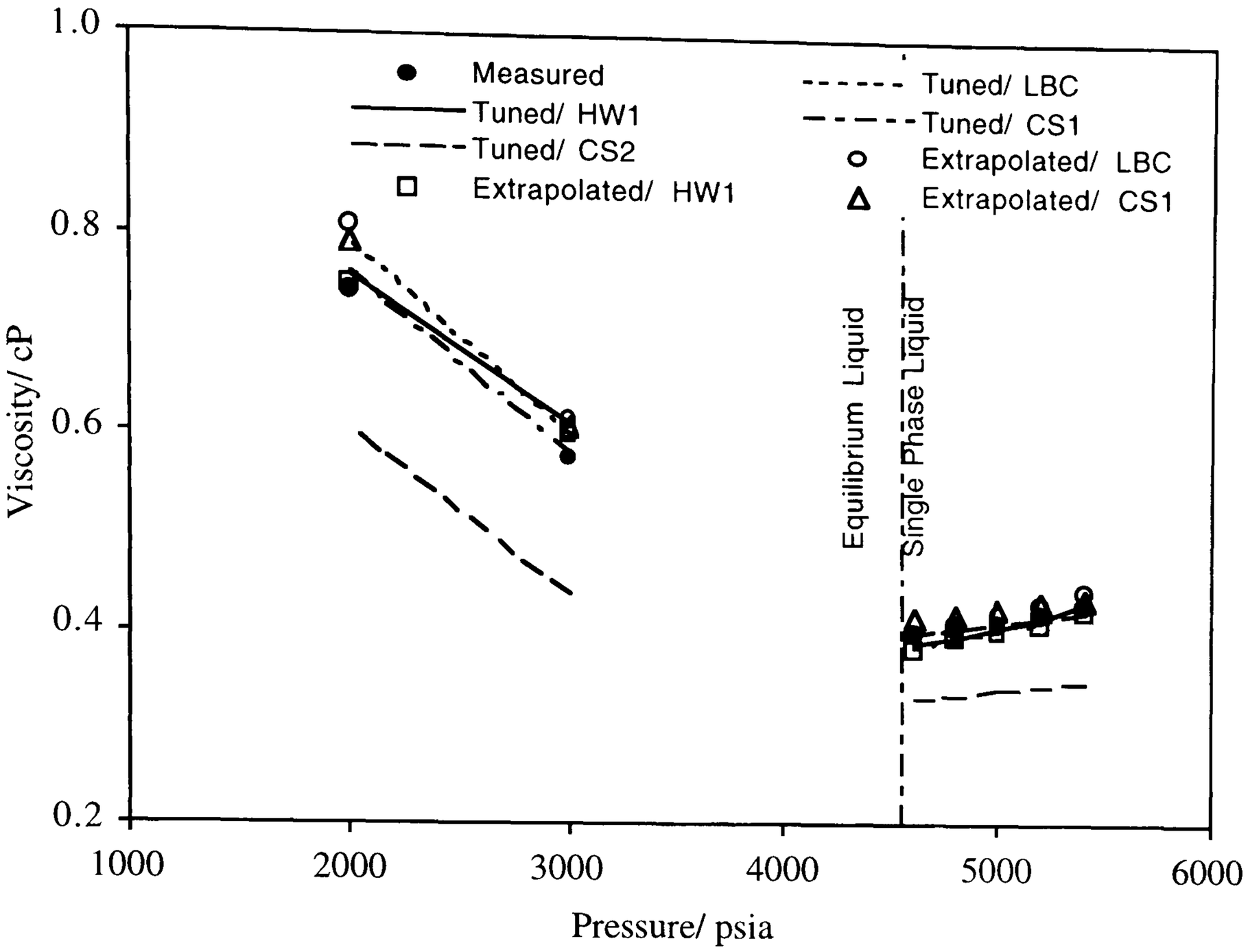

Figure 7.30 - Experimental and Predicted Viscosities Versus Pressure of the Original Volatile Oil LRA97-1 at 37.8 °C, With Extrapolated and Adjusted C7+ Properties.

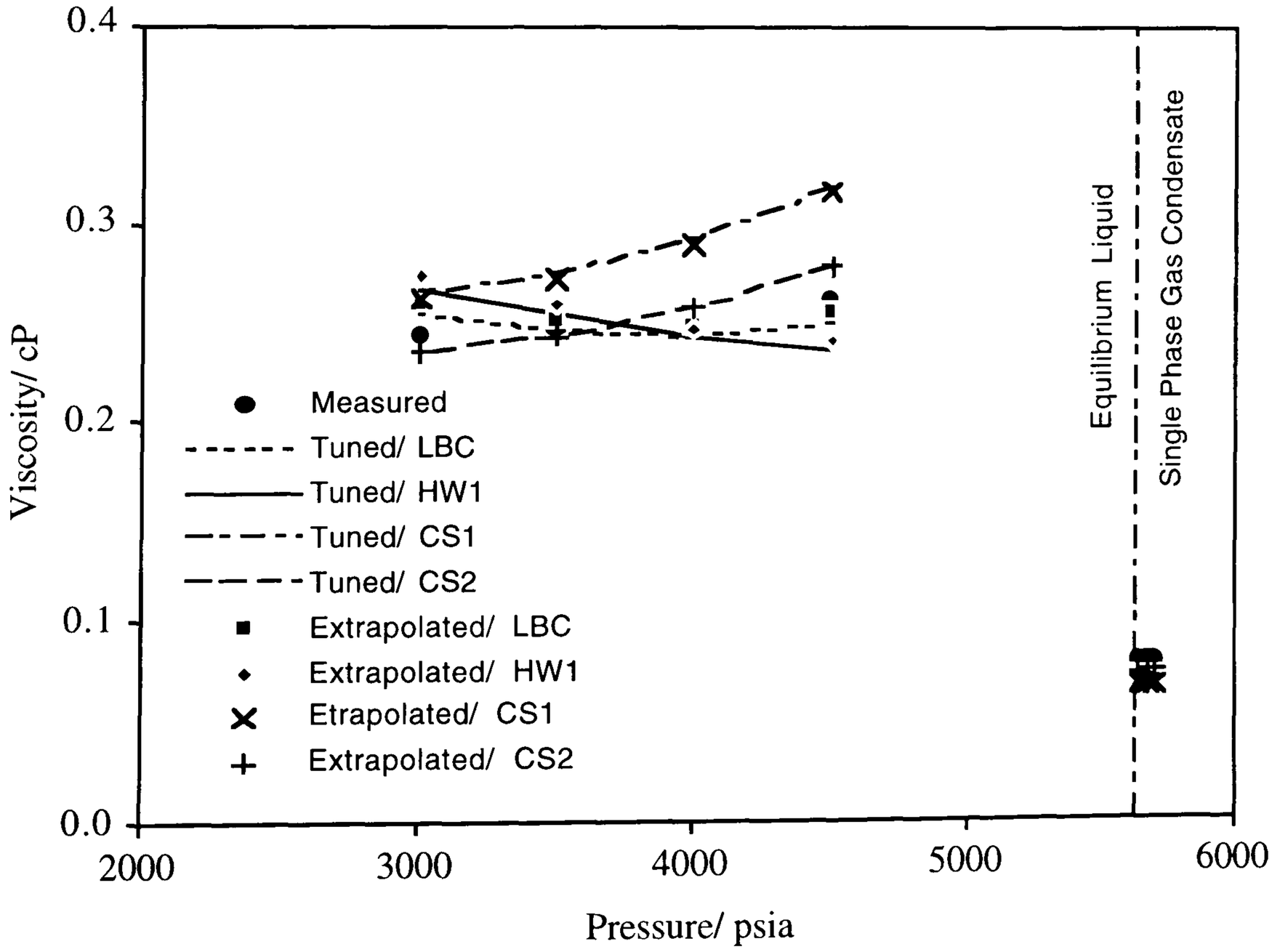

Figure 7.31 - Experimental and Predicted Viscosities Versus Pressure of the Original Gas Condensate GCB98-1 at 37.8 °C, With Extrapolated and Adjusted C7+ Properties.

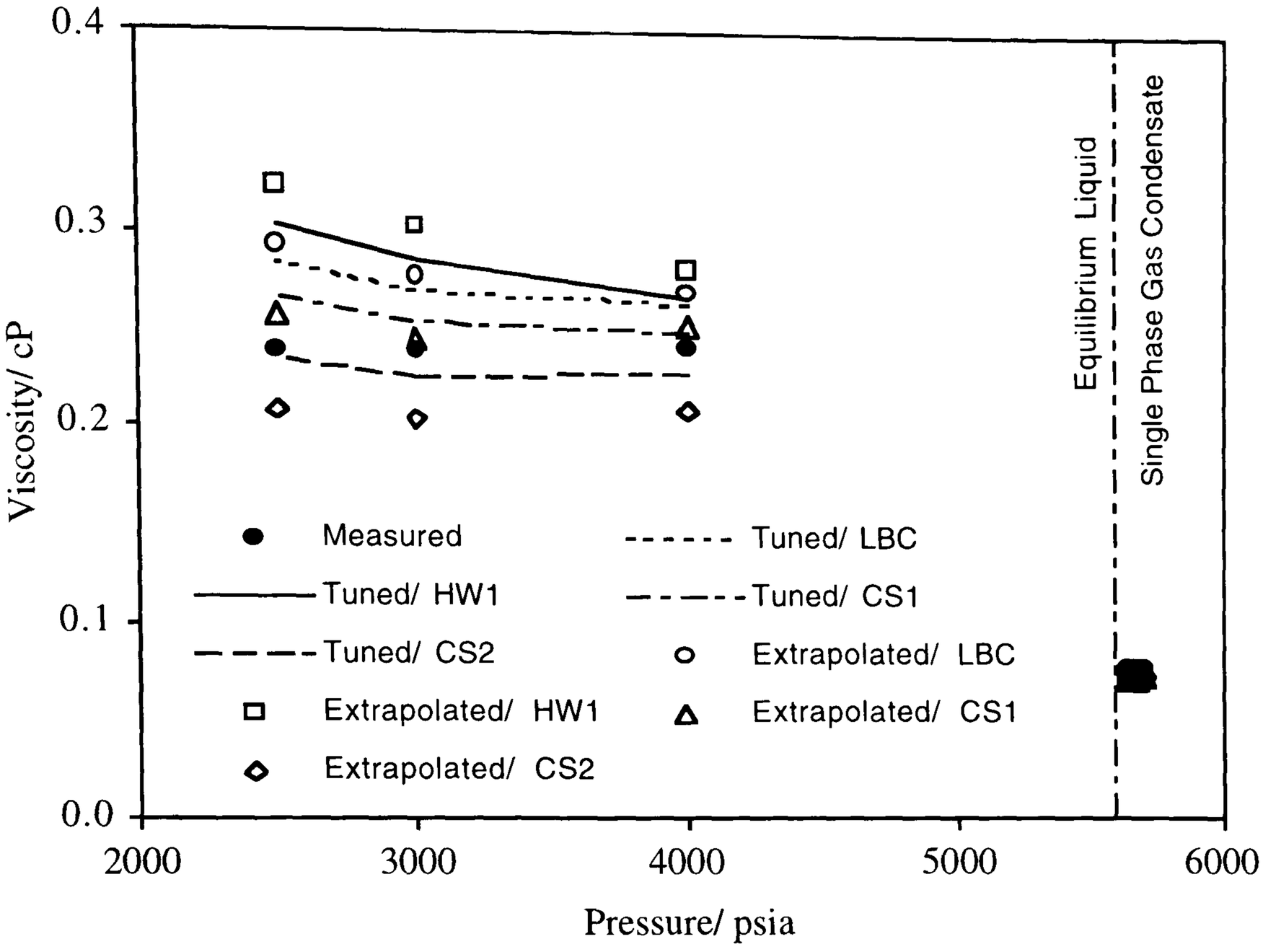

Figure 7.32 - Experimental and Predicted Viscosities Versus Pressure of the Original Gas Condensate GCB98-2 at 37.8 °C, With Extrapolated and Adjusted C7+ Properties.

CHAPTER 8

CONCLUSIONS AND RECOMMENDATIONS

Surface and viscous forces play a major role in the flow characteristics of fluids in petroleum reservoirs, hence, in the recovery of hydrocarbons. In reservoir engineering, surface forces are expressed by the interfacial tension (IFT) between different co-existing phases at equilibrium and the contact angle between the reservoir rock and in-situ fluids; whereas viscous forces are expressed by the viscosity of the flowing phases. The determination and evaluation of these properties are essential in planning, management and operation of reservoirs for optimum recovery.

In light of the experimental data and modelling work presented in the preceding chapters of this thesis, the conclusions and recommendations for further work are stated below.

8.1 CONCLUSIONS

Evaluation of the Meniscus Height Technique for Interfacial Tension Measurement.

Accurate and reliable information on interfacial tension (IFT) is of major importance in the petroleum industry. The relative permeability relationships which determine the flow behaviour of reservoir fluids in porous media strongly depend on the interfacial tension at high pressure conditions. Therefore, it is important to acquire reliable IFT data at wider conditions of pressure and temperature. Evaluation on the measurement of IFT by both the pendant drop and meniscus height techniques has concluded the following:

- Measured IFTs by the pendant drop and meniscus height techniques for different reservoir processes were in close agreement which is within ±2% in most cases (Figures 4.1, 4.3, 7.2 and 7.5). This in turn endorses the meniscus height technique as a rigorous method for measuring the IFT, with no additional effort, while conducting conventional PVT analysis.

The Variation of Gas-Oil-Solid Contact Angle with Interfacial Tension. Literature reports on capillary pressure data on chalk and sandstone cores have suggested to change the contact angle for low interfacial tension values while transposing laboratory capillary pressure data to reservoir conditions. However, there exists little information on the variation of contact angle with pertinent parameters in the literature. The exploratory study into the variation of contact angle with interfacial tension has provided some stimulating results both from a theoretical as well as a practical perspectives, which are summarised below:

- A novel technique (Section 2.4.2, page 18) based on the filament rise in a square capillary tube was employed for measuring the vapour-liquid-solid contact angle at conditions relevant to reservoir operation. The technique could readily be incorporated into conventional PVT analysis of reservoir fluids.
- The variation of IFT and contact angle (Section 3.3, page 27) for a variety of binary and multi-component real reservoir fluids has shown that the contact angle remains relatively constant for a wide range of IFT values and then decreases as the fluid approaches its critical region (Figure 3.3). The results have also shown that the current practice of assuming zero or constant angle is invalid at low IFT values, and a capillary pressure curves which take contact angle variation into account must be incorporated for multi-phase flow simulation.
- The generated data on binary fluid systems (Tables 3.5 through 3.8) were used to develop a generalised correlation (Equation 3.2) between the contact angle, interfacial tension and convergence pressure (Section 3.4, page 29). Predictions from the developed correlation were compared against measured data of two multi-component reservoir fluids and found to be in good agreement (Figures 3.4 and 3.5).

The Modified Residual Viscosity Correlation. In multi-phase flow calculations, reliable information on the viscosity of all flowing phases over a wide range of equilibrium conditions is essential for optimum process design and operational management. Viscosity predictive techniques used by the petroleum industry have been observed to behave un-reliably for dense fluids. The residual viscosity method by Lohrenz-Bray-Clark (LBC) has been modified and the modification was evaluated as summarised below:

- A systematic investigation of density and viscosity of pure compounds at various pressures and temperatures indicated the need to include both structural and thermal effects, in addition to density, for accurate viscosity prediction (Figures 5.6 and 5.7). The residual viscosity correlation by Jossi-Steil-Thodos (JST) (Equation (5.13), page 54, developed for pure hydrocarbons) has been modified by incorporating the above-mentioned effects.
- The modified correlations (Equations 5.27 and 5.28, page 60-61) has been used for calculating mixture viscosity for a variety of binary hydrocarbon and carbon dioxide systems and proved to be superior to all tested viscosity prediction methods, Figures 5.11 through 5.15.
- Viscosity prediction for a variety of multi-component fluids, using the modified correlations (Equations 5.27 and 5.28, page 60-61), at wider conditions (with and without water) proved its reliability and superiority to the residual viscosity models (LBC, page 55, and HW1 page 57) and the corresponding states model (CS1, page 52, and CS2 page 53), Figures 5.16 through 5.26.
- The modified correlations (Equations 5.27 and 5.28, page 60-61) have been used for calculating mixture viscosity for binary systems of Methane/Methylcyclohexane and Methane/cis-Decahydronaphthanlene, at a wide conditions of temperature, pressure and composition. The predictions from the modified correlation were comparable to those of the LBC method. However, at higher concentrations of cis-Decahydronaphthanlene, both the LBC and the modified correlation were seen to largely deviate from experimental values, Figures 5.27 and 5.28.

Near-Critical Viscosity Enhancement Study. Reliable understanding and description of the critical behaviour of fluids is needed for many innovative applications such as enhanced oil recovery and high pressure-high temperature fluid processes. The viscosity of under-saturated fluids normally decreases with decreasing pressure. However, viscosity enhancement was observed for near-critical binary and multi-component real reservoir fluids. This behaviour has not been previously reported for fluids with phase behaviour similar to real reservoir fluids. The conclusions and findings reached in this area are summarised below:

- The measurement of viscosity of several near critical mixtures, representative of those discovered in HPHT reservoirs and IOR processes, exhibited viscosity enhancement near the critical region, similar to those of pure compounds reported in the literature. Viscosity enhancement in excess of 10% was observed, reaching its maximum at the saturation pressure (Figures 6.4 and 6.5). The observed enhancement is significant and should be taken into account in flow simulation at such conditions.
- Models normally used for predicting viscosity of reservoir fluids were observed to behave unreliably in the vicinity of critical point (Figure 6.6). A simple two-parameter corresponding state viscosity model has been developed, using critical enhancement data on pure fluids, (Section 6.7, pagse 79-81). The developed model (Equation 6.7, page 80), for the critical region, successfully predicted the near critical viscosity enhancement of all tested fluids. The relative deviations were observed to increase further away from the critical point (Figures 6.19 through 6.25).
- The deviations of model prediction from experimental data for tested fluids were investigated by including the molecular weight as the third parameter. No obvious trend between the disappearance of viscosity enhancement with the component molecular weight was detected (Figure 6.26).

Contamination of Reservoir Fluids with Oil-based Mud Filtrate. The properties of the original reservoir fluid are essential in the design of process facilities as well as reservoir management. Despite advances in downhole sampling tools, obtaining a mud-free reservoir fluid sample still remains a challenge. To retrieve the properties of the

original fluid, from contaminated samples, predictive tools are often used. A number of volatile oil and gas condensate samples have been purposely contaminated with different mud filtrates at various levels. The samples, original and contaminated, have been fully characterised, and tested experimentally at the reservoir and surface conditions. The contamination level was increased incrementally in the tests to the extent of converting the gas condensate samples to volatile oil systems. Using the developed methodology (Sections 7.3.2 and 7.4.2) for retrieving the interfacial and viscosity of the original (un-contaminated) reservoir fluid, the following conclusions can be made:

- The interfacial tension of the un-contaminated fluid can be predicted, with reasonable accuracy, by extrapolating the parachor value of the plus-fraction, obtained from tuned models of the contaminated samples, to 0% contamination (Figures 7.10 through 7.14).
- The un-tuned viscosity models poorly predicted the single phase oil viscosities, while they reliably predicted the viscosities of the saturated vapour. The un-tuned one- and two-reference fluid(s) corresponding states models (CS1 and CS2) performed very well for predicting the viscosities of the single phase condensate, while those of the residual viscosity models (LBC and HW1) predicted the viscosity of the saturated liquids with reasonable accuracy (Tables 7.19 through 7.22).
- The deviations of predicted viscosity of the original single and saturated fluid phases using the model with tuned C7+ critical properties determined by extrapolation to zero contamination are in close agreement (Figures 7.30 through 7.32). This in turn demonstrated the reliability of the method used in retrieving the viscosity of un-contaminated reservoir fluids from contaminated samples

8.2 RECOMMENDATIONS

- The exploratory study into contact angle and interfacial tension for hydrocarbon mixtures has provided some stimulating results. It is recommended that recovery schemes where surface or capillary forces dominate, in the flow characteristics of

fluids, should be re-evaluated by including the contact angle in the capillary pressure functions.

- More research should be conducted to tie-in the observed commencement of the decline of contact angle with interfacial tension (IFT) with the line breakage between IFT and vapour-liquid density difference, which was previously noticed in this laboratory as well as by other investigators. Interestingly to note that all of these effects happen in the vicinity of critical region.
- To improve viscosity prediction of dense phases, the developed correlation should be incorporated in numerical reservoir simulators.
- To improve the viscosity prediction for dense aromatic compounds and naphtenes, it is advisable that more experiments should be performed. In light of these results and those from the literature, a more systematic investigation could be conducted to assess model deviation and improve model prediction.
- During the contamination studies, it was assumed that there is no inter-phase exchange between mud filtrate and formation hydrocarbon. This assumption is valid when dealing with oils. However for gas condensate samples, exchange of components between these fluids and the drilling fluid is expected. An investigation into such process would be desirable to gain an understanding into its effects on measured fluid properties.

APPENDIX A

A.1 DERIVATION OF EQUATIONS FOR PROPAGATION OF ERROR ANALYSIS

The fact that measuring devices never provide the true value follow that when someone uses data containing standard errors in mathematical calculations, the errors are propagated by these calculations. The following general equation for the variance is of wide application in the area of error propagations[1]:

$$E_f{}^2(f) = \left(\frac{\partial f}{\partial A}E_A\right)^2 + \left(\frac{\partial f}{\partial B}E_B\right)^2 + \ldots + \left(\frac{\partial f}{\partial N}E_N\right)^2 \qquad \text{(A.1)}$$

where;

f	:the calculated function or dependant variable.
A, B, ..., N	:terms which the function f depends on.
E	:standard error associated with each term in function f.

The above formulation was applied for the calculation of the overall propagated errors on the computed contact angle, using Equation (2.4). For the contact angle function, Equation (A.1) can be written as:

$$E^2(\tan(\theta)) = \left(\frac{\partial \tan(\theta)}{\partial R_c}E_{R_c}\right)^2 + \left(\frac{\partial \tan(\theta)}{\partial R_t}E_{R_t}\right)^2 \qquad \text{(A.2)}$$

Since the radius of curvature of liquid filament (R_t) is not a measurable quantity, errors arise in its calculated value, using a rearranged form of Equation (2.5). These errors are propagated from errors in the measured vapour-liquid density difference ($\Delta\rho$), the height of liquid filament rise (ΔZ), the IFT between equilibrated vapour and liquid phases (σ), and the radius of curvature of the meniscus (R_b). Therefore, error function of the form similar to Equation (A.1) must be derived for R_t as follow:

$$E^2(R_t) = \left(\frac{\partial R_t}{\partial R_b} E_{R_b}\right)^2 + \left(\frac{\partial R_t}{\partial Z} E_Z\right)^2 + \left(\frac{\partial R_t}{\partial \sigma} E_\sigma\right)^2 + \left(\frac{\partial R_t}{\partial \Delta\rho} E_{\Delta\rho}\right)^2 \qquad \text{(A.3)}$$

The derivatives which go into Equations (A.2) and (A.3) are derived below.

A.2.1 Derivatives of tan(θ) With Respect to R_b and R_t

The derivatives of the tangent of contact angle, tan(θ), as a function of R_c and R_t can be obtained by taking the derivative of Equation (2.4) with respect to R_c and R_t which are shown below:

$$\frac{\partial \tan(\theta)}{\partial R_c} = -\frac{1}{\sqrt{2}} \left[\frac{\left\{ \left(\sqrt[4]{R_t^2 + R_c\sqrt{2R_t^2 - R_c^2}} \right)\left(1 + \frac{2R_c}{2\sqrt{2R_t^2 - R_c^2}} \right) \right\} - \left\{ \left(R_c - \sqrt{2R_t^2 - R_c^2} \right)\left(\frac{\left(-R_c^2 \Big/ \sqrt{2R_t^2 - R_c^2} \right) + \left(\sqrt{2R_t^2 - R_c^2} \right)}{4\left(R_t^2 + R_c\sqrt{2R_t^2 - R_c^2} \right)^{-3/4}} \right) \right\}}{\sqrt{R_t^2 + R_c\sqrt{2R_t^2 - R_c^2}}} \right] \qquad \text{(A.4)}$$

$$\frac{\partial \tan(\theta)}{\partial R_t} = -\frac{1}{\sqrt{2}} \left[\frac{\left\{ \left(\sqrt[4]{R_t^2 + R_c\sqrt{2R_t^2 - R_c^2}} \right) \left(-\frac{4R_t}{2\sqrt{2R_t^2 - R_c^2}} \right) \right\} - \left\{ \left(R_c - \sqrt{2R_t^2 - R_c^2} \right) \left(\frac{(2R_t) + \left(\frac{4R_t}{2R_c\sqrt{2R_t^2 - R_c^2}} \right)}{4\left(R_t^2 + R_c\sqrt{2R_t^2 - R_c^2} \right)^{-3/4}} \right) \right\}}{\sqrt{R_t^2 + R_c\sqrt{2R_t^2 - R_c^2}}} \right] \quad \text{(A.5)}$$

Substituting Equations (A.4) and (A.5) into Equation (A.2), the resulting overall error in the measured contact angle can be computed by Equation (A.6) below;

$$E^2(\tan(\theta)) = \left(-\frac{1}{\sqrt{2}} \left[\frac{\left\{ \left(\sqrt[4]{R_t^2 + R_c\sqrt{2R_t^2 - R_c^2}} \right) \left(1 + \frac{2R_c}{2\sqrt{2R_t^2 - R_c^2}} \right) \right\} - \left\{ \left(R_c - \sqrt{2R_t^2 - R_c^2} \right) \left(\frac{\left(\frac{-R_c^2}{\sqrt{2R_t^2 - R_c^2}} \right) + \left(\sqrt{2R_t^2 - R_c^2} \right)}{4\left(R_t^2 + R_c\sqrt{2R_t^2 - R_c^2} \right)^{-3/4}} \right) \right\}}{\sqrt{R_t^2 + R_c\sqrt{2R_t^2 - R_c^2}}} \right] E_{R_c} \right)^2 +$$

$$\left(-\frac{1}{\sqrt{2}} \left[\frac{\left\{ \left(\sqrt[4]{R_t^2 + R_c\sqrt{2R_t^2 - R_c^2}} \right) \left(1 + \frac{2R_c}{2\sqrt{2R_t^2 - R_c^2}} \right) \right\} - \left\{ \left(R_c - \sqrt{2R_t^2 - R_c^2} \right) \left(\frac{\left(\frac{4R_t}{\sqrt{2R_t^2 - R_c^2}} \right) + (2R_t)}{4\left(R_t^2 + R_c\sqrt{2R_t^2 - R_c^2} \right)^{-3/4}} \right) \right\}}{\sqrt{R_t^2 + R_c\sqrt{2R_t^2 - R_c^2}}} \right] E_{R_t} \right)^2 \qquad \text{(A.6)}$$

In computing the propagated error in the measured contact angle, E_{Rc} has only standard error with a value of ±0.003 mm. However E_{Rt} must be computed from terms associated with the calculated R_t which are described below.

Derivatives of R_t With Respect to $\Delta\rho$, ΔZ, σ, and R_b. Errors in the calculated values of R_t could have propagated through mathematical calculation of errors in the

measured vapour-liquid density difference, $\Delta\rho$, the height of liquid filament rise (ΔZ), the IFT between vapour and liquid phases, σ, and the radius of the curvature of the meniscus, R_b. Similar functions of the form of Equation (A.1) can, therefore, be written for R_t where the derivatives invloved are derived as shown below:

$$\frac{\partial R_t}{\partial \Delta\rho} = -\frac{\left(\sigma R_b^2 g \Delta Z\right)}{\left(R_b \Delta\rho g \Delta Z + 2\sigma\right)^2} \tag{A.7}$$

$$\frac{\partial R_t}{\partial \Delta Z} = -\frac{\left(\sigma R_b^2 \Delta\rho g\right)}{\left(R_b \Delta\rho g \Delta Z + 2\sigma\right)^2} \tag{A.8}$$

$$\frac{\partial R_t}{\partial \sigma} = \frac{R_b\left(R_b \Delta\rho g \Delta Z + 2\sigma\right) - 2\sigma R_b}{\left(R_b \Delta\rho g \Delta Z + 2\sigma\right)^2} \tag{A.9}$$

$$\frac{\partial R_t}{\partial R_b} = \frac{\sigma\left(R_b \Delta\rho g \Delta Z + 2\sigma\right) - \sigma R_b \Delta\rho g \Delta Z}{\left(R_b \Delta\rho g \Delta Z + 2\sigma\right)^2} \tag{A.10}$$

In Equations (A.7) through (A.10), $\Delta\rho$ is calculated by taking the difference between measured densities of the equilibrium vapour and liquid phases. Hence, in addition to standard errors associated to measured density, additional error propagtes by this simple mathematical operation which could effect its calculated value. Similar to the vapour-liquid density difference, IFT (σ), also contains propagated errors as a result of using Equations (2.2) or (2.3). While, ΔZ and R_b have only standard resolution errors associated with their dimensioning devices.

The propagated error equation for the vapour-liquid density difference and IFT are derived below.

Propagated Error Equation for the Calculated Vapour-Liquid Density Difference. Errors propagate in substraction operation according to the form below:

$$E_{Diff} = \sqrt{E_A^2 + E_B^2} \tag{A.11}$$

Therefore, errors in the calculated vapour-liquid density difference ($\Delta\rho$) can propagates as:

$$\Delta\rho = \Delta\rho_{calc.} \pm \sqrt{2} E_\rho \tag{A.12}$$

Propagated Error Equation for the Calculated **IFT.** Formulations, similar to those above, can be employed to calculate propagated errors for IFT measured by either the classical pendant drop or the meniscus height techniques[2,3]. The propagated errors for the IFT calculated by pendant drop method[2], Equation (2.2), can be estimated from Equation (A.13), below:

$$E[\sigma] = g\sqrt{\left(\frac{\partial\sigma}{\partial\Delta\rho}E_{\Delta\rho}\right)^2 + \left(\frac{\partial\sigma}{\partial d_e}E_{d_e}\right)^2 + \left(\frac{\partial\sigma}{\partial 1/H}E_{1/H}\right)^2} \tag{A.13}$$

The derivatives of each of the terms above are computed from the following set of equation:

$$\frac{\partial\sigma}{\partial\Delta\rho} = \frac{gd_e^2}{H} \tag{A.14}$$

$$\frac{\partial\sigma}{\partial d_e} = \frac{2\Delta\rho g d_e}{H} \tag{A.15}$$

$$\frac{\partial\sigma}{\partial 1/H} = \Delta\rho g d_e^2 \tag{A.16}$$

Substituting Equations (A.14) through (A.16) into Equations (A.13), the resulting overall error in the calculated IFT using pendant drop method, Equation (2.2), can be computed from Equation (A.17) below;

$$E[\sigma] = \sqrt{\left(\frac{gd_e^2}{H}E_{\Delta\rho}\right)^2 + \left(\frac{2gd_e}{H}E_{d_e}\right)^2 + \left(\Delta\rho g d_e^2 E_{1/H}\right)^2} \qquad \text{(A.17)}$$

Where; the values of $E_{\Delta\rho}$ is obtained from Equation (A.12) and $E_{1/H}$ is computed. using the quotient rule below;

$$E_{1/H} = \frac{d_s}{d_e}\sqrt{\left(\frac{E_{d_s}^2}{d_s}\right)^2 + \left(\frac{E_{d_e}}{d_e}\right)^2} \qquad \text{(A.18)}$$

If the IFT is calculated using the meniscus height technique[3], Equation (2.3), its propagated error function can be computted as follow;

$$E[\sigma] = g\sqrt{\left(\frac{\partial\sigma}{\partial\Delta\rho}E_{\Delta\rho}\right)^2 + \left(\frac{\partial\sigma}{\partial h}E_h\right)^2} \qquad \text{(A.19)}$$

The derivatives of each of the terms in Equation (A.19) can be computed from Equations (A.20) and (A.21) below;

$$\frac{\partial\sigma}{\partial\Delta\rho} = \frac{gh^2}{2} \qquad \text{(A.20)}$$

$$\frac{\partial\sigma}{\partial h} = \Delta\rho g h \qquad \text{(A.21)}$$

Substituting Equations (A.20) and (A.21) into Equation (A.19), the resulting overall error in the calculated IFT using Equation (2.3) can be computed from Equation (A.22);

$$E[\sigma] = \sqrt{\left(\frac{gh^2}{2}E_{\Delta\rho}\right)^2 + \left(\Delta\rho g h E_h\right)^2} \qquad \text{(A.22)}$$

REFERENCES

[1] Crandall, K.C and Seabloom, R.W.,:Engineering Fundamentals In Measurements. Probability, Statistics, and Dimensions", McGrew-Hill General Engineering Series. San Francisco, (1970).

[2] Andreas, J.M., Hauser, E.A., and Tucker, W.B. :"Boundary Tension by Pendant Drops," Presented at the 50th Colloid Symposium, held at Cambridge, Massachusetts (1938).

[3] Danesh, A., Todd, A.C., Somerville, J and Dandekar, A : "Direct Measurement of Interfacial Tension, Density, Volume and Compositions of Gas Condensate Systems", Trans I Chem E, **68A**, 325 - 330, (1990).

APPENDIX B

B.1 PRINCIPLE OF CORRESPONDING STATE METHODS

This section contains the various expressions and formulations used by the different corresponding state-based viscosity predictive methods, as described in Section 5.6 of Chapter 5.

B.1.1 The Extended Corresponding State Method (TRAPP)

Ely and Hanley[1] have presented a corresponding state model for the prediction of fluid viscosity. The viscosity of a fluid at a given density and temperature is calculated using the Equation (5.7) below;

$$\eta(\rho,T) = \eta_{ref}\left(\rho_{ref},T_{ref}\right) F_{\eta} \tag{5.7}$$

where;

$\eta(\rho,T)$: viscosity of fluid of interest.

$\eta_{ref}(\rho_{ref},T_{ref})$: viscosity of reference fluid.

ρ_{ref} , T_{ref}: equivalent density and temperature, evaluated from Equations (B.1).and (B.2).

$$T_{ref} = \frac{T}{f_x} \tag{B.1}$$

$$\rho_{ref} = \rho.h_x \tag{B.2}$$

F_η: corresponding state reducing factor, evaluated from Equations (B.3).

$$F_\eta = \left(\frac{MW_x}{MW_{ref}} \right)^{1/2} f_x^{1/2} \, h_x^{-2/3} \tag{B.3}$$

In case of mixtures, MW_x, f_i and h_i are evaluated from Equations (B.4) through (B.9), below;

$$f_x = \frac{\sum_i \sum_j x_i x_j f_{ij} h_{ij}}{h_x} \tag{B.4}$$

$$h_x = \sum_i \sum_j x_i x_j h_{ij} \tag{B.5}$$

$$MW_x = \left(\sum_i \sum_j x_i \, x_j \, f_{ij}^{1/2} h_{ij}^{4/23} \mathrm{MW}_{ij}^{1/2} \right)^2 \Big/ f_x \, h_x^{8/3} \tag{B.6}$$

where;

$$f_{ij} = \left(f_i f_j \right)^{0.5} \tag{B.7}$$

$$h_{ij} = \frac{1}{8} \left(h_i^{\frac{1}{3}} + h_j^{\frac{1}{3}} \right)^3 \tag{B.8}$$

$$MW_{ij} = 2 MW_i \, MW_j \Big/ \left(MW_i + MW_j \right) \tag{B.9}$$

where x_i and MW_i are the mole fraction and molecular weight of component i in the mixture.

The TRAPP method uses two shape factors, $\Theta(T_r, V_r, \omega)$ and $\Phi(T_r, V_r, \omega)$, to account for deviations from the corresponding state principle. The shape factors for each ith component are related to the corresponding state reducing ratios, (f_i and h_i) as shown in Equations (B.10) through (B.15):

$$f_i = \left(\frac{T_{ci}}{T_{ref}} \right) \Theta_i \tag{B.10}$$

$$h_i = \left(\frac{V_{ci}}{V_{ref}}\right)\Phi_i \tag{B.11}$$

$$\Theta_i = 1 + \left(\omega_i - \omega_{ref}\right) F\left(V_i, T_{ri}\right) \tag{B.12}$$

$$\Phi_i = \left(1 + \left(\omega_i - \omega_{ref}\right) G\left(V_i, T_{ri}\right)\right) \frac{Z_{c,ref}}{Z_{ci}} \tag{B.13}$$

where;

$$F\left(V_{ri}, T_{ri}\right) = 0.090569 - 0.862762\ \ln\left(T_{ri}\right) + \left(0.316636 - \frac{0.465684}{T_{ri}}\right)\left(V_{ri} - 0.5\right) \tag{B.14}$$

$$G\left(V_{ri}, T_{ri}\right) = 0.394901\ \left(V_{ri} - 1.023545\right) - 0.932813\ \left(V_{ri} - 0.754639\right)\ \ln\left(T_{ri}\right) \tag{B.15}$$

V_{ri}, T_{ri}: reduced volume and reduced temperature, respectively.

Z_c: critical compressibility factor.

However, since the density (or volume) of fluid for which the viscosity is to be calculated is not known, an iterative procedure is needed, hence, to the determination of Θ and Φ, since they are both function of V_r. To accomplish this iterative procedure, an initial value of V_r is set for each i th component in the fluid mixture. The initial values used to start this iterative procedure are 2.0 and 0.5 for the vapour and liquid phases, respectively.

The calculated fluid density calculated by the 33-parameter Benedict-Webb-Rubin (BWR) EOS in the form suggested by McCarty[2] is then converted into volume using the apparent fluid molecular weight and then the reduced volume is calculated and compared with the assumed values. The above calculations are repeated until convergence between calculated and assumed values is attained. The methane viscosity is calculated by Equation (B.16);

$$\eta_{ref}\left(\rho, T\right) = \eta_o\left(T_{ref}\right) + \eta_1\left(T_{ref}\right)\rho_{ref} + \eta_2\left(\rho_{ref}, T_{ref}\right) \tag{B.17}$$

For calculating the dilute gas coefficient, $\eta_o(T)$, Equation (B.18) can be used;

$$\eta_o(T) = \sum_{i=1}^{9} GV_i.T^{\frac{i-4}{3}} \tag{B.18}$$

$$\eta_1(T) = A + B.\left[C - \ln\left(\frac{T}{F}\right)\right]^2 \tag{B.19}$$

The terms $\Delta\eta^1(\rho,T)$ and $\Delta\eta^2(\rho,T)$, which govern the dense fluid region, can be obtained from Equations (B.20) and (B.21),

$$\Delta\eta^1(\rho,T) = \exp\left(j_1 + {}^{j_4}\!/_{T}\right)\left[\exp\left(\rho^{0.1}\left(j_2 + {}^{j_3}\!/_{T^{3/2}}\right) + \Psi\rho^{0.5}\left(j_5 + {}^{j_6}\!/_{T} + {}^{j_7}\!/_{T^2}\right)\right) - 1.0\right] \qquad \text{(B.20)}$$

$$\Delta\eta^2(\rho,T) = \exp\left(k_1 + {}^{k_4}\!/_{T}\right)\left[\exp\left(\rho^{0.1}\left(k_2 + {}^{k_3}\!/_{T^{3/2}}\right) + \Psi\rho^{0.5}\left(k_5 + {}^{k_6}\!/_{T} + {}^{k_7}\!/_{T^2}\right)\right) - 1.0\right] \qquad \text{(B.21)}$$

and Ψ is included to account for the high density behaviour of the transport viscosity as defined by Equation (B.22);

$$\Psi = \frac{\rho - \rho_{cref}}{\rho_{cref}} \qquad \text{(B.22)}$$

F_1 and F_2 are coefficients calculated from Equations (B.23) through (B.26) below:

$$F_1 = \frac{HTAN + 1}{2} \qquad \text{(B.23)}$$

$$F_2 = \frac{1 - HTAN}{2} \qquad \text{(B.24)}$$

$$HTAN = \frac{\exp(\Delta T) - \exp(-\Delta T)}{\exp(\Delta T) + \exp(-\Delta T)} \qquad \text{(B.25)}$$

$$\Delta T = T - T_f \qquad \text{(B.26)}$$

The values for the constant GV_i, A, B, C, F, j_i and k_i are listed in Tables B.1 through B.4.

Table B.1 - Methane Dilute Gas Coefficient, GV_i, Values for Equation (B.18)

GV_i	Methane
GV_1	-2.090975×10^5
GV_2	2.647269×10^5
GV_3	-1.472818×10^5
GV_4	4.716740×10^4
GV_5	-9.491872×10^3
GV_6	1.219979×10^3
GV_7	-96.27993
GV_8	4.274152
GV_9	-8.141531×10^{-2}

Table B.2 - Methane Coefficients A, B, C & F Values for Equation (B.19).

Coefficient	Value
A	1.696985927
B	-0.133372346
C	1.4
F	168.0

Table B.3 - Methane Coefficients, j_i, Values for Equation (B.20).

i	j_i
1	-10.3506
2	17.5716
3	-3019.39
4	-188.730
5	0.0429036
6	14B.290
7	6127.68

Table B.4 - Methane Coefficients, k_i, Values for Equation (B.21).

i	k_i
1	-9.74602
2	18.0834
3	-4126.66
4	44.6055
5	0.976544
6	81.8134
7	15649.9

B.1.2 The One-reference Fluid Method

As discussed in Chapter 5, the viscosity of any substance, using the above method, can be determined from Equation (5.8)[3,4];

$$\eta(P,T) = \left(\frac{\eta_c}{\eta_{c,ref}}\right)\eta_{ref}\left(P_{ref}, T_{ref}\right)F_\eta \qquad (5.8)$$

where,

P_{ref} , T_{ref}: equivalent pressure and temperature, respectively, evaluated from Equations (B.27) and (B.28) below;

$$P_{ref} = \frac{PP_{cref}}{P_c\ \alpha} \qquad (B.27)$$

$$T_{ref} = \frac{TT_{cref}}{T_c\ \alpha} \qquad (B.28)$$

F_η: corresponding state reducing factor, taken as the ratio of the rotational coupling factor of fluid of interest and the reference fluid. The rotational coupling factors for the reference fluid and the fluid of interest are evaluated from Equations (5.29) and (5.30).

$$\alpha_{RC} = 1 + 8.374x10^{-4}\ \rho_r{}^{4.265} \qquad (B.29)$$

$$\alpha = 1 + 7.747x10^{-5}\ \rho_r{}^{4.265} MW^{0.8579} \qquad (B.30)$$

where;

$$\rho_r = \frac{\rho_{RC}\left(\frac{T.T_{cref}}{T_c}, \frac{P.P_{cref}}{P_c}\right)}{\rho_{cref}} \tag{B.31}$$

The viscosity of the reference component (methane), η_{ref} (ρ,T), can be calculated from Equations (B.18) through (B.26).

For mixture, the following mixing rules are applied for calculating its properties[5];

$$T_{cmix} = \frac{\sum_i \sum_j x_i\, x_j \left[\left(\frac{T_{ci}}{P_{ci}}\right)^{1/3} + \left(\frac{T_{cj}}{P_{cj}}\right)^{1/3}\right]^3 \left[T_c\, T_{cj}\right]^{1/2}}{\sum_i \sum_j x_i\, x_j \left[\left(\frac{T_{ci}}{P_{ci}}\right)^{1/3} + \left(\frac{T_{cj}}{P_{cj}}\right)^{1/3}\right]^3} \tag{B.32}$$

$$P_{cmix} = \frac{8\sum_i \sum_j x_i\, x_j \left[\left(\frac{T_{ci}}{P_{ci}}\right)^{1/3} + \left(\frac{T_{cj}}{P_{cj}}\right)^{1/3}\right]^3 \left[T_c\, T_{cj}\right]^{1/2}}{\left(\sum_i \sum_j x_i x_j \left[\left(\frac{T_{ci}}{P_{ci}}\right)^{1/3} + \left(\frac{T_{cj}}{P_{cj}}\right)^{1/3}\right]^3\right)^2} \tag{B.33}$$

$$MW = MW_n + 1.304x10^{-4}\left(MW_w^{2.303} - MW_n^{2.303}\right) \tag{B.34}$$

where;

$$MW_w = \frac{\sum_i x_i\, MW_i^2}{\sum_i x_i\, MW_i} \tag{B.35}$$

$$MW_n = \sum_i x_i\, MW_i \tag{B.36}$$

B.1.3 The Two-reference Fluids Method

Based on the above method, the viscosity of any fluid system can be calculated from Equation (5.10) using the expression below[6];

$$\eta(P,T) = \frac{\eta_c \eta_1(T_1,P_1)}{\eta_{c1}} \left(\frac{\eta_2(T_2,P_2)\eta_{c1}}{\eta_1(T_1,P_1)\eta_{c2}} \right)^K \tag{5.10}$$

where;

K: an interpolating factor, $K = \dfrac{MW - MW_1}{MW_2 - MW_1}$ (5.11)

The subscripts 1 and 2 refer to methane and n-Decane components, respectively. methane and n-Decane viscosities are calculated from Equation (B.37) below;

$$\eta_{ref}(\rho,T) = \eta_o(T) + \eta_1(T)\rho + \eta_2(\rho,T) \tag{B.37}$$

The density of reference components is evaluated from Adachi-Lu-Sugie (ALS)-EOS in the form suggested by Jensen[7] using equivalent pressure and temperature, as calculated below:

$$P_{1,2} = \frac{PP_{c1,2}}{P_{cx}} \quad \text{and} \quad T_{1,2} = \frac{TT_{c1,2}}{T_{cx}} \tag{B.38}$$

For calculating the dilute gas coefficient, $\eta_o(T)$, Equation (B.18) can be used. The GV_i values of both substances are listed in Table B.5.

Table B.5 - Methane and n-Decane Dilute Gas Coefficient, GV_i, Values for Equation (B.18)

GV_i	Methane	n-Decane
GV_1	-2.090975×10^5	0.2640
GV_2	2.647269×10^5	0.9487
GV_3	-1.472818×10^5	71.0
GV_4	4.716740×10^4	0
GV_5	-9.491872×10^3	0
GV_6	1.219979×10^3	0
GV_7	-96.27993	0
GV_8	4.274152	0
GV_9	-8.141531×10^{-2}	0

The density correlation coefficient term, $\eta_1(T)$ can also be obtained from Equation (B.19) using appropriate constants, temperature and pressure for each reference component. The values of A, B, C and F constants for Methane and n-Decane are listed in Table B.6.

Table B.6 - Methane and n-Decane Coefficients (A, B, C & F) Values for Equation (B.19) Used by the two-reference Corresponding State Method.

Coefficient	Methane	n-Decane
A*100	23946	0.00248
B	343.79	81.35
C	0.4487	5.9583
F	168.0	490.0

For the dense fluid term, $\eta_2(\rho,T)$, Equation (B.20) can also be used with the tabulated j_i values for both Methane and n-Decane of Table B.6.

Table B.6 - n-Decane Coefficients, j_i, Values for Equation (B.20) Used by the Two-Reference Corresponding State Method.

j_i	Methane	n-Decane
j_1	-22.768	-11.739
j_2	30.574	16.092
j_3	-1.4929×10^4	-1.8464×10^4
j_4	1.0615×10^3	-811.3
j_5	-1.4748	1.9745;
j_6	290.62	898.45
j_7	3.0396×10^4	11.9620×10^4

The method can also be used for calculating the viscosity of mixtures using Equations (B.32) and (B.33) for mixture critical properties and Equation (B.39) through (B.41) for molecular weight;

$$MW_x = MW_n + 0.00867358\left(MW_w^{1.56079} - MW_n^{1.56079}\right) \tag{B.39}$$

where;

$$MW_w = \frac{\sum_i x_i \, MW_i^2}{\sum_i x_i \, MW_i} \tag{B.40}$$

$$MW_n = \sum_i x_i \, MW_i \tag{B.41}$$

REFERENCES

[1] Ely, J. F. and Hanley, H. J. M. : "Prediction of the Viscosity and Thermal Conductivity in Hydrocarbon Mixtures- Computer Program, TRAPP", Proceedings of the 60th Annual Convention of Gas Processors Association, 20-29. (March, 1981).

[2] McCarty, R. D. : "Conformal Solution Theory for Viscosity and Thermal Conductivity of Mixtures", Mol. Phy., **31**, 825, (1976).

[3] Pedersen, K. S., Fredensland, Aa., Christensen, P. L. and Thomassen, P.: "Viscosity of Crude Oils", Chem. Eng. Sci., **39**, 1011-1016, (1984).

[4] Pedersen, K. S., and Fredenslund, Aa. : "An Improved Corresponding States Model for the Prediction of Oil and Gas Viscosities and Thermal Conductivities," Chem. Eng. Sci., **42**, 182-186, (1987).

[5] Mo, K. C. and Gubbins, K. E. : "A Modified Benedict-Webb-Rubin Equation of States for Methane Using Recent Experimental Data", Cryog., **14**, 276, (1974).

[6] Petersen, Aa., K., Knudsen, K. and Fredenslund, Aa. : "Prediction of Viscosities of Hydrocarbon Mixtures," Fluid Phase Equilib., **70**, 293-308, (1991).

[7] Jensen, B. H. : Densities, Viscosities and Phase Equilibria in Enhanced Oil Recovery, Ph.D. Dissertation, Institute for Kemiteknik, The Technical University of Denmark, (1987).